Understanding substrate and inhibitor interactions with Mo-nitrogenase



Ting Chen

Somerville College

Michaelmas Term 2019

A Thesis submitted to the Board of the Faculty of Physical Sciences, for the degree of

Doctor of Philosophy, University of Oxford

Abstract

Understanding substrate and inhibitor interactions with MoFe nitrogenase

Ting Chen, Somerville College, University of Oxford

A thesis submitted for the degree of Doctor of Philosophy, Michaelmas Term 2019

The nitrogenase enzyme is a metalloenzyme that plays a key role in the biological nitrogen cycle. Nitrogenase fixes nitrogen by catalysing the reduction of dinitrogen in the atmosphere to ammonia. The enzyme is a protein expressed by free-living soil bacteria and symbiotic bacteria living in the roots of certain plants. The dinitrogen reduction mechanism of the enzyme remains poorly understood. This thesis describes using electrochemistry and Infrared spectroscopy to study the mechanism of molybdenum (Mo)-nitrogenase. In order to overcome the complexity of electron transfer by the native reductant Fe protein coupled to the hydrolysis of ATP, a carbon working electrode was used instead of Fe protein as a reductant to supply electrons to MoFe protein. A series of known inhibitors and different possible substrates of nitrogenase (including protons, dinitrogen, acetylene, isocyanides and carbon monoxide) was introduced into this spectroelectrochemical study. Meanwhile, genetic variants of nitrogenase were also studied to determine the role of specific amino acids in the protein by this approach.

Following the previous study of nitrogenase MoFe protein in the Vincent group, an attachment approach was developed to immobilise protein onto the carbon working electrode in the spectroelectrochemical cell. Consistent with an earlier electrochemical study of MoFe protein trapped in Nafion, the attached MoFe protein was shown to commence proton reduction at about -0.9 V. The interaction between MoFe protein and inhibitor, carbon monoxide was studied by IR spectroelectrochemistry. The results from both infrared spectroscopy and electrochemistry were consistent with a previous study under catalytic turnover conditions, and also showed that CO binds to the MoFe protein at around -0.9 V and below. For the first time direct electron transfer from a carbon working electrode to one of the variants of the nitrogenase MoFe protein (α -64$^{Tyr \rightarrow His}$) was observed, together with preliminary evidence of electron transfer to the wild type MoFe protein.

Acetylene is known to be a non-natural substrate of nitrogenase, and was shown to inhibit the proton reduction current by the MoFe protein at -0.9 V and below. Inhibition was irreversible when CO was flushed out with Ar at -0.9 V, but Ar was able to recover some of the proton

reduction activity at more negative potentials. The product ethylene was followed by GC analysis, which confirmed acetylene reduction by MoFe protein at about -0.9 V and more negative.

When isocyanide was introduced to MoFe protein, a shift in the peak of v(NC) from isocyanide to higher wavenumber compared to that in free solution was observed even at a mild potential. This suggests that isocyanide binds to a more oxidized redox state of the MoFe protein compared to the state needed for proton reduction, CO binding and acetylene reduction. Preliminary evidence for methylamine as the product was obtained by GC at much lower potentials.

These results establish, for the first time, the potentials at which different ligands bind to the MoFe protein, and thus should help in establishing aspects of the mechanism of substrate reduction by nitrogenase.

Acknowledgements

I would first like to give my deepest thank to Professor Kylie Vincent, my supervisor. Thanks for her giving me the chance to do PhD degree at the University of Oxford. Thanks for her inspiration and guidance to my research program. Thanks for her patient help and encouragement in daily life, especially the thesis writing.

Afterwards, I would thank Dr Philip Ash who gave me the training about research skills in our lab through the early days of my D.Phil. Your talent capability saves me and my experiments many times in the suffering time. I am grateful for all discussion with you and your help with data analysis.

I thank Prof Lance Seefeldt for providing the precious nitrogenase samples and giving me the chance to visit your lab at Utah State University. In addition, thanks to Dr Zhiyong Yang and Dr Artavazd Badalyan for uncomplaining assistance with my acetylene experiments.

My special thanks to all the Vincent group members past and present. I would like to say thanks to Dr Holly Reeve for her great organisation skill and daily help in the lab. The advice from Dr Jack Rowbotham and Jake Nicholson helped me determine amine groups by GC. I would like to thank the hard work by Part II student: Benjamin Rackham, for carrying out some experiments under my supervision. I am thankful to Michael Posidias' help with the UV-vis and carrying gas cylinders with me these years.

I am grateful to all the friends I have made and met during my D.Phil. for enriching my daily life and giving me unforgettable memories in Oxford over the past four years.

Finally, I would like to thank the great support from my family since I was born. Mom, thank you for accompanying me during this hardest time. Dad, I miss you so much.

Abbreviations

A	amperes
Å	Angstrom (10^{-10} m)
ADP	adenosine diphosphate
ATP	adenosine triphosphate
ATR	attenuated total reflectance
°C	degrees Centigrade
Da	Dalton
E	electrode potential
E_m	midpoint potential
$E°$	standard reduction potential
EPR	electron paramagnetic resonance
ENDOR	electron nuclear double resonance
Eu-L	Europium-ligands complexes
IR	infrared
I	current
K	Kelvin
NMR	nuclear magnetic resonance
O.D.	optical density
ppm	parts per million
s	second(s)
SCE	saturated calomel electrode
SEC	spectroelectrochemistry
SHE	standard hydrogen electrode
t	time
T	temperature
UV-vis	ultraviolet-visible
V	volts
64H	variant α-$64^{\mathrm{Tyr\rightarrow His}}$ MoFe protein
98H	variant β-$98^{\mathrm{Tyr\rightarrow His}}$ MoFe protein
70A	variant α-$70^{\mathrm{Val\rightarrow Ala}}$ MoFe protein

Table of Contents

ABSTRACT ..... **III**

ACKNOWLEDGEMENTS ..... **V**

ABBREVIATIONS ..... **VII**

TABLE OF CONTENT ..... **III**

CHAPTER 1

INTRODUCTION **1**

1.1 NITROGEN CYCLE AND NITROGEN FIXATION 2

1.1.1 Nitrogen cycle *2*

1.1.2 Non-biological nitrogen fixation *6*

1.1.3 Biological nitrogen fixation *8*

1.2 NITROGENASE ENZYMES 10

1.2.1 V-nitrogenase *11*

1.2.2 Fe-nitrogenase *11*

1.3 MO-NITROGENASE ENZYME 13

1.3.1 Fe protein of Mo-nitrogenase *14*

1.3.2 MoFe protein of Mo-nitrogenase *15*

1.4 THE CURRENT MECHANISMS OF MO-NITROGENASE 19

1.4.1 Electron transfer in nitrogenase *19*

1.4.2 Catalytic mechanism *21*

1.4.3 Reaction pathway *24*

1.4.4 Substrates and inhibitors of nitrogenase *25*

1.4.5 Techniques for studies of nitrogenase *28*

1.5 AIM AND SCOPE OF THIS THESIS 31

1.5.1 Developing an approach for MoFe protein immobilisation *31*

1.5.2 Study of ligands binding to the MoFe protein *31*

BIBLIOGRAPHY 33

CHAPTER 2

THEORY AND METHODOLOGY 39

2.1 ELECTROCHEMISTRY 40

2.2.1 Electrode process and interface *40*

2.1.2 Electron transfer *43*

2.1.3 Equilibrium electrochemistry *46*

2.14 Electrochemical techniques *50*

2.2 INFRARED SPECTROSCOPY 55

2.2.1 Molecular vibration *55*

2.2.2 Infrared red spectroscopy *58*

2.2.3 IR spectra of metal carbonyls and isocyanides *60*

2.2.4 The attenuated total reflectance (ATR) technique *62*

2.3 OTHER EXPERIMENTAL TECHNIQUES 64

2.3.1 Chemicals *64*

2.3.2 Experimental preparation *69*

2.3.3 Spectroelectrochemical cell *70*

BIBLIOGRAPHY 78

CHAPTER 3

APPROACH DEVELOPMENT 80

3.1 NITROGENASE PROTEIN IMMOBILISATION 81

3.1.1 Nitrogenase SEC in Nafion *81*

3.1.2 Protein film infrared electrochemistry *86*

3.1.3 Covalent attachment and carbon modification *89*

3.2 REDOX MEDIATORS 97

3.2.1 Substrates/inhibitors with mediator solution 98

3.2.2 Cobaltocene 102

BIBLIOGRAPHY 104

CHAPTER 4

NITROGENASE MOFE PROTEIN CATALYSED PROTON REDUCTION AND CO INHIBITION 105

4.1 INTRODUCTION 106

4.1.1 Proton reduction by nitrogenase 106

4.1.2 Previous study of CO binding to nitrogenase as an inhibitor 107

4.1.3 CO reduction as a substrate 111

4.2 ELECTROCHEMICAL PROTON REDUCTION AND CO INHIBITION 112

4.2.1 Effect of CO on proton reduction by the MoFe protein 114

4.2.2 Electrochemistry of MoFe protein in the presence of CO 117

4.3 CO BINDING TO MOFE PROTEIN 117

4.3.1 Wild Type MoFe protein 117

4.3.2 Variant α-70$^{Val\rightarrow Ala}$ MoFe protein 124

4.3.3 Variant α-64$^{Tyr\rightarrow His}$ MoFe protein 125

4.3.4 The reversibility of CO binding 129

4.4 USING THE ATTACHMENT APPROACH 131

4.4.1 Wild type MoFe protein 131

4.4.2 Variant β-98$^{Tyr\rightarrow His}$ MoFe protein 134

4.5 DISCUSSION 136

4.5.1 CO inhibition of wildtype and variant MoFe protein 136

4.5.2 v(CO) peaks from CO coordination 137

4.5.3 Different sample handling approaches 138

4.5.4 The potential scale 138

BIBLIOGRAPHY 140

CHAPTER 5

STUDY OF ACETYLENE REDUCTION BY NITROGENASE MOFE PROTEIN 142

5.1 INTRODUCTION 143

5.2 ELECTROCHEMISTRY OF ACETYLENE REDUCTION 145

5.2.1 Variant β-98$^{Tyr\rightarrow His}$ MoFe protein 147

5.3.2 Variant α-70$^{Val\rightarrow Ala}$ MoFe protein 153

5.3.3 Wild Type MoFe protein 154

5.3 INFRARED SPECTROSCOPY OF ALKYNES REDUCTION 155

5.3.1 Using acetylene as a ligand 156

5.3.2 Using propargyl alcohol as a ligand 157

5.4 ETHYLENE DETERMINATION BY GC 159

5.4.1 Acetylene reduction by wild type MoFe protein 160

5.4.2 Partial pressure to the acetylene reduction reaction 164

5.4.3 Other proteins 166

5.5 DISCUSSION 168

BIBLIOGRAPHY 172

CHAPTER 6

STUDY OF ISOCYANIDE BINDING TO THE METAL CENTRES OF NITROGENASE 173

6.1 INTRODUCTION 174

6.1.1 Isocyanide binding to isolated FeMo cofactor 174

6.1.2 Reducing isocyanides by nitrogenase 175

6.2 ELECTROCHEMICAL INVESTIGATION OF ISOCYANIDE INHIBITION OF MOFE PROTEIN 177

6.3 IR SEC STUDY OF ISOCYANIDE BINDING TO MOFE PROTEIN 179

6.3.1 Isocyanide in the solution 180

6.3.2 Variant β-98$^{Tyr\rightarrow His}$ MoFe protein 183

6.3.3 Variant α-70$^{Val\rightarrow Ala}$ MoFe protein 186

6.3.4 Wild Type MoFe protein 191

6.3.5 Ethyl isocyanide *198*

6.3.6 Methylene blue as an extra mediator *202*

6.4 PRODUCTS DETERMINATION BY CHROMATOGRAPHY 206

6.5 DISCUSSION 208

6.5.1 Isocyanide bound peaks *208*

6.5.2 Methylamine determination *210*

6.5.3 The potential scale *211*

BIBLIOGRAPHY 212

CHAPTER 7

CONCLUSION 213

BIBLIOGRAPHY 217

Chapter 1

Introduction

The nitrogenase enzyme is expressed by free-living soil bacteria and symbiotic bacteria living in the roots of certain plants. The mechanism of the enzyme remains poorly understood. My project uses electrochemistry and Infrared spectroscopy to study the mechanism of Mo-nitrogenase. This includes looking at its reactions with a range of different possible substrates (including protons, dinitrogen, acetylene, isocyanides and carbon dioxide) and known inhibitors of the enzyme. Genetic variants of nitrogenase will also be studied to determine the role of specific amino acids in the protein.

1.1 Nitrogen cycle and nitrogen fixation

1.1.1 Nitrogen cycle

The nitrogen cycle is the biogeochemical cycle affecting most of the molecules containing nitrogen, including proteins, nucleic acids, chlorophyll, enzymes and other cellular constituents. Although nitrogen is in its -3 redox state in all these molecules, the majority of nitrogen is dinitrogen gas (N_2) in the atmosphere. However, the nitrogen in earth's atmosphere has limited availability for living organisms, leading to a scarcity of usable nitrogen in many types of ecosystems. The global nitrogen cycle on the earth is shown in Figure 1-1 which consists of several processes of transformation between different forms of nitrogen.

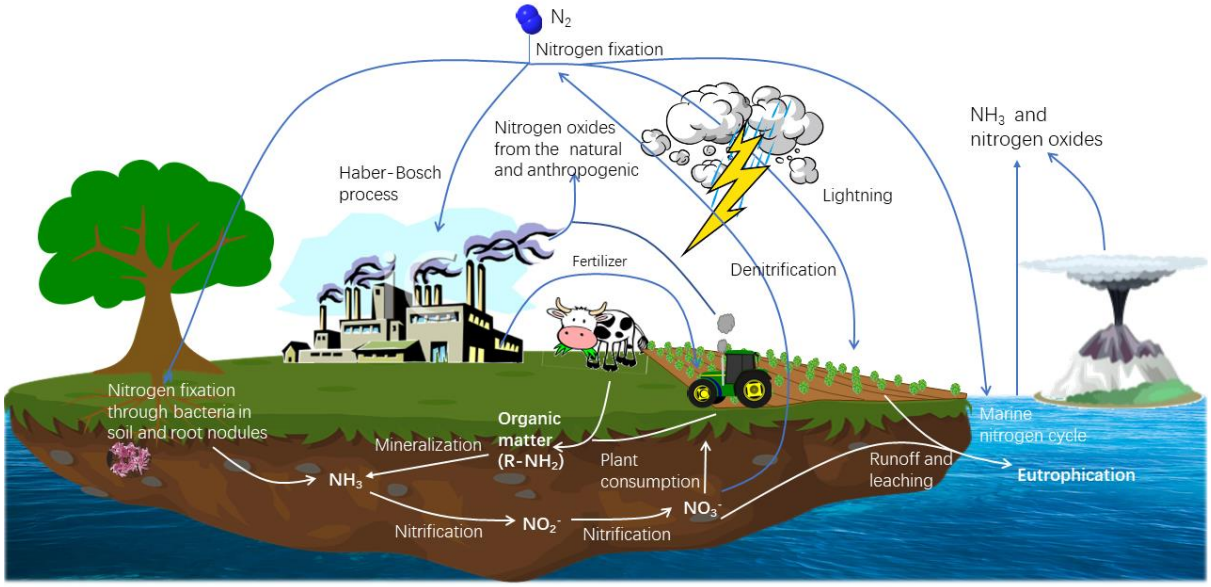


Figure 1-1: The global nitrogen cycle shows most nitrogen transformations on the earth.

The nitrogen cycle contains large-scale transfers of N between the atmosphere and the biosphere. Nitrogen inputs to the biosphere occur both because of natural processes (biological fixation and lightning) and industrial fixation. Nitrogen is finally returned to the atmosphere as dinitrogen gas, but small quantities of atmospheric nitrogen oxides are released in the process of microbial transformation of nitrogen. There are natural and anthropogenic contributions to atmospheric

nitrogen oxide emissions, both of which occur mainly due to microbial transformations of nitrogen from terra and marine environments. In nature, the Nitrogen cycle can be viewed as a series of catalysed redox reactions by enzymes which lead to an accessible supply of reduced nitrogen compounds as shown in Figure 1-2.

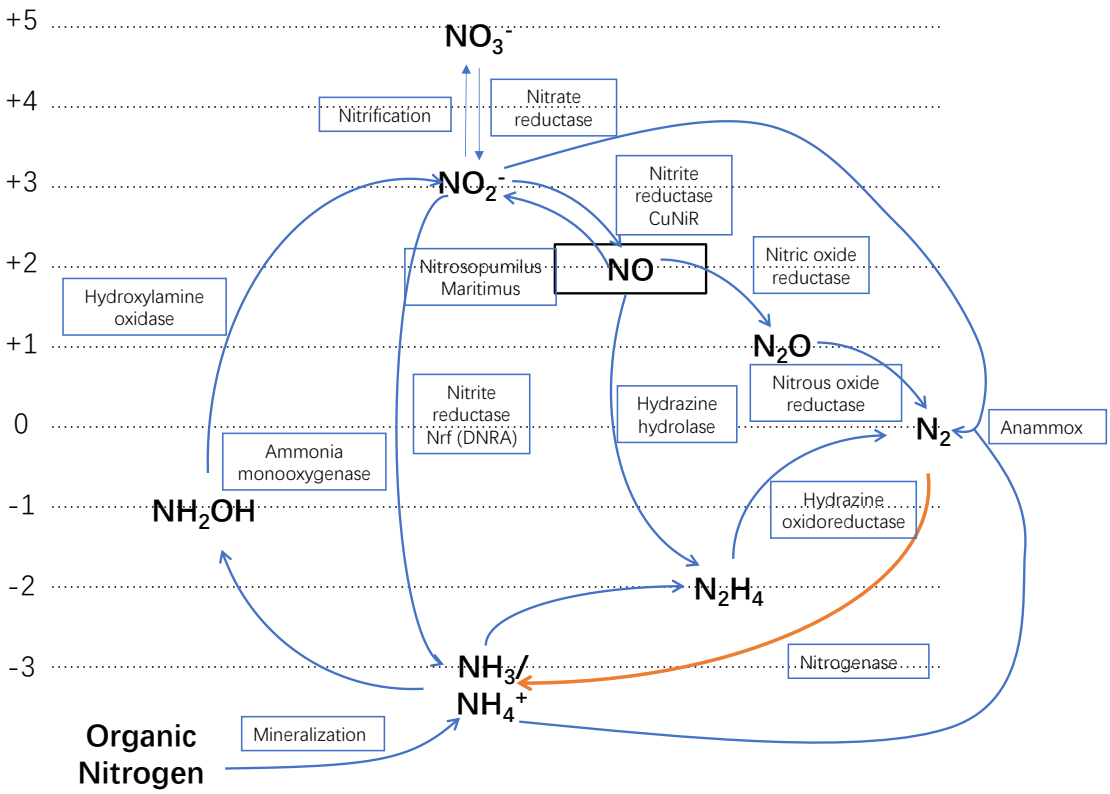


Figure 1-2: A diagram of major biological transformations in the nitrogen cycle by enzymes. The oxidation numbers of nitrogen are indicated on the left.

Nitrification

Nitrification is the process that converts ammonia to nitrite and then to nitrate, which mostly occurs aerobically and is carried out exclusively by prokaryotes. There are two distinct steps of nitrification in different types of microorganisms. The first step is from ammonia to nitrate (Figure 1-2) which is carried out by *Nitrosomonas europaea*.[1] The oxidation of NH_3 to NO_2^- is a two-step process catalysed by ammonia monooxygenase (*amo*)[2] and hydroxylamine oxidoreductase (hao)[3].

Aerobic ammonia oxidizers convert ammonia to nitrite via the intermediate hydroxylamine by these two enzymes.

Ammonia monooxygenase: $NH_4^+ + O_2 + 2e^- + H^+ \rightarrow NH_2OH + H_2O$

Hydroxylamine oxidoreductase: $NH_2OH + H_2O \rightarrow NO_2^- + 4e^- + 5H^+$

The second step in nitrification is the oxidation of nitrite (NO_2^-) to nitrate (NO_3^-) shown in Figure 1-2 by nitrite oxidoreductase (*nxr*).[4]

Nitrite oxidoreductase: $NO_2^- + H_2O \rightarrow NO_3^2 + 2e^- + 2H^+$; $E^{0\prime}(NO_3^-/NO_2^-)$ = +0.43 V

All these oxidisers are ubiquitous in aerobic environments in the natural environment, but they play a very important role in wastewater treatment which needs to remove potentially harmful ammonium to maintain a healthy aquatic environment.

Anammox

Anammox is a process by which bacteria oxidize ammonia by using nitrite as the electron acceptor to produce dinitrogen gas (Figure 1-2), and is carried out by prokaryotes.[5] Anammox bacteria were first discovered in anoxic bioreactors of wastewater treatment plants but have since been found in a variety of aquatic systems.

Anammox: $NH_4^+ + NO_2^- \rightarrow N_2 + 2H_2O$

Denitrification

Denitrification is a series of processes that reduce nitrate to dinitrogen gas via intermediate nitrogen oxides, as shown in in Figure 1-2, thus removing bioavailable nitrogen and returning it to the Earth's atmosphere. Enzymes of these processes are nitrate reductases[6], nitrite reductases[7], nitric oxide reductases[8] and nitrous oxide reductases[9]. It is significant that denitrification can remove fixed nitrogen (i.e., nitrate) from the ecosystem and return it to the atmosphere in a biologically inert form (N_2) which can remove unwanted nitrates from the waste water effluent.

Mineralization

When an organism expels waste or dies, the initial forms of nitrogen in its tissues are organic (like amino acids and DNA). Various fungi and bacteria then convert organic nitrogen to inorganic nitrogen back into the ecosystem as ammonia in the process known as Mineralization (ammonification). The ammonia then becomes available for uptake by plants and other microorganisms for growth.

Nitrogen fixation

The conversion of dinitrogen gas into ammonia and nitrogen oxides through atmospheric, industrial and biological fixation processes is called nitrogen fixation. To be taken up by plants, atmospheric nitrogen must be processed, or "fixed", into a usable form for the synthesis of amino acids and nucleic acids, so it is central to agricultural production.

Table 1-1: Amount of nitrogen fixed on a global scale

TYPE OF NITROGEN FIXATION	**N_2 FIXED (10^9 KG PER YEAR)**
NON-BIOLOGICAL (TOTAL)	~80
INDUSTRIAL	~50
COMBUSTION	~20
LIGHTNING	~10
BIOLOGICAL (TOTAL)	~175
AGRICULTURAL LAND	~90
FOREST AND NON-AGRICULTURAL LAND	~50
SEA	~35
DATA FROM VARIOUS SOURCES, COMPILED BY DF BEZDICEK & AC KENNEDY.[10]	

About 10 billion kg/year (Table 1-1) dinitrogen is fixed by lightning strikes[10] which break dinitrogen molecules and enable their atoms to combine with oxygen in the air forming nitrogen oxides. These dissolve in the rain forming nitrous acid or nitric acid, that are carried to the earth forming nitrates in the soil. However, most natural nitrogen fixation is done by free-living bacteria or bacteria that are symbiotic with plants, known as diazotrophs.

1.1.2 Non-biological nitrogen fixation

Harber-Bosch process

Throughout the 19th century, the demand for ammonia and nitrates as fertilisers and industrial raw material had been steadily increasing. However, the main source was mining nitre deposits until German chemist Fritz Haber successfully fixed N_2 in a laboratory in 1909.[11] In 1913, barely five years later, a research team from BASF, led by Carl Bosch, developed the first industrial-scale application of the Haber process, sometimes called the Haber-Bosch process. This synthesis process of ammonia from dinitrogen and hydrogen gas used an iron-based catalyst at high temperatures and pressures (about 400 °C and 200 bars), which earned two Nobel prizes (Haber in 1918 and Bosch in 1931). Interestingly, Gerhard Ertl won the Nobel Prize in 2007 "for his studies of chemical processes on solid surfaces," which was mainly for determining the mechanism of the Haber Bosch process on the catalyst surface.

In the Haber-Bosch process, dinitrogen and dihydrogen molecules adsorb on the iron-based catalyst surface, then the intramolecular bonds are split, and the two different species recombine to form the product ammonia. The rate-determining step of this reaction is the cleavage of the dinitrogen triple bond. The high temperature is required to overcome this kinetic barrier, while the high pressure is applied in order to shift the thermodynamic equilibrium of the reaction towards the formation of ammonia molecules. The key steps in the reaction mechanism are shown below.[12]

$$N_{2(g)} \rightarrow N_{2(ad)} \rightarrow 2N_{(ad)}$$

$$H_{2(g)} \rightarrow H_{2(ad)} \rightarrow 2H_{(ad)}$$

$$N_{(ad)} + H_{(ad)} \rightarrow NH_{(ad)} \xrightarrow{+H_{(ad)}} NH_{2(ad)} \xrightarrow{+H_{(ad)}} NH_{3(ad)} \rightarrow NH_{3(g)}$$

Alternative catalytic process

The commercial Haber Bosch process uses a heterogeneous catalyst based on iron and promoted with Al_2O_3 and potassium. It is well accepted that the relative catalytic activity of different metallic catalysts can be related to their binding energies with nitrogen adsorption species in terms of a volcano-type dependence relationship. If the adsorption of dinitrogen is too weak or too strong, on the metal, this decreases the activity of the catalytic reaction.[13] N_2 dissociation is rate-limiting when catalytic metals have low binding energies. And when metals have high binding energies, N_2 dissociation happens, but desorption of the atomic nitrogen is much slower, which limits the number of available binding sites and slows the catalytic rate.[14]

Metal complexes like Mo- and W- are used as homogeneous catalysts for N_2 reduction to NH_3.[15,16] An Fe complex was reported in 2013 to reduce nitrogen to ammonia in the presence of a strong reductant (KC_8).[17] Moreover, it appears that reduction reactions in all these cases required 6 electrons (no electrons used for H_2 production) and involved many intermediate species (M-$N_xH_y^{n+}$). H_2 reduction is found as competing reaction with N_2 reduction with these metal complexes as catalysts.[18]

Recently, the electrochemical N_2 reduction reaction coupled with water oxidation (half-reaction) at ambient temperature and pressure has been demonstrated, with unique advantages. Nevertheless, the faradaic efficiency of the nitrogen reduction reaction is low at the potentials required for this reaction, due to the competing hydrogen evolution reaction. For example, using

a Pt electrode and a Nafion electrolyte only gives a production rate of $9.37 \times 10^{-6}\ mol \cdot m^{-2} \cdot s^{-1}$ at 353 K after applying a potential of -1.2 V, and a faradaic efficiency of 0.83%.[19]

Photochemical reduction of dinitrogen gas to ammonia has also been demonstrated in numerous experiments,[20] not only with artificial catalysts like Bi_2MoO_6,[21] but also from Mo- and Fe-containing biomimetic clusters (chalcogels) under mild condition.[22]

Plasma catalysis was able to synthesise ammonia on lab-scale at atmospheric pressure and close to ambient temperature (413 K).[23] The yield of ammonia produced is reasonably high[24], but the energy efficiencies are quite low (25−30 g-NH_3/kWh[25] compared to around 500 g-NH_3/kWh[26] for large-scale Haber−Bosch process) in many experiments.

1.1.3 Biological nitrogen fixation

In the biosphere, only a special group of microorganisms called diazotrophs is responsible for conversion of dinitrogen into biologically accessible ammonia. All the nitrogen-fixing organisms are prokaryotes (bacteria as shown in Table 1-2), some of which live independently of other organisms, the so-called free-living nitrogen-fixing bacteria (e.g. *Azotobacter*). Others live in intimate symbiotic associations with plants or with other organisms (e.g. root exudates from legume plants, like peas, clover and soybeans, serve as a signal to certain species of Rhizobium, which are nitrogen-fixing bacteria). Under nitrogen-deficient conditions, the host plant will form a symbiotic relationship with nitrogen-fixing bacteria by developing the root nodules.

Some of these bacteria are phototrophic, others are chemotrophic (i.e., they use chemicals as their energy source instead of light). Although there are great physiological and phylogenetic differences among the organisms carrying out nitrogen fixation, they all have a similar enzyme complex called nitrogenase that catalyses the reduction of N_2 to NH_3.

The nitrogenase enzyme complex is highly sensitive to dioxygen. It will be inactivated when the enzyme is exposed to dioxygen because this reacts with the iron sulfur clusters of the proteins.

This can be a big problem for aerobic species such as cyanobacteria generating oxygen during photosynthesis and the free-living aerobic bacteria in soils, like *Azotobacter* and *Rhizobium*. *Azotobacter* have the highest known rate of respiratory metabolism of any organism, so they might protect the enzyme by maintaining a very low level of oxygen in their cells to overcome this problem. *Azotobacter* species can also produce large amounts of extracellular polysaccharide. These bacteria can control the diffusion rate of oxygen to the cells by maintaining water within the polysaccharide slime layer. In the symbiotic nitrogen-fixing organisms like Rhizobium, the root nodules can contain oxygen-scavenging molecules such as leghaemoglobin, which may control the supply of oxygen. Some of the cyanobacteria have another mechanism for protecting nitrogenase, where nitrogen fixation occurs in special cells (heterocysts) possessing only photosystem I (used to generate ATP by light-mediated reactions); in contrast the other cells have both photosystem I and photosystem II which produces oxygen when light energy is used to split water to supply H_2 for the synthesis of organic compounds.

Table 1-2: Examples of nitrogen-fixing bacteria

Free-living nitrogen-fixing bacteria		**Symbiotic with plants**	
Aerobic	**Anaerobic**	**Legumes**	**Other plants**
Azotobacter *Beijerinckia* *Klebsiella* (some) Cyanobacteria (some)*	*Clostridium* (some) *Desulfovibrio* Purple sulphur bacteria* Purple non-sulphur bacteria* Green sulphur bacteria*	*Rhizobium*	*Frankia* *Azospirillum*
*** denotes a photosynthetic bacterium**			

Marine nitrogen fixation

In the open ocean, as on land, fixed nitrogen is one of the most important growth-limiting means of sustenance for photosynthetic organisms (primary producers) such as marine bacteria and algae. Nitrogen can also serve as an energy source or as an oxidant for these marine bacteria and archaea. The biological fixation of dinitrogen by marine bacteria is the major source of nitrogen to the ocean.[27,28] This process contributes significantly to sustain primary production and maintain the global nitrogen stock.

The single major nitrogen source to the ocean is considered to be the nitrogen-fixing photoautotrophic bacterium of the genus *Trichodesmium*, a species that occurs globally in tropical and subtropical waters.[29] However, numerous other nitrogen-fixing bacteria have been described which may raise the estimate of the global nitrogen input to the oceans significantly.[30] Moreover, nitrogen fixation seems to be a significant process not only in tropical surface waters and some benthic systems,[31] but also in anoxic waters, at the seafloor,[32] in estuaries and in river plumes where diatom diazotroph associations prevail.[33,34]

1.2 Nitrogenase enzymes

Although there is great physiological and phylogenetic diversity among the organisms that carry out nitrogen fixation on the earth, they all have a similar enzyme complex called nitrogenase that catalyses the reduction of N_2 to NH_3, which is used as a genetic marker for nitrogen fixation.[35]

Three kinds of nitrogenase have been demonstrated to exist in diazotrophs: the Mo-nitrogenase, the V-nitrogenase, and the Fe-nitrogenase.[36] Despite differences in their metal content, these three nitrogenase enzymes are structurally, mechanistically, and phylogenetically similar. The structural components of the Mo-nitrogenase are encoded by *nifH*, *nifD* and *nifK* genes. The V-nitrogenase is encoded by *vnfH, vnfD, vnfG* and *vnfK*, and the Fe-nitrogenase components are products of *anfH, anfD, anfG* and *anfK* genes.

1.2.1 V-nitrogenase

In 1901, Beijerinck discovered and described the first representative of the genus, *Azotobacter chroococcum* which was able to grow on any fixed nitrogen source.[37] Molybdenum from Na_2MoO_4 and vanadium from $NaVO_3$ played key roles in stimulation of nitrogen fixation by trace elements.[38] Mo had been found to be much more significant for N_2-dependent growth than V in *Azotobacter* which indicated that Mo was significant for nitrogen fixation. Biological nitrogen fixation was found to be a MgATP-dependent process and the enzyme could be extracted from other diazotrophs like *Clostridium pasteurianum*, *Azotobacter vinelandii*, and *Rhodosporillum rubrum*. For many years, studies focused on Mo-dependent nitrogen fixation in which the two-component protein system was responsible, in the form of Mo-nitrogenase.[39]

It was not until 1982 that the existence of an "alternative" nitrogen fixation enzyme was demonstrated by V-induced, diazotrophic response of *Azotobacter vinelandii* mutants that carried lesions of structural genes of Mo-nitrogenase.[40] This was later proved by the purification of V-nitrogenase from Tungsten (W)-tolerant mutants of *Azotobacter chroococum*[41] and *Azotobacter vinelandii*[42,43], which fixed nitrogen in the presence of Na_2WO_4.

The Fe proteins of V- and Mo-nitrogenases encoded by *vnfH* and *nifH*, respectively—share about 91% sequence identity.[44] While the α- and β-subunits of the VFe protein (encoded by *vnfD* and *vnfK*) share about 33% and 32% sequence identity, respectively, with the α- and β-subunits of the MoFe protein (encoded by nifD and nifK).[44] The VFe protein purified from *Azotobacter chroococcum* is consistent with $\alpha_2\beta_2\gamma_2$-hexametric composition[45] and purified from *Azotobacter vinelandii* is a mixture of $\alpha\beta_2$- trimer and $\alpha_2\beta_2$-tetramer, with minor amounts of the γ-subunit associated with both structures.[46]

Like Mo-nitrogenase, V-nitrogenase can reduce the physiological substrate (N_2) and alternative substrates like protons (H^+), acetylene (C_2H_2) and cyanide (CN^-).[41] Further studies by stopped-flow

spectrometry show that the association of the two-component proteins, MgATP hydrolysis and electron transfer are very similar between two enzymes.[47] At standard temperature (30 ℃), the specific activity of V-nitrogenase is much lower than that of Mo-nitrogenase both in *in vivo* and *in vitro* assays. However, when the temperature is lowered (below 5 ℃), V-nitrogenase becomes more active that its Mo-counterpart.[48] V-nitrogenase shows an increased preference for protons as a competitive substrate to N_2 or C_2H_2, which leads to increased H_2 evolution.[49] This feature makes V-nitrogenase form about 5% additional C_2H_6 in acetylene reduction reactions, compared to Mo-nitrogenase.[50]

1.2.2 Fe-nitrogenase

The second "alternative" nitrogenase was purified from *Azotobacter vinelandii* in 1988, and was expressed only in the absence of both Mo and V. It was found to be a two-component enzyme, known as Fe-nitrogenase.[43] The Fe-only nitrogenase is the least understood of the three homologous nitrogenases. This enzyme has been isolated from *Rhodospirillum rubrum* and *Rhodobacter capsulatus* as well.[51] The Fe protein component of the Fe-nitrogenase is structurally similar to Fe protein from the Mo-nitrogenase from spectroscopic studies.[52] The FeFe protein also has an additional γ-subunit which is encoded by *anfG*, $\alpha_2\beta_2\gamma_2$ and forms a heterohexamer. Recently *in vitro* and *in vivo* studies found that the Fe-nitrogenase from *Rhodopseudomonas palustris* has the highest CO_2 to CH_4 reduction.[53,54] The nitrogen reduction reactions of all three nitrogenases are presented below.

Mo-nitrogenase: $N_2 + 8H^+ + 8e^- + 16MgATP \rightarrow 2NH_3 + H_2 + 16MgADP + 16P_i$

V-nitrogenase: $N_2 + 12H^+ + 12e^- + 24MgATP \rightarrow 2NH_3 + 3H_2 + 24MgADP + 24P_i$

Fe-nitrogenase: $N_2 + 24H^+ + 24e^- + 24MgATP \rightarrow 2NH_3 + 9H_2 + 24MgADP + 24P_i$

1.3 Mo-nitrogenase enzyme

The most widespread and intensively characterised system is the Mo-nitrogenase, which is a complex two-component metalloenzyme. The Mo-nitrogenase has been isolated from *Azotobacter vinelandii, Klebsiella pneumoniae*, and *C. pasteurianum*.[55] The smaller dimeric component of Mo-nitrogenase, known as the Fe protein (dinitrogenase reductase NifH protein), functions as an ATP-dependent electron donor to the larger heterotetrameric component, known as the MoFe protein (dinitrogenase, comprising 2NifD and 2NifK subunits), which contains the enzyme active site (Figure 1-3). Both nitrogenase component proteins are extremely oxygen-sensitive.

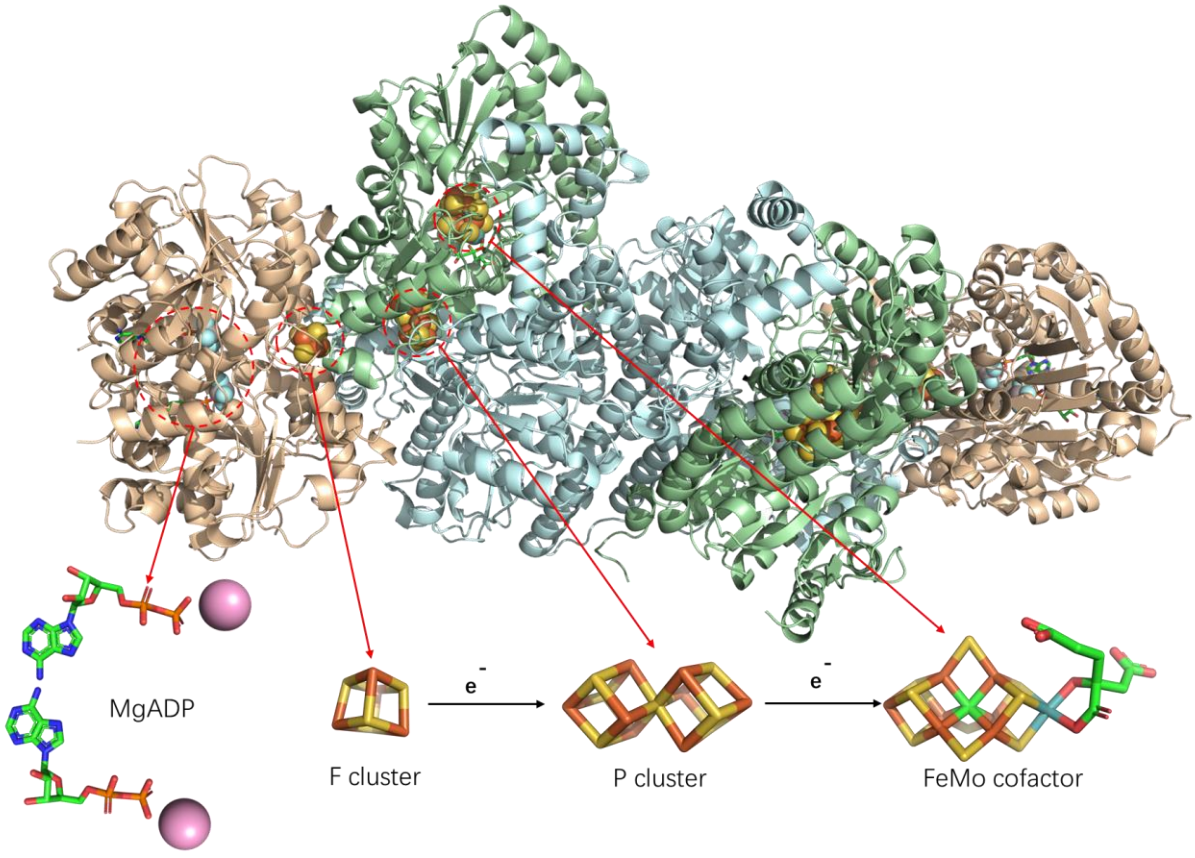


Figure 1-3: Structure of a complex between the Fe protein (wheat) and MoFe protein (α-subunit is shown as pale green and β-subunit is shown as pale cyan) of Mo-nitrogenase from *Azotobacter vinelandii* (1N2C from RCSB PDB) showing locations of its prosthetic groups and electron transfer

between metal clusters using Pymol. All cofactors are shown in stick format with Fe, S, N, P, Mg, O, C and Mo atoms represented as brown, yellow, blue, orange, pink, red, green and cyan, respectively.

1.3.1 Fe protein of Mo-nitrogenase

The Fe protein of Mo-nitrogenase is an α_2-homodimer (Mr ≈ 64 kDa) containing one ATP binding site in each subunit and a [4Fe-4S] cluster bridge in between. The [4Fe-4S] cluster is coordinated by four thiol groups from cysteine amino acid residues as shown in Figure 1-4.[56] The Fe protein is classed as a member of a family of nucleotide-utilizing proteins[57,58] and works as an ATP-dependent reductase in the nitrogenase catalytic system due to the fact that it serves as an electron transmitter to the MoFe protein during enzyme turnover. It is encoded by *nifH* and also called nitrogenase reductase or component II. The Fe protein requires hydrolysis of a pair of ATP molecules to complete each electron transfer from the [4Fe-4S] cluster and dissociate. This Fe protein component is the only known reductant which can activate the MoFe protein to reduce dinitrogen to ammonia efficiently.

Apart from shuttling electrons during catalysis, the Fe protein also participates in the biosynthesis of the MoFe protein as well. The Fe protein plays a key role by inserting the Mo atom and an R-homocitrate molecule into a precursor cluster to complete the maturation of the FeMoco active site.[59] Recently, Hu et al. found that Fe protein of Mo- and V-nitrogenase is able to reduce CO_2 to CO both *in vitro* and *in vivo* under ambient conditions.[60]

The [4Fe-4S] cluster has two oxidation states which may both be involved in the electron transfer to the MoFe protein: $[4Fe\text{-}4S]^{+}$ and $[4Fe\text{-}4S]^{2+}$.[61] The redox potentials are not well defined in the literature, butit was found that the all-ferrous state $[4Fe\text{-}4S]^{0}$ could be achieved using low potential reductants like Eu^{II}-DTPA.[62]

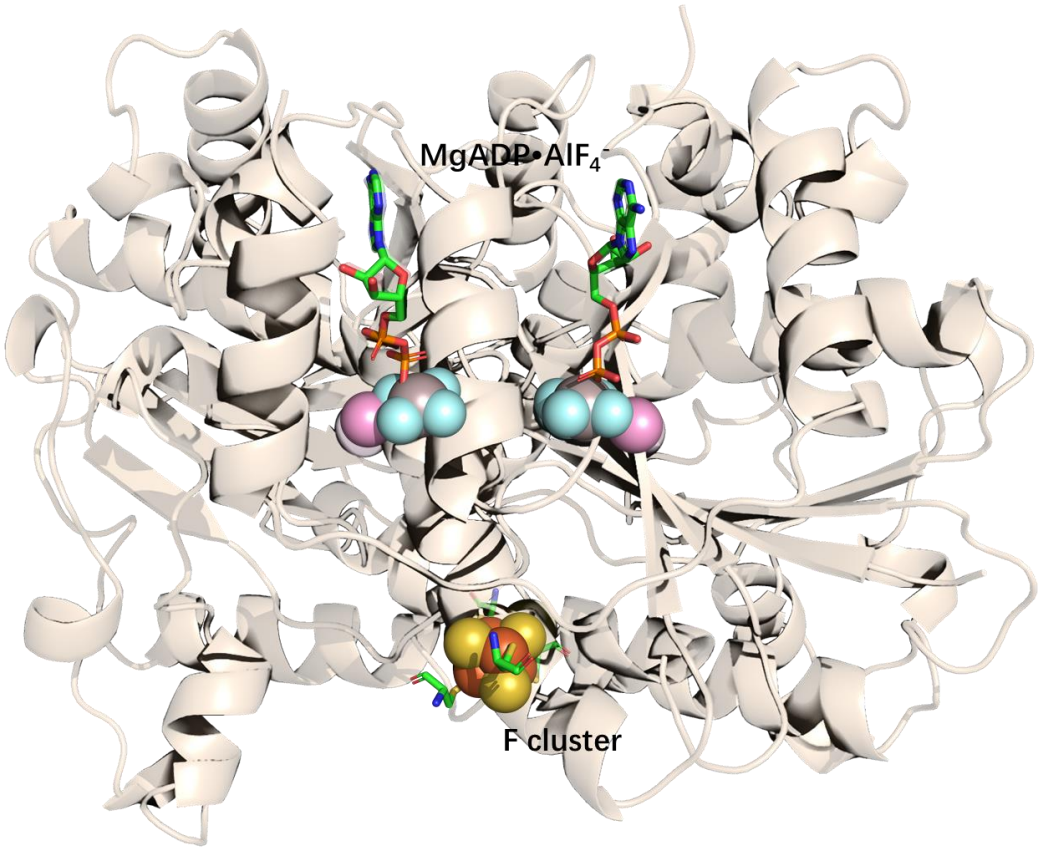


Figure 1-4: A presentation of the structure of the MgADP·AlF_4^--stabilized Fe protein (wheat) of nitrogenase. MgADP·AlF_4^- and F cluster, which is a [4Fe-4S] cluster ligated by four cysteine amino acids shown as space-filling models. PYMOL was used to create this figure (1N2C from RCSB PDB) with Fe, S, N, P, O, C Mg, Al and F atoms represented as brown, yellow, blue, orange, red, green pink, grey and pale cyan, respectively.

1.3.2 MoFe protein of Mo-nitrogenase

The MoFe protein ($M_r \approx 250$ kDa) is the catalytic partner of the Fe protein in nitrogenase catalysis. The crystal structure of the MoFe protein is an $\alpha_2\beta_2$ heterotetramer where the α-subunit is encoded by *nifD* and the β-subunit is encoded by *nifK* (shown in Figure 1-5).[63] The MoFe protein consists of a [7Fe–8S] P-cluster involved in mediating electrons to the [7Fe–9S–Mo–C–homocitrate] FeMo-cofactor (M cluster), the active site of nitrogenase for substrate reduction.[64,65]

P cluster

The P cluster of nitrogenase is a [8Fe-7S] cluster which is bridged between the α- and β-subunits at a position that is 10 Å below the surface of the protein.[66,65] It can be viewed as two [4Fe-3S] partial clusters bridged by sulphide and is coordinated with six cysteine residues (shown in Figure 1-5), three from the α-subunit (α-62^{Cys}, α-88^{Cys} and α-154^{Cys}) and three from the β-subunit (β-70^{Cys}, β-95^{Cys} and β-153^{Cys}). Each of α-88^{Cys} and β-95^{Cys} coordinate two Fe atoms, and the other cysteines each coordinate one Fe atom.[67] The P cluster serves as a mediating centre in the electron transfer pathway, from the [4Fe-4S] of the Fe protein to the FeMoco of the MoFe protein. Additionally, the biosynthesis of the P cluster also requires the presence of both the Fe protein and ATP.

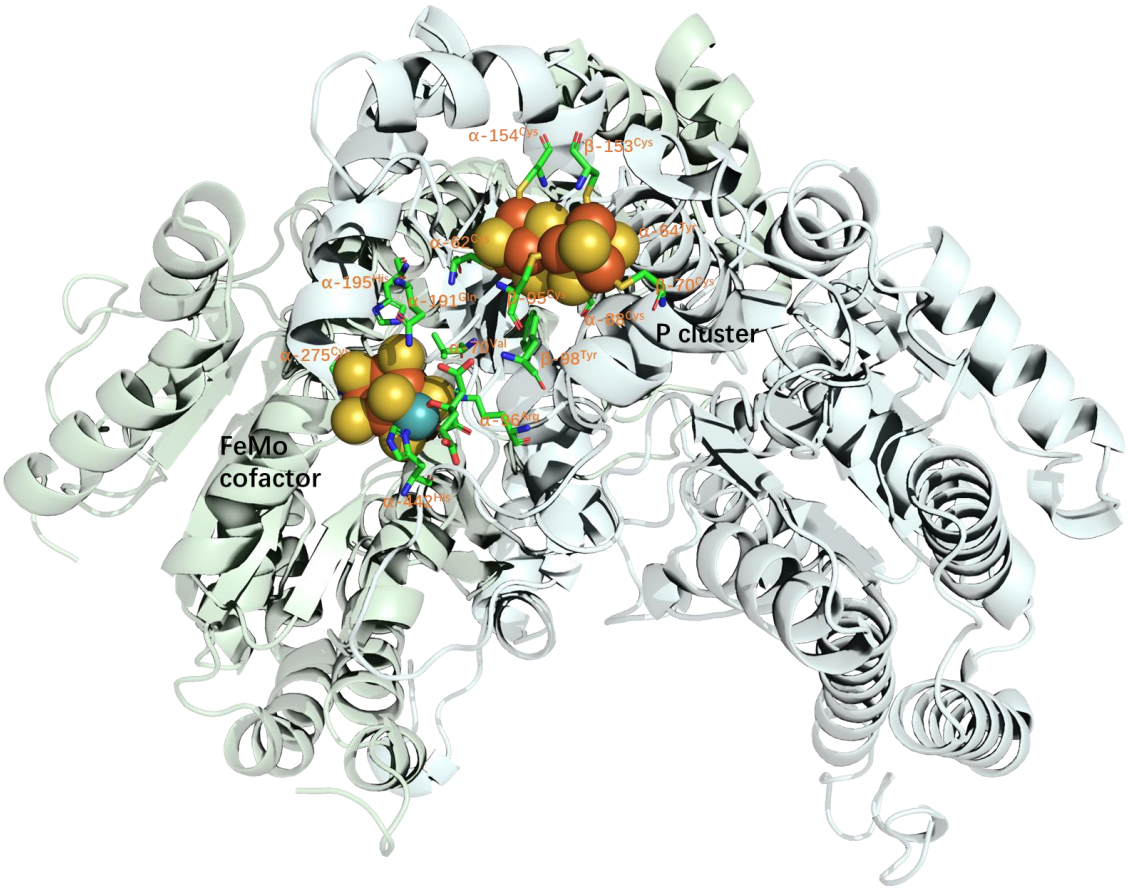


Figure 1-5: The structure of one catalytic half of the MoFe protein is an $\alpha_2\beta_2$ heterotetramer where the α-subunit (pale green) houses the FeMo cofactor and P cluster, which is at the interface of the α-subunit and β-subunit (pale cyan). Residues α-442^{His}, α-195^{His}, α-191^{Gln}, α-96^{Arg} and α-70^{Val} coordinate the

FeMo-cofactor, which is a [7Fe–9S–Mo] cluster with a central carbide and R-homocitrate ligand on Mo. Residues α-154^{Cys}, α-88^{Cys}, α-64^{Tyr}, α-62^{Cys}, β-153^{Cys}, β-98^{Tye}, β-95^{Cys} and β-70^{Cys} coordinate the P cluster which is a [8Fe-7S] cluster. PYMOL was used to create this figure (1N2C from RCSB PDB) with Fe, S, N, P, O, C and Mo atoms represented as brown, yellow, blue, orange, red, green and cyan, respectively.

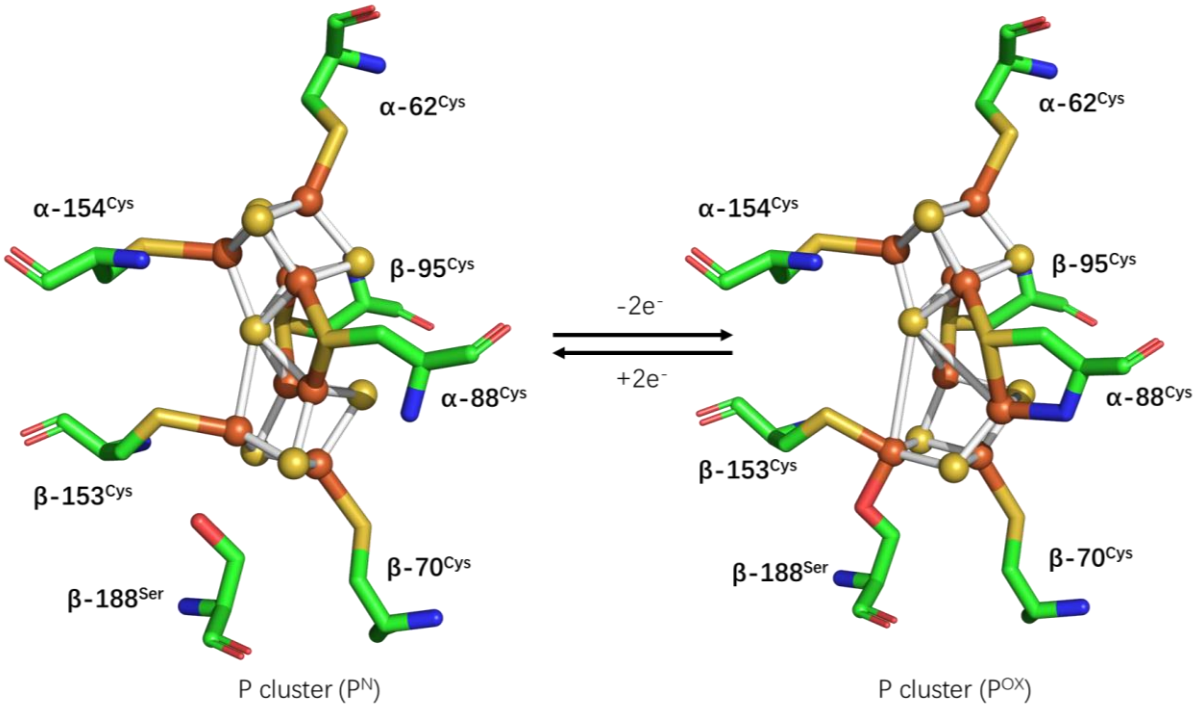


Figure 1-6: The structures of P^{N} and P^{OX} states of P cluster. The clusters are shown as ball-and-stick models and residues are shown as sticks. PYMOL was used to create this figure (3MIN and 2MIN from RCSB PDB, respectively) with the atom colours as those in Figure 1-5.

The P cluster exists in the all ferrous oxidation state in the resting state (P^{N}) and can be oxidised to various oxidation states although only the first two or three states are likely to be involved in the biological electron transfer process: P^{+}, P^{2+} and P^{3+}.[68] It was found that the oxidation of P^{N}-cluster to P^{2+} (P^{OX})-cluster resulted in conformational changes of the core structure (Figure 1-6), in which two additional bonds form to the P^{OX}-cluster.[69] One of these is from residue β-188^{Ser}, which coordinates an Fe atom through an oxygen atom, and the other is from residue α-88^{Cys} which coordinates an Fe atom through a backbone amide as shown in Figure 1-6.

FeMo cofactor

The active site of Mo-nitrogenase, FeMo cofactor or M cluster, is a [Mo-7Fe-9S-C-homocitrate] complex, which can be viewed as [4Fe-3S] and [Mo-3Fe-3S] clusters bridged by three μ_2-sulfides (S^{2-}) and one μ_6-carbide (C^{4-}) in the centre (Figure 1-5).[64,65] The FeMo cofactor is buried within the α-subunit, 14 Å away from the P cluster. In addition, the FeMo cofactor also contains an organic homocitrate moiety attached through its 2-hydroxy and 2-carboxyl groups to the Mo atom.[63] This unusual cluster resides in each α-subunit and is bound to the surrounding protein via only two amino acid residues, one is α-275^{Cys} via a thiol group to the terminal Fe atom and the other is α-442^{His} via an imidazole group to the opposite Mo atom.[70]

Previous studies showed that substitution of the homocitrate with other homocitrate analogues, likes citrate and isocitrate, resulted in malfunctioning nitrogenase.[71] The presence of the homocitrate ligand not only contributes an overall negative charge to FeMo cofactor, but is also able to assist in the assembly of FeMoco in the MoFe protein during the final step of biosynthesis.[59,72] The FeMoco cluster including R-homocitrate can be extracted as an intact entity into the organic solvent N-methylformamide (NMF).[73,74] The extracted FeMo cofactor was shown to be anionic[75] despite a proposed charge of +1 or +3 from the core metal-sulfur cluster in the resting state.[76,77] The overall negative charge of the FeMo cofactor is contributed by its homocitrate which is -4 if the hydroxyl group is deprotonated. The extracted (isolated) FeMo cofactor can bind carbon monoxide (CO), and cyanide (CN^-) at certain reduction states.[78,79]

Although it has been established that FeMoco is the active site of the enzyme, at which the substrates are bound and reduced, there is controversy about the position of substrate binding site on the cofactor.

1.4 The current mechanisms of Mo-nitrogenase

Therefore, the exact mechanism of nitrogen reduction by nitrogenase is still unknown, and the major challenges are around the complex electron transfer pathway and uncontrollable side reactions of proton reduction.

1.4.1 Electron transfer in nitrogenase

In the earlier studies of electron transfer in nitrogenase, the hydrolysis of 2 ATP to 2 ADP and $2P_i$ was assumed to be coupled to the transfer of one electron from the Fe protein to the MoFe protein.[80] In the last few years, studies have suggested a different model by showing that ATP hydrolysis happens after the electron transfer to the MoFe protein.[81] The key steps of this new model are shown in Figure 1-7 which indicates that ATP binding to the Fe protein is important to activate Fe protein for binding to the MoFe protein. The energy of ATP hydrolysis is used to weaken the binding of the Fe protein and the MoFe protein and for dissociation at the end of the cycle after P_i release which is the rate-limiting step.[82]

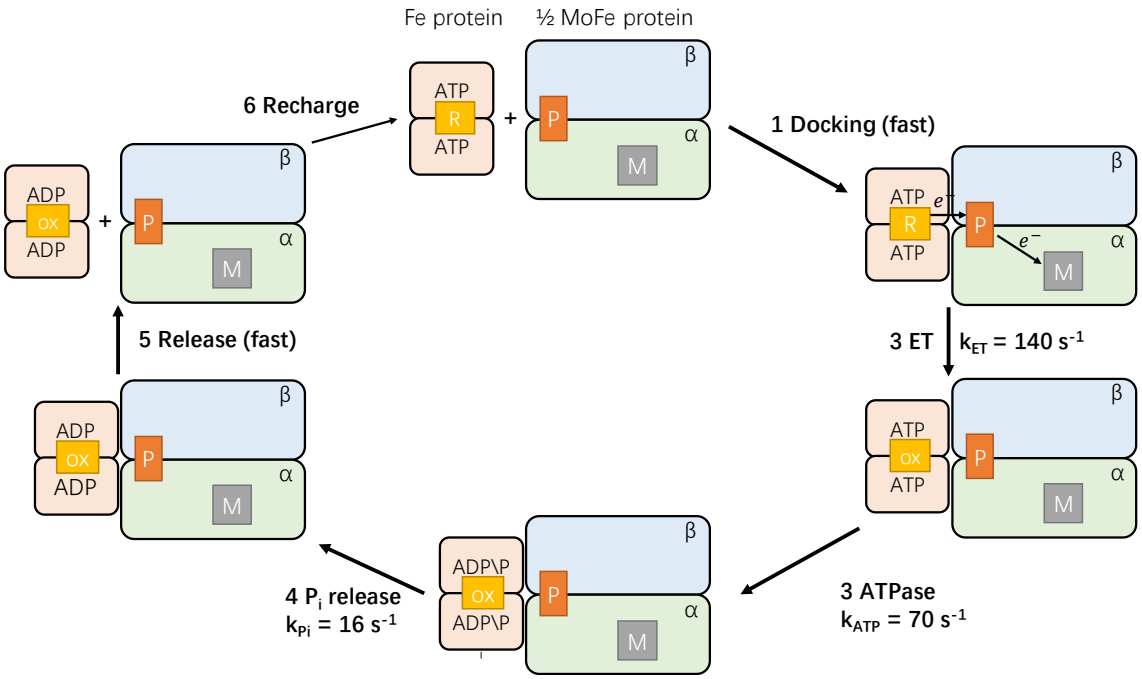


Figure 1-7: Scheme for the key procedures during electron transfer between the nitrogenase Fe protein and the MoFe protein. The MoFe protein is shown as one αβ pair (α-subunit, pale green; β-subunit, pale cyan) containing a P cluster (P) and FeMo cofactor (M). The Fe protein dimer (wheat), with one [4Fe-4S] cluster (R or ox) and two bound ATP, associates with the MoFe protein (top). This association initiates a gated electron transfer event from the P cluster to FeMo-co with a rate constant (k_{ET}) of 140 s^{-1} at 25 °C, with rapid follow up electron transfer from the Fe protein to the oxidised P cluster. The next step is ATP hydrolysis with a rate constant k_{ATP} of 70 s^{-1}, followed by P_i release with a rate constant k_{Pi} of 16 s^{-1}, and then the fast dissociation of the two proteins.

It was earlier proposed that ATP binding to the Fe protein of nitrogenase energised the F cluster for electron transfer by docking of the Fe protein with the MoFe protein, and that the two-protein complex is more stable.[83] The F cluster is close to the surface of the Fe protein after ATP binding which strengthens the electronic coupling to the P cluster of the MoFe protein.[84,85] After the docking of the Fe protein and MoFe protein, a conformational change within the MoFe protein might occur which opens the gate for electron transfer from P cluster to FeMo cofactor. Moreover, this docking may further increase the electron tunnelling from the Fe protein to the MoFe protein due to the distance shortening.

It was found that the P cluster in the resting state (P^N) has all ferrous oxidation state.[77] Since there is no known example of enzyme Fe-S cluster below the ferrous oxidation state, the model that the Fe protein would first transfer an electron to the P cluster has a problem. Instead, a 'deficit-spending' electron transfer model explains that the gated P cluster to FeMo cofactor electron transfer occurs first, following by fast reduction of the oxidised P cluster by the Fe protein (Figure 1-8). And this model was supported by studies on variants of MoFe proteins.[86]

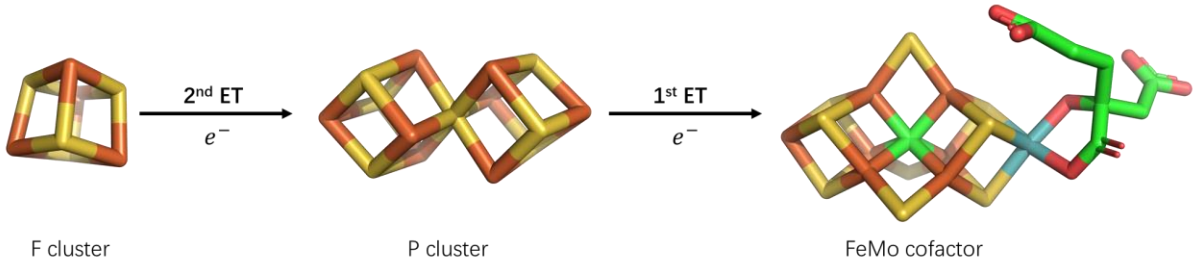


Figure 1-8: A schematic representation of electron transfer (ET) process from the F cluster of the Fe protein to the metal clusters of MoFe protein. The first ET event is proposed to be from the P cluster to the M cluster, while the second electron transfer event is from the Fe protein to the oxidised P cluster.

1.4.2 Catalytic mechanism

In dinitrogen reduction by Mo-nitrogenase, 8 electrons are required to reduce N_2 to NH_3. A "kinetic" foundation of a nitrogenase mechanism was developed by many groups, especially Lowe and Thorneley and co-workers,[57] which describes the kinetics of N_2 transformations among intermediates (shown as E_n), where n is the number of steps of electron/proton transfer to MoFe protein shown in Figure 1-8 A. A mechanism based on the Lowe and Thorneley (LT) kinetic model was proposed by Hoffman et al. more recently.[87] One electron transfer from Fe protein to MoFe protein is coupled to binding and hydrolysis of two MgATP. Electrons are accumulated on the FeMo cofactor with the P cluster acting as a "deficit-spending" electron shuttle between the two-component proteins.

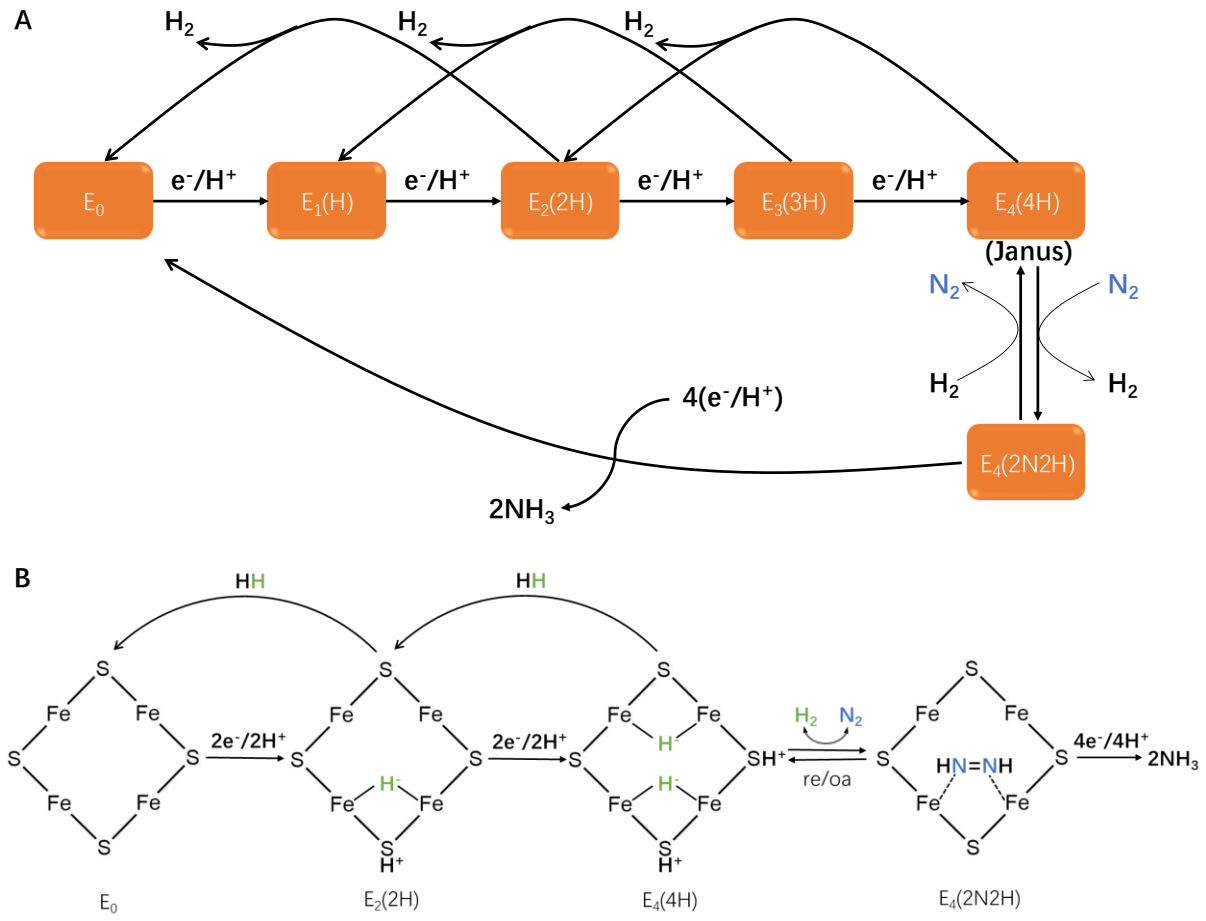


Figure 1-9: A simple model for nitrogenase-mediated nitrogen fixation. (A) Simplified representation of the Lowe–Thorneley (LT) kinetic scheme for nitrogen reduction. (B) Simplified scheme of the N_2 activation mechanism, with cartoons of the Fe 2, 3, 6, 7 face (as shown in Figure 1-10) of FeMo-cofactor in the E_0, E_2, and E_4 states (designation from the LT kinetic model) showing hydrides and protons, and showing both the re/oa equilibrium with loss of H_2 and binding/reduction of N_2 (going right) and the two steps of H_2 generation by hydride protonation that occur in the absence of N_2 (going left). The exact location of the bound hydrides and protons is proposed but not established.[52]

Figure 1-9 B shows how electrons and protons might accumulate on the FeMo cofactor of the MoFe protein and how the enzyme is activated for N_2 binding and reduction.[87] N_2 cannot be bound and reduced by nitrogenase until four electrons and protons are accumulated on the FeMo cofactor to create the $E_4(4H)$ intermediate. This $E_4(4H)$ intermediate has two Fe-H-Fe bridging hydrides which are built up in the four steps. N_2 binding and reduction to the first bound

intermediate (E_4(2N2H)) [88,89] which is a diazene-metal complex with a combination of two hydrides to release H_2 in a reductive elimination (*re*). An oxidative addition (*oa*) of H_2, is coupled with this reversible *re* step which leads to N_2 release from the E_4(2N2H) state.[90,91] This reversibility of *re/oa* step is consistent with the early findings that two HD are formed for every D_2 consumed in the turnover studies when D_2 and N_2 are present. The oa of D_2 by the E_4(2N2H) with the release of N_2 results in this observation. And each of the deuterides reacts with H^+ from the solvent, forming two HD.[92,93]

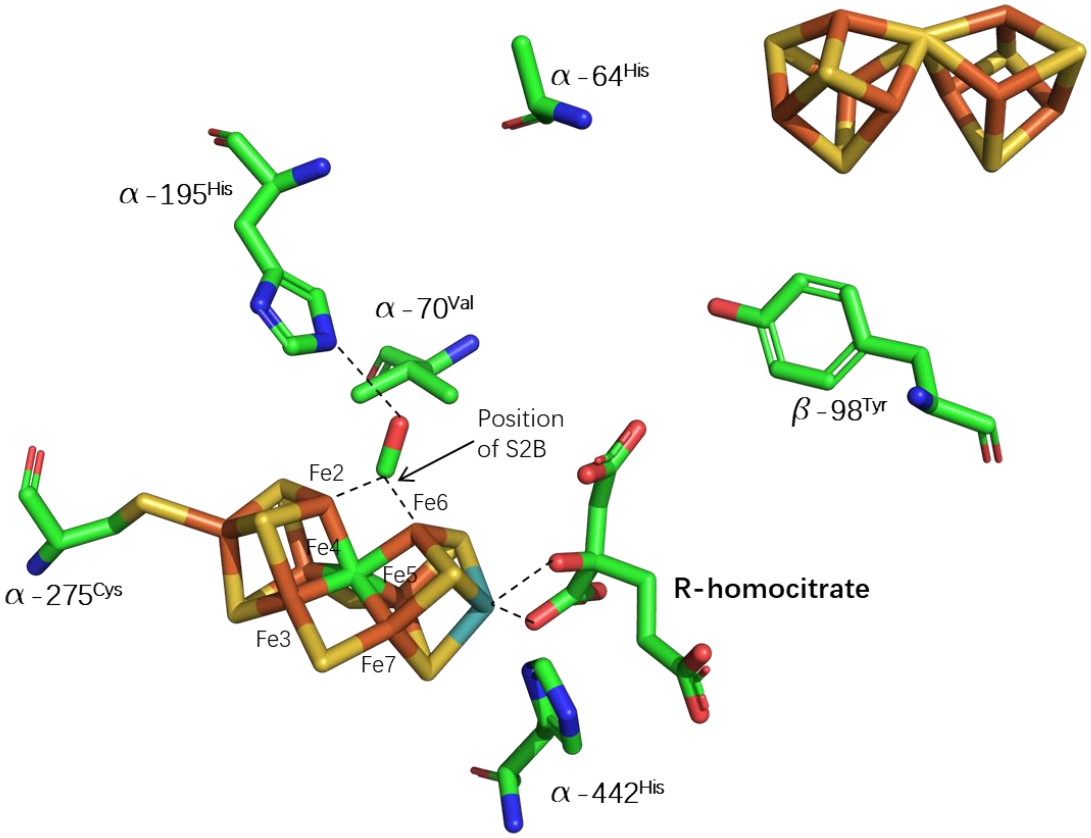


Figure 1-10: Detailed diagram of the FeMo cofactor and surrounding environment, numbering Fe atoms and S atoms mentioned (generated from 4TKV PDB file).

Some computational studies have also proposed a possible mechanism for dinitrogen reduction. Varley et al. used density functional theory (DFT) calculations to explain how the dissociation of the μ_2-S2B site (as shown in Figure 1-10) as H_2S from the FeMo cofactor unveils a highly active Fe

site.[94] This calculation was based on the recent crystal structure supporting the reversible displacement of a belt-sulfur atom by CO.[95] In this model, the dissociation of a belt-sulfur atom is an initiation step of the dinitrogen reduction process. The reversibility of this process and subsequent resealing of the active Fe site by H_2S reabsorption is required to free the second NH_3 and release H_2 which is consistent with the LT kinetic model.[95]

1.4.3 Reaction pathway

It is the key to the elucidation of the dinitrogen reduction pathway for the second half of the LT kinetic scheme, the reaction pathway for N_2 reduction that begins with the E_4 state.[57,96] These invoke distinctly different intermediates which are trapped during turnover by the MoFe protein. It has proven difficult to achieve this in practice as the catalytic reaction could not be synchronised. So far, two different reaction mechanisms have been proposed: distal and alternating. In the distal mechanism, the distal N atom of N_2 is hydrogenated in three steps until the first NH_3 product is released, and then the remaining N atom from nitrido is hydrogenated three more times to liberate the second NH_3 (Figure 1-11). This pathway is associated with the Chatt[97] or Chatt-Schrock cycle[98] with the mechanism of dinitrogen cleavage being a mononuclear.[87]

The other proposed mechanism is known as the alternating pathway, in which N_2 is bound and protonated at either one or more binding sites (suggested to apply to catalysis at Fe of FeMo cofactor).[99,100] In the alternating scheme, the first two hydrogenations generate a diazene intermediate, and then form hydrazine by next two hydrogenations, two NH_3 are released near the end of the cycle (Figure 1-11). This scheme is mainly supported by the observation that nitrogenase is able to reduce hydrazine, one of the potential intermediates proposed in the pathway.[87]

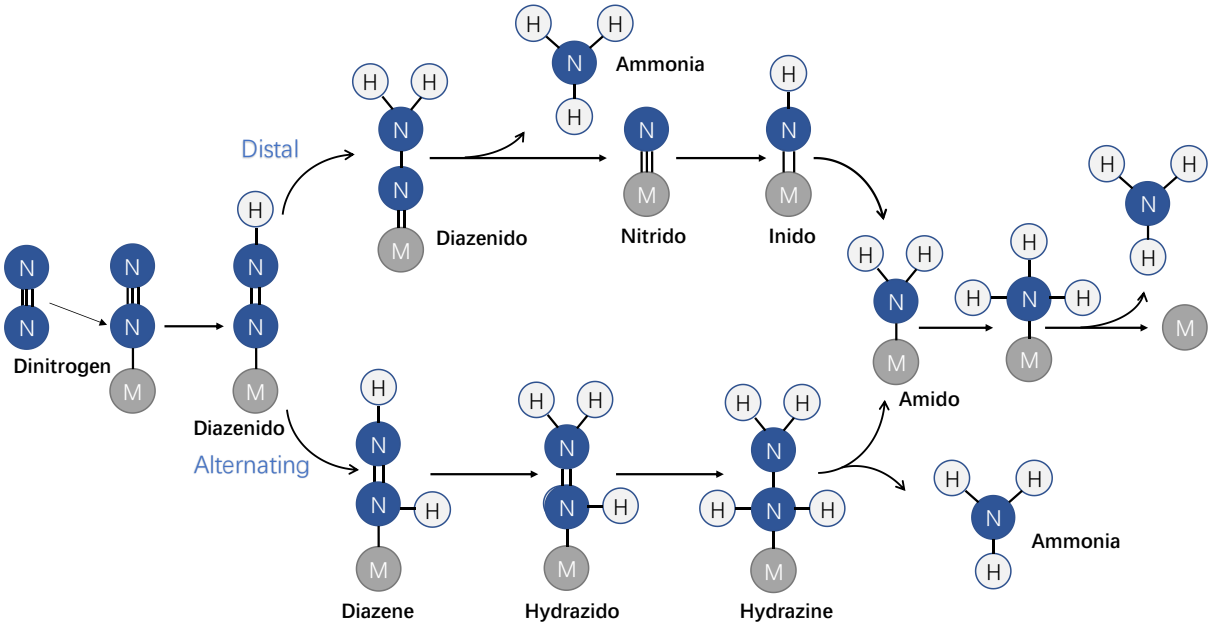


Figure 1-11: Comparison of distal and alternating pathways for proposed nitrogen reaction by nitrogenase (M represents the binding site on the FeMoco cluster).

1.4.4 Substrates and inhibitors of nitrogenase

Apart from physiological substrates, dinitrogen and protons, Mo-nitrogenase is also capable of catalysing the reduction of other small multiply-bonded substrates such as ethene, acetylene (ethyne) and propyne. It is still unclear whether these reactions may be involved in the physiological function of the enzyme or be a part of an ancient metabolic pathway. On the other hand, some small molecules act as inhibitors of nitrogenase like CO, CN^-, NO.

Dinitrogen

Dinitrogen is the main physiological substrate of nitrogenase for the production of ammonia. Although dinitrogen is abundant in the atmosphere, it is unreactive with most reducing agents under mild conditions. There are many factors that contribute to the inertness of the dinitrogen molecule. The triple bond between the two N atoms is one of the strongest bonds among molecules (bond dissociation enthalpy 946 kJ mol^{-1}), which requires a large amount of energy to cleave it. The dinitrogen molecule has ten valence electrons with the electron configuration

$1\sigma_g^2 1\sigma_u^2 1\pi_u^4 2\sigma_g^2$. A large energy gap between the highest occupied molecular orbital (HOMO) and the lowest unoccupied molecular orbital (LUMO) makes it difficult to accept electrons from a mild reducing reagent. Also, the low polarizability of the dinitrogen molecule makes it unreactive for the formation of coordination complexes.

Nitrogenase is able to reduce dinitrogen and some nitrogen-containing substrates like hydrazine (N_2H_4) and azide (N_3^-) to ammonia under ambient conditions. Hydrazine and azide could also be reduced to ammonia by the MoFe protein with electrons supplied by strong reducing reagents like Eu-DTPA,[101] without the Fe protein and ATP. However, conditions are yet to be defined for ATP-independent N_2 reduction by the MoFe protein.[102] Brown et al. used cadmium sulfide (CdS) nanocrystals to photosensitise the MoFe protein to reduce N_2 to NH_3 and the turnover rate could reach 63% of the ATP-dependent reaction rate for the nitrogenase under optimal conditions.[103]

Carbon monoxide

Carbon monoxide (CO) is a diatomic gas which is isoelectronic with dinitrogen. It has a triple bond with a bond length similar to that dinitrogen but a larger bond dissociation energy (1072 $kJ.mol^{-1}$). It has the electron configuration $1\sigma^2 2\sigma^2 1\pi^4 3\sigma^2$. The HOMO (3σ) has non-bonding character and is localised on the carbon atom, while the LUMO (2π) is antibonding.

CO is a strong-field ligand with poor σ-donor but good π-acceptor characteristics. It can form a coordination complex with low oxidation state metal centres via π back bonding. The HOMO of CO donates its 'lone pair' of electrons to the metal d-orbitals to form a σ bond, while the π* LUMO of CO accepts electrons from the d orbitals of the metal to form a π bond. This π-back donation strengthens the bond between the metal and CO (M–CO) but weakens the triple bond of CO since the antibonding π* orbital is occupied.

Previous studies show that CO acts as a non-competitive inhibitor for nitrogenase. However, Ribbe and co-worker found that V-nitrogenase can reduce CO to CH_4, C_2H_4, C_2H_6 and other short-chain

hydrocarbons.[104] A study by Seefeldt and co-workers showed that modified MoFe protein, α-70$^{Val\rightarrow Ala/Gly}$, is also able to catalyse the reduction of CO to hydrocarbons.[105] Ribbe and co-workers demonstrated slow CO reduction of wild-type Mo-nitrogenase from *Azotobacter vinelandii*, resulting in the formation of small hydrocarbon chains.[106] Both Mo- and V-nitrogenase exhibited a similar hydrocarbon product distribution, but CH_4, the one-carbon product was not found in the experiment of Mo-nitrogenase.

Chapter 4 shows some infrared spectroscopic results under electrochemical control involving the MoFe protein and CO. Some CO binding peaks clearly appeared at negative potentials in the infrared spectra.

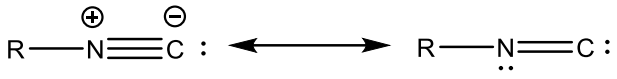
Acetylene

Acetylene (ethyne, $HC \equiv CH$) is a hydrocarbon and the simplest alkyne which has a C-C triple bond. In each carbon atom, the 2s orbital hybridizes with one 2p orbital thus forming a linear sp hybrid. The other two 2p orbitals ($2p_y$ and $2p_z$) of each carbon remain unhybridized and combine to give two mutually perpendicular π orbitals. The two sp hybridized orbitals overlap to form a strong σ valence bond between the carbons and overlap with a hydrogen 1s atomic orbitals.[107]

Acetylene is one of the earliest studied non-native substrates of nitrogenase, and is used in specific activity assays for nitrogenase. In Mo-nitrogenase, the main reduction product of acetylene is ethylene with a very small amount of ethane,[108,109] while V-and Fe-nitrogenase have both ethylene and ethane as reduction products from acetylene.[50,110] Acetylene was found to be reduced to ethylene in an ATP-independent process by the MoFe protein at negative potentials (see Chapter 5 for more detail).

Isocyanide

Isocyanide (RNC) is an isomer of cyanide which is isoelectric with CO and N_2. Isocyanides are described by two resonance structures, one with a triple bond between the nitrogen and the carbon and one with a double bond between as shown below.



As a ligand, RNC has poorer π-acceptor character than CO but stronger σ-donor which is able to coordinate with higher oxidation number metal centres. It was reported that methyl isocyanide can be reduced to methylamine, methane and other hydrocarbons by nitrogenase (see Chapter 6 for more detail).[111,112]

1.4.5 Techniques for studies of nitrogenase

Nitrogenase has been of great interest since biological nitrogen fixation was discovered in 1880, with the enzyme first extracted in 1960. Many advanced physical techniques have been employed to study nitrogenase. A large amount of data on structure and mechanism have been gathered to try to solve the puzzle of this enzyme, however, some pieces of information are still missing from the whole picture.

X-ray Crystallography

Protein X-ray crystallography is an essential technique used to determine the structure of proteins. Crystal structural information is the basis for further studies on catalytic mechanisms. In this technique, a three-dimensional view of the electron density is obtained by Fourier analysis of diffraction data. And then, the molecular architecture models are built by fitting atoms within the electron density maps.

The major challenge in this method is to obtain large and well-ordered crystals, which are directly related to the quality of electron density maps derived from diffraction patterns for fine resolution

and accurate structural determination. The crystal structure of nitrogenase protein was first reported by Rees and co-workers in 1992, showing the structure of the active site as a [Mo-7Fe-8S] cluster ligated with R-homocitrate.[63,113,114] Then Einsle et al. reported the existence of the internal atom in the active site which was discovered later in the high resolution (1.16 Å) crystal structure.[64]

The nature of the central atom at the active site of nitrogenases was not identified using X-ray crystallography as it is difficult to distinguish between light atoms by XRD. Using X-ray emission spectroscopy (XES), in particular Fe valence-to-core, an X-ray technique that can differentiate C from N or O, carbon was found to fit the XES data from nitrogenase MoFe protein, isolated FeMoco, and the FeMoco-deficient ΔnifB protein.[115]

X-ray absorption spectroscopy

X-ray absorption spectroscopy (XAS) is one of X-ray based techniques that have been used to study nitrogenase. Unlike X-ray crystallography, which requires a single crystal for obtaining proper diffraction patterns to resolve a complete 3D structure of the enzyme. XAS can yield limited structural information more flexibly, as it can probe a variety of sample types, like amorphous solid samples, frozen solutions, solutions, and gases. It is an element-specific and local bonding-sensitive spectroscopic technique. For nitrogenase, XAS was used to determine the electronic structure of the metal clusters. The structures of MoFe and VFe protein, including their isolated cofactors, were investigated in the extended X-ray absorption fine structure (EXAFS) region.

Electron paramagnetic resonance spectroscopy

Electron paramagnetic resonance (EPR) spectroscopy is exploited to study systems with unpaired electrons which is widely used to study Fe in the redox site of metalloproteins. The basic concepts of EPR are analogous to those of nuclear magnetic resonance (NMR), but it is electron spins that are excited instead of the spins of atomic nuclei. An EPR spectrum of the MoFe protein of

nitrogenase in the resting state showed that the FeMoco exhibits an S=3/2 rhombic signal but the P cluster is EPR silent (S=0), presumably as all Fe are in the 2+ oxidation state. Under turnover conditions, the S=3/2 EPR signal from the FeMoco disappeared. In addition, the isolated FeMoco in NMF exhibited the S=3/2 EPR signal in the dithionite-reduced state and is EPR silent in the oxidised state,[116] similar to that of the enzyme-bound FeMoco. For the Fe protein, the dithionite-reduced [4Fe-4S]$^{+}$ cluster exhibits both S=1/2 and S=3/2 EPR signals, which disappear when the cluster is oxidised to [4Fe-4S]$^{2+}$.[57] Moreover, the interactions between the protein and inhibitors can be monitored by a change in EPR signals. For instance, when CO binds to the cofactor during turnover, it exhibits different sets of EPR signals depending on the partial pressure of CO.[117]

Electrochemistry

Electrochemical techniques are useful for studying a dynamic system like a redox enzyme. In the case of nitrogenase, due to the restriction on direct electrochemical control of the large enzyme, a mediated electrochemical approach is often applied to study the redox properties of the enzyme. The midpoint potential of clusters has been determined by potentiometric titration with redox mediators in conjunction with EPR spectroscopy (more detail shown in Chapter 4).

The redox property of the isolated FeMoco has also been investigated using electrochemical measurements. A cyclic voltammogram of the extracted FeMo cofactor in NMF shows -0.3 V and -0.94 V as the midpoint potential for the first two processes.[78,116] The isolated VFe cofactor from V-nitrogenase has the potentials of these two processes in lower potential (ca. -0.41 V and -1.06 V).[118]

Infrared spectroscopy

Infrared spectroscopy is based on the absorption of mid-infrared light in the range 400-4000 cm^{-1} by a molecule. An IR spectrum shows transitions in the vibrational energy levels of molecules and gives information on the chemical bonds present and thus the molecular structure. Infrared spectroscopy can be used to characterise exogenous ligand binding to metal centres inside

nitrogenase. Many small π-acid ligands, such as CO, CN and isocyanide (RNC), have strong absorption bands in a part of the IR region which is clear of other protein vibrational features. Furthermore, these small molecules also work as substrates and inhibitors of nitrogenase which could help determine the mechanism of reduction reaction by nitrogenase (more detail is shown in Chapter 4-6).

1.5 Aim and scope of this thesis

The focus of his thesis is to study interactions between ligands and the MoFe protein using an IR spectroelectrochemical technique. In this thesis, substrates and inhibitors of nitrogenase are used to understand the mechanism of ligands binding to the active site of the MoFe protein under electrochemical control with a series of redox mediators. Wild type and variants of the MoFe protein are applied to learn the function of amino acid residues near the FeMo cofactor and P cluster of the nitrogenase.

1.5.1 Developing an approach for MoFe protein immobilisation

From a previous study in the Vincent group, an entrapment approach for the MoFe protein in a Nafion polymer electrolyte had been developed for the spectroelectrochemical study. However, some problems with reproducibility using this method were encountered at the beginning of my project. Therefore, new approaches for MoFe protein immobilisation were developed as described in Chapter 3.

1.5.2 Study of ligands binding to the MoFe protein

Based on the immobilisation approaches, the experimental results are shown in Chapter 4-6, which are divided by different ligands. In Chapter 4, the interactions between CO and the MoFe protein are presented and discussed from the spectroelectrochemical study. CO is able to inhibit the proton reduction current by the MoFe protein at negative potentials and its binding to the active site is shown as CO-bound peaks in the Infrared spectra.

In Chapter 5, acetylene was found to inhibit the proton reduction current of the MoFe protein, andthe recovery of current from this inhibition occurred after flushing the acetylene away. The reduction product of acetylene, as determined by GC during a visit to the Seefeldt group labs is presented and discussed.

Chapter 6 shows the results of isocyanide, especially methyl isocyanide, binding to the MoFe protein at two different potentials. Some distinct *v*(NC) peaks appeared under different conditions.

Bibliography

1 D. J. Arp, L. A. Sayavedra-Soto and N. G. Hommes, *Arch. Microbiol.*, 2002, **178**, 250–255.

2 M. Könneke, A. E. Bernhard, J. R. De La Torre, C. B. Walker, J. B. Waterbury and D. A. Stahl, *Nature*, 2005, **437**, 543–546.

3 N. Igarashi, H. Moriyama, T. Fujiwara, Y. Fukumori and N. Tanaka, *Nat. Struct. Biol.*, 1997, **4**, 276–284.

4 E. Bock, H. Sundermeyer-Klinger and E. Stackebrandt, *Arch. Microbiol.*, 1983, **136**, 281–284.

5 M. Strous, E. Van Gerven, P. Zheng, J. G. Kuenen and M. S. M. Jetten, *Water Res.*, 1997, **31**, 1955–1962.

6 S. Lücker, M. Wagner, F. Maixner, E. Pelletier, H. Koch, B. Vacherie, T. Rattei, J. S. S. Damsté, E. Spieck, D. Le Paslier and H. Daims, *Proc. Natl. Acad. Sci. U. S. A.*, 2010, **107**, 13479–13484.

7 M. Nojiri, H. Koteishi, T. Nakagami, K. Kobayashi, T. Inoue, K. Yamaguchi and S. Suzuki, *Nature*, 2009, **462**, 117–120.

8 R. K. Poole, *Biochem. Soc. Trans.*, 2005, **33**, 176 LP – 180.

9 D. Richardson, H. Felgate, N. Watmough, A. Thomson and E. Baggs, *Trends Biotechnol.*, 2009, **27**, 388–397.

10 A. Kennedy and D. Bezdicek, *Microorganisms in Action*, Blackwell Scientific Publications, Boston, 1998.

11 F. Haber, *Naturwissenschaften*, 1923, **11**, 339–340.

12 and F. A. A. Shriver, D. F., Mark T. Weller, Tina Overton, Jonathan Rourke, *Inorganic Chemistry*, N.Y. : W. H. Freeman and Company, New York, Sixth Edit., 2014.

13 and C. J. H. J. Logadottir, T. H. Rod, J. K. Nørskov, B. Hammer, S. Dahl, *J. Catal.*, 2001, **197**, 229–231.

14 C. J. H. Jacobsen, S. Dahl, B. G. S. Clausen, S. Bahn, A. Logadottir and J. K. Nørskov, *J. Am. Chem. Soc.*, 2001, **123**, 8404–8405.

15 J. Chatt, J. R. Dilworth and R. L. Richards, *Chem. Rev.*, 1978, **78**, 589–625.

16 C. J. Pickett and J. Talarmin, *Nature*, 1985, **317**, 652–653.

17 J. S. Anderson, J. Rittle and J. C. Peters, *Nature*, 2013, **501**, 84–87.

18 J. G. Chen, R. M. Crooks, L. C. Seefeldt, K. L. Bren, R. Morris Bullock, M. Y. Darensbourg, P. L. Holland, B. Hoffman, M. J. Janik, A. K. Jones, M. G. Kanatzidis, P. King, K. M. Lancaster, S. V. Lymar, P. Pfromm, W. F. Schneider and R. R. Schrock, *Science*, 2018, **360**, eaar6611.

19 R. Lan and S. Tao, *RSC Adv.*, 2013, **3**, 18016–18021.

20 A. J. Medford and M. C. Hatzell, *ACS Catal.*, 2017, **7**, 2624–2643.

21 Y. Hao, X. Dong, S. Zhai, H. Ma, X. Wang and X. Zhang, *Chem. - A Eur. J.*, 2016, **22**, 18722–18728.

22 J. Liu, M. S. Kelley, W. Wu, A. Banerjee, A. P. Douvalis, J. Wu, Y. Zhang, G. C. Schatz and M. G. Kanatzidis, *Proc. Natl. Acad. Sci. U. S. A.*, 2016, **113**, 5530–5535.

23 J. H. van Helden, W. Wagemans, G. Yagci, R. A. B. Zijlmans, D. C. Schram, R. Engeln, G. Lombardi, G. D. Stancu and J. Röpcke, *J. Appl. Phys.*, 2007, **101**, 43305.

24 J. Hong, S. Prawer and A. B. Murphy, *ACS Sustain. Chem. Eng.*, 2018, **6**, 15–31.

25 T. Kim, H. H.; Teramoto, Y.; Ogata, A.; Takagi, H.; Nanba, *Plasma Chem. Plasma Process.*, 2016, **36**, 45–72.

26 I. Rafiqul, C. Weber, B. Lehmann and A. Voss, *Energy*, 2005, **30**, 2487–2504.

27 N. Gruber, *The Dynamics of the Marine Nitrogen Cycle and its Influence on Atmospheric CO2 Variations BT - The Ocean Carbon Cycle and Climate*, Springer Netherlands, Dordrecht, 2004.

28 N. Gruber, in *Nitrogen in the Marine Environment (Second Edition)*, eds. D. G. Capone, D. A. Bronk, M. R. Mulholland and E. J. B. T. Carpenter, Academic Press, San Diego, 2008, pp. 1–50.

29 D. G. Capone, J. A. Burns, J. P. Montoya, A. Subramaniam, C. Mahaffey, T. Gunderson, A. F. Michaels and E. J. Carpenter, *Global Biogeochem. Cycles*, 2005, **19**.

30 J. P. Zehr, E. J. Carpenter and T. A. Villareal, *Trends Microbiol.*, 2000, **8**, 68–73.

31 R. A. Herbert, *FEMS Microbiol. Rev.*, 1999, **23**, 563–590.

32 A. E. Dekas, R. S. Poretsky and V. J. Orphan, *Science*, 2009, **326**, 422 LP – 426.

33 E. J. Carpenter, J. P. Montoya, J. Burns, M. R. Mulholland, A. Subramaniam and D. G. Capone, *Mar. Ecol. Prog. Ser.*, 1999, **185**, 273–283.

34 J. Grosse, D. Bombar, H. N. Doan, L. N. Nguyen and M. Voss, *Limnol. Oceanogr.*, 2010, **55**, 1668–1680.

35 F. Mus, A. B. Alleman, N. Pence, L. C. Seefeldt and J. W. Peters, *Metallomics*, 2018, **10**, 523–538.

36 L. S. Hartmann and S. R. Barnum, *J. Mol. Evol.*, 2010, **71**, 70–85.

37 R. D. Joerger, P. E. Bishop and H. J. Evans, *CRC Crit. Rev. Microbiol.*, 1988, **16**, 1–14.

38 H. Bortels, *Zentralbl. Bakteriol. Parasitenkd.*, 1936, **95**, 193–218.

39 W. A. Bulen and J. R. LeComte, *Proc. Natl. Acad. Sci.*, 1966, **56**, 979 LP – 986.

40 P. E. Bishop, D. M. Jarlenski and D. R. Hetherington, *J. Bacteriol.*, 1982, **150**, 1244–1251.

41 R. R. Eady, R. L. Robson, T. H. Richardson, R. W. Miller and M. Hawkins, *Biochem. J.*, 1987, **244**, 197–207.

42 G. D. Riddle, J. G. Simonson, B. J. Hales and H. D. Braymer, *J. Bacteriol.*, 1982, **152**, 72–80.

43 J. R. Chisnell, R. Premakumar and P. E. Bishop, *J. Bacteriol.*, 1988, **170**, 27–33.

44 Y. Hu, C. C. Lee and M. W. Ribbe, *Dalt. Trans.*, 2012, **41**, 1118–1127.

45 R. R. Eady, *Coord. Chem. Rev.*, 2003, **237**, 23–30.

46 C. Z. Blanchard and B. J. Hales, *Biochemistry*, 1996, **35**, 472–478.

47 R. N. Thorneley, N. H. J. Bergström, R. R. Eady and D. J. Lowe, *Biochem. J.*, 1989, **257**, 789–794.

48 R. W. Miller and R. R. Eady, *Biochem. J.*, 1988, **256**, 429 LP – 432.

49 R. L. Robson, R. R. Eady, T. H. Richardson, R. W. Miller, M. Hawkins and J. R. Postgate, *Nature*, 1986, **322**, 388–390.

50 M. J. Dilworth, R. R. Eady, R. L. Robson and R. W. Miller, *Nature*, 1987, **327**, 167–168.

51 R. R. Eady and R. R. Eady, 1996, **96**, 3013–3030.

52 D. F. Harris, D. A. Lukoyanov, S. Shaw, P. Compton, M. Tokmina-Lukaszewska, B. Bothner, N. Kelleher, D. R. Dean, B. M. Hoffman and L. C. Seefeldt, *Biochemistry*, 2018, **57**, 701–710.

53 B. Hu, D. F. Harris, D. R. Dean, T. L. Liu, Z. Yang and L. C. Seefeldt, *Bioelectrochemistry*, 2018, **120**, 104–109.

54 Y. Zheng, D. F. Harris, Z. Yu, Y. Fu, S. Poudel, R. N. Ledbetter, K. R. Fixen, Z. Y. Yang, E. S. Boyd, M. E. Lidstrom, L. C. Seefeldt and C. S. Harwood, *Nat. Microbiol.*, 2018, **3**, 281–286.

55 Y. Hu and M. W. Ribbe, *J. Biol. Inorg. Chem.*, 2015, **20**, 435–445.

56 J. B. Howard and D. C. Rees, *Chem. Rev.*, 1996, **96**, 2965–2982.

57 B. K. Burgess and D. J. Lowe, *Chem. Rev.*, 1996, **96**, 2983–3011.

58 J. Christiansen, D. R. Dean and L. C. Seefeldt, *Annu. Rev. Plant Physiol. Plant Mol. Biol.*, 2001, **52**, 269–295.

59 Y. Hu and M. W. Ribbe, *Microbiol. Mol. Biol. Rev.*, 2011, **75**, 664–677.

60 J. G. Rebelein, M. T. Stiebritz, C. C. Lee and Y. Hu, *Nat. Chem. Biol.*, 2017, **13**, 147–149.

61 L. C. Seefeldt, B. M. Hoffman and D. R. Dean, *Annu. Rev. Biochem.*, 2009, **78**, 701–722.

62 K. A. Vincent, G. J. Tilley, N. C. Quammie, I. Streeter, B. K. Burgess, M. R. Cheesman and F. A. Armstrong, *Chem. Commun.*, 2003, **3**, 2590–2591.

63 J. Kirn and D. C. Rees, *Nature*, 1992, **360**, 553–560.

64 O. Einsle, F. A. Tezcan, S. L. A. Andrade, B. Schmid, M. Yoshida, J. B. Howard and D. C. Rees, *Science*, 2002, **297**, 1696–1700.

65 T. Spatzal, M. Aksoyoglu, L. Zhang, S. L. A. Andrade, E. Schleicher, S. Weber, D. C. Rees and O. Einsle, *Science*, 2011, **334**, 940.

66 B. E. Smith, *Science*, 2002, **297**, 1654–1655.

67 M. K. Chan, J. Kim and D. C. Rees, *Science*, 1993, **260**, 792 LP – 794.

68 K. Rupnik, C. C. Lee, J. A. Wiig, Y. Hu, M. W. Ribbe and B. J. Hales, *Biochemistry*, 2014, **53**, 1108–1116.

69 J. W. Peters, M. H. B. Stowell, S. M. Soltis, M. G. Finnegan, M. K. Johnson and D. C. Rees, *Biochemistry*, 1997, **36**, 1181–1187.

70 K. M. Lancaster, M. Roemelt, P. Ettenhuber, Y. Hu, M. W. Ribbe, F. Neese, U. Bergmann and S. DeBeer, *Science*, 2011, **334**, 974.

71 C. Rüttimann-Johnson, P. Rangaraj, V. K. Shah and P. W. Ludden, *J. Biol. Chem.*, 2001, **276**, 4522–4526.

72 H. U. Yilin and M. W. Ribbe, *Acc. Chem. Res.*, 2010, **43**, 475–484.

73 A. W. Fay, C.-C. Lee, J. A. Wiig, Y. Hu and M. W. Ribbe, ed. M. W. Ribbe, Humana Press, Totowa, NJ, 2011, pp. 239–248.

74 V. K. Shah and W. J. Brill, *Proc. Natl. Acad. Sci.*, 1977, **74**, 3249 LP – 3253.

75 B. K. BURGESS, *Biol. Nitrogen Fixat.*, 1990, **90**, 1377.

76 H.-I. Lee, B. J. Hales and B. M. Hoffman, *J. Am. Chem. Soc.*, 1997, **119**, 11395–11400.

77 S. J. Yoo, H. C. Angove, V. Papaefthymiou, B. K. Burgess and E. Münck, *J. Am. Chem. Soc.*, 2000, **122**, 4926–4936.

78 C. J. Pickett, K. A. Vincent, S. K. Ibrahim, C. A. Gormal, B. E. Smith and S. P. Best, *Chem. - A Eur. J.*, 2003, **9**, 76–87.

79 C. J. Pickett, K. A. Vincent, S. K. Ibrahim, C. A. Gormal, B. E. Smith, S. A. Fairhurst and S. P. Best, *Chem. - A Eur. J.*, 2004, **10**, 4770–4776.

80 J. E. MCNARY and R. H. BURRIS, *J. Bacteriol.*, 1962, **84**, 598–599.

81 S. Duval, K. Danyal, S. Shaw, A. K. Lytle, D. R. Dean, B. M. Hoffman, E. Antony and L. C. Seefeldt, *Proc. Natl. Acad. Sci.*, 2013, **110**, 16414–16419.

82 Z.-Y. Yang, R. Ledbetter, S. Shaw, N. Pence, M. Tokmina-Lukaszewska, B. Eilers, Q. Guo, N. Pokhrel, V. L. Cash, D. R. Dean, E. Antony, B. Bothner, J. W. Peters and L. C. Seefeldt, *Biochemistry*, 2016, **55**, 3625–3635.

83 I. V Kurnikov, A. K. Charnley and D. N. Beratan, *J. Phys. Chem. B*, 2001, **105**, 5359–5367.

84 F. A. Tezcan, J. T. Kaiser, J. B. Howard and D. C. Rees, *J. Am. Chem. Soc.*, 2015, **137**, 146–149.

85 C. P. Owens, F. E. H. Katz, C. H. Carter, M. A. Luca and F. A. Tezcan, *J. Am. Chem. Soc.*, 2015, **137**, 12704–12712.

86 K. Danyal, D. R. Dean, B. M. Hoffman and L. C. Seefeldt, *Biochemistry*, 2011, **50**, 9255–9263.

87 B. M. Hoffman, D. Lukoyanov, Z. Y. Yang, D. R. Dean and L. C. Seefeldt, *Chem. Rev.*, 2014, **114**, 4041–4062.

88 D. Lukoyanov, N. Khadka, Z.-Y. Yang, D. R. Dean, L. C. Seefeldt and B. M. Hoffman, *J. Am. Chem. Soc.*, 2016, **138**, 1320–1327.

89 D. Lukoyanov, N. Khadka, Z.-Y. Yang, D. R. Dean, L. C. Seefeldt and B. M. Hoffman, *J. Am. Chem. Soc.*, 2016, **138**, 10674–10683.

90 D. Lukoyanov, Z. Y. Yang, N. Khadka, D. R. Dean, L. C. Seefeldt and B. M. Hoffman, *J. Am. Chem. Soc.*, 2015, **137**, 3610–3615.

91 D. Lukoyanov, Z.-Y. Yang, B. M. Barney, D. R. Dean, L. C. Seefeldt and B. M. Hoffman, *Proc. Natl. Acad. Sci.*, 2012, **109**, 5583–5587.

92 B. K. Burgess, S. Wherland, W. E. Newton and E. I. Stiefel, *Biochemistry*, 1981, **20**, 5140–5146.

93 J. H. Guth and R. H. Burris, *Biochemistry*, 1983, **22**, 5111–5122.

94 J. B. Varley, Y. Wang, K. Chan, F. Studt and J. K. Nørskov, *Phys. Chem. Chem. Phys.*, 2015, **17**, 29541–29547.

95 T. Spatzal, K. A. Perez, O. Einsle, J. B. Howard and D. C. Rees, *Science*, 2014, **345**, 1620–1623.

96 F. Neese, *Angew. Chemie Int. Ed.*, 2006, **45**, 196–199.

97 B. A. MacKay and M. D. Fryzuk, *Chem. Rev.*, 2004, **104**, 385–402.

98 H.-P. Jia and E. A. Quadrelli, *Chem. Soc. Rev.*, 2014, **43**, 547–564.

99 Y. Tanabe and Y. Nishibayashi, *Coord. Chem. Rev.*, 2013, **257**, 2551–2564.

100 B. Hinnemann and J. K. Nørskov, *Top. Catal.*, 2006, **37**, 55–70.

101 K. Danyal, A. J. Rasmussen, S. M. Keable, B. S. Inglet, S. Shaw, O. A. Zadvornyy, S. Duval, D. R. Dean, S. Raugei, J. W. Peters and L. C. Seefeldt, *Biochemistry*, 2015, **54**, 2456–2462.

102 C. C. Lee, Y. Hu and M. W. Ribbe, *Proc. Natl. Acad. Sci.*, 2012, **109**, 6922–6926.

103 K. A. Brown, D. F. Harris, M. B. Wilker, A. Rasmussen, N. Khadka, H. Hamby, S. Keable, G. Dukovic, J. W. Peters, L. C. Seefeldt and P. W. King, *Science*, 2016, **352**, 448–450.

104 C. C. Lee, Y. Hu and M. W. Ribbe, *Angew. Chemie - Int. Ed.*, 2011, **50**, 5545–5547.

105 Z. Y. Yang, D. R. Dean and L. C. Seefeldt, *J. Biol. Chem.*, 2011, **286**, 19417–19421.

106 Y. Hu, C. C. Lee and M. W. Ribbe, *Science*, 2011, **333**, 753–755.

107 J. Clayden, N. Greeves and S. G. Warren, *Organic chemistry*, Oxford University Press, Oxford, 2nd edn., 2012.

108 M. J. Dilworth, *Biochim. Biophys. Acta - Rev. Biomembr.*, 1966, **127**, 285–294.

109 M. J. Dilworth, M. E. Eldridge and R. R. Eady, *Biochem. J.*, 1993, **289**, 395–400.

110 K. Schneider, U. Gollan, S. Selsemeier-Voigt, W. Plass and M. Mtiller, *Naturwissenschaften*, 1994, **81**, 405–408.

111 M. Kelly, *Biochem. J.*, 1968, **107**, 1–6.

112 J. F. Rubinson, J. L. Corbin and B. K. Burgess, *Biochemistry*, 1983, **22**, 6260–6268.

113 M. M. Georgiadis, H. Komiya, P. Chakrabarti, D. Woo, J. J. Kornuc and D. C. Rees, *Science*, 1992, **257**, 1653 LP – 1659.

114 J. Kim and D. C. Rees, *Science*, 1992, **257**, 1677 LP – 1682.

115 K. M. Lancaster, M. Roemelt, P. Ettenhuber, Y. Hu, M. W. Ribbe, F. Neese, U. Bergmann and S. DeBeer, *Science*, 2011, **334**, 974 LP – 977.

116 F. A. Schultz, S. F. Gheller, S. Lough, B. K. Burgess and W. E. Newton, *J. Am. Chem. Soc.*, 1985, **107**, 5364–5368.

117 L. Yan, V. Pelmenschikov, C. H. Dapper, A. D. Scott, W. E. Newton and S. P. Cramer, *Chem. - A Eur. J.*, 2012, **18**, 16349–16357.

118 B. R. Lydon, C. C. Lee, K. Tanifuji, N. S. Sickerman, M. P. Newcomb, Y. Hu, M. Ribbe and J. Yang, *ChemBioChem*, 2019, **20**, 1–7.

Chapter 2

Theory and Methodology

Native nitrogenase is a redox enzyme that reduces nitrogen to ammonia. Electron from the Fe protein, in conjunction with ATP hydrolysis, are transferred to the P cluster and FeMo cofactor in MoFe protein. The electrochemical method allowed the active site to reduce substrate without Fe protein and ATP hydrolysis. Thus a new way to investigate nitrogenase has been established in this thesis.

Infrared spectroscopy coupled with electrochemistry allows studying the process of substrate reduction by nitrogenase while also observing spectroscopic changes. The fundamental theory of IR spectroscopy, especially the attenuated total reflectance IR spectroscopy, will be presented in this chapter which the main approach used in my studies.

2.1 Electrochemistry

Electrochemistry is one area of chemistry which studies the relationship between chemicals and electricity. The chemical process not only depends on the electrode but also the entire system including the solvent, electrolyte, membrane, wires and connections.

2.2.1 Electrode process and interface

Electrode/solution interface

A layer of atoms at the surface of the electrode comes in contact with the electrolyte (the solution with its solutes). The atoms at the surface get an excess charge (either positive or negative) as the electrode is polarized. The structure of the electrode/solution interface has various interactions as shown in Figure 2-1.

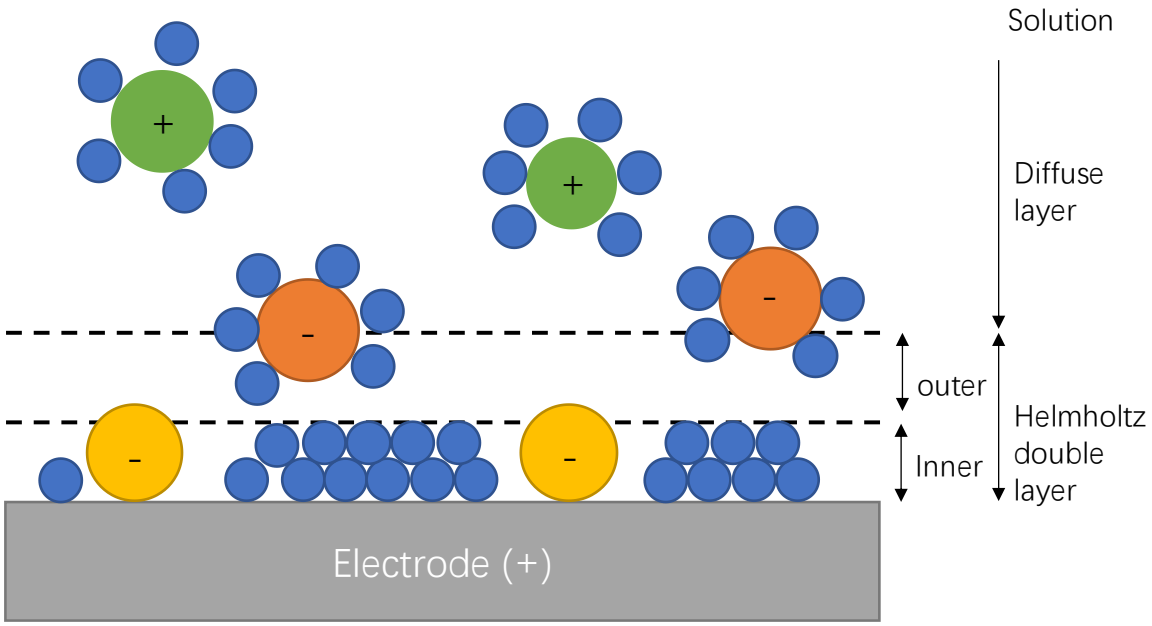


Figure 2-1: general representation of electrode/solution interface showing a specifically adsorbed anion on the electrode( ), non-specifically interacting anion and cation (and) and solvent molecules ( ).

In the solution of Figure 2-1, the solvent molecule moves and rolls randomly due to Brownian motion and convection. The molecules close to the electrode surface align themselves and touch

the electrode. The molecules in this layer of solvent are much ordered than those in the bulk solution, and this inner layer is referred to as the inner Helmholtz plane (IHP). The orientation of a molecule is felt as the increase of the distance to the surface of electrode.[1,2]

The solutes will approach the surface of the electrode next to the inner layer. The solvated anion will move from solution and form the outer layer called the outer Helmholtz plane (OHP). The solvated ions are non-specifically adsorbed as they are surrounded by a layer of solvent molecules.

The layer of well-ordered solvent molecules and ions is considered as the electrical double layer which is about 0.5 nm thick. Due to the effect of Brownian motion, the next layer below bulk solution is the diffusion layer where opposite charged ions to the electrode dominate (cations in the example shown in Figure 2-1).

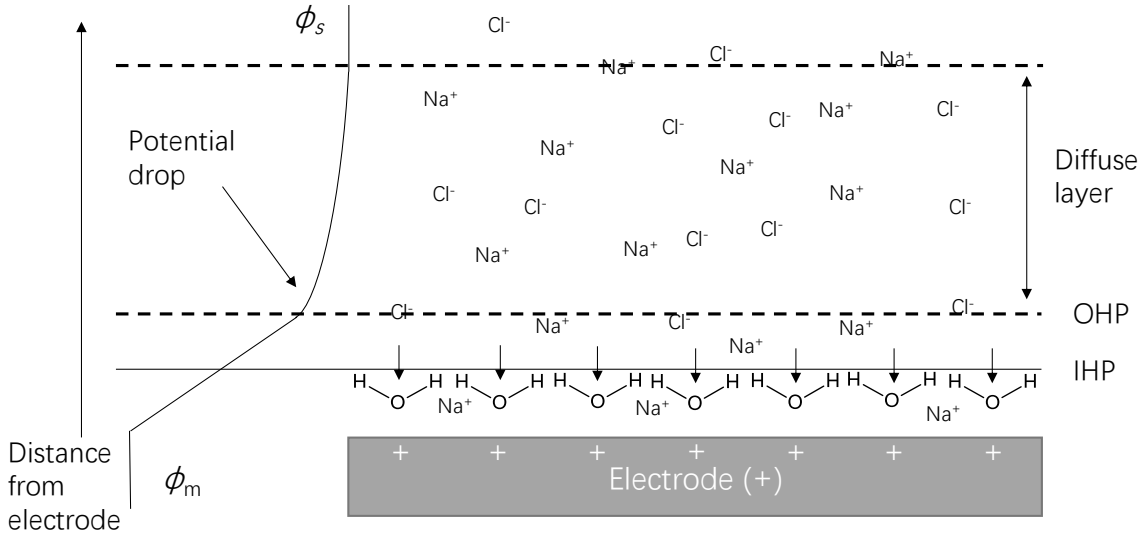


Figure 2-2: Graham model for the electrode solution interface and change in potential with distance from the electrode. Movement and orientation of solvent dipole moment (↓) in the positive electrode polarization (excess positive charge on the surface)

Figure 2-2 shows a simple model of an electrode/NaCl solution. The potential (ϕ) does not change on the electrode, but instead rapidly decreases in the Helmholtz plane, and this change is gradually lost in the diffusion layer and becomes stable in the bulk solution.

Ideal polarizable and non-polarizable electrode

The glassy carbon electrode in water is an example of an ideal polarizable electrode which holds a potential proportional to the charge removed. Due to no chemical reactions happening on the surface of the carbon electrode, the current at positive and negative potentials is insignificant within a certain range. Oxidation of water and reduction of protons will occur at extreme polarization as shown in Figure 2-3.

The Ag/AgCl electrode is an example of the ideal non-polarizable electrode as a redox reaction happens at the electrode to affect polarization by either oxidation (Ag to Ag^+) or reduction (Ag^+ to Ag). This behaviour will make the current rise suddenly when the potential is changed.

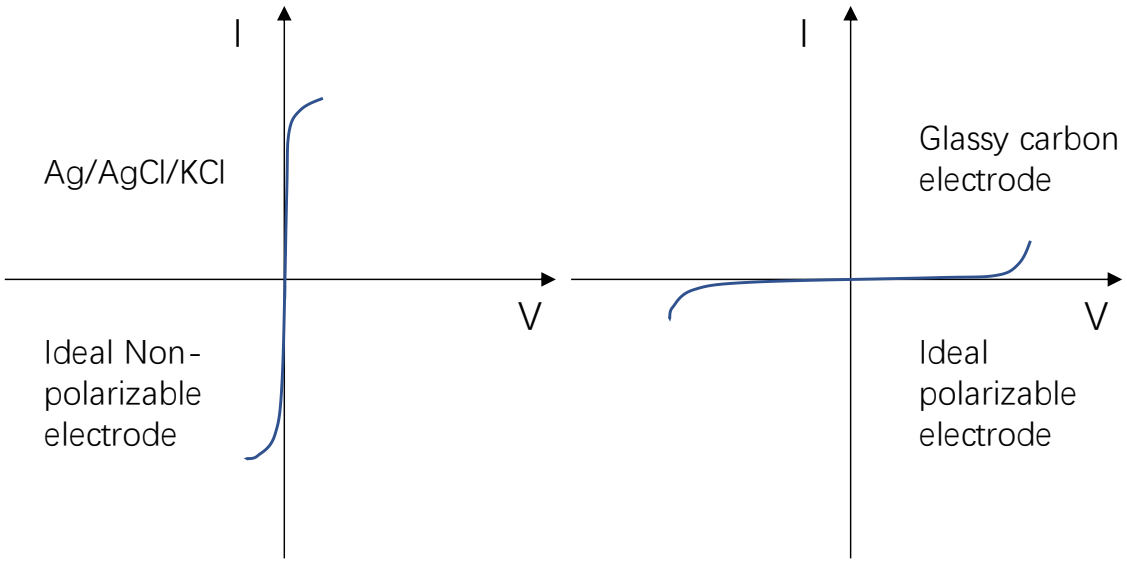


Figure 2-3: Current / Potential (I/V) curves for an ideal nom-polarizable electrode (Ag/AgCl electrode) and an ideal polarizable electrode (carbon electrode).

2.1.2 Electron transfer

Electrode potential

Due to the immobilisation of MoFe protein on the working electrode (carbon), electrons might directly transfer, via the P cluster, to the active site of nitrogenase. Heterogeneous electron transfer is the electron transfer process from the atoms on the electrode to a species in solution, or vice versa. The electron exchange could also happen in homogeneous phase via transfer between molecules in solution.

The simple model of electron transfer from an electrode to an enzyme is shown in Figure 2-4 which considers the Fermi level of the electrode and the energy of the frontier orbitals of the redox centres of the enzyme being reduced or oxidised. The energy of the electron in an electrode is defined by the electrode potential which could be controlled by applying a voltage (V). If the average energy of the Fermi level is not equal to that of the enzyme or solution, a flow of electrons from or to the electrode can cause a redox reaction to happen.[3]

The Fermi level of the electrode can be increased and decreased by applying a potential to the electrode in the negative or positive direction. If the energy of the Fermi level raised by the applied potential is higher than the lowest unoccupied molecule orbital (LUMO) of a redox molecule, then electrons can transfer from the electrode to this redox molecule. Similarly, if the energy of the Fermi level lowered by the applied potential is below the highest occupied molecule orbital (HOMO) of the redox species, electrons can flow back to the electrode from the HOMO of the molecule. The difference between the electron flux to the electrode (ja), and from the electrode (jc) is current flux/net current density ($j_0 = j_a - j_c$).

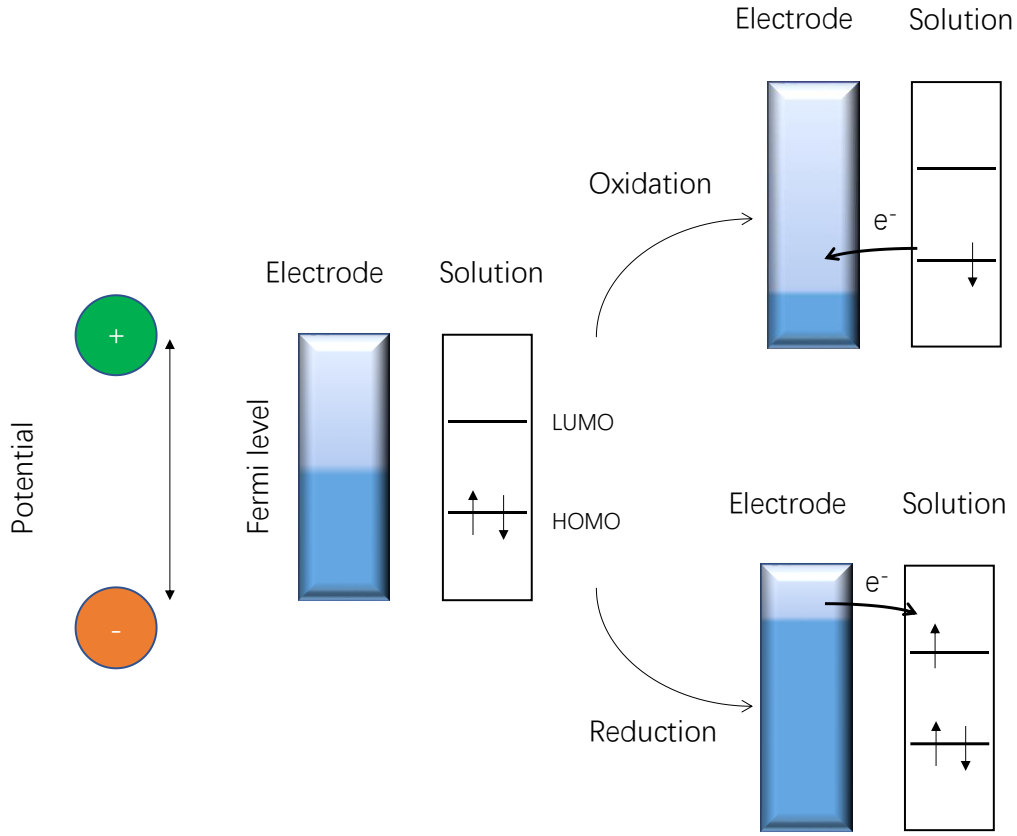


Figure 2-4: Simple description of changes in the Fermi level of the electrode. A positive potential lowers the Fermi level of the electrode below the HOMO of redox species, and a negative potential raises the Fermi level of the electrode above the LUMO of redox species. Electrons can enter and leave the electrode via this change.

Mass transport

As nitrogenase is quite a large protein, even with the Fe protein removed in my research, the MoFe protein still has a molecular mass of 250 kDa which is about 4 times that of a NiFe hydrogenase (100 kDa), for example[4]. The active site of nitrogenase, FeMo cofactor, is deeply buried in the enzyme (10 Å)[5] is therefore direct electron transfer for most variants and wild type MoFe protein is unlikely. Therefore, small molecule redox mediators and their mass transport should also be considered in electron transfer to the MoFe protein.

Three different but important mechanisms of mass transport play a key role in dynamic electrochemistry. The random movemenment of all small particles, molecules and ions in solution

is called diffusion. Diffusion is the dominant mass transport mechanism in the space close to the electrode. The speed of ions and molecules depend on their size, mass, the viscosity and the temperature of the solution. Diffusion leads to a random movement of all species. There will be a net movement of species close to the electrode surface in response to application of a potential. [6]

The rate of species moving within this diffusion zone is described by Fick's first and second laws of diffusion where concentration is a function of time and position. The first law states how the flux (J) is proportional to the concentration gradient $\frac{\partial C}{\partial x}$ and related to the diffusion coefficient D.

$$\mathrm{J(x,t)} = -\mathrm{D}\frac{\partial C(x,t)}{\partial x}$$

Fick's second law considers that concentration varying with time is related to the Laplacian operator (∇^2) of the concentration gradient. Forms of ∇^2 for different geometries are given in Table 2.1. Fick's second law permits us to calculate how concentration will change with time in an electrochemical experiment.

$$\frac{\partial C}{\partial t} = D\nabla^2 C$$

Table 2-1 Forms of the Laplacian Operator for Different Geometries[7]

Type	Variables	∇^2	Example
Linear	x	$\frac{\partial^2}{\partial x^2}$	Shielded disk electrode
Spherical	r	$\frac{\partial^2}{\partial x^2} + \frac{2}{r}\cdot\frac{\partial}{\partial r}$	Hanging drop electrode
Cylindrical (axial)	r	$\frac{\partial^2}{\partial x^2} + \frac{1}{r}\cdot\frac{\partial}{\partial r}$	Wire electrode
Disk	r, z	$\frac{\partial^2}{\partial x^2} + \frac{1}{r}\cdot\frac{\partial}{\partial r} + \frac{\partial^2}{\partial z^2}$	Inlaid disk ultramicroelectrode

Band	x, z	$\frac{\partial^2}{\partial x^2} + \frac{\partial^2}{\partial z^2}$	Inlaid band electrode

Migration is caused by electrostatic interactions where charged chemicals will move along the electric field gradient, because of the Coulombic force, from the bulk solution (far away from the electrode). The positively charged ions will move to a negatively charged electrode and vice versa where the concentration gradient is negligible.. The flux due to migration (a linear mass transport system) can be described as the contribution to the current by each species in the equation below. A is a cross-sectional area (cm^2), D is the diffusion coefficient (cm^2s^{-1}), C is the concentration (M) and $\frac{\partial \emptyset}{\partial x}$ is the electric field gradient (Vcm^{-1}).

$$i_j = \frac{{z_j}^2 F^2 A D_j C_j}{RT} \cdot \frac{\partial \emptyset}{\partial x}$$

Convection is described as the movement of species within the bulk solution which is the most primary mechanism over large distances (<0.5 mm). This mechanism affects my electrochemical experiments in the cell as a solution flow by a pump is used in most of my experiments.

When the electrode potential (polarization) is changed, the rate of electron transfer between the electrode and an enzyme may not significantly change, as it will be affected by a combination of factors, including overpotential of the redox catalytic site, conductivity through the enzyme, concentration of enzyme and solutes, mass-transport of mediators and substrates.

2.1.3 Equilibrium electrochemistry

In dynamic electrochemistry, the process of removing or giving electrons to species involves a change of energy. A redox reaction consists of two half-reactions (reduction and oxidation).

For an overall redox reaction as shown:

$$A_{ox} + B_{red} \leftrightarrow A_{red} + B_{ox}$$

It can be thought of as a combination of two entirely separate reactions (half-reactions):

$$A_{ox} + \mathrm{n}e^- \leftrightarrow A_{red}$$

$$B_{red} \leftrightarrow B_{ox} + ne^-$$

Each of these half-reactions has its own half-cell reduction potential (E^0) reported under standard conditions (293 K, 1 atm and unit activity of species). It is impossible to measure the half-cell potential itself, but the potential could be measured when it is combined with another half-cell such as the standard or normal hydrogen electrode (SHE or NHE), which by definition has a potential of 0 V at all temperature. Another reference electrode, saturated calomel electrode (SCE) instead of SHE is used in my experiments with nitrogenase, because it gives a convenient, reproducible potential and no side reactions with the protein.

Nernst equation

The reduction potential for a reaction (or half-cell reaction) can be determined by the Nernst equation. The relationship between the equilibrium potential and the concentrations of reduced and oxidised species is shown below:

$$E_A = E_A^0 + \frac{RT}{nF}\ln\frac{A_{ox}}{A_{red}}$$

$$E_B = E_B^0 + \frac{RT}{nF}\ln\frac{B_{ox}}{B_{red}}$$

Where E is the electrode potential, E^0 is the standard reduction potential of each species, R is the gas constant, T is the absolute temperature and F is the Faraday constant.

The overall voltage difference (E) could be determined by the difference between the two half-cell potentials. If one is the reference electrode, the potential of another half reaction is very easy determine or control.

$$\mathrm{E} = E_{cathode} - E_{anode} = E_A - E_B = E_A^0 - E_B^0 + \frac{RT}{nF}\ln\frac{A_{ox}B_{red}}{A_{red}B_{ox}}$$

The standard Gibbs free energy of the redox reaction, $\Delta_r G^0$ is related to the standard reduction potential (E^0) as shown:

$$\Delta_r G^0 = -RT \ln K = -nF(E_A^0 - E_B^0)$$

Kinetic of electrochemical reaction

The electron transfer across an interface is the key step of electrochemical reactions. The equilibria can be predicted by the thermodynamics of the processes. The movement of charge depends on the current (I), but is also proportional to the surface area of the electrode (A). So, the current density (j, A cm^{-2}) is a combination of these two factors. The net current density (j) is the flow of electrons between the electrode and a redox species which is a sum of the anodic and cathodic current densities (j_a and j_c) as shown below:

$$j = j_a - j_c$$

The rate of electrons flow to each electrode is proportional to the amount of reduced or oxidised species in solution which can be related to the concentrations at the distance of 0 from the electrode surface.

Rate of oxidation $= \frac{\partial OX}{\partial t} = k_c[OX]_{x=0}$

Rate of reduction $= \frac{\partial Red}{\partial t} = k_a[Red]_{x=0}$

Where k_a and k_c are the rate constants for the electron transfer to and from the electrode, and [OX] and [Red] are the concentrations of oxidised and reduced species formed at the electrode. From Faraday's law and constant, the current densities are related to the redox reaction rate.

$$j_c = vF\frac{\partial OX}{\partial t} = vFk_c[OX]_{x=0}$$

$$j_a = vF\frac{\partial Red}{\partial t} = vFk_a[Red]_{x=0}$$

Where *v* is the number of electrons in each reaction.

Therefore, if we consider the mediator involved in the experiment which is used to transfer an electron to the active site of the MoFe protein, each reaction requires activation to overcome a kinetic barrier ($\Delta G^{\ddagger}$, the Gibbs free energy of the formation of the transition state). As the electron transfer is reversible and rapid, the extra changes of structure with electron transfer can be considered as a single elementary step. And the reaction coordinate can be defined as shown in Figure 2-5. Transition state theory and the Eyring-Polanyi equation will be used to determine the reaction rate for electron transfer.[8,9]

$$k_{ET} = \kappa \frac{k_B T}{h} \cdot \exp\left(\frac{-\Delta G^{\ddagger}}{k_B T}\right)$$

Where κ is the transmission coefficient, k_B is the Boltzmann constant, *h* is the Planck constant, and *T* is the absolute temperature.

The kinetic barrier ($\Delta G^{\ddagger}$) is calculated by Marcus theory as shown below:

$$\Delta G^{\ddagger} = \frac{(\lambda + \Delta G^{0})^2}{4\lambda}$$

$$\Delta G^{0} \approx vF\eta$$

where λ is the reorganisation energy for electron transfer and η is the overpotential.

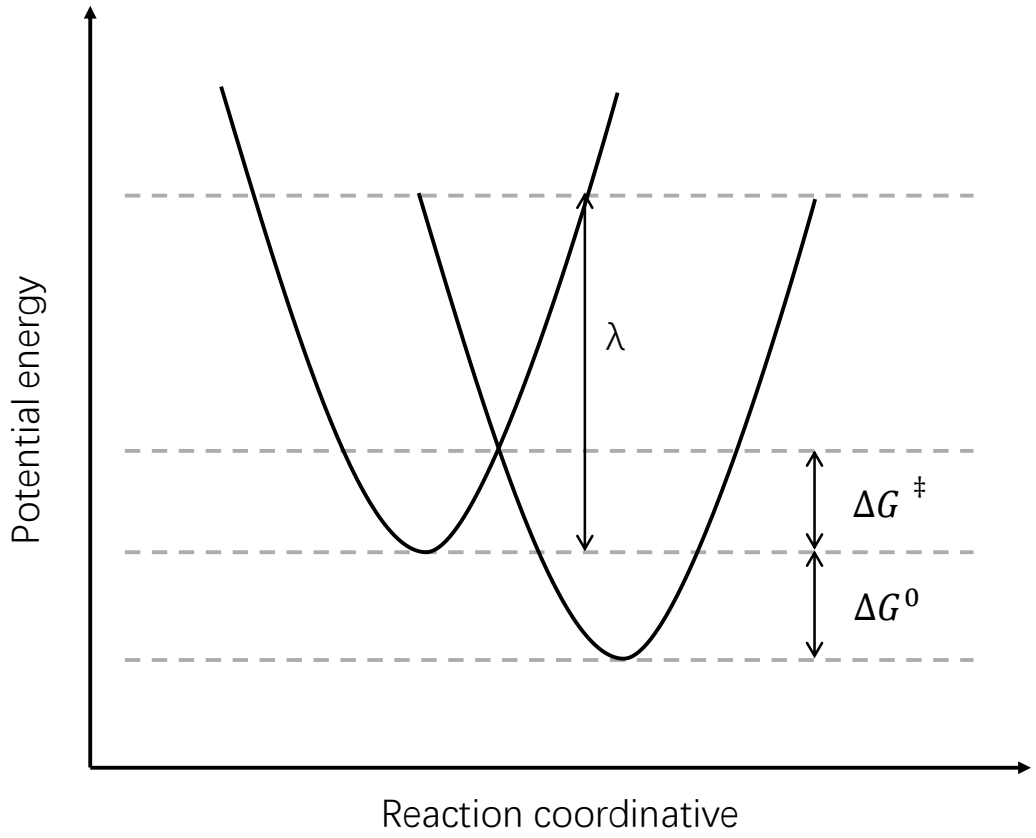


Figure 2-5: Electronic energy surfaces for an electron transfer reaction.

2.14 Electrochemical techniques

The three-electrode system

Current flow can be carried out with two electrodes where two half-cell reactions occur in dynamic electrochemistry. The interesting reaction will occur at the working electrode (WE) and the opposite half-cell reaction happen at the counter electrode (CE). Because there is always a continuous current through the counter electrode, it is difficult to measure the potential of a catalytic reaction happening at the working electrode accurately. Therefore an additional reference electrode (RE) is included, as mentioned above (SHE or SCE). The reference electrode will undergo polarization (changing the concentration of redox species at the electrode, which will make the potential vary) if a significantly large current goes through the reference electrode. Athree electrode system is used to solve this problem by having a working, counter and reference

electrode, with the reference connected via a voltmeter to the working electrode as shown in Figure 2-6. In this setup, there is almost no current passing through the reference electrode and its composition will not change over time. Therefore, it is possible to measure the potential of the working electrode with respect to the reference, but also to adjust the potential of the working electrode.

The current which can be measured by an ammeter will mostly flow between the working electrode and counter electrode. This current will be limited by the slowest reaction in the circuit, so it is important to use a much larger surface area of the counter electrode than that of the working electrode so that current flow at the counter electrode does not limit processes at the working electrode.

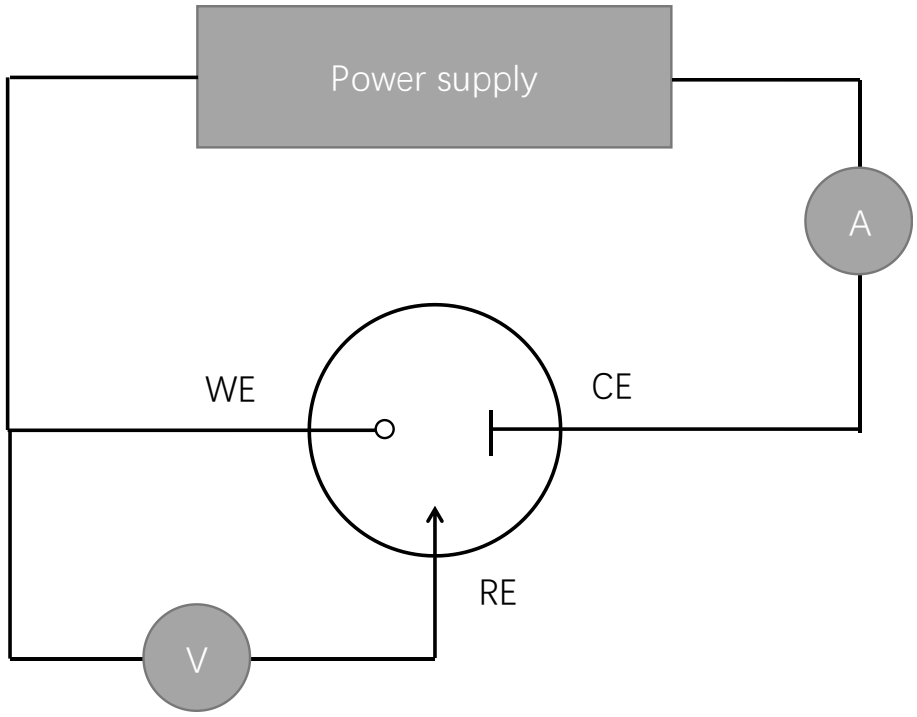
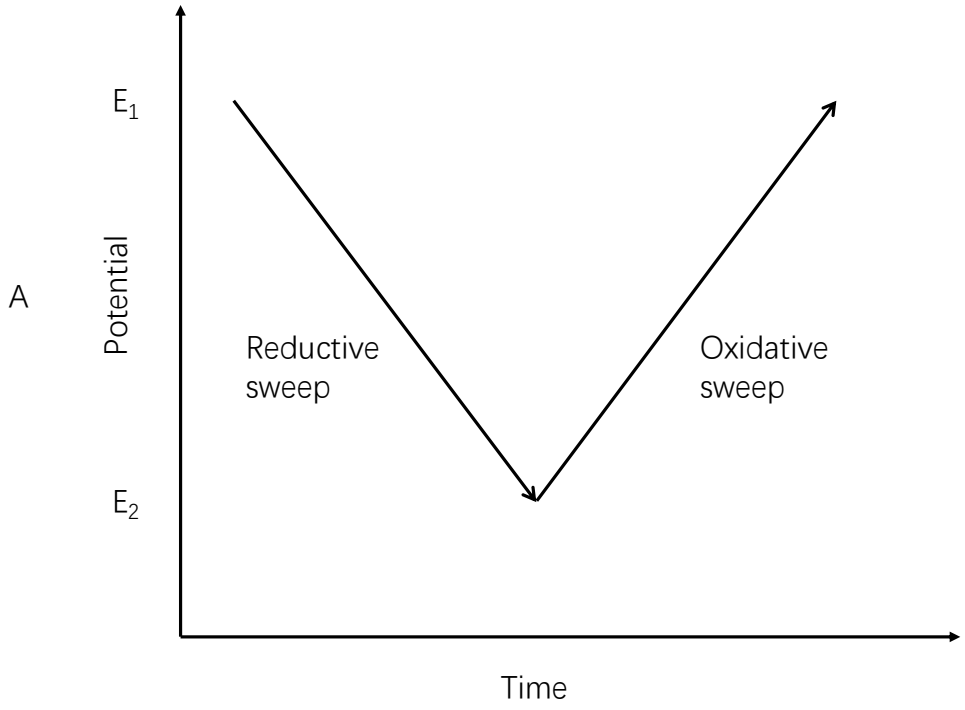


Figure 2-6: A schematic circuit for a three-electrode cell showing the working electrode (WE), counter electrode (CE), reference electrode (RE), voltmeter (V) and ammeter (A).

Two different methods of electrochemistry using a three-electrode arrangement are used in my thesis work: cyclic voltammetry and chronoamperometry, both of which involve controlling the potential and measuring the resultant current in the cell.

Cyclic voltammetry

Voltammetric techniques are quite an important part of electroanalytical chemistry. The current resulting from application of a controlled potential at the working electrode is recorded. Cyclic voltammetry (CV) is an extension of linear sweep voltammetry in which potential is swept from an initial value (E_1) to a final value (E_2). The scan direction in CV is reversed again to complete a cycle. Figure 2-7 (A) shows how potentials is changed with time in cyclic voltammetry. The range of potentials between E_1 and E_2 should cover the redox potentials of the studied species.



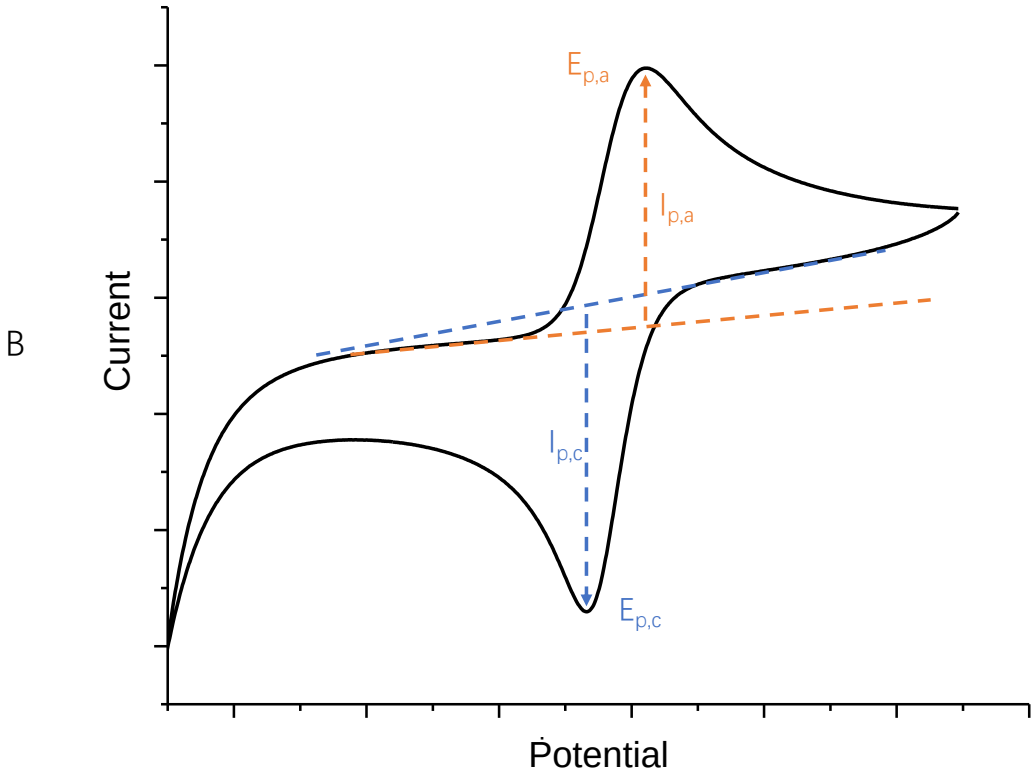


Figure 2-7: (A) Potential applied as function of time during cyclic voltammetry. (B) A typical sample of a diffusion-controlled cyclic voltammogram for a redox species at a glassy carbon working electrode showing the anodic and cathodic potentials ($E_{p,a}$ and $E_{p,c}$) and the anodic and cathodic peak current ($I_{p,a}$ and $I_{p,c}$).

In a CV experiment as shown in Figure 2-7 (B), the first half-wave is equivalent to linear sweep voltammetry. The current dramatically increases when the potential is close to the reduction peak potential ($E_{p,c}$). At $E_{p,c}$, the current reachs the value $I_{p,c}$, and the rate of reduction is a maximum. After the reduction peak, the concentration of oxidized species in the diffusion layer is lower than that of the reduced species and the current decreases in the subsequent part of the potential sweep. The current will fall to zero in an ideal condition if there is no oxidized species to be reduced in bulk solution. The at very negative potentials is due to proton reduction at the =glassy carbonworking electrode. During the opposite potential sweep, the first process is seen to be reversible. The reduced form is re-oxidised near the oxidation peak potential ($E_{p,a}$). A midpoint

potential can be determined at the average of $E_{p,c}$ and $E_{p,a}$ which corresponds to the standard reduction potential of a redox species.

Chronoamperometry

In the case of a nitrogenase experiment, chronoamperometry (CA) is used to observe current change as a function of time at low potentials. A series of potentials applied to the working electrode enable changes in the activity of the enzyme itself.

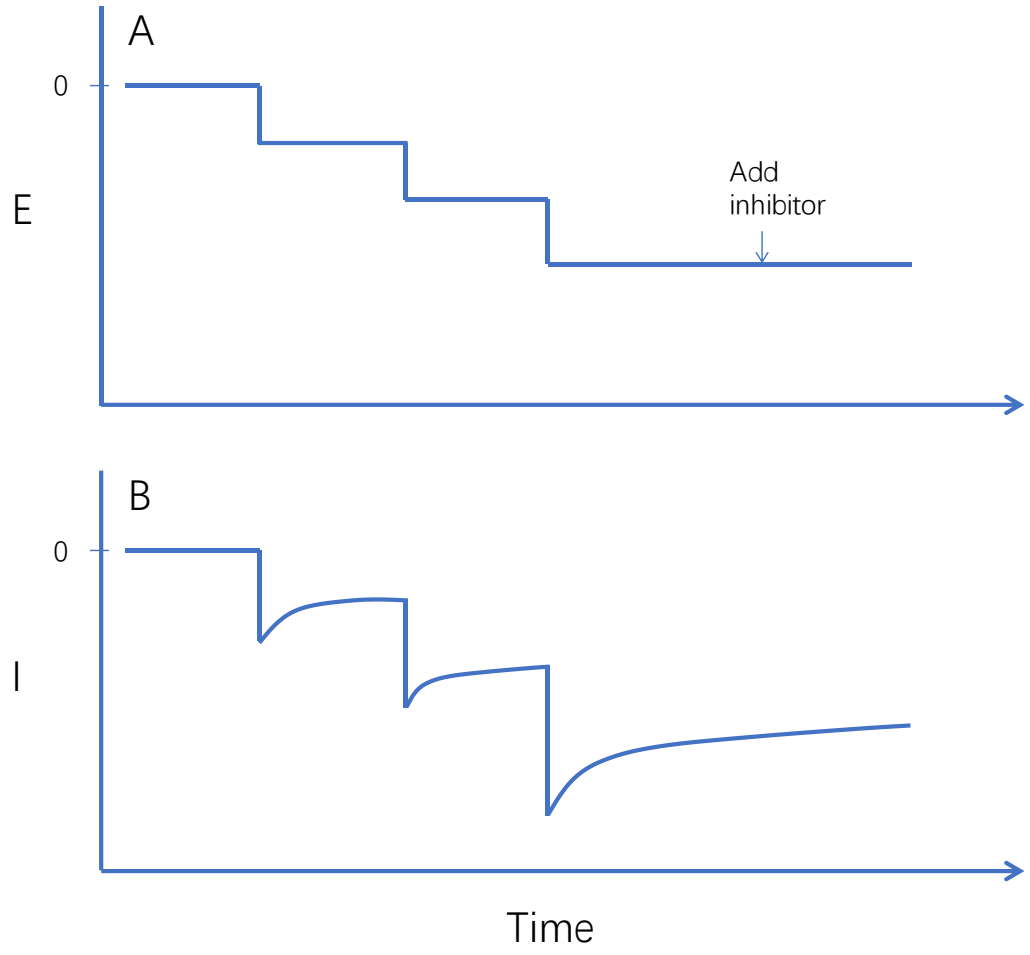


Figure 2-8: A plot of applied potential (A) and current response (B) as a function of time in a chronoamperometry experiment for a reductive catalytic process.

Figure 2-8 (A) shows how the potential is controlled in a chronoamperogram. Potential at the working electrode where the enzyme is immobilised is adjusted by a series of potentials. The

current at each potential as a result of reactions at the working electrode is recorded as shown in Figure 2-8 (B). The current always takes a while to stabilise after a potential step due to equilibration of charge at the electrode surface, as = shown in Figure 2-8 (B) (non-Faradaic contribution). The lower potential will increase the driving force for the catalytic process which has an effect on the heterogeneous electron transfer and causes a greater magnitude of current. In a stationary solution, the Faradaic current decays over time after each step and this can be explained by the Cottrell equation as shown below:

$$\mathrm{I} = \frac{nFAc_j^0\sqrt{D_j}}{\sqrt{\pi t}}$$

Where A is the area of electrode surface (cm^2), c_j^0 is an initial concentration of reducible analyte j (mol/cm^3), D_j is the diffusion coefficient for species j (cm^2/s).

The model will be much more complicated in a real experiment when enzyme was adsorbed onto the working electrode. The current is shown to be the sum of two contributions, a substrate-concentration independent non-Faradaic current and a Faradaic catalytic current (usually H^+ reduction to H_2 by nitrogenase). When studying inhibition by CO, the inhibitor diffusion and equilibration should also be considered in the system.[10]

2.2 Infrared Spectroscopy

2.2.1 Molecular vibrations

Molecular vibrations can result from the simple stretching of a diatomic molecule to the much more complex motion of atoms in a complicated compound. A molecule that consists of N atoms has 3N degrees of freedom. Three of them are from the translational motion in mutually perpendicular directions, the x, y and z axes. And another three represent the rotational motion about these three axes. And the remaining 3N-6 degrees are the number of vibrational modes for

a non-linear molecule, while a linear molecule has 3N-5 degrees as the rotation about its molecular axis cannot be observed.[11]

Each vibrational mode is due to the displacements of the atoms from their equilibrium positions and have a certain characteristic frequency. These frequencies can be represented by the potential energy of a harmonic oscillator as shown in Figure 2-9 as a function of the distance between atoms.

In Figure 2-9, the harmonic oscillator is well fitted to the low frequency (v) value which can be described by the following equation:

$$V_{in} = hn_i(v_i + \frac{1}{2})$$

Where h is Planck's constant, n_i is the fundamental frequency of the particular mode, and v_i is the vibrational quantum number of the i^{th} mode (v_i = 0; 1; 2; . . .). The energy difference for transitions between the ground state (v_i = 0) and the first excited state (v_i = 1) is consistent with the energy of the radiation in the mid-infrared spectrum region (400 to 4000 cm^{-1}).

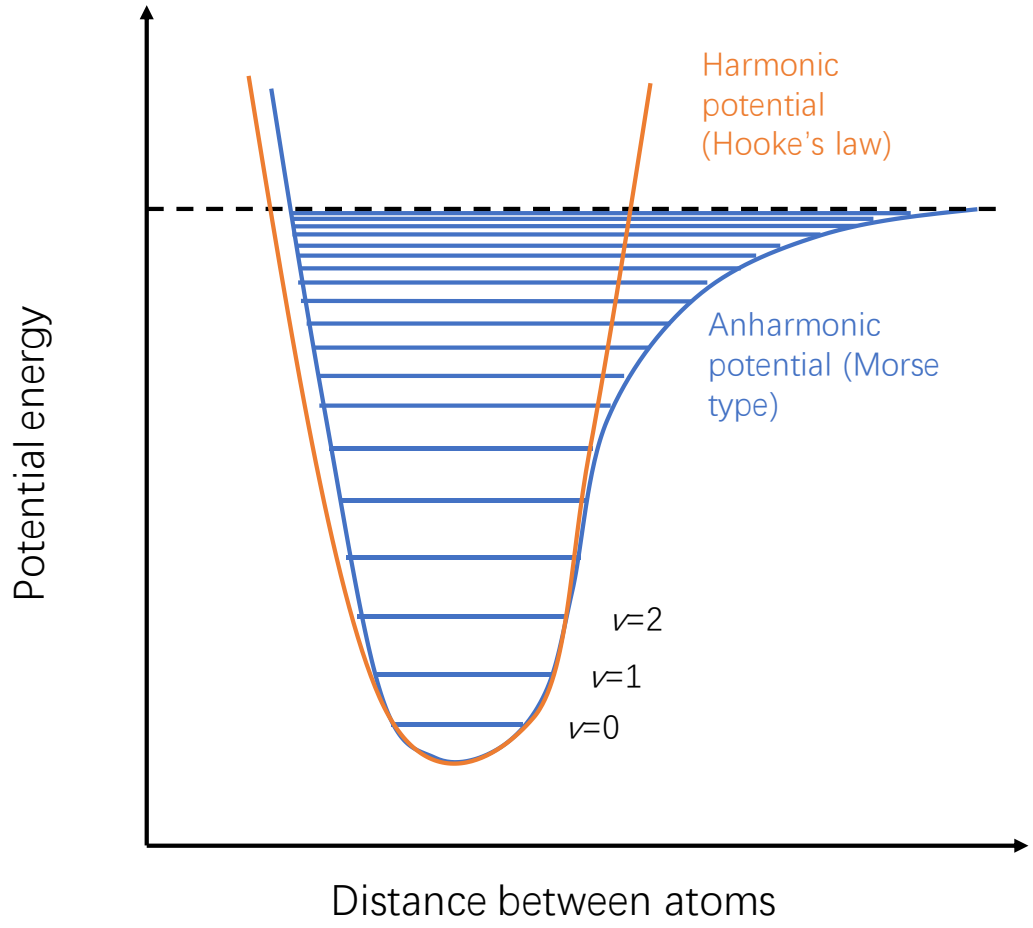


Figure 2-9: Potential energy of a diatomic molecule as a function of the distance of atoms with vibration for a harmonic oscillator (orange) and an anharmonic Morse oscillator (blue).

The actual vibration of potential energy (Morse type) is shown in Figure 2-9 (blue line) which is valid in large v_i. And the potential energy is described as the expression below:

$$V_{iv} = hv_i\left(v_i + \frac{1}{2}\right) + hv_i x_i\left(v_i + \frac{1}{2}\right)^2$$

Where x_i is the anharmonicity constant which is dimensionless and typically has values between -0.001 and -0.02, depending on the mode.

2.2.2 Infrared spectroscopy

The selection rule for 'IR active' vibrational modes is that the transition must involve a change in the dipole moment. A sample irradiated with mid-infrared light can absorb photons of energy equivalent to the energy difference between two states, typically, the ground state, and an excited vibrational state. If the infrared radiation has a frequency equal to the frequency of a molecular vibration causing a change of dipole moment, it will be absorbed.

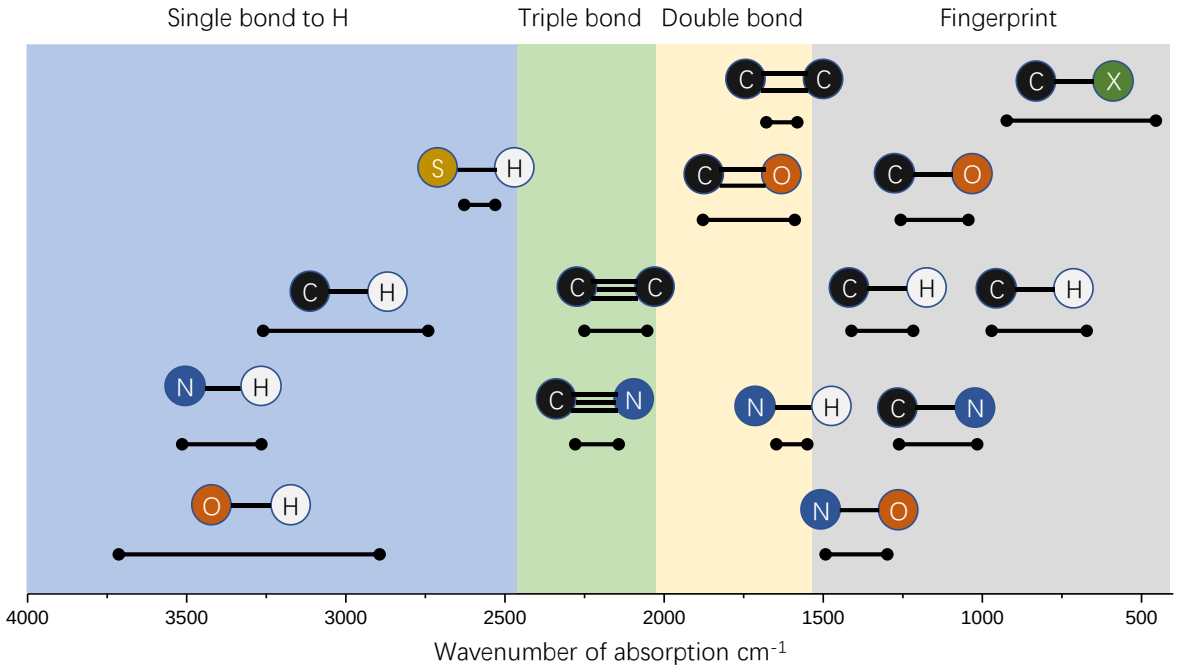


Figure 2-10: The fundamental stretching wavenumber of some common functional groups in the mid-IR region.

Certain groups of atoms have a large displacement in their vibrational modes while the rest of the molecule is almost stationary during such a transition. The frequency of such modes is characteristic of the specific functional group in which the motion is centred and is minimally affected by the properties of the nearby atoms in the molecule. Therefore certain chemical functional groups in a molecule have spectral features within a specific region of the spectrum which has enabled development of spectra/structure correlation tables. Figure 2-10 shows some primary information of infrared spectroscopic absorptions by frequency regions.

One of the advantages of infrared spectroscopy is that species in all phases of matter can be studied. Infrared spectra of solids, liquids and gasses have different characteristics. The spectra of small molecules in the gas phase show considerable fine structure due to transitions between the quantized rotational energy levels occuring at the same time as other vibrational transitions. For large molecule in the vapour phase, the individual rotational transitions are very similar which make the peaks resolved.

The rotational energy levels of diatomic molecules are characterized by a single rotational quantum number *J.* The rotational energy is shown below:

$$E_j = BJ(J+1)$$

Where B is the rotational constant as shown:

$$\mathrm{B} = \frac{h}{8\pi^2 Ic}$$

Where *I* is the moment of inertia of the molecule and c is the velocity of light. The selection rule of vibrational transitions between rotational energy states for the linear molecule is

$$\Delta \mathrm{J} = \pm 1$$

So that,

$$E_J - E_{j-1} = BJ(J+1) - BJ(J-1) = 2BJ$$

The pure rotation spectrum would be a series of lines with the same spacing of 2B cm^{-1}.

Beer's law (Bouguer-Lambert-Beer law) is the fundamental law of quantitative spectroscopy as well as infrared spectroscopy. The transmittance of any sample at wavenumber $\overline{\nu}$ (cm^{-1}) is referred to as the ratio of the radiant power from the rear ($I(\overline{\nu})$) and front ($I_0(\overline{\nu})$) face of the sample. Beer's law is given as:

$$T(\bar{\nu}) = \frac{I(\bar{\nu})}{I_0(\bar{\nu})} = e^{[-\alpha(\bar{\nu})b]}$$

Where b is the thickness (cm) of the sample, $\alpha(\bar{\nu})$ is the linear absorbance coefficient (cm^{-1}) at $\bar{\nu}$. The absorbance of the sample (a mixture) at $\bar{\nu}$, $A(\bar{\nu})$, is given by the base 10 logarithms of $\frac{1}{T(\bar{\nu})}$:

$$A(\bar{\nu}) = log_{10}\frac{1}{T(\bar{\nu})} = a_i(\bar{\nu})bc_i$$

Where c_i is the concentration of each component of the sample, a_i is the molar extinction coefficient (also known as molar absorptivity) and is typically reported in units of $M^{-1}cm^{-1}$.

2.2.3 IR spectra of metal carbonyls and isocyanides

Metal-bound carbonyls have a strong and sharp CO stretching peak in the infrared spectrum, generally between 2100 cm^{-1} and 1800 cm^{-1}, because the *ν*(CO) is free from coupling with other modes. The *ν*(CO) often gives important information about the bonding and structure of carbonyl complexes. As CO is one of the important inhibitors of nitrogenase, the study of CO binding to nitrogenase could be used to understand the mechanism of CO binding and how CO can be reduced as a non-native substrate of nitrogenase.

The free CO peak is at 2155 cm^{-1}, while *ν*(CO) from most carbonyl compounds is shifted to lower frequency due to the poor σ-donor but a strong π-acceptor character of CO. From Molecular Orbital theory, the σ-bond is formed from the donation of electrons (5σ) from the CO to the metal which increases the strength of the C-O bond slightly, while the π-bond is formed by back bonding from the filled *d*π orbitals of the metal to an empty antibonding orbital of CO which decreases the strength of the CO bond.[12] (See Figure 2-11.)

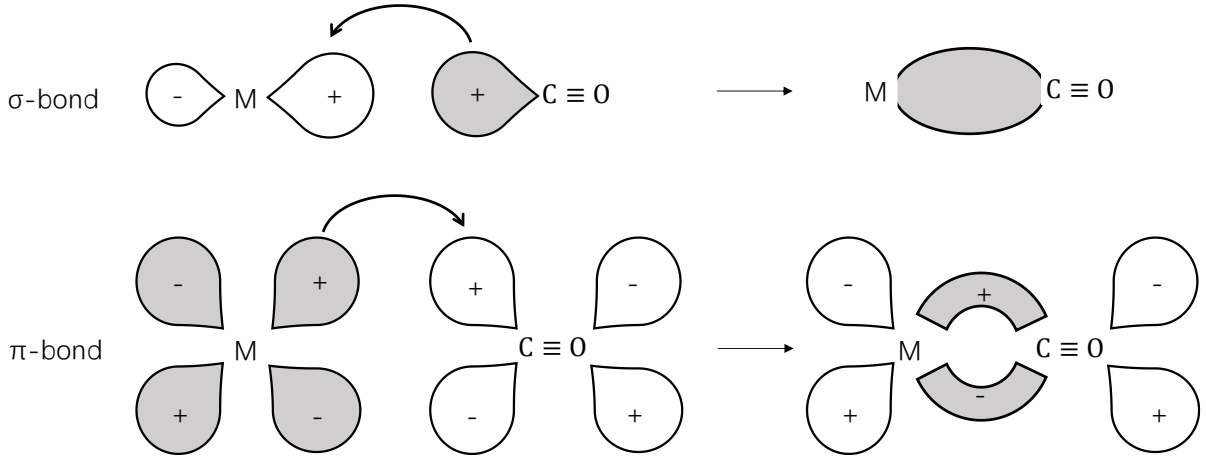


Figure 2-11 The σ and π bonding in metal carbonyls. The $2p\pi^*$ is an antibonding orbital and therefore donation into this orbital weakens the CO bond, causing *ν*(CO) to shift to lower wavenumber.

The *ν*(CO) for CO bound in a bridging mode between two metal centres is typically in the range 1900-1800 cm^{-1} which is much lower than the wavenumber of terminal CO ligands, (2100-1900 cm^{-1}). The *ν*(CO) is also lowered as the net negative charge on a complex increases as shown in the table below:

Table 2-2: Vibrational frequencies of *ν*(CO) mononuclear tetracarbonyls show the effect of net charge on a metal carbonyl.

Compound	*ν*(CO)/cm^{-1}	Ref
$Ni(CO)_4$	2094	[13]
$[Co(CO)_4]^-$	1946	[14]
$[Fe(CO)_4]^{2-}$	1788	[15]

In the case of isocyanide (isonitrile, $R\text{-}N^+\equiv C^-$), the σ-interactions with metal centres is significant wherease π-bonding interactions contribute to the bonding only slightly. Thus, isocyanide complexes are also formed with higher oxidation state metals that will not bind CO.

The distance between carbon and nitrogen is much shorter than in cyanides (R-C≡N). And isocyanides exhibit a strong *v*(NC) vibrational band between 2187 cm^{-1} and 2110 cm^{-1}.[16] In the study by Cotton and Zingales,[17] the back donation of electrons from the metal to the ligand is great when isocyanides combine with zero-valent metals like Cr(0), and the *v*(NC) is then shifted to lower wavenumber than that of the free isocyanide in solution. For mono- and dipositive metals, little or no back bonding occurs and the stretching band of isocyanides moves to a higher wavenumber due to the inductive effect of the metal ion to raise the NC bond.

Carbon monoxide and isocyanide will be described as inhibitors of the MoFe protein in the spectroelectrochemical study in the later chapters. The position of bound *v*(CO) and *v*(NC) bands will give valuable mechanistic insight into the enzymatic activity and redox chemistry of the MoFe protein.

2.2.4 ATR-IR Spectrometry

In most of my experiments, ATR-IR spectroscopy is used to investigate infrared characteristic features of nitrogenase under electrochemical control.

In the Vincent group, an ATR-IR spectroscopy technique combined with electrochemistry has been developed for studying biological redox systems, for example, hydrogenase[4] and nitrogenase[18].

2.2.4 The attenuated total reflectance (ATR) technique

The attenuated total reflectance technique is used to carry out the spectroscopic part of the experiments. Samples are put on an IRE (Internal Reflection Element) with a high refractive index and excellent IR transmitting properties (Figure 2-12), here, silicon. Compared to transmission IR, ATR is quite quick, non-destructive and requires no sample preparation. The spectral information of a sample which is too thick or strongly absorbing to be analysed by transmission methods can be obtained from reflection phenomena.

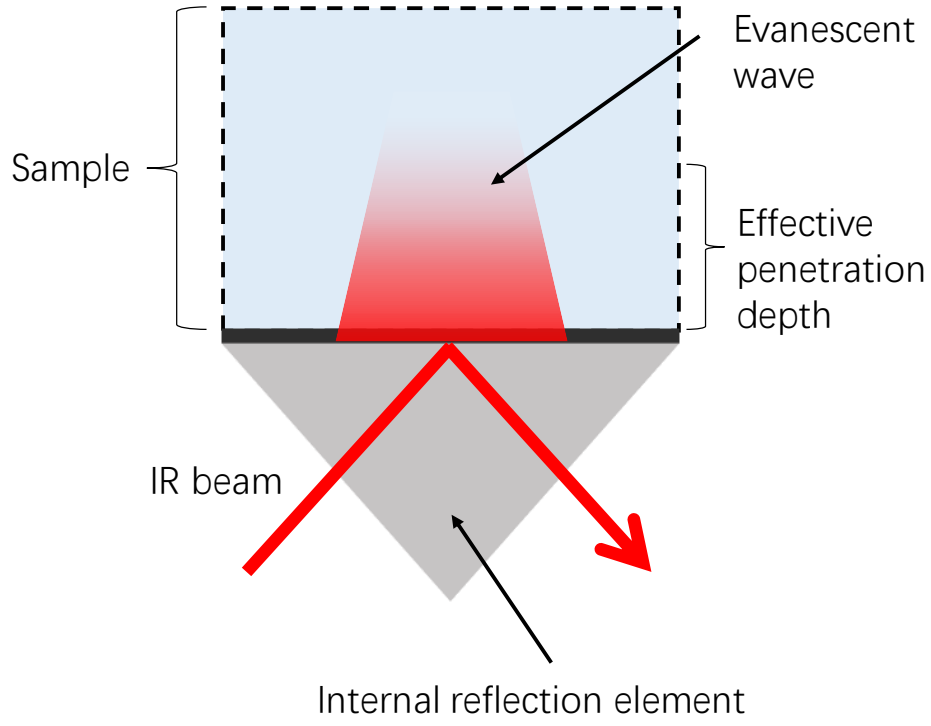


Figure 2-12: Diagram of a single reflection ATR crystal representing internal reflection at the surface.

A single reflection crystal is normally used in micro-ATR work and a multiple reflectance ATR crystal is often used for bulk samples as well as my program. An ATR accessory provides an IR spectrum of a sample because the radiation at the reflection point probes the sample with an 'evanescent wave'.[19]

When radiation passes from one transparent medium (with refractive index n_1) to another (with refractive index n_2), the relationship of the angle of incidence θ_1, the angle of refraction θ_2 is given by Snell's law:

$$n_1 \sin \theta_1 = n_2 \sin \theta_2$$

Typical crystals such as Si, Ge, or diamond have much higher refractive indexes than that of samples which will result in an internal reflection at moderate angles of incidence. The reflected radiation penetrates the sample boundary as the evanescent wave. The electric field amplitude of

this wave displaces decays exponentially with the distance from the surface. The effective penetration depth (dp) is expressed as:

$$\mathrm{dp} = \frac{\lambda}{2\pi n_1 \sqrt{\sin^2\theta - (\frac{n_2}{n_1})^2}}$$

Where, λ equals the wavelength of the radiation. From this equation, the penetration depth is a function of the wavelength λ and the sampling depth of the ATR method is approximately 2-15 μm.

2.3 Other experimental techniques

Due to the oxygen-sensitivity of nitrogenase, all chemicals and parts of the cell need to have oxygen removed before coming in contact with the protein and were therefore handled in an anaerobic glovebox (< 1 ppm, Glove Box Technology Ltd). The preparation of chemicals and samples was done in a wet glovebox, and the sealed spectroelectrochemical (SEC) cell was then moved to a dry glovebox which is maintained at a dew point of ca. -75 to -85 °C to minimise contributions of water vapour to the infrared spectrum.

2.3.1 Chemicals

All chemicals in solid or liquid were purchased from Sigma Aldrich, unless specifically mentioned. Gases were from gas cylinders purchased from BOC.

Buffer solution

The MoFe protein in most experiments was in 100 mM Tris-HCl buffer pH 8.0 with the same concentration of NaCl as the electrolyte. Trizma base and NaCl were first dissolved in Ultra-high purity water (MilliQ Millipore, 18 MΩ·cm) to reach 100 mM concentration. A pH meter and probe (Mettler Toledo) were used to adjust the pH of the buffer using concentrated (37%) HCl which leads to minimal change in concentration. The Tris-HCl buffer was then bubbled with N_2 gas for at

least 4 hours before transferring to the anaerobic glovebox. The buffer was then stirred overnight in the glovebox with cap untightened to get rid of residual O_2 before use.

Mediators

A series of [$Eu^{III/II}$-L] complexes (Eu-L), where L (structures shown in Figure 2-13) is 1,2-bis(o-aminophenoxy)ethane-N,N,N',N'-tetraacetate (BAPTA), ethylene glycol-bis(β-aminoethyl ether)-N,N,N',N'-tetraacetate (EGTA) or diethylenetriamine-N,N,N',N'',N''-pentaacetate (DTPA), has been developed and used as a redox mediator cocktail for the study of MoFe protein of the nitrogenase enzyme at low potential by a previous Vincent group member.[18]

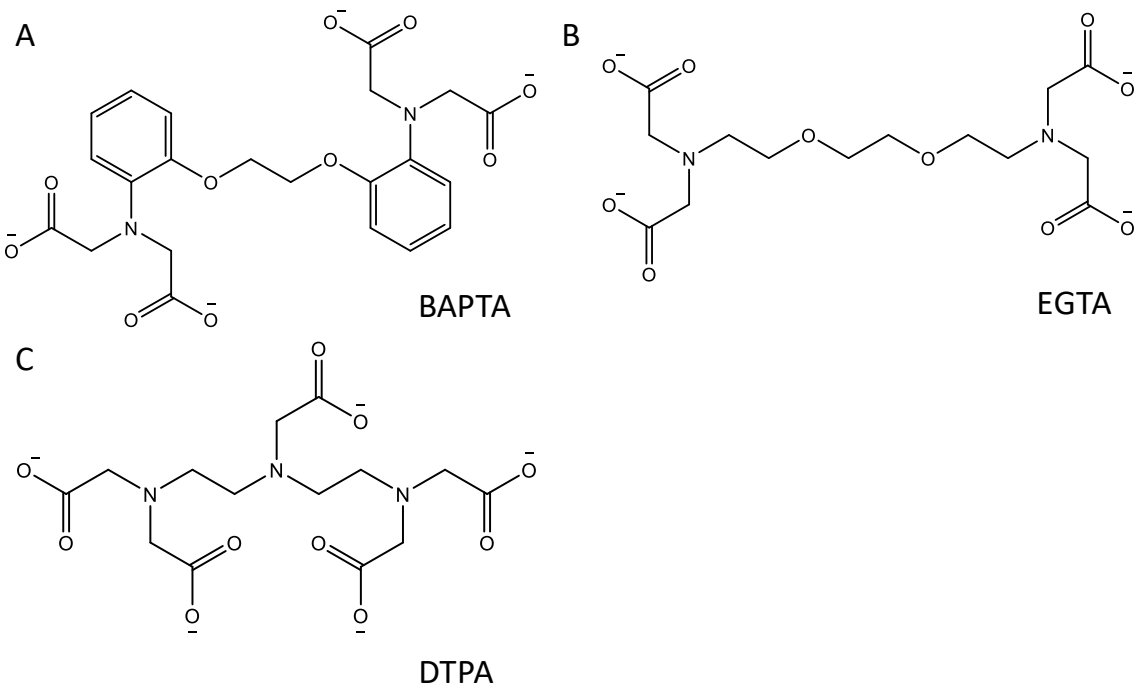


Figure 2-13: Structures of BAPTA, DTPA and EGTA used in Eu-L mediators.

Europium has the most accessible +II oxidation state of all the lanthanides. This is because of the $4f^7$ electron configuration (half-filled shell) in the Eu^{II} ion, which gives rise to a particularly high third ionisation energy. This is due to the maximum loss of exchange energy resulting from the decrease in the number of electrons with a parallel spin in going to the $4f^6$ Eu^{III} ion which gives europium rich redox chemistry that is incredibly rare amongst the lanthanides and leads to many

possible applications.[20] The redox potential of the $Eu^{3+/2+}$ couple in aqueous solution is commonly reported as around -0.35 V at neutral pH.[21] Although, the Eu^{3+} ions are not readily soluble in aqueous solution at neutral pH, chelating with this series of polyaminocarboxylate ligands here gives complexes for which the redox potential is shifted in a negative direction by stabilising the +III oxidation state.

The advantage of the $Eu^{III/II}$ couple with ligands is effective reversibility, and both the oxidised and reduced states are fairly stable kinetically in aqueous solution at neutral pH. The complexes form quickly after the addition of the ligand and can be rapidly electrochemically reduced. These Eu-L complexes have redox potentials over a suitable range for the low potentials used in the experiments. Although they are all thermodynamically susceptible to oxidation by H^+, this reaction is sufficiently slow that the redox couples are pseudo reversible. They can become reduced at the electrode and oxidised by transferring electrons to the redox sites in the MoFe protein.

Samples of BAPTA (4.76 mg), EGTA (3.8 mg), DTPA (3.93 mg) and Eu_2O_3 (5.28 mg, Alfa Aesar) were weighed and taken into the glovebox. The chemicals were held under N_2 purge in the antechamber of the glovebox for at least 2 min to minimise oxygen. The polyaminocarboxylate ligands were dissolved in 200 µL of 0.25 M NaOH solution (deoxygenated) individually and Eu_2O_3 was dissolved in 300 µL of 0.5 M HCl solution (deoxygenated), with the solutions being shaken until all species were well-dissolved. The Eu^{3+} solution was is divided and added to each ligand solution evenly to make an Eu-L mediator stock solution. The 0.25 mM mediator solution used in the study of nitrogenase was made by adding each mediator stock solution to the relevant amount of Tri-HCl buffer (described above) in a crimp-top vial.

Cyclic voltammetry was employed to study electrochemical properties of the chosen Eu ligand complexes. All Eu^{III}-ligand complexes were formed by adding each ligand to Eu^{3+} solution at a molar ratio of 1:1. Experiments were performed under anaerobic conditions in the N_2-filled

glovebox and a three-electrode electrochemical system was used comprising a glassy carbon working electrode, Pt wire counter electrode and SCE reference electrode.

Figure 2-14 shows the result of a cyclic voltammetry experiment on the Eu^{III}-ligand complexes (Eu-BAPTA, Eu-EGTA, and Eu-DTPA). The average midpoint potential of Eu-BAPTA is about -0.63 V vs SHE (standard hydrogen electrode). The values of Eu-EGTA (-0.865 V) and Eu-DTPA (-1.087 V) agree with previous studies (Table 2-3)[22].

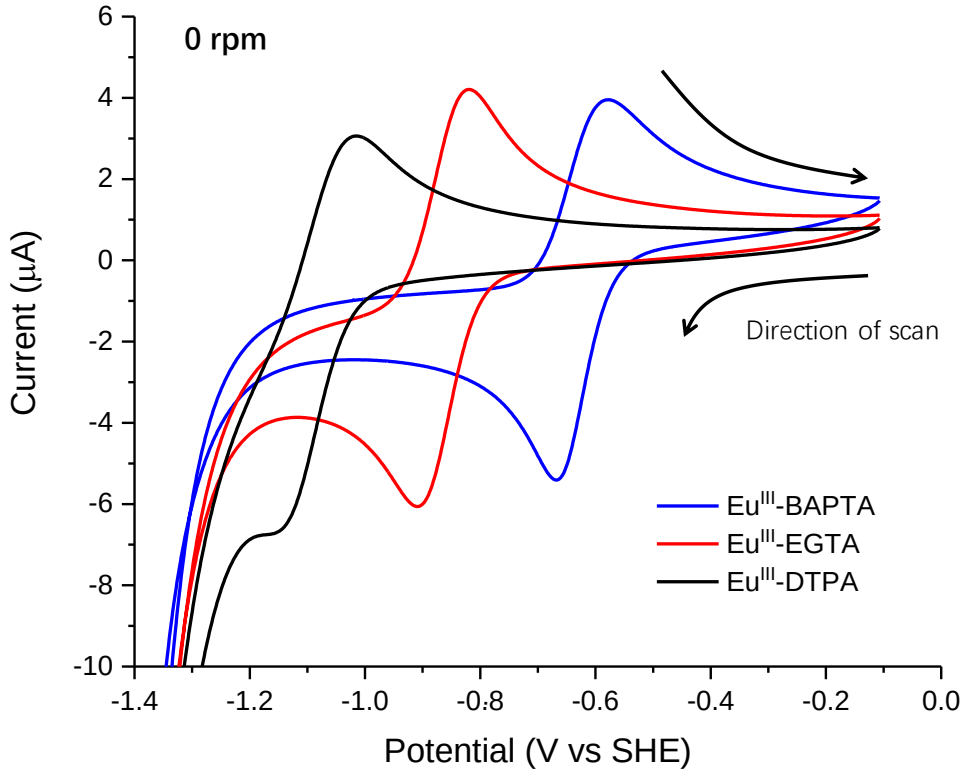


Figure 2-14: Cyclic voltammograms of Eu^{III}-BAPTA, Eu^{III}-EGTA and Eu^{III}-DTPA, each of concentration 2 mM, in 100 mM pH 8 Tris-HCl buffer, scan rate 10 mV s^{-1}.

Table 2-3: Redox potential, peak separation for a series of $Eu^{III/II}$-L complexes from the voltammograms presented in Figure 2-14.

Redox Couple	$E°_{pH\ 8.0}$ / mV vs SHE	ΔE_{pp} / mV [a]
$Eu^{III/II}$-BAPTA	−630	49
$Eu^{III/II}$-EGTA	−865	52
$Eu^{III/II}$-DTPA	−1087	78

a. The ideal for a one-electron process would be 59 mV. These are probably distorted by the proton reduction that occurs at low potential and will be better if scanned over a shorter scan range.

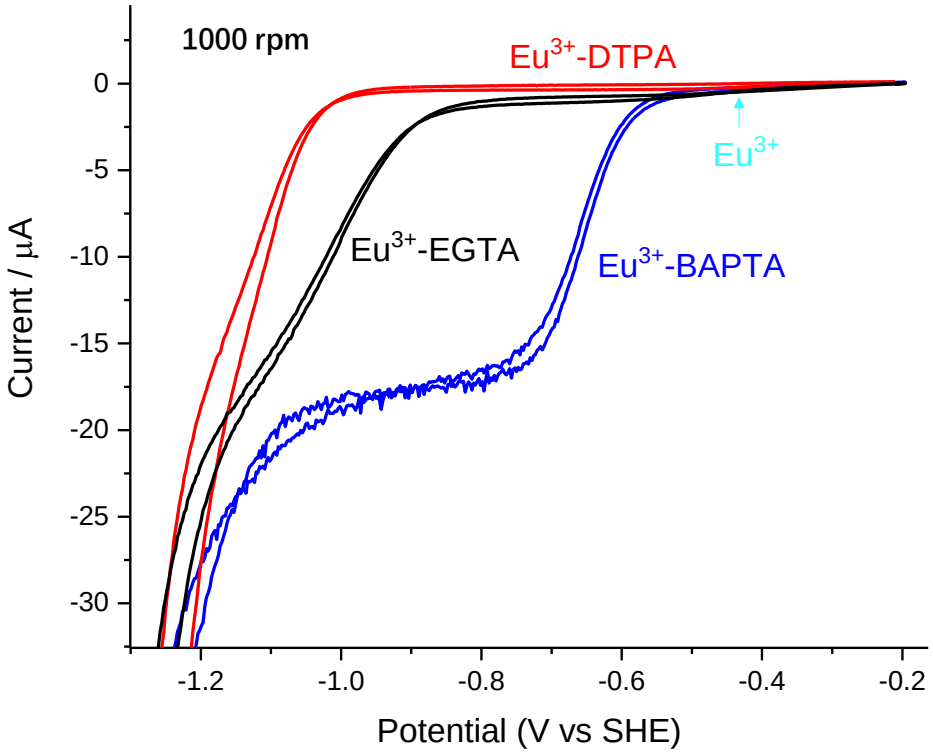


Figure 2-15: Cyclic voltammograms of Eu^{III}-BAPTA, Eu^{III}-EGTA and Eu^{III}-DTPA, each of concentration 2 mM, in 100 mM pH 8 Tris-HCl buffer, scan rate 10 mV s^{-1}, rotation rate 1000 rpm.

Figure 2-15 presents cyclic voltammograms of these three complexes at 1000 rpm rotation of the working electrode. In this case, there is no return oxidation current observed on the return sweep because the reduced form is spun away to the bulk solution from the diffusion layer of the working

electrode. Figure 2-15 also shows the effect of the proton reduction occurring at low potential on the shape of the cyclic voltammetry.

Based on the mid-potential of these three Eu^{III} complexes, they were chosen to form a cocktail of redox mediators to cover a range of potentials in which redox processes are likely to occur at the active site of nitrogenase. This cocktail of mediators is collectively referred to as Eu-L throughout this thesis.

All other mediators used in my programs like cobaltocene and methylene blue were prepared by dissolving deoxygenated compounds into Tris-HCl buffer in the glovebox to the concentration specified.

Reagents

The isocyanide solution was made by injecting pure methyl isocyanide (made by a previous group member, Pathinan Paengnakorn) or ethyl isocyanide (Hansa Fine Chemical) into the deoxygenated Eu-L mediator solution in a sealed crimp-top vial in the fume hood and transferring to the glovebox immediately. The vial was cooled on ice to minimise evaporation during Ar gas bubbling in the headspace for 2 min before use.

The acetylene gas used in experiments carried out in Oxford was generated by reacting calcium carbide (CaC_2) with O_2-free water in a custom-made Burris Bottle inside the glove box.

2.3.2 Experimental preparation

Anaerobic handling of nitrogenase

In this work, both wild-type and amino acid substituted MoFe proteins from *A. vinelandii* were provided by collaborator, Lance Seefeldt, the Department of Chemistry and Biochemistry, Utah State University, USA. Cell growth and protein isolation procedures are described elsewhere.[23] The protein was stored in a cryogenic vial (Nalgene) and frozen by snap freezing in liquid nitrogen

to keep the activity of the enzyme during storage. A low temperature was maintained during transport from Utah State University to University of Oxford by keeeping sealed samples on dry ice.

The nitrogenase protein was stored in a Dewar filled with liquid nitrogen in the Vincent group. A tablet of the frozen enzyme (~50 µL) was picked up and quickly put into a cryogenic vial with a drilled hole in the lid to keep pressure enable deoxygenating in the glove box antechamber. The vial was left in a vacuum flask filled with nitrogen transferred to a glovebox after deoxygenating. The protein solution was then slowly thawed and separated into aliquots of suitable volume for one experiment (2 nmol) in small Eppendorf tubes. The aliquots were snap frozen and stored in the fridge of the glovebox (-35 ℃) for later experiments.

Flow system and mass flow controller

SEC experiments were mostly conducted with a flow of electrolyte solution over the protein. The flow system consisted of a peristaltic pump (Watson Marlow 120U) and tubing equipped with appropriate fittings for the cell (diameter 0.1 mm, Kinetic Technologies).

A flow rate of gas was regulated by a mass flow controller (Brooks, controlled by Brooks Smart Interface). Gases were passed through an oxygen scrubbing filter (Restek Super Clean gas filter, <1 ppm O_2) before going into the anaerobic glovebox.

2.3.3 Spectroelectrochemical cell

The SEC cell used in this work was designed by R. Hidalgo Gonzalez (a previous member in the Vincent group) and constructed by the PTCL workshop, Department of Chemistry. Figure 2-16 shows the SEC cell design fitted with a trapezoidal prism. The whole-cell body and base plate were made of polyether ether ketone (PEEK). The set up was designed to make it possible to introduce gas or solution either directly into solution in the back of the cell or via the flow system while a constant potential was applied to the cell. The ATR element used in this study is a Si multibounce

internal reflection element (8.39x5x1 mm^3 with an incidence angle of 39°, Crystal GmbH), with calculated penetration depth (dp) in an aqueous solution of ca. 0.50 µm.

For electrochemical control of protein, three modified electrodes (as shown in Figure 2-16) were designed and located via the top of the spectroelectrochemical cell. Electrodes were connected to a potentiostat (Autolab 128N or 302) to study the effect of different potentials on ligand binding to nitrogenase MoFe protein and to control the reaction between enzyme and substrates.

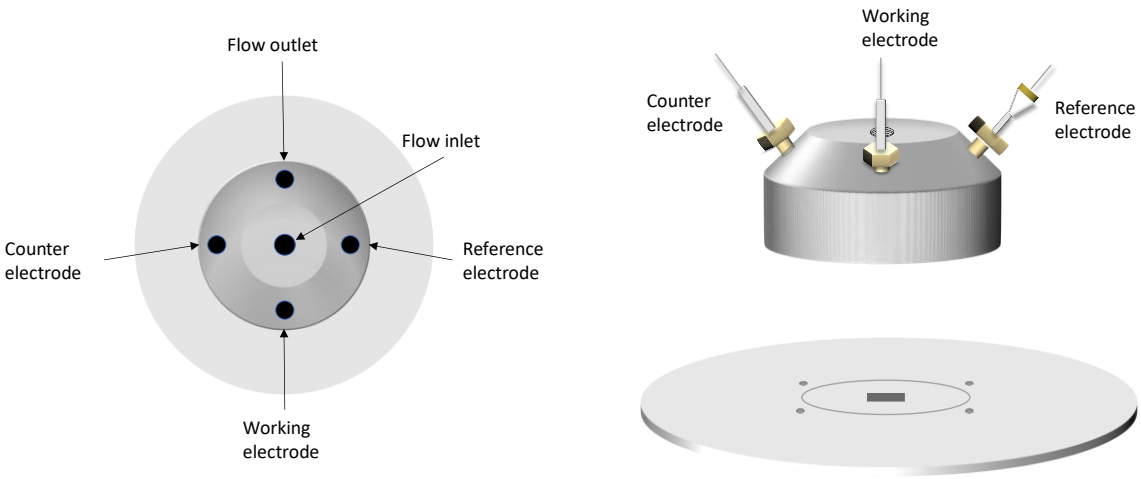


Figure 2-16: A diagram of the ATR-IR spectroelectrochemical cell with three electrodes used for nitrogenase experiments.

Reference electrode

Due to the Ag/AgCl reference electrode being incompatible with the Tris-HCl buffer used with nitrogenase, a saturated calomel reference electrode (SCE) was employed in this project to avoid the small concentration of Ag ions reacting with proteins and producing an insoluble precipitate in the porous liquid junction structure of the electrode. A SCE reference is based on the reaction between elemental mercury (Hg) and mercury chloride (calomel, Hg_2Cl_2), and the aqueous phase in contact with the mercury and the mercury chloride is a saturated solution of potassium chloride (KCl). The potential of the SCE is -0.241 V *vs*. SHE at 25 °C.[24] The electrode potential is based on the following reaction:

$Hg_2Cl_{2\,(s)} + 2e^- \leftrightarrow 2Hg_{(l)} + 2Cl^-$

A small leak-free saturated calomel reference electrode was designed to fit into the spectroelectrochemical cell as shown in Figure 2-17. The top part of the SCE comprises Hg and Hg_2Cl_2 (Fisher) in a micro-point pipette tip sealed by a rubber stopper (top) and glass wool (bottom). The polyetherether ketone tube contains a saturated KCl solution and with a nonporous junction to maintain a concentrated chloride solution which is taken from an inoperative Ag/AgCl leak-free reference electrode (Warner Instruments). The electrode was sealed using silicone sealant to the cell, which is easy to open again for repairs to the reference electrode.

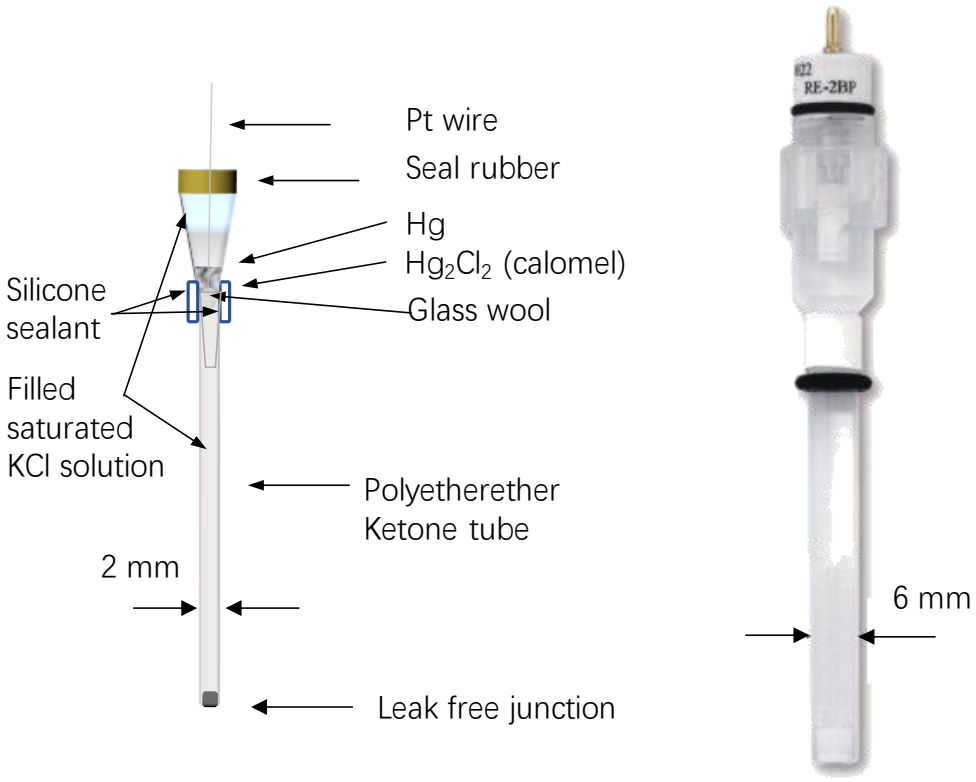


Figure 2-17 : Design of a mini leak-free saturated calomel reference (left) for the ATR-IR spectroelectrochemical cell, and comparison with a commercial saturated calomel reference electrode (right, RE-2BP, ALS).

Counter electrode

The counter (auxiliary) electrode serves with the working electrode, to provide a circuit through which current is either applied or measured. The counter electrode in the spectroelectrochemical study is a Pt wire (diameter 0.2 mm) in a Teflon tube sealed by epoxy resin. To ensure that the current can pass through it fast enough to allow a reaction to be controlled and measured smoothly, the naked part of the Pt wire is located in the solution flow (between the inlet and outlet channels).

Working electrode connections

A solid carbon rod is used as the working electrode connector for nitrogenase protein study with a high surface area carbon paper and carbon particle network as the working electrode. Using carbon as a working electrode can minimise proton reduction at the very negative potentials, and carbon does not react with exogenous ligands of interest.

A piece of carbon paper (made of carbon fibres) is placed between the carbon nanoparticle layer modified with the enzyme, and the carbon rod, and this carbon paper with ca. the size of the ATR prism is pressed down against the particle layer by the carbon rod when the ATR-IR spectroelectrochemical cell is closed. The connection across the carbon layer means the majority of enzyme molecules should be in electronic contact as shown in Figure 2-18.

To have an effective connection to the potentiostat, the carbon rod is twisted by platinum wire and packed in a Teflon tube. Epoxy resin is used to seal the end of the tube allowing only the carbon part to be in the solution in order to avoid side reactions from Pt wire in the solution and keep the cell airtight. The Pt wire is connected to a cable from the controlling potentiostat hardware.

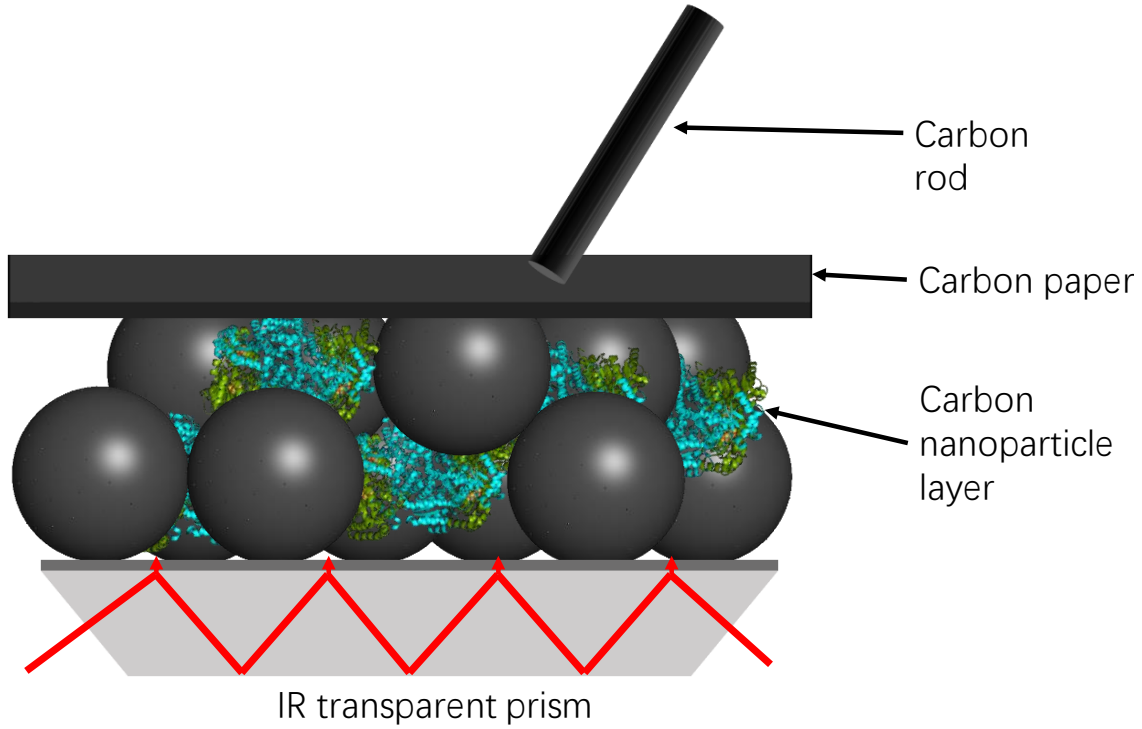


Figure 2-18: A diagram displaying the working electrode connection (not to scale). The carbon nanoparticle film with adsorbed MoFe protein is deposited on the IR transparent prism. A piece of carbon paper is pushed against the film by a carbon rod to have an efficient electrical conductivity.

Daily maintenance

The SEC cell including electrodes and tubing was flushed with plenty of water by the pump after an experiment. Working and counter electrodes were not moved from the top of the cell after cleaning, but the reference electrode was removed and stored in saturated KCl solution to keep the potential accurate. The potential of the home-made reference electrode was checked against the potential of a commercial saturated calomel reference electrode by a voltammeter before using in an experiment. If the value between the two references was not stable or larger than 7 mV, the silicone sealant between the top and tube of the home-made reference electrode was opened and saturated KCl solution was refilled slowly to vent bubbles which may have formed in the tube. The resistance of the working and counter electrodes was also checked to ensure that the electrodes are not damaged.

After rinsing with water, the prism was sonicated two times with the appropriate amount of 98% H_2SO_4 for 5 min and 15 min. Then the prism was sonicated in 70% HNO_3 solution for 1 hour. It was then rinsed with plenty of water after sonicating with the acid.

Operation

Most of the experiments described in this thesis involve studying changes of the infrared spectrum when changing the potential at the working electrode where enzymes are immobilised. Control experiments of substrates/inhibitors over a series of potentials were tested first in the presence or absence of the enzyme. Normally, each potential would be held for at least 30 min toallow a slow reaction to happen. For cases where a reaction was observed at a given potential, the new potential was applied after there was no further change in the infrared spectrum over 10 min.

In each experiment, a series of infrared spectra are recorded. Figure 2-19 presents a simple set of operations which were used to process infared spectra. Panel (A) shows two infrared absorbance spectra taken at two different potentials, -0.7 V (blue line) and -0.9 V (red line) in a spectroelectrochemical study of interactions between MoFe protein and CO. These spectra could not directly be used to provide information on the protein sample on the Si prism (ATR crystal) due to the influence of water in the cell. The subtracted result between two spectra (difference spectrum, -0.9 V minus -0.7 V) shown in Figure 2-19 (B) presents far more details of the changes with potential. The spectrum in Figure 2-19 (D) focusses on the metal carbonyl v(CO) stretching region, and has the absorbance scale a thousand times enlarged compared to the original spectra. In addition to the broad v(CO) bands of interest, this spectrum also shows some finer peaks due to changes water vapour in the sampling environment. Since the optics are open to the glove box, this change is water vapour might result from slight leaking of the flow tubing or normal dehydration from operation of the dry glovebox after bringing in the cell. Therefore a water vapour spectrum as shown in Figure 2-19 (C) is required to subtract these changes (a fractional contribution from the water vapour spectrum is substracted to take the known water vapour

peaks to zero). The resulting 'water vapour corrected' spectrum is shown in Figure 2-19 (E), and more clearly displays the differential absorbance resulting from interactions of the MoFe protein and CO on stepping from -0.7 V to -0.9 V.

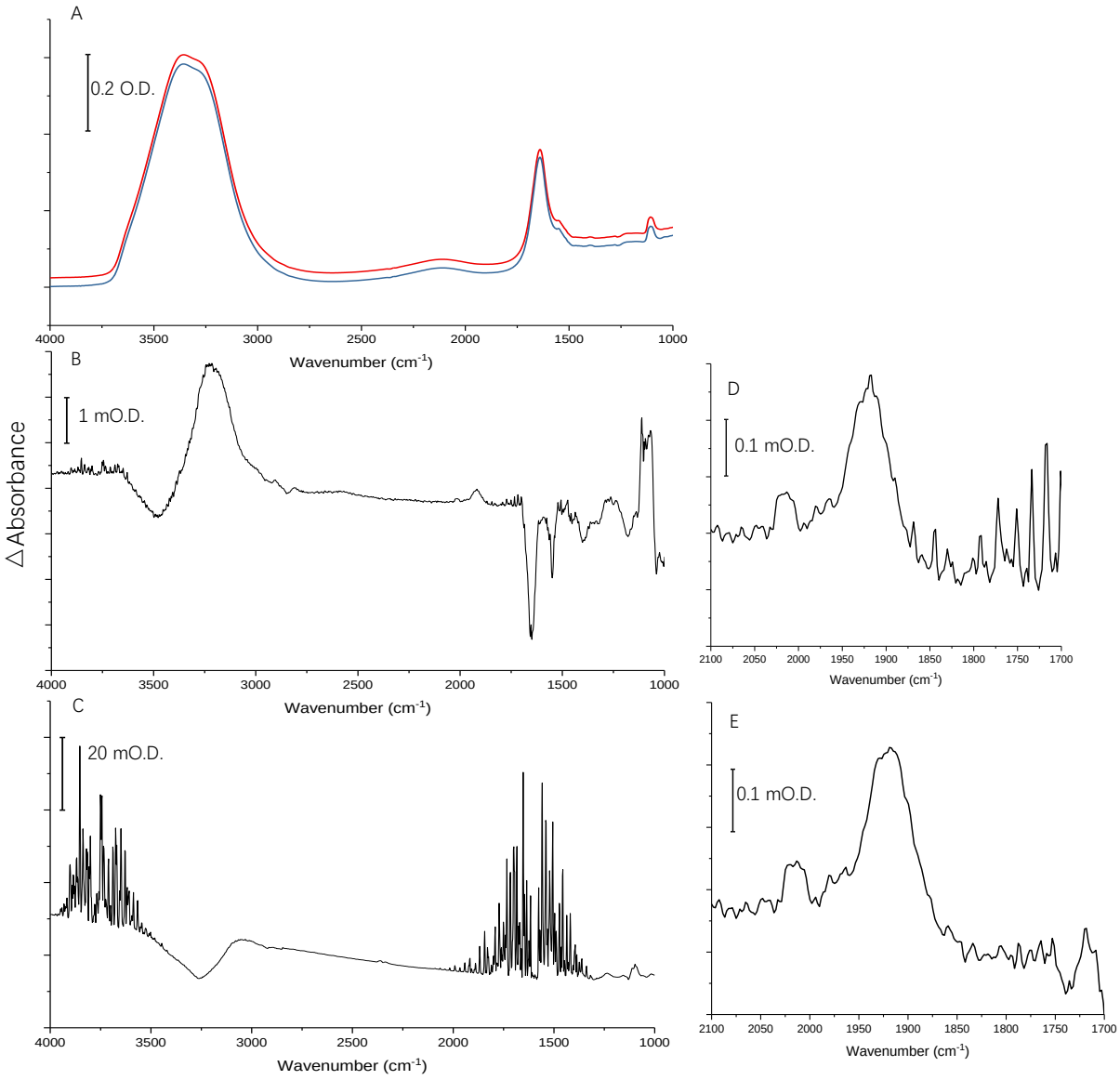


Figure 2-19: IR absorbance spectra show the experimental operations performed to work up a spectroelectrochemical experiment. (A) shows two spectra at different potentials (— -0.7 V, — -0.9 V) under saturated CO solution (Tris-HCl, pH 8.0 with Eu-L). (B) shows the difference between the two spectra from panel (A) after spectral subtraction. (D) is the zoom view of the spectra in the range of the metal carbonyl stretching modes. (E) is processed from the spectrum (D) after subtractingthe water

vapour spectrum (C). For these experiments, the MoFe protein was immobilised on the working electrode by direct adsorption.

There is a small but significant combination band (IR and Raman) of the bending and libration modes of liquid water at about 2125 cm^{-1} which is also evident in Figure 2-19 (A). Due to slight changes in water close to the electrode with potential, this combination peak would change the baseline of spectra when different potentials are applied, so a linear baseline correction is a reasonable operation to remove the slope in a narrow region of interest during spectral analysis.

Bibliography

1 P. Zanello and N. G. Conelly, *Inorganic Electrochemistry: Theory, Practice and Application*, The Royal Society of Chemistry, Cambridge, 2003.

2 P. W. Atkins, J. De Paula and J. Keeler, *Atkins' Physical Chemistry*, Oxford University Press, Oxford, 11th edn., 2047.

3 W. R. Browne, *Electrochemistry*, Oxford University Press, Oxford, 2018.

4 R. Hidalgo, P. A. Ash, A. J. Healy and K. A. Vincent, *Angew. Chemie - Int. Ed.*, 2015, **54**, 7110–7113.

5 J. Kirn and D. C. Rees, *Nature*, 1992, **360**, 553–560.

6 A. J. Bard and L. R. Faulkner, *Electrochemical Methods Fundamentals and Application*, John Wiley & Sons, New York, 2nd edn., 2001.

7 J.Crank, *The Mathematics of Diffusion*, CLARENDON PRESS, Oxford, 1975.

8 J. A. Stubbe, D. G. Nocera, C. S. Yee and M. C. Y. Chang, *Chem. Rev.*, 2003, 103, 2167–2201.

9 P. N. Bartlett, *Bioelectrochemsitry: Fundamentals,Experimnetal Techniques and applications*, Wiley, 2008.

10 C. Léger and P. Bertrand, *Chem. Rev.*, 2008, **108**, 2379–2438.

11 P. R. Griffiths and J. a. De Haseth, *Fourier Transform Infrared Spectrometry, Second Edition*, 2006.

12 K. Nakamoto, *Infrared and Raman Spectra of Inorganic and Coordination Compounds*, John Wiley & Sons, New Jersey, 6th edn., 2009.

13 G. B. and M. Bigorgne, *Spectrochim. Acta*, 1971, **27A**, 139.

14 Walter F. Edgell and John Lyford IV, *J . Chem. Phys*, 1970, **52**, 4329.

15 and S. B. H. Stammreich, K. Kawai, Yara Tavares, P. Krumholz, J. Behmoiras, *J . Chem. Phys*, 1960, **32**, 1482.

16 R. W. Stephany, M. J. A. de Bie and W. Drenth, *Org. Magn. Reson.*, 1974, **6**, 45–47.

17 F. A. Cotton and F. Zingales, *J. Am. Chem. Soc.*, 1961, **83**, 351–355.

18 P. Paengnakorn, P. A. Ash, S. Shaw, K. Danyal, T. Chen, D. R. Dean, L. C. Seefeldt and K. A. Vincent, *Chem. Sci.*, 2017, **8**, 18967–18971.

19 P. j. Larkin, *IR and Raman spectroscopy principles and spectral interpretation*, Elsevier Inc., 2nd edn., 2017.

20 N. Kaltsoyannis and P. Scott, *The f element*, Oxford University Press, 1999.

21 L. R. Morss and H. O. Haug, *J. Chem. Thermodyn.*, 1973, **5**, 513–524.

22 K. A. Vincent, G. J. Tilley, N. C. Quammie, I. Streeter, B. K. Burgess, M. R. Cheesman and F. A. Armstrong, *Chem. Commun.*, 2003, **3**, 2590–2591.

23 J. Christiansen, P. J. Goodwin, W. N. Lanzilotta, L. C. Seefeldt and D. R. Dean, *Biochemistry*, 1998, **37**, 12611–12623.

24 J. W. Beams, A. J. Weed and E. G. Pickels, *Science*, 1933, **78**, 338–340.

Chapter 3

Approach development

Although the spectroelectrochemical approach developed in the Vincent group works well for hydrogenase, there are a number of reasons why this method is not suitable for nitrogenase. Pathinan Paengnakorn, a previous D.Phil. student in Vincent group was able to study CO binding to the MoFe protein trapped in a Nafion network system. However, there were a lot of disadvantages to the Nafion approach, including the fact that Nafion obscures the spectrum below about 1400 cm^{-1}, and irreversible side reactions were observed between some nitrogenase substrates and Nafion. Therefore, a new spectroelectrochemical approach needed to be worked out in order to develop these studies further.

3.1 Nitrogenase protein immobilisation

In order to collect infrared and electrochemical data under solution flow, the enzyme needs to be trapped on the IR transparent prism efficiently. Due to the specific properties of the protein under study (size, surface charge and hydrophobicity) and substrates/inhibitors, a distinct approach must be developed to fit each target enzyme.

A previous DPhil student in the Vincent group, Pathinan Paengnakorn, worked on nitrogenase using a Nafion-based working electrode for the study of CO binding to MoFe protein under potential control.[1] Nitrogenase MoFe protein was trapped in a layer of Nafion surrounding the carbon electrode with the Nafion titrated to a biologically compatible pH with buffer. This approach to nitrogenase spectroelectrochemical study was explored first.

3.1.1 Nitrogenase SEC in Nafion

An aqueous Nafion suspension (a sulfonated tetrafluoroethylene-based fluoropolymer-copolymer as shown in Figure 3-1) is the first of a class of synthetic polymers with ionic properties, known as ionomers, discovered in the late 1960s by Walther Grot of DuPont.[2] It is commonly used as an ionic conductor in fuel cells because of its excellent thermal and mechanical stability. At the beginning of this project, Nafion was adapted for use in combination with carbon nanoparticles to create a high surface-area working electrode to study the electrocatalytic properties of enzymes.

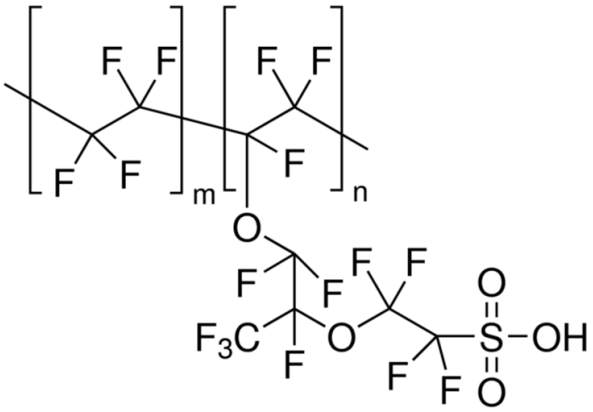
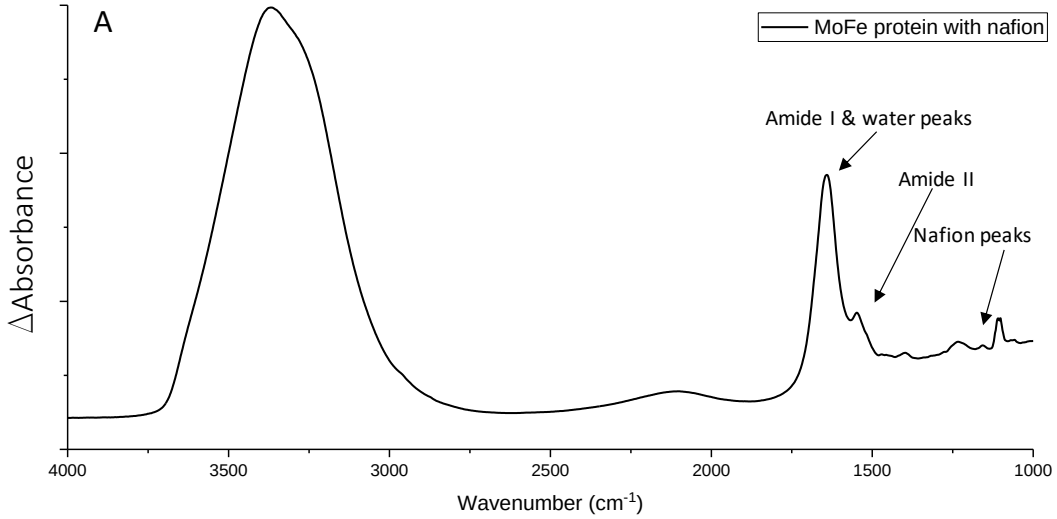


Figure 3-1: Structure of Nafion perfluorinated membrane used to trap enzyme on the ATR-IR prism.

The aqueous Nafion solution for enzyme was prepared by mixing with Tris-HCl buffer titrated to pH 8.0 with NaOH. Protein was mixed with aqueous Nafion suspension and put on the prism located on the SEC cell baseplate as shown in Section 2.3.3. The mixture was then partially dehydrated before covering with carbon paper. The SEC Cell with three electrodes was then screwed onto the baseplate and filled with buffer solution. Gaseous reagents were bubbled into the headspace of a crimp-top vial and were flowed into the cell by a peristaltic pump.



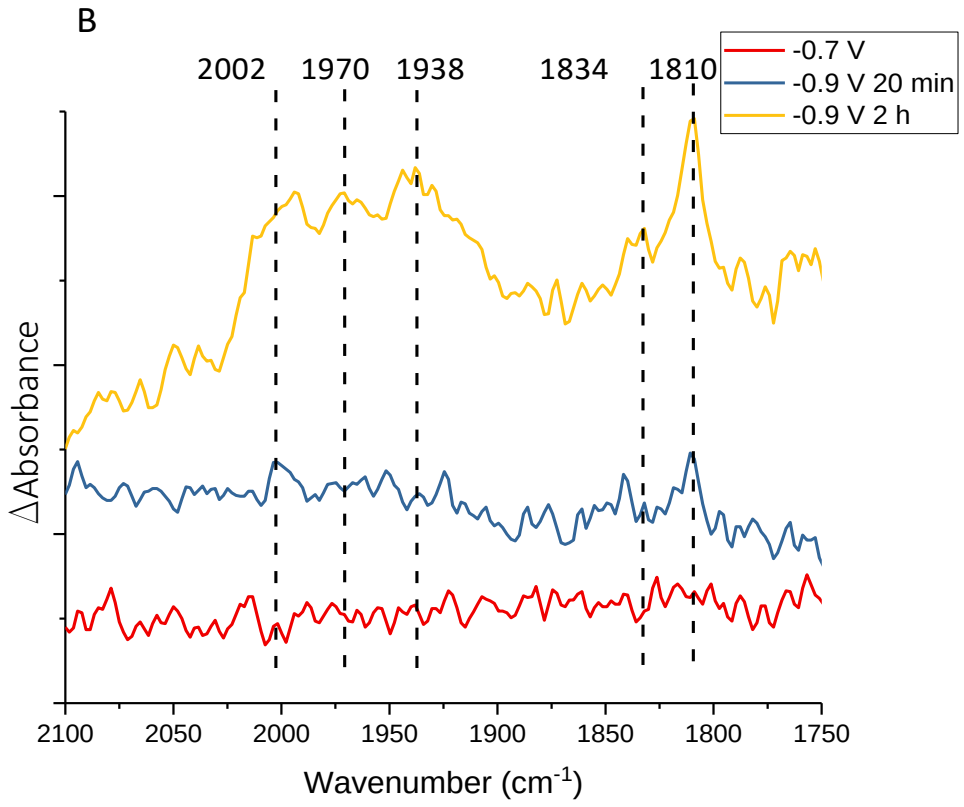


Figure 3-2: IR spectra of wild type MoFe protein trapped in a Nafion network surrounded by CO saturated Tris-HCl buffer pH 8.0. (A) shows a wide wavenumber range. The peaks of Amide I & II, O-H bending from water and Nafion are prominent. (B) displays absorbance spectra of CO binding to the active site of MoFe protein which took 2 hours to be observed at -0.9 V with CO saturated solution in the cell (—).

Figure 3-5 (A) shows a spectrum of the Nafion film with MoFe protein before applying a potential. It shows the vibrational bands in the range from 3000 cm^{-1} to 3500 cm^{-1} which is a symmetric stretch (ν_1), asymmetric stretch (ν_3) and overtone of bending stretch (ν_2) of water. Additionally, a bending vibration of water appears between 1500 cm^{-1} and 1700 cm^{-1}, which are close to the peaks known as amide I & II (~1650 cm^{-1} & 1550 cm^{-1}) from proteins. The combination of ν_2 and libration can be observed at about 2125 cm^{-1}. The bands of Nafion block the range from 1250-1050 cm^{-1}. No strong interfering peaks appear between 2200-1800 cm^{-1} where interesting substrates/inhibitors like CO and CN- ligands bound to the active site would give stretching bands.

In experiments using the MoFe protein trapped in an aqueous Nafion suspension, it took about 2 hours before clear peaks of CO-metal species were observed as shown in Figure 3-2 (B) when the MoFe protein was exposed to CO saturated mediator solution at -0.9 V. A weak low frequency feature at 1810 cm $^{-1}$ appeared within about 20 min, and is likely to arise from a bridged Fe-CO-Fe species forming at low CO concentration.[3] This would be consistent with a low effective CO concentration due to difficulty in CO passing through the Nafion film to bind to MoFe protein. The broad peak between 1900 cm^{-1} and 2010 cm $^{-1}$ appeared later in the experiment, and is consistent with terminal bound CO-metal species in the literature.[4]

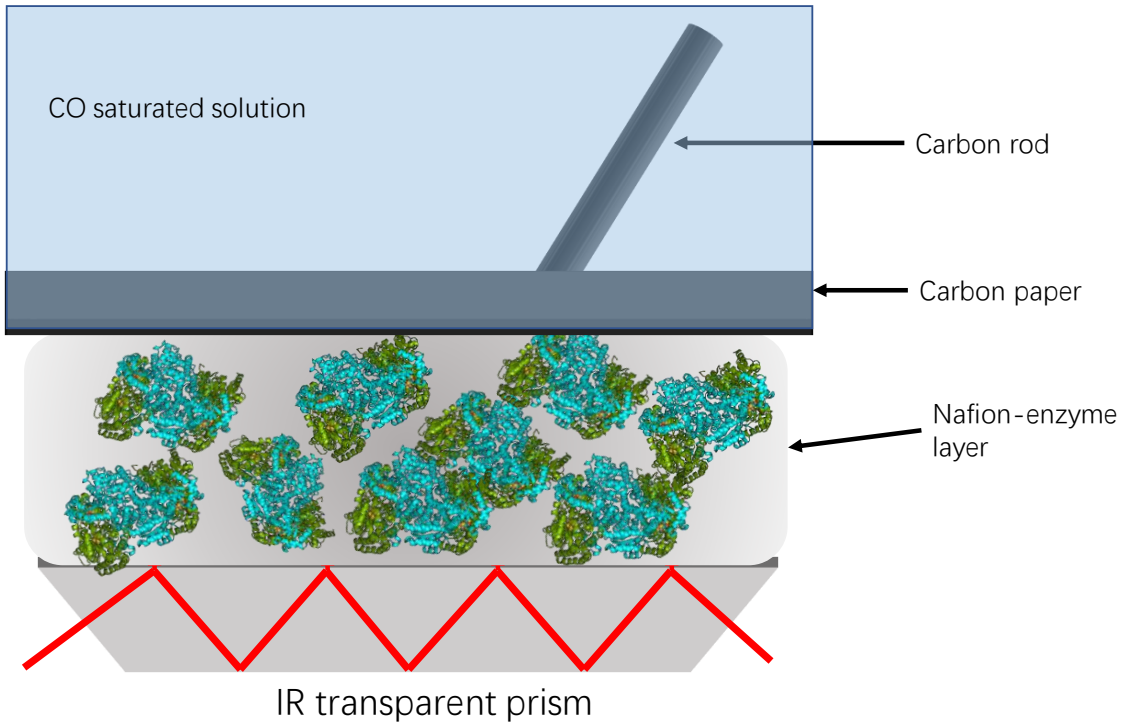


Figure 3-3: A diagram displaying how the Nafion film with MoFe protein is deposited on the IR transparent prism in saturated CO solution in a SEC cell (not to scale).

The decrease of catalytic proton reduction current from CO inhibition occurred fast after introducing CO, but the higher wavenumber bound CO-metal could not be observed at -0.9 V until 2 hours had elapsed. As shown in Figure 3-3, the MoFe protein is trapped in the Nafion film such that the enzyme close to the carbon paper can respond to an electrochemical signal efficiently.

After bubbling CO gas, the proton reduction by this portion of the enzyme is quickly inhibited by CO, whereas the enzyme in the region where the evanescent wave penetrates is hardly touched by CO which would be why there is little change in the infrared spectrum over the metal carbonyl range until much later.

Using Nafion as an immobilisation approach enables the enzyme to be trapped onto the prism in the SEC cell. However, in experiments on nitrogenase, Nafion causes some limitations. It would be difficult to observe peaks below 1400 cm^{-1} where asymmetric and symmetric stretches of CF_2 from Nafion bands occur. The appearance of negative peaks between 1700 cm^{-1} and 1450 cm^{-1} indicates dramatic loss of protein over time during experiments, as shown in Figure 3-4. Some side reactions between substrates like methyl isocyanide and Nafion were observed in the study from the previous member (Pathinan Paengnakorn) of the Vincent group.

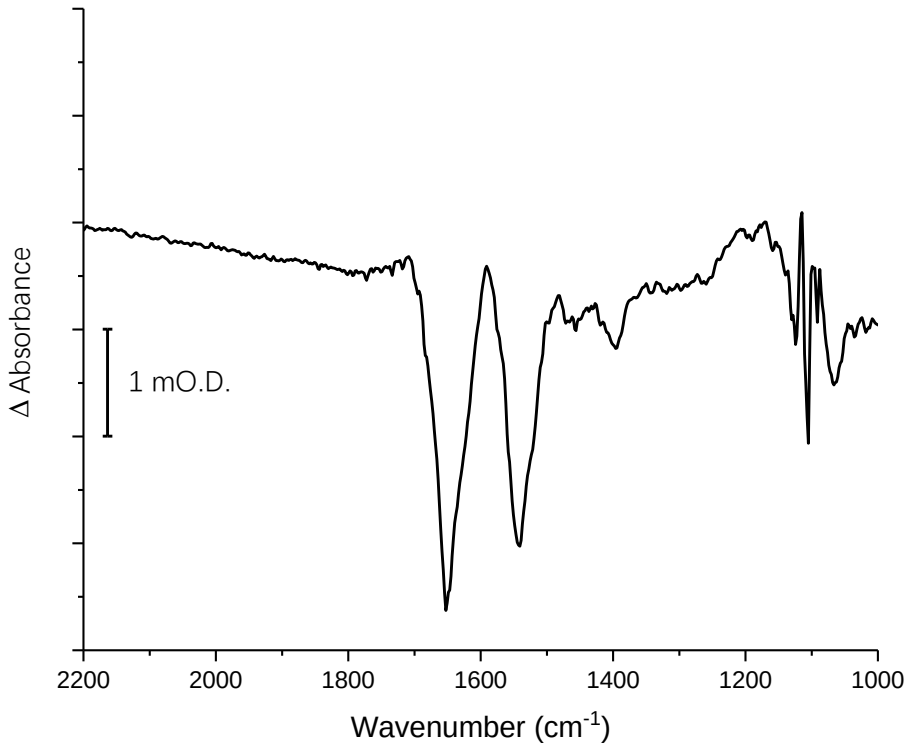


Figure 3-4: Difference spectrum of Nafion film with MoFe protein at -0.9 V showing changes below 1700 cm^{-1} in amide and water bands after 10 min at the same potential. These would obscure spectral

change in this range, but also shows that the protein is not trapped in a stable way in the Nafion film. Signal-to-noise ratio is poor below 1400 cm^{-1} due to strong IR absorption by Nafion.

3.1.2 Protein film infrared electrochemistry

Protein film infrared electrochemistry (PFIRE) is a method coupling PFE (Protein Film Electrochemistry) with ATR-IR spectroscopy, allowing electrochemical control of the enzyme and simultaneous collection of infrared spectra. This technique has been successfully applied to NiFe hydrogenase in the Vincent group[5] with the enzymes physically adsorbed on commercial carbon black particles with high surface area, BP2000 (BLACK PEARLS 2000 Carbon Black, CABOT), to a high loading by simply mixing enzyme solution with particles at low temperature for several hours.

Attempts were made to extend this physical adsorption approach to nitrogenase MoFe protein. To try this, carbon particles were prepared as a 20 mg/mL suspension in Tris-HCl buffer, and sonicated in an in Ultrasonic Bath (from Ultrawave) for 1 hour, to allow particles to distribute evenly in solution. Then 2 nmol protein was left to adsorb in a 5 µL particle suspension on ice for 2 hours. This mixture was loaded onto the prism and allowed to partially dry to form a particle layer on the prism.

The black trace in Figure 3-5 shows significant amide II band, indicating that there was quite a lot of enzyme immobilised on the carbon electrode. Without Nafion impeding reactant access, the ligand was able to bind enzyme directly and the ligand-cluster binding peaks clearly appeared. The infrared spectrum (blue line) in Figure 3-6 displayed that CO bound rapidly to the MoFe protein when the potential was changed from -0.7 V to -0.9 V. The Infrared response was much quicker and stronger than in the experiment with the Nafion membrane. The bands continued to grow over 1 hour and the position of peaks was slightly different compared to the Nafion experiments indicating different CO-metal species formation, possibly due to improved mass transfer in film. More detail of infrared data for CO binding will be displayed in Chapter 4 using this approach to immobilise enzyme.

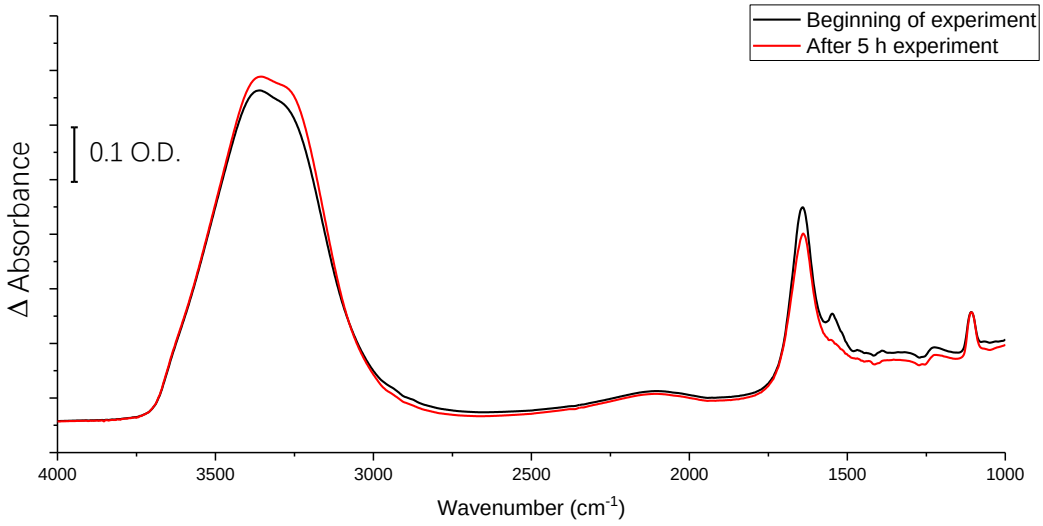


Figure 3-5: The spectra of nitrogenase MoFe protein physically adsorbed on carbon particle at the beginning in black line and the end of the experiment in red line (512 scans, 4 cm^{-1} resolution).

The red spectrum in Figure 3-5 shows a substantial depletion of the amide II band which indicated that a significant amount of protein is lost during a 5-hour experiment under solution flow. Electron transfer via the working electrode connection through carbon, from carbon rod to carbon paper and carbon particles, clearly allows control over the redox state of the enzyme. The high surface area of the electrode gave sufficient protein coverage for a strong IR signal. However, it was found that the MoFe protein is not adsorbed well enough to sustain the loading during an experiment. Thus, efforts were made to explore different strategies to improve nitrogenase loading onto the carbon particles on the ATR-IR prism.

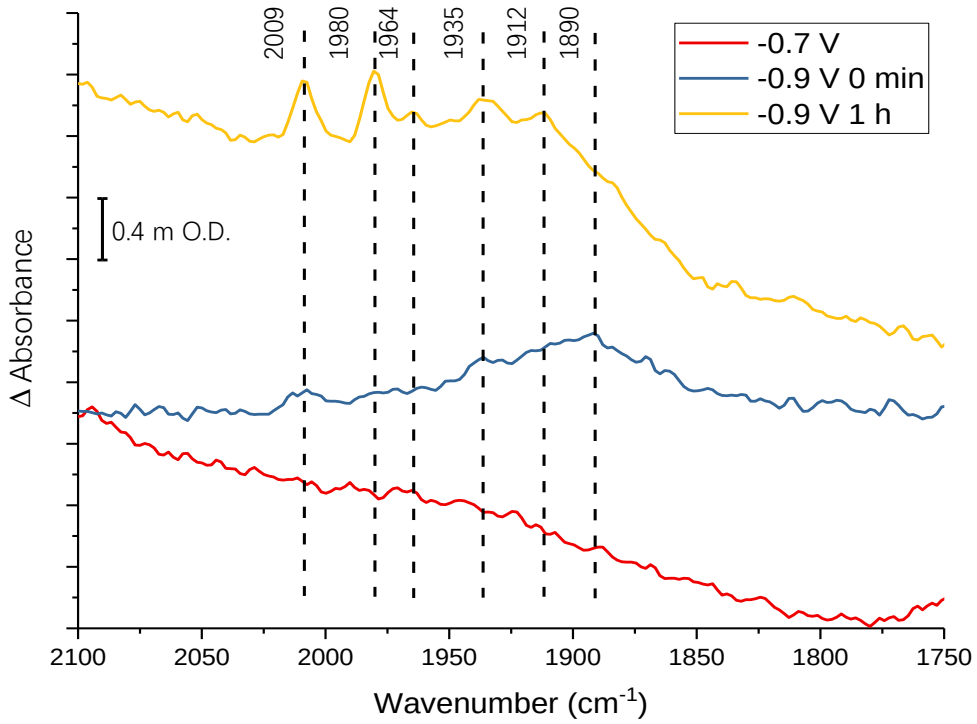


Figure 3-6: Infrared spectra of MoFe protein absorbed in carbon nanoparticle (BP2000) in CO saturated solution controlled by electrochemistry. No CO binding peak appeared at -0.7 V (—), but peaks arose immediately after applying the potential of -0.9 V (—). Different species were formed over time (—). Each spectrum is processed against a background spectrum at –0.7 V prior to addition of CO (512 scans, 4 cm^{-1} resolution).

It was shown in this approach that electron transfer from the working electrode to the enzyme on a high surface area carbon particle does give a clearer spectral response to binding of the inhibitor CO. This method allows the monitoring of coordination changes in the active of the MoFe protein, by means of IR spectroscopy, whilst it is engaging in catalytic proton reduction turnover. No side reaction or interference in the useful region of IR spectrum was observed from the carbon particles. However, much improvement is needed to increase the stability of the protein film to solution flow.

3.1.3 Covalent attachment and carbon modification

To increase the stability of immobilisation of the MoFe protein in the carbon particle film, covalent bonding was considered instead of just physical adsorption. Various functional groups such as the hydroxyl (-OH) or carboxyl group (-COOH) are found on the surface of carbon particles, so, a peptide bond was judged suitable to fix the enzyme to carboxyl groups through lysine residues, which have the side chain lysyl ($-(CH2)_4NH_2$). There are a number of lysines (shown in Figure 3-7) in the MoFe protein, and about 80% of lysyl side chains are on the surface of the MoFe protein (displayed in Figure 3-7) and thus should be able to support covalent bonds to carboxyl groups to give a stable network in the particle film.

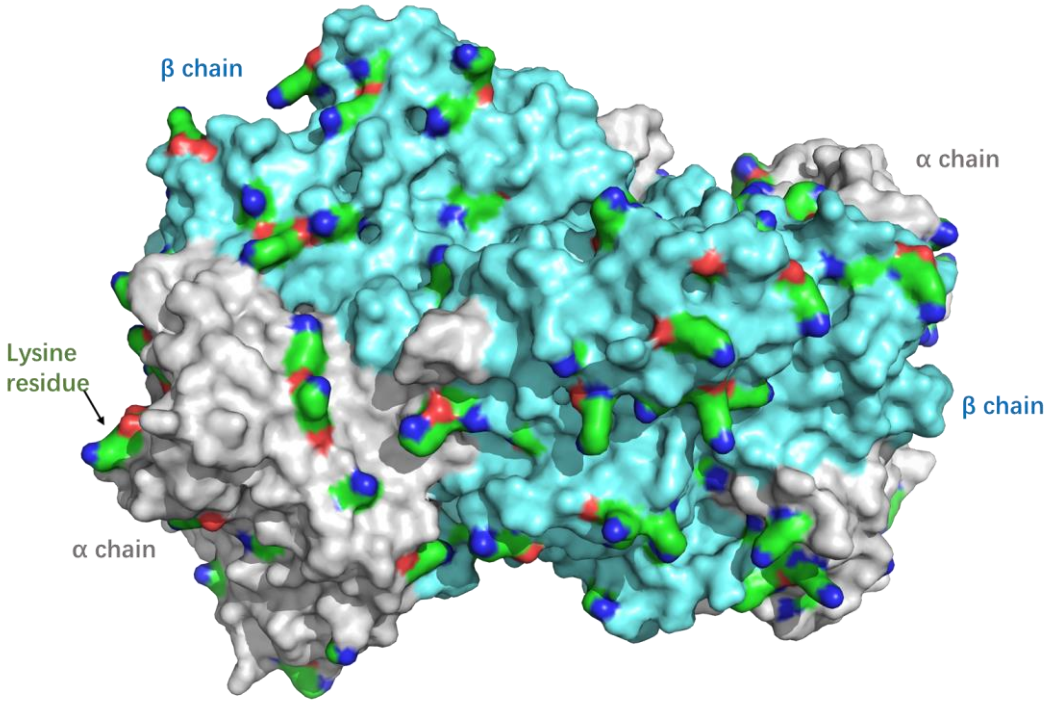


Figure 3-7: The surface of MoFe protein (PDB: 1M1N) shows the structure of the $\alpha_2\beta_2$ heterotetramer (α chain in grey, β chain in cyan) and lysine residues on the surface of the protein (coloured by elements).

Table 3-1: Calculated number of lysine groups in and on the surface of the MoFe protein

Chain of MoFe protein	Total lysine groups	Surface lysine groups
α chain	36	~30
β chain	38	~31

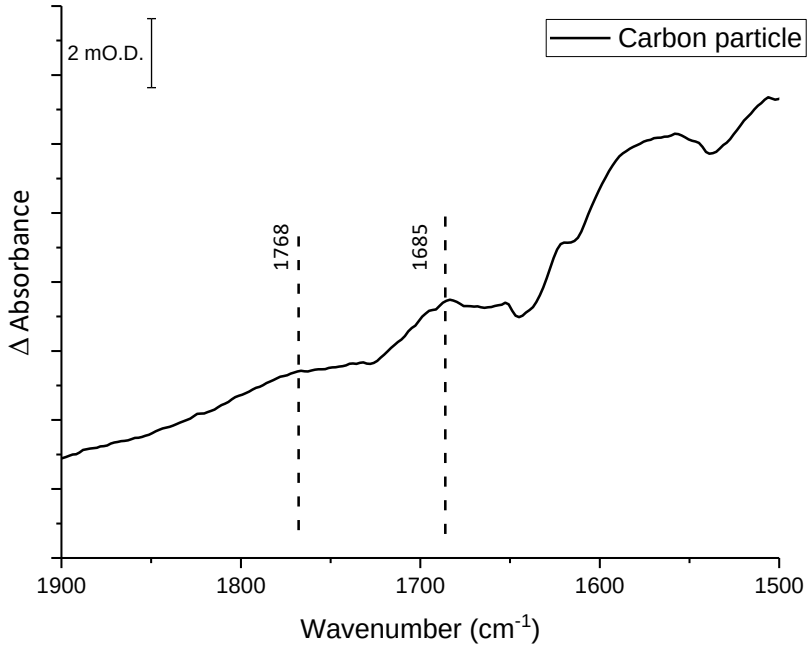


Figure 3-8: Infrared spectrum of carbon particle on the ATR-IR prism shows some carboxyl groups on the carbon film with the bare prism as background (512 scans, 4 cm^{-1} resolution).

To define the feasibility of enzyme binding to carbon particles, the number of carboxyl groups on the carbon was considered by the intensity of the carboxyl peak in the infrared spectrum. The carbonyl stretching C=O of carboxyl groups may appear as an intense band from 1760 cm^{-1} to 1660 cm^{-1}, the exact position of this band depends on the environment of the carboxylic acid. Figure 3-8 shows the spectrum of bare carbon particles used for physical adsorption on the prism. Two weak peaks appear at 1768 and 1685 cm^{-1}. Although a BP2000 carbon particle itself contains some

carboxyl groups, these are still unlikely to be sufficient to form covalent bonds with lysine groups on the surface of the MoFe protein.

To increase the possibility for the covalent bonds between enzyme and carbon particles, the carbon particles were modified to increase the number of carboxyl groups. These can be introduced by mechanical[6], chemical[7] or electrochemical[8] routes. Three different chemical ways were tried to enhance the number of carboxyl groups on the carbon surface.

Acid treatment

Yudianti used a mixture of nitric and sulfuric acid (3:1) to functionalize Multi-Wall Carbon Nanotubes (MWCNTs) by chemical oxidation to get more carboxyl groups[9]. Following this method, 20 mg BP 2000 carbon particles were suspended in a mixture of 70% nitric (0.75 mL) and 98% sulfuric (0.25 mL) acid. The carbon particles then were sonicated overnight, before centrifuging and washing with distilled water to a neutral pH. A 5 µL aliquot of the particle suspension was placed on the prism to obtain the infrared spectrum shown in Figure 3-9. The carbonyl vibrational band from carboxyl groups is clear at 1721 cm^{-1} indicating an increase of carboxylation on the surface of the functionalized carbon particles.[10]

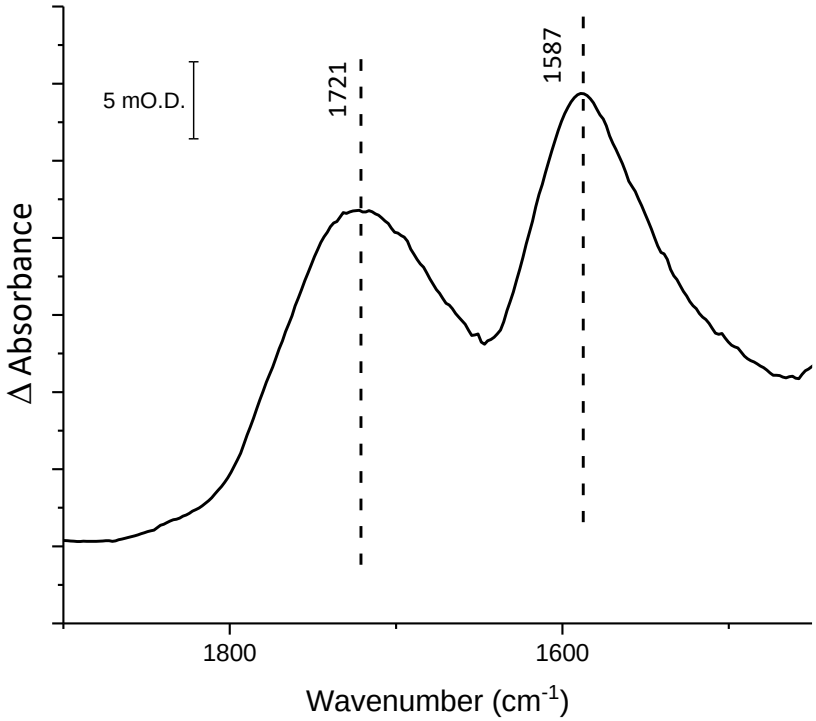


Figure 3-9: Infrared spectrum of carbon particles treated by nitric and sulphuric acid (3:1) with the bare prism as background (512 scans, 4 cm^{-1} resolution).

Another method to increase oxygenated acidic surface groups on the carbon surface was tested by using a mixture of acetic anhydride and nitric acid.[11]

To a suspension of 20 mg carbon particles in 0.8 mL acetic anhydride, 0.2 mL 70% nitric acid was added gradually at below 5 °C over 5 hours. Then the reaction was allowed to carry on at room temperature for another 5 hours and the particles were then washed with distilled water until the filtrate was neutral. Again, a 5 µL aliquot of particles was dropped on the prism to collect a spectrum for information on surface functional groups. From the spectrum in Figure 3-10, we can observe two *ν*(C=O) peaks in the region between 1700 cm^{-1} and 1800 cm^{-1}. However, the intensity of the peak was a bit weaker than that of the particles oxidised in sulphuric and nitric acid.

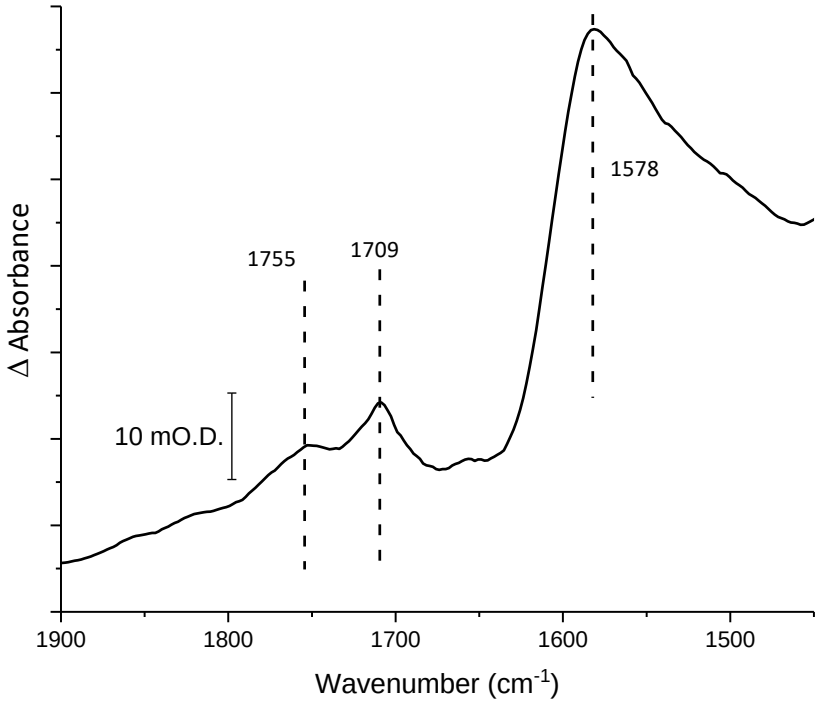


Figure 3-10: Infrared spectrum of carbon particles treated by nitric and acetic anhydride (1:4) with the bare prism as background (512 scans, 4 cm^{-1} resolution).

Oxidation

Apart from treating with acid, using oxidant can also be a good way to increase the functional groups on carbon. Suryanto and Zhao used a piranha solution (H_2SO_4 : H_2O_2, 3:1) to treat carbon particles and got information of ketonic (-C=O) and hydroxyl (-C-O) groups from the XPS spectrum.[12] The purpose of using piranha solution as a soft oxidation method was to introduce oxygen functional groups without destroying their structural integrity due to acid corrosion.[13]

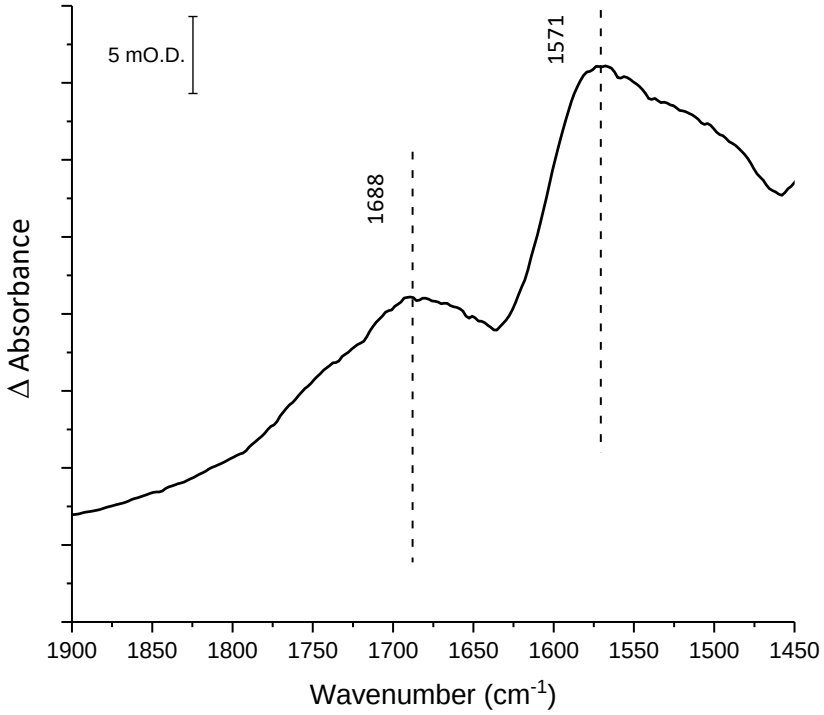


Figure 3-11: Infrared spectrum of carbon particles treated by piranha solution with the bare prism as background (512 scans, 4 cm^{-1} resolution).

Following a modified method from Suryanto and Zhao, a 20 mg aliquot of carbon particle was subjected to ultrasonication in 25 mL of 98% H_2SO_4 in a round-bottomed flask for 30 min. The homogenous carbon particle-H_2SO_4 suspension was magnetically stirred and 5 mL of 30% hydrogen peroxide solution was cautiously added to prevent overheating of the mixture. The mixture was continuously stirred for 4 hours in the 3:1 piranha mixture. The final solution was washed with distilled water to neutral pH. From spectra (Figure 3-11), there was a broad peak between 1800 cm^{-1} and 1600 cm^{-1} consistent with C=O functional groups on the carbon surface.

Although the carboxyl group coverage on the carbon particles increased by acid treatment and oxidisation approaches, there was not much covalent bond formed after mixing the MoFe protein with modified carbon particles which were activated by EDC and NHSS as mentioned in the next section. Time-consuming preparation of carbon particles and adjustment of pH was also a disadvantage for use in a daily experiment.

π - stacked 1-pyrenebutyric acid

Krishnan and Armstrong used derivatised pyrene-modified carbon nanotubes to aid immobilisation of *E. coli* hydrogenase 1 on multi-wall carbon nanotubes which were coated onto a pyrolytic graphite edge disk electrode for a special fuel cell.[14] A similar strategy was explored for immobilisation of nitrogenase MoFe protein onto carbon black particles, as shown schematically in Figure 3-12.

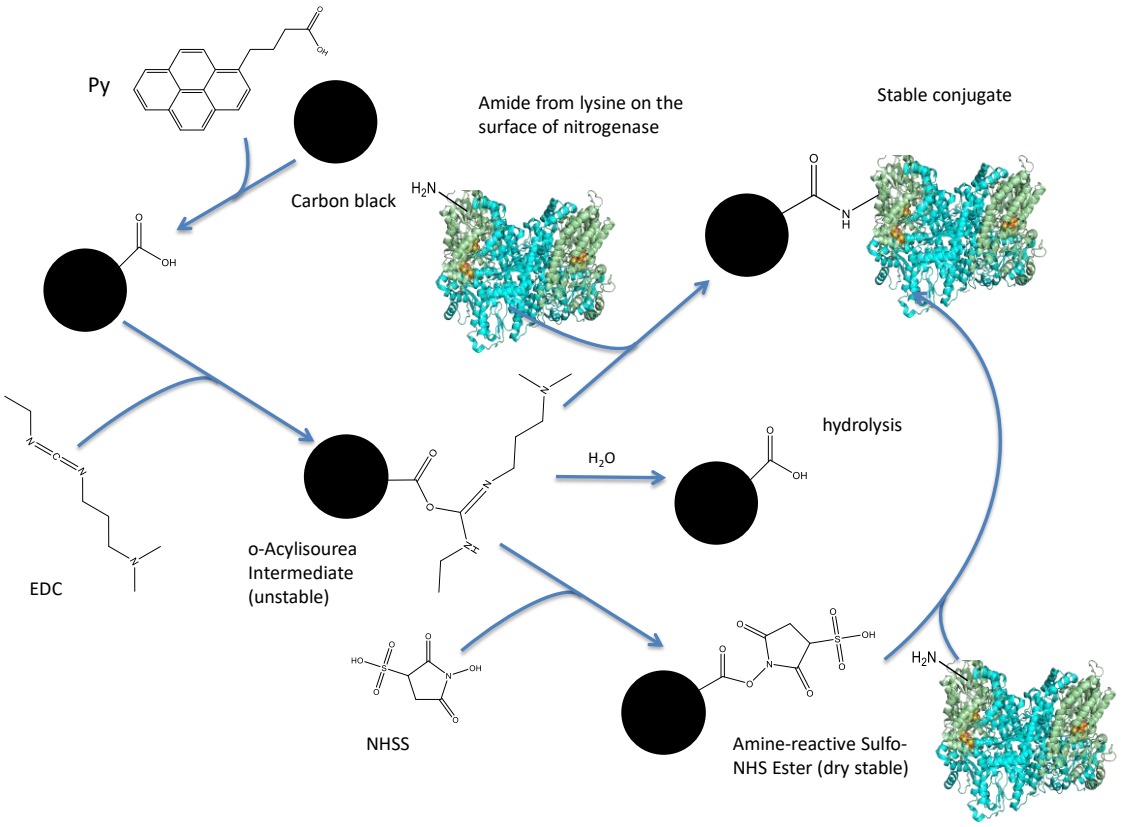


Figure 3-12: Scheme of BP2000 coupling with MoFe protein via 1-pyrenebutyric acid (Py), 1-ethyl-3-(3-dimethylaminopropyl) (EDC) and N-hydroxy sulfosuccinimide (NHSS).

An aliquot of 20 mg/mL carbon black (BP2000) was mixed with 10 mM 1-pyrenebutyric acid (Py) in DMF (dimethyl formamide) and stored at 4 ℃ for 10 hours. Then the suspension was rinsed with DMF and water to remove the Py that was not firmly stacked on the carbon. The amount of carboxyl groups modified on the carbon particles was then determined by the infrared spectrum

as shown in Figure 3-13. A dominant peak at 1652 cm^{-1} is assigned as *v*(CO) from carboxylic group which appears at much lower wavenumber, likely because of aromatic conjugation. The intensity of this band suggests a high level of -COOH groups on the carbon particle

To immobilise the protein, the free carboxylic group from Py was activated for 1 hour using a freshly prepared solution of 0.4 M EDC (1-ethyl-3-(3-dimethylaminopropyl) carbodiimide) and 0.1 M NHSS (N-hydroxy sulfosuccinimide) in the glovebox before treating with 2 nmol nitrogenase MoFe protein for 4 hours to make covalent attachments through the lysine residues on the surface. The non-coupled protein was then rinsed off with Buffer and the modified particles were loaded onto the ATR-IR prism.

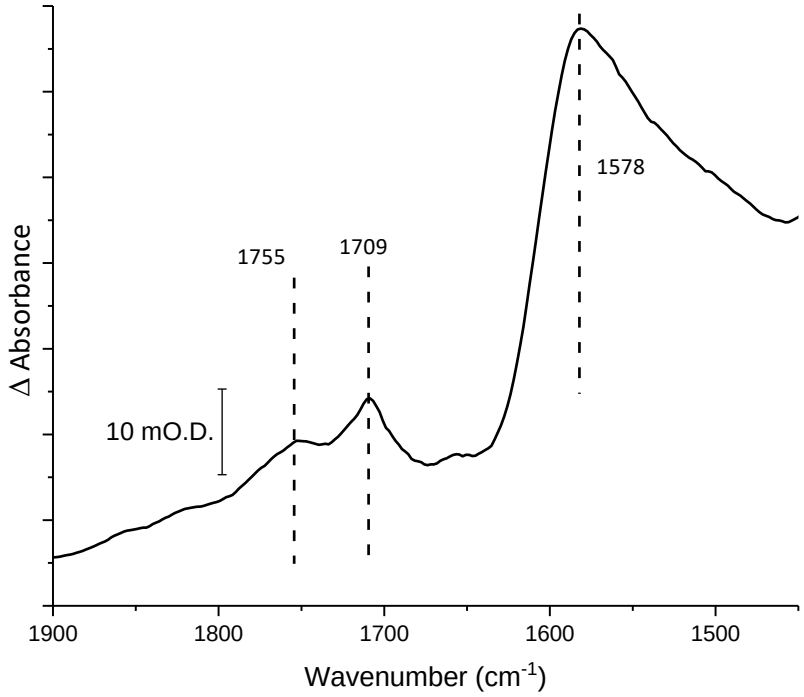


Figure 3-13: Infrared spectrum of carbon particles treated with 1-pyrenebutyric acid with the bare prism as background (512 scans, 4 cm^{-1} resolution).

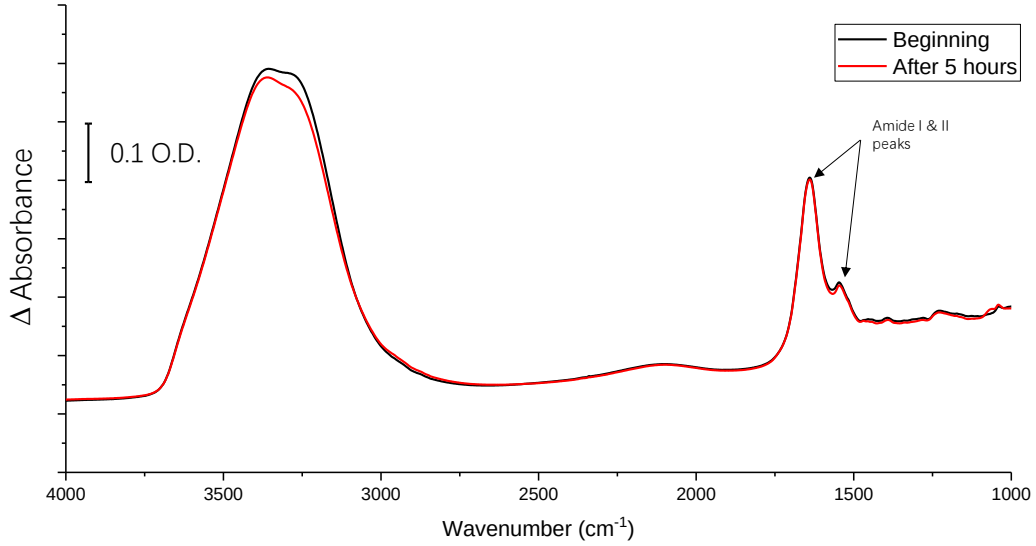


Figure 3-14: The spectra of nitrogenase MoFe protein attached to modified carbon through covalent bonds, shown at the beginning in black and the end of the experiment in red (512 scans, 4 cm^{-1} resolution).

Figure 3-14 shows spectra from an experiment designed to explore the stability of an enzyme film coupled to the Py-modified particles under solution flow for 5 hours. It is clear that the two amide peaks did not decrease significantly during this period by naked eyes. This improvement (compared to Figure 3-5) provides much more scope for infrared experiments on MoFe proteins and allows us to design much longer experiments for further understanding reactivity of the enzyme.

3.2 Redox mediators

Another challenge for electron transfer from electrodes, instead of from the native Fe protein, to MoFe protein is the size of the enzyme. Unlike the study of small metalloproteins like ferredoxin (12-14 kDa) or hydrogenase (80 – 90 kDa), the size of MoFe protein (250kDa) means diffusion will be very slow in solution, and when then the enzyme is immobilised, it may not be able to exchange electrons with the carbon working electrode efficiently. Meanwhile, the active site of nitrogenase

is buried deep inside the protein unit. Electron transfer may not proceed through the native transfer route.

In order to study the redox property of MoFe protein under electrochemical control, a set of redox mediators was included in the solution. These redox mediators can help electron transfer most efficiently when the solution potential (E_h) is near to the mediator mid-potential (E_m). A mixture of different redox mediators with E_m covering the potential range of redox potentials of a protein is commonly used. However, nitrogenase operates at a particularly negative potential. Thus, appropriate selection of redox mediators is critical to establish a system suitable for studying the redox processes of the MoFe protein.

A set of experiments was designed to test the compatibility of different redox mediators for the MoFe protein by Part II student Benjamin Rackham (2018) under my supervision.

3.2.1 Substrates/inhibitors with mediator solution

A series of control experiments were set up to study interactions between Eu-L mediators (as described in section 2.3.1) and substrates/inhibitors (carbon monoxide, hydrazine, azide and acetylene) commonly used to understand the mechanism of the nitrogenase protein.

A sealed electrochemical cell was used to perform cyclic voltammetry on solutions of each of the Eu^{III}-L complexes under a gas flow of 10 mL min^{-1} of N_2 and CO gas in turn. The voltammograms are shown in Figure 3-15, CO does not appear to change the shapes of CVs or shift the potentials of any of the complexes significantly, suggesting that there is no interaction between CO and any of these Eu^{III} or Eu^{II} species. Minor differences in shape may simply arise from some concentration of the solution by evaporation or contamination of the working electrode surface over multiple cycles.

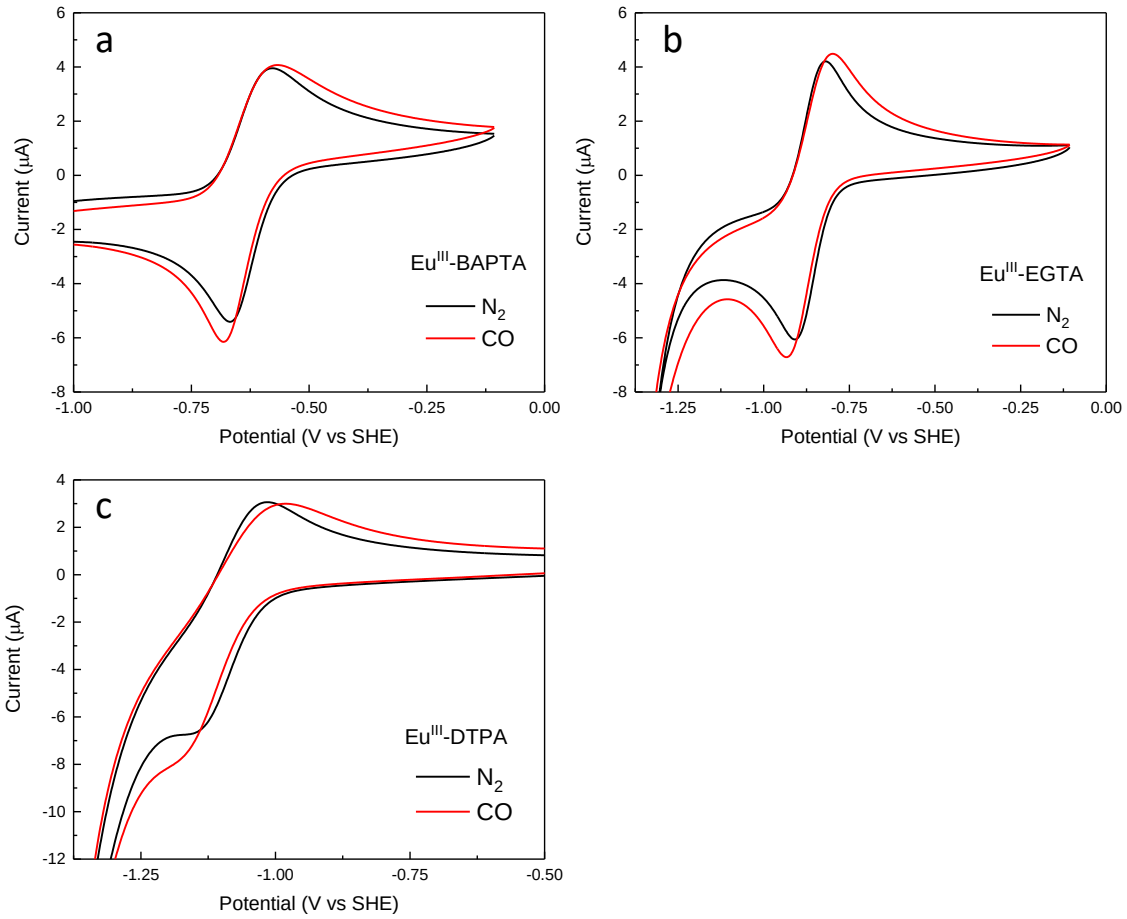


Figure 3-15: Cyclic voltammograms (10 mV s^{-1}) under 10 mL min^{-1} flow rate of N_2 (black) or CO (red) of (a) Eu^{III}-BAPTA, (b) Eu^{III}-EGTA and (b) Eu^{III}-DTPA, each 2 mM in 100 mM, pH 8.0 Tris-HCl buffer.

Figure 3-16 shows voltammograms recorded of the Eu^{III}-L complexes, first in the absence of hydrazine (black) and then after addition of hydrazine dihydrochloride at a concentration of 20 mM (red), with the pH adjusted by addition of 1 M NaOH (aq). The low potential proton reduction current is much larger in magnitude in the presence of hydrazine, but otherwise the shapes of CVs and the mid potentials of the $Eu^{III/II}$ peaks remain largely unchanged.

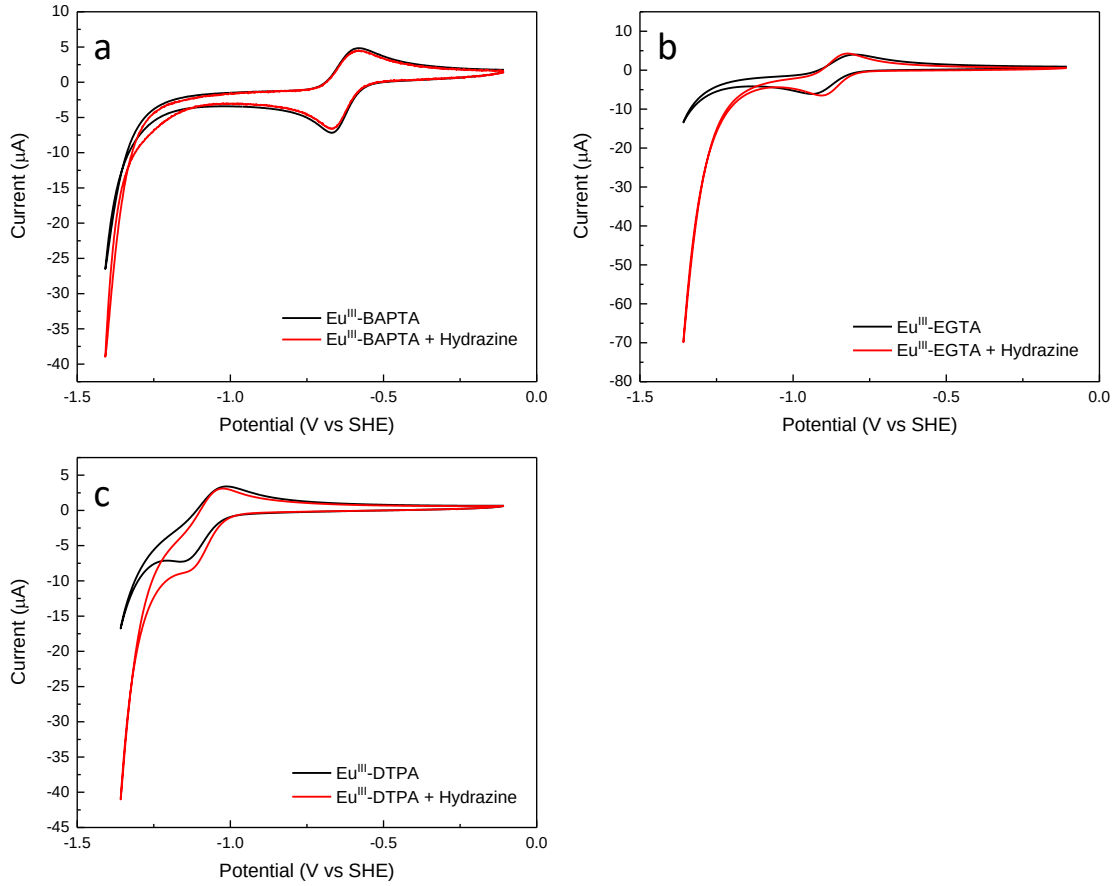


Figure 3-16: Cyclic voltammograms (10 mV s^{-1}) of samples before (black) and after (red) addition of hydrazine (20 mM) of (a) Eu^{III}-BAPTA, (b) Eu^{III}-EGTA and (c) Eu^{III}-DTPA, each 2 mM in 100 mM, pH 8.0 Tris-HCl buffer.

Voltammograms of the Eu^{III}-L complexes, first in the absence of azide (black) and then after addition of sodium azide at a concentration of 20 mM (red), are shown in Figure 3-17. There is no change in the mid potentials of the $Eu^{III/II}$ peaks upon the addition of azide. The magnitude of the current at low potential is greater for all solutions in the presence of azide, otherwise the Eu^{III}-L voltammograms remain largely unchanged.

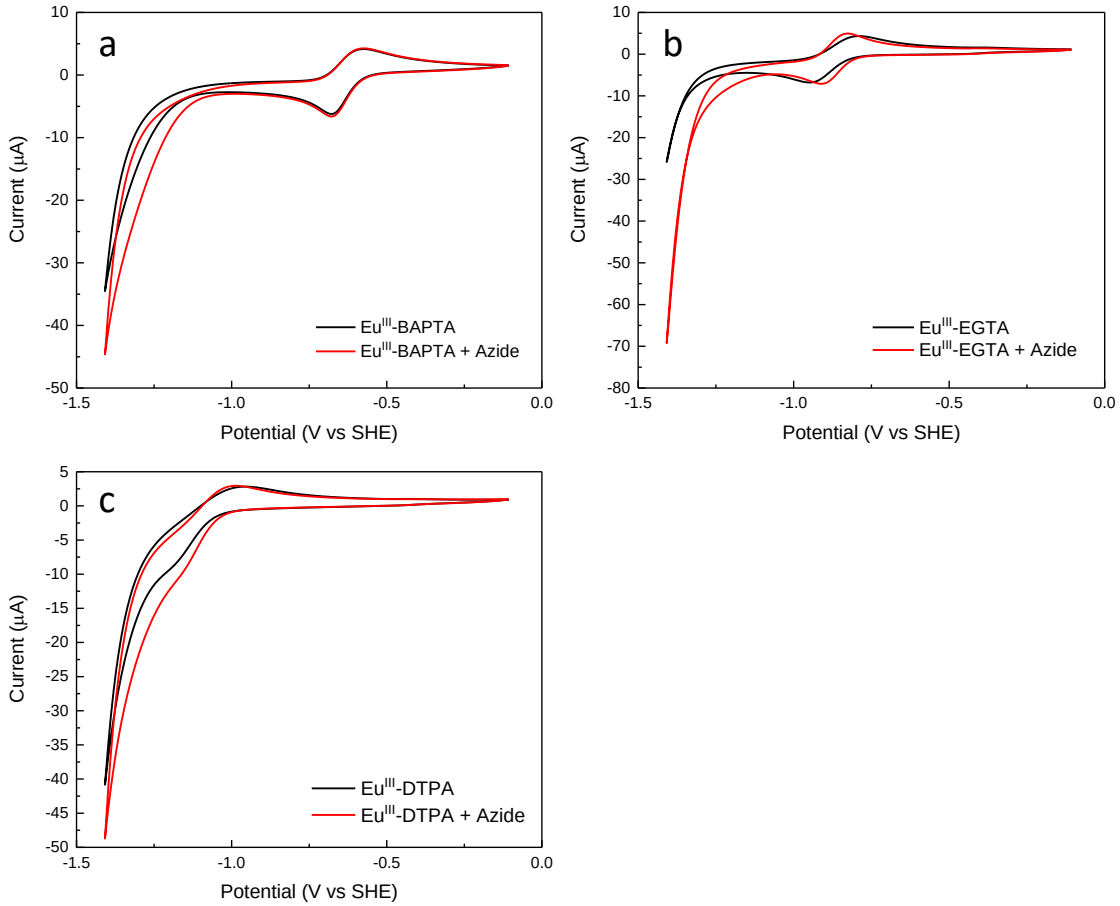


Figure 3-17: Cyclic voltammograms (10 mV s^{-1}) of samples before (black) and after (red) addition of sodium azide (20 mM) of (a) Eu^{III}-BAPTA, (b) Eu^{III}-EGTA and (c) Eu^{III}-DTPA. Each 2 mM in 100 mM, pH 8.0 Tris-HCl buffer.

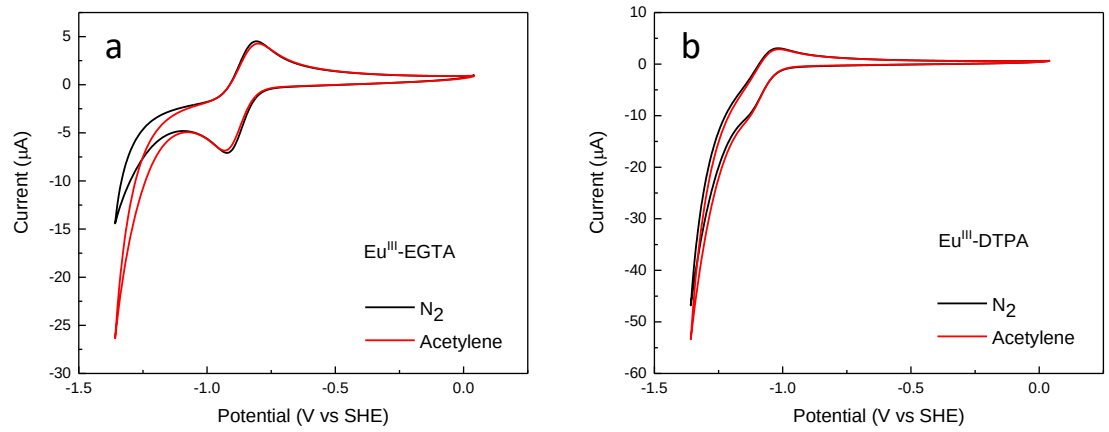


Figure 3-18: Cyclic voltammograms (10 mV s^{-1}) of samples under N_2 (black) or acetylene (red) gas: (a) Eu^{III}-EGTA and (b) Eu^{III}-DTPA. Each 2 mM in 100 mM, pH 8.0 Tris-HCl buffer.

Cyclic voltammetry was performed on solutions of Eu^{III}-EGTA and Eu^{III}-DTPA, each under N_2 gas at a gas flow rate of 10 mL min^{-1} and then after the solution had been exposed to a flow of acetylene gas. The voltammograms are shown in Figure 3-18. For both samples the reduction current at a low potential is greater in magnitude under acetylene than N_2, but the potential of the $Eu^{III/II}$ couple remains the same and the shapes of the voltammograms of the EGTA and DTPA complexes are largely unchanged.

3.2.2 Cobaltocene

Milton et al successfully used cobaltocene as a mediator to enable nitrogenase MoFe protein to reduce N_3^- and NO_2^- in a Fe protein-independent system using a polymer as the enzyme immobilisation approach[15].

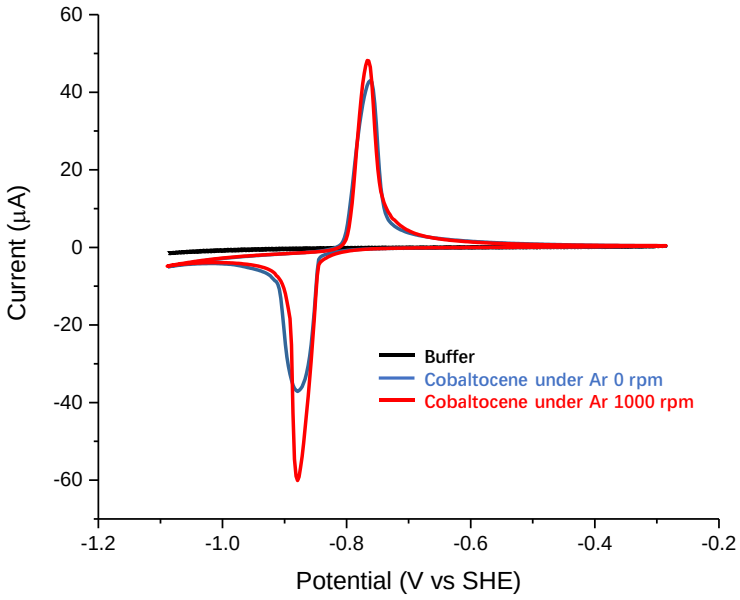


Figure 3-19: Cyclic voltammograms of cobaltocene (concentration 2 mM), in 100 mM pH 8 Tris-HCl buffer, scan rate 10 mVs^{-1}.

To see the feasibility of introducing this mediator into our system, cyclic voltammetry was run (Figure 3-19) to study the properties of this mediator. All experiments were under Ar to avoid any side effect from N_2. The CVs show clear reduction and oxidation peaks of cobaltocene in Tris-HCl

buffer, at -0.879 V and -0.766 V suggesting a mid-potential is close to Eu-EGTA. However, the symmetrical shape of these peaks and the fact that a similar shape of CV was collected at 1000 rpm indicates that some cobaltocene is deposited onto the working electrodeSo, cobaltocene is unsuitable as a soluble mediator in my system.

Bibliography

1 P. Paengnakorn, University of Oxford, 2014.

2 C. M. Moore, N. L. Akers, A. D. Hill, Z. C. Johnson and S. D. Minteer, *Biomacromolecules*, 2004, **5**, 1241–1247.

3 C. J. Pickett, K. A. Vincent, S. K. Ibrahim, C. A. Gormal, B. E. Smith, S. A. Fairhurst and S. P. Best, *Chem. - A Eur. J.*, 2004, **10**, 4770–4776.

4 S. J. George, G. A. Ashby, C. W. Wharton and R. N. F. Thorneley, *J. Am. Chem. Soc.*, 1997, **119**, 6450–6451.

5 R. Hidalgo, P. A. Ash, A. J. Healy and K. A. Vincent, *Angew. Chemie - Int. Ed.*, 2015, **54**, 7110–7113.

6 J. Boudou, J. I. Paredes, A. Cuesta, J. Boudou, J. I. Paredes, A. Cuesta and J. M. D. T. Oxygen, *Carbon N. Y.*, 2003, **41**, 41–56.

7 F. Xie, J. Phillips, I. F. Silva, M. C. Palma and J. A. Menéndez, *Carbon N. Y.*, 2000, **38**, 691–700.

8 C. C. Hu and C. C. Wang, *J. Power Sources*, 2004, **125**, 299–308.

9 R. Yudianti, *Open Mater. Sci. J.*, 2011, **5**, 242–247.

10 M. Vesali Naseh, A. Khodadadi, Y. Mortazavi, O. a. Sahraei, F. Pourfayaz and S. M. Sedghi, *Eng. Technol.*, 2009, **49**, 177–179.

11 N. Tsubokawa, T. Satoh, M. Murota, S. Sato and H. Shimizu, *Polym. Adv. Technol.*, 2001, **12**, 596–602.

12 B. H. R. Suryanto and C. Zhao, *Chem. Commun.*, 2016, **52**, 6439–6442.

13 V. Datsyuk, M. Kalyva, K. Papagelis, J. Parthenios, D. Tasis, A. Siokou, I. Kallitsis and C. Galiotis, *Carbon N. Y.*, 2008, **46**, 833–840.

14 S. Krishnan and F. A. Armstrong, *Chem. Sci.*, 2012, **3**, 1015–1023.

15 R. D. Milton, S. Abdellaoui, N. Khadka, D. R. Dean, D. Leech, L. C. Seefeldt and S. D. Minteer, *Energy Environ. Sci.*, 2016, **9**, 2550–2554.

Chapter 4

Nitrogenase MoFe protein catalysed proton reduction and CO inhibition

This chapter focuses on CO inhibition of proton reduction and its binding to the MoFe protein and characterisation of the interaction between CO and the metal clusters of the MoFe protein and several genetic variants. Variants α- $64^{Tyr\text{-}His}$, α-$70^{Val\text{-}Ala}$ and β-$98^{Tyr\rightarrow His}$ were used to study the role of specific amino acid residues around the active site of the MoFe protein in controlling its chemistry.

4.1 Introduction

Since it is isoelectronic with dinitrogen, carbon monoxide is used as a model to study aspects of dinitrogen binding to nitrogenase. As an IR-chromophore, the CO can be used as a useful probe to study the binding mechanism of nitrogenase MoFe protein using the spectroelectrochemical cell and the immobilisation approaches discussed in Chapter 3.

4.1.1 Proton reduction by nitrogenase

In nitrogenase, catalysis of proton reduction to dihydrogen, also referred to as H_2 evolution, occurs when the MoFe protein is under turnover conditions in the absence of other substrates. This reaction requires two electrons transferred by the Fe protein, each electron transfer coupling with the hydrolysis of two ATP molecules. It has been reported that proton reduction reactivity strongly depends on pH value and an optimum pH for proton reduction under Ar for *A. vinelandii* nitrogenase was found to be at pH 7.5, giving catalytic activity ca. 500 nmol H_2 per minute per mg total protein[1]. It was shown that the rate decreased by 50% at pH lower than 6.3 and higher than 9.0.[1] In this project, Tris-HCl buffer was used as the electrolyte solution which was not the best pH conditionfor proton reduction by nitrogenase, but was a compromise to limit background proton reduction at the working electrode at negative potentials.

Reduction of protons is competitive with reduction of dinitrogen under the turnover condition of nitrogenase.[2] It has been found that dinitrogen can only partly suppress this proton reduction and the limiting ratio between these two reactions depends on the type of nitrogenase and experimental conditions. For instance, the limiting stoichiometry of reduced N_2 to produced H_2 in the cases of Mo-nitrogenase and V- nitrogenase are 1:1 and 1:3.5, respectively.[3,4]

A complete mechanism of the proton reduction and the importance of this reaction to the main dinitrogen fixation process are still unknown. Both experimental and computational studies have indicated that binding of protons and release of dihydrogen happen at the early oxidation states

of the enzyme, either two- or four-electron reduced state.[5-6] It has been suggested that proton binding to the active site involves the formation of a metal hydride, with the production of dihydrogen via a reductive elimination pathway,[7,8] thus leaving the FeMo catalytic centre reduced by 2 electrons. It has been proposed that this may be important in accumulating the electrons needed for N_2 reduction.[9]

The catalytic capability of hydrogen production in nitrogenase has been compared to those of Mo-containing heterogeneous catalysts such as molybdenum disulphide (MoS_2). This inorganic Mo compound was found to be able to catalyse proton reduction with low over-potential under mild conditions,[10] so it has been of interest as an alternative catalyst for industrial hydrogen production [11,12]as well as reducing nitrogen by Mo-based catalysts.[13,14] Therefore the Mo atom on the FeMoco might be involved in the proton reduction activity of the enzyme.[1,8]

4.1.2 Previous study of CO binding to nitrogenase as an inhibitor

Carbon monoxide is a well-known inhibitor to all three nitrogenases. It is reported that CO inhibits all known substrate reduction. The inhibition of proton reduction by CO is weak and has only been detected in a basic solution. Literature shows that CO binds to the active centre of the nitrogenase, for instance, the substitution of the homocitrate ligand and some nearby amino acid residues directly affects CO inhibition. It was found that CO can bind to native nitrogenase only at its reduced state, not at the resting state.

According to an IR spectroscopic study by George et al. using a stopped-flow IR (SF-IR) technique (Figure 4-1 A), evidence for CO binding to wild type Mo-nitrogenase was in agreement with EPR and ENDOR results as they exhibited two sets of ν(CO) absorption bands under corresponding conditions. Under the 'lo-CO' condition, a transient ν(CO) peak was observed at 1904 cm^{-1} for a short time before it evolved to a ν(CO) peak at 1715 cm^{-1}.[15,16] It was thought that the former peak arose from terminal CO binding to the intermediate complex and the latter was assigned as

bridging CO bound to another Fe atom. On the other hand, under the 'hi-CO' condition, ν(CO) peaks were observed at 1880, 1906, 1936 and 1960 cm^{-1}, all assigned as terminal CO binding.[16] It was suggested that these species were the result of CO binding to separate sites or different redox states of the metal cluster, including some EPR-silent states. Another SF-IR study of steric effects on the FeMoco-CO complex demonstrated that changing the side chain size of α-70^{Val} amino acid residues located above the 4Fe-4S face of the FeMoco cluster resulted in an IR wavenumber shift of *ν*(CO) peaks under 'hi-CO' condition.[17] It was observed that MoFe protein variants substituted with a less bulky residue, α-$70^{Val \rightarrow Ala}$, show a shift of the *ν*(CO) peak of both 'lo-CO' and 'hi-CO' forms to higher wavenumber, shown in Figure 4-1 B. Later, it was found that this α-70^{Gly} MoFe protein variant was capable of CO reduction into hydrocarbons.[18] This suggested that the shorter side chain of glycine amino acid might open up more space near the FeMoco allowing CO to bind to a different site and be reduced.

A study on CO inhibition of azide reduction using the SF-IR approach by Tolland *et al.* showed that addition of azide had no impact on the formation of 'lo-CO' and 'hi-CO' bands, consistent with CO as a non-competitive inhibitor for azide reduction and CO having a different binding site from azide.[15]

The susceptibility of the bound CO ligands to photolysis was investigated using EPR and SF-IR spectroscopy. In the EPR study, it was shown that the 'hi-CO' complex converts to the 'lo-CO' one after irradiation under visible light at 12 K and this 'lo-CO' product was converted back to the 'hi-CO' form by increasing the temperature to 77 K, with the calculated activation energy of the reaction being 3.9 $kJ.mol^{-1}$.[19] In contrast, it was found that the protein sample with 'lo-CO' and 'hi(5)-CO' (S = 3/2) signals was photo-stable.[19] A SF-IR study on photolysis at low temperature (4 K) showed that photolysis of CO-bound wild type MoFe protein resulted in loss of the new 'hi-CO' peak at 1973 cm^{-1} and the appearance of peaks at 2135 and 2123 cm^{-1}, assigned as two free CO molecules trapped inside the protein.[20] Another study of different variants reported that changing

the α-195$^{His \rightarrow Gln}$ amino acid residue resulted in a new EPR-silent CO-bound MoFe protein, assigned as two terminal CO ligands that coupled to each other with a separation of 2.7 Å.[21]

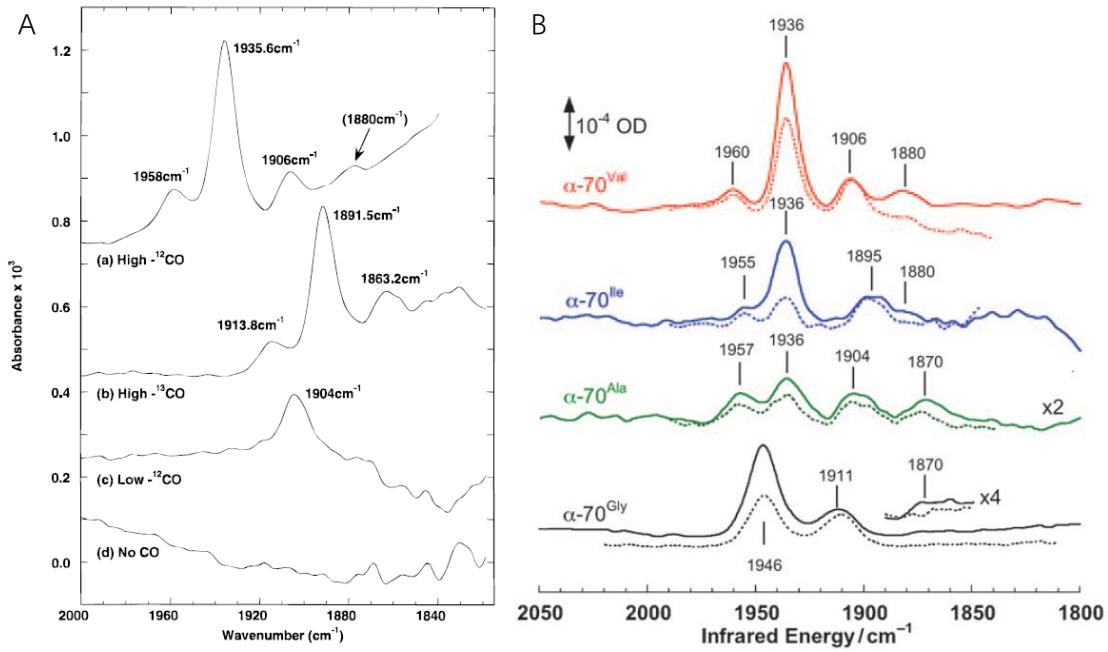


Figure 4-1: IR spectra of the nitrogenase. A, transient infrared spectra of *Klebsiella pneumoniae* nitrogenase-CO complex. These are illustrative spectra obtained by averaging the data sets over 4-54 s after mixing. All samples contained MoFe protein, Fe protein, 25 mM HEPES pH 7.3 buffer, 10 mM $MgCl_2$, 10 mM sodium dithionite, and 10 mM ATP. No creatine kinase regenerating system was used. CO concentrations assume buffer saturated with CO is 1 mM: (a) ~0.5 mM CO (high CO) and (b) ~0.5 mM ^{13}CO (high ^{13}CO). The reduced intensity compared to (a) is due to the presence of 15% $^{13}C^{18}O$: (c) ~60 μM CO (low CO) and (d) no CO. Copyright (c) 1997 American Chemical Society. B, hi-CO complex formed under the turnover condition with the Fe protein and ATP. Spectra averaged 25–35 s (solid line) and 6–14 s (broken line) after mixing, were obtained by the stopped-flow method) Copyright (c) 2011 Wiley-VCH Verlag GmbH & Co. KGaA, Weinheim.

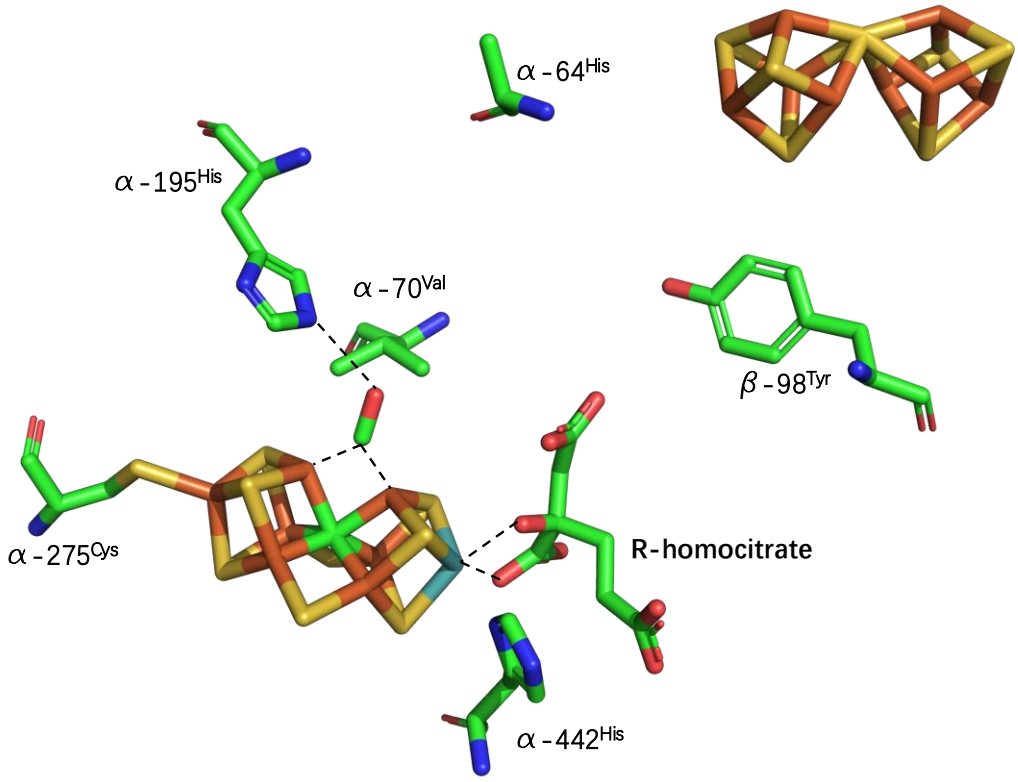


Figure 4-2: A structure of CO-bound FeMoco of the MoFe protein from *A. vinelandii*. (generated from PDB file 4TKV). The coordinated amino acids and some nearby residues were located as in the MoFe protein.

Recently, a crystal structure of CO-bound nitrogenase was reported by Rees and co-workers. In the presence of Fe protein and ATP, it showed that CO was bound to the FeMoco by replacing an S atom on the central Fe-S core and forming bridging bonds between two Fe atoms on the site near the α-70Val and α-195^{His} residues shown in Figure 4-2.[22] It was suggested that S displacement could be the result of proton donation from the α-195^{His} residues and the position of the bound CO was within H-bonding distance of the α-195^{His} residue. The bond length between CO and Fe was determined to be 1.86 Å, shorter than the bond length between Fe and the original bridging S at 2.20 Å.174 The coordination with CO was found to also change the geometry of the FeMoco by shortening the distance between the two Fe atoms to which CO bound (2.5 Å), relative to other pairs of Fe atoms on the Fe-S core (2.6 Å). Moreover, it was reported that the MoFe protein was

reactivated upon removal of CO and the S atom was reinserted into the FeMoco. These findings indicate that CO binding is reversible under the experimental conditions used. Although this CO-bound structure was generated under different conditions from previous EPR and SF-IR studies, so it cannot be directly linked to any previously assigned state, it is possible that it could be related to the lo-CO complex.

The structure reported by Rees and co-workers provides new evidence that the CO binding site is on the FeMo cofactor near the α-70^{Val} residue.[22] This structure gives new insight into the study of the CO inhibition and the mechanism of nitrogenase.[22] However, questions remain about the binding mechanism and which redox state of the active site CO binds to.

4.1.3 CO reduction as a substrate

Carbon monoxide (CO) is not reduced by the wild-type Mo-nitrogenase. In recent years, several groups reported that CO can be reduced to short chain hydrocarbons by Mo-nitrogenase and by V-nitrogenase. Ribbe and co-workers reported that V-dependent nitrogenase (*vnfH*-encoded Fe protein; *vnf*DGK-encoded VFe protein) from *A. vinelandii* can catalyse the reduction of CO to small hydrocarbon products such as C_2H_4, C_2H_6 and C_3H_8 by gas chromatography–mass spectrometry (GC-MS).[23] Later, they found that Mo-nitrogenase also catalyses this reaction in large scale, but with relatively lower rate compared to V-nitrogenase (~0.1% in H_2O and ~2% in D_2O), but no methane was determined in either experiment (H_2O and D_2O)[24] Another study by Seefeldt and co-workers showed that α-70^{Ala}, α-70^{Gly}, α-70^{Ala}/α-96^{His} and α-70^{Ala}/α-191^{Ala} MoFe protein variants are capable of CO reduction (ca. 6 and 7 nmol C_2H_4 per nmol protein per hour for the α-70^{Ala} and α-70^{Gly} variants, respectively).[18] It was found that increasing the CO pressure in the reaction not only yielded more products but also made the formation of longer chain hydrocarbons a more favourable reaction. From this observation, they proposed a mechanism of nitrogenase-catalysed hydrocarbon formation, paralleling the Fischer-Tropsch reaction. In this mechanism, two CO molecules bind to the FeMoco at two adjacent sites, and then the bound-CO pair is partially

reduced to a -CH intermediate. This intermediate can either be fully reduced to methane or coupled together to form longer hydrocarbon chain products.

As well as native ATP-driven reaction with Fe protein as reductant, CO reduction was also observed in ATP-independent systems with different nitrogenase variants. With Eu^{II}-DTPA as reductant, catalysis of CO reduction by isolated FeMoco and FeVco has been reported (ca.55 and 20 nmol CH_4 per µmol cofactor per hour, respectively),[25] showing that capabilities of CO reduction are not limited to the active site inside the protein. It has also been shown that nitrogenase variants with only P-cluster or P-cluster precursor are able to catalyse the conversion of CO to hydrocarbons (6 and 83 nmol CH_4 per µmol protein per hour, respectively).[26]

This discovery of CO reduction activity in nitrogenase has revealed a new aspect for the study of CO binding to the protein. The spectroscopic investigation of the interaction between CO and the active site under electrochemical control could be the next step toward understanding the CO reduction mechanism of nitrogenase, with implications for catalyst design for hydrocarbon formation as well as N_2 fixation.

4.2 Electrochemical proton reduction and CO inhibition

In this section, the MoFe protein of nitrogenase from *Azotobacter vinelandii* was studied in the absence of its Fe protein and ATP using the spectroelectrochemical cell described in Chapter 3.

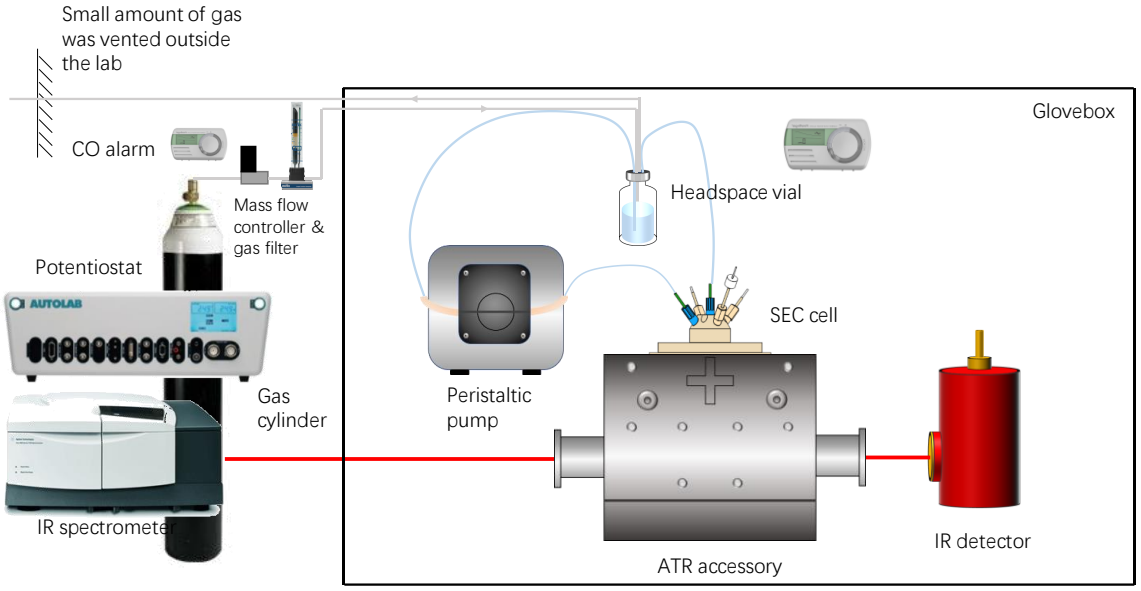


Figure 4-3: A schematic diagram of the spectroelectrochemical (SEC) cell with a flow system inside the anaerobic glove box and the infrared spectrometer, and the potentiostat for controlling the experiment.

The immobilisation of MoFe protein started with the direct adsorption onto carbon particles, and there is some investigation into using this attachment approach to carry out experiments later in this chapter. A chronoamperometric technique was used to explore the effect of CO on the electrocatalytic proton reduction by MoFe protein. For this experiment, the SEC cell was equipped with a flow system to allow change of gas-saturated solution flowing into the cell during the experiment. CO gas from a gas cylinder was purified by passing through an O_2 scrubbing filter (Restek Super Clean gas filter, <1 ppm O_2) before bubbling into redox mediator solution inside a glove box as illustrated in Figure 4-3. The mass flow controller (Brooks Instruments) was set up to control the different gases and to make it possible to have specific concentrations of dissolved gas in solution throughout the experiment. For safety, CO alarms (Fireangel) were placed both inside and outside the glovebox in case of leaks. Due to the small flow rate (20 mL/min) in normal experiments, the outlet of gas line from the glovebox is vented to the atmosphere outside of the building.

4.2.1 Effect of CO on proton reduction by the MoFe protein

In a series of control experiments without MoFe protein (Figure 4-4), a sequence of potential steps was applied to the working electrode in the cell containing buffered electrolyte (black), Eu-L mediators in a buffer (red) and Eu-L mediators in the presence of CO-saturated solution (blue). Each potential was held for at least 5 minutes to allow the system to equilibrate and obtain a steady current ahead of the next potential step. The working electrode was first held at 0 V and a series of more negative potentials were applied in -0.1 V steps to a final potential of −1.2 V. This large potential range covered all the reduction potentials of Eu(III)-BAPTA, Eu(III)-EGTA and Eu(III)-DTPA (Figure 4-4).

From these control experiments, all three currents slightly increased in magnitude as the potential was stepped to more negative values and were quite similar to each other. This confirmed that proton reduction by the carbon working electrode was not observed significantly in this potential window, and that background proton reduction by the Eu-L mediators was not significant at pH 8.

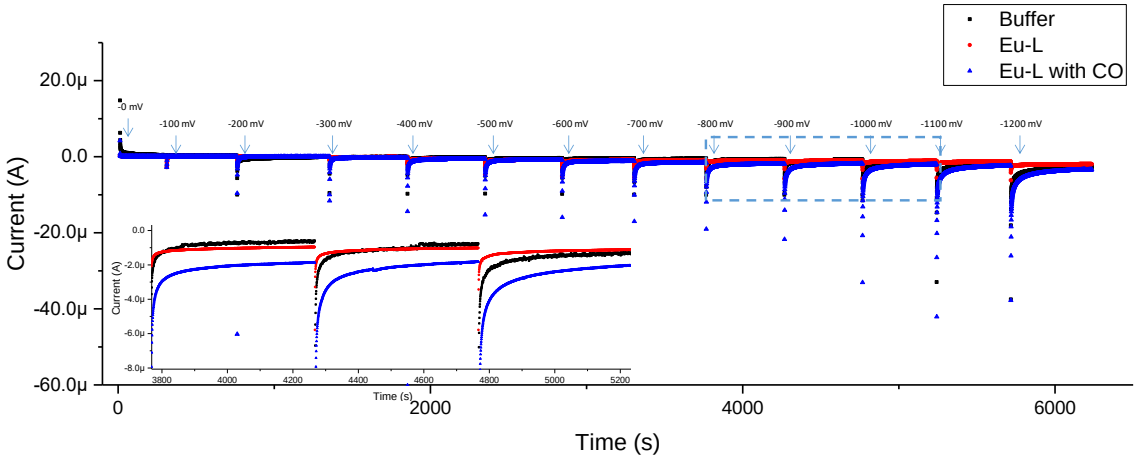


Figure 4-4: Chronoamperograms of Tris-HCl pH 8.0 buffer (●), Eu-ligand mediator solution (●) and the mediator solution with CO gas flow (20 mL/min, ●). The Eu-L cocktail solution consists of Eu-BAPTA, Eu-EGTA, and Eu-DTPA 0.25 mM in total, in the electrochemical cell. A sequence of potential steps from 0 V to -1.2 V (V vs SHE each step is -0.1 V) was applied at the indicated times. Inset showing a zoom-in of a range of interest from -0.8 V to -1.0 V where MoFe protein has a redox reaction.

Figure 4-5 shows a current-time trace in which the Eu-L mediator solution was used to initiate electrochemically-driven proton reduction by nitrogenase MoFe protein. Using 2 nmol wild type nitrogenase MoFe protein as the sample, adsorbed onto a 20 mg/mL carbon particle suspension (as shown in Section 3.1.2), and argon-saturated Tris-HCl pH 8.0 buffer with Eu-L mediator cocktail as background electrolyte flowing through the cell, the trace in Figure 4-5 shows no significant increase in reduction current when the working electrode potential was held at values from -0 V to -0.7 V (vs SHE).

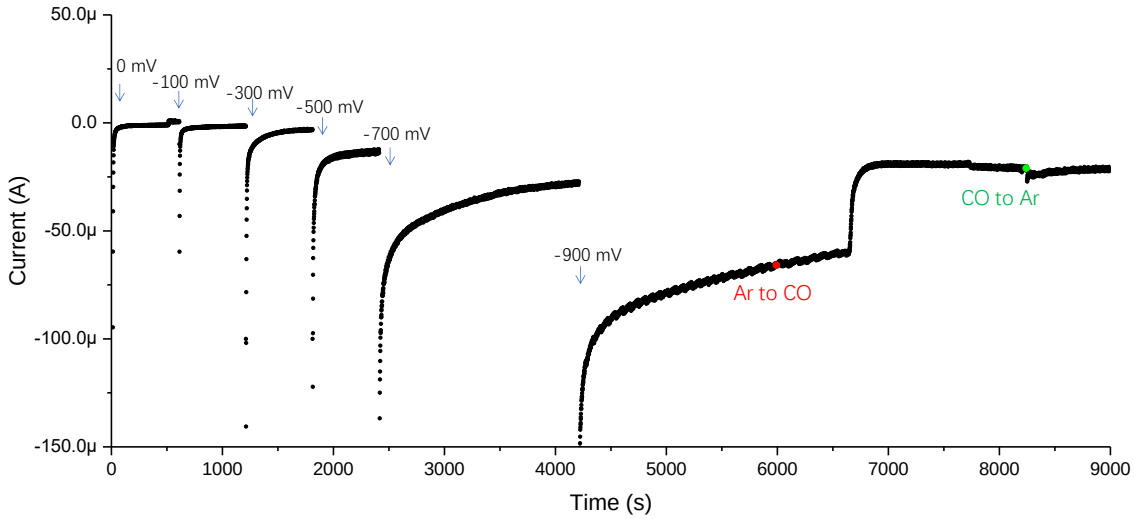


Figure 4-5: Current-time trace for an electrochemical experiment on wild type MoFe protein showing the effect of CO on the electrocatalytic proton reduction current. At the point shown in ●, Ar to CO, the flow solution (Tris-HCl, pH 8.0 containing Eu-L) was flushed with 100% CO gas, while the Ar-saturated buffer was flushed through the cell at the point shown in ●, CO to Ar.

After application of a -0.9 V potential, a more dramatic catalytic current step was observed. The catalytic current reached about –50 μA and was fairly stable until the introduction of a 100% CO atmosphere to the Tris-HCl buffer into the cell (Ar to CO) at approximately 6000 s. After a short lag time, due to equilibration of the buffer with CO, the electrocatalytic current decreased in magnitude to -20 μA which is similar to the background current of the Eu-L solution with CO in Figure 4-5.

After ca 30 min the gas atmosphere was changed back to Ar (CO to Ar, Figure 4-5). There is no significant change in reduction current. Therefore, the result indicates that CO can inhibit the electrocatalytic proton reduction process by nitrogenase, and that this inhibition appears to be irreversible, at least at -0.9 V.

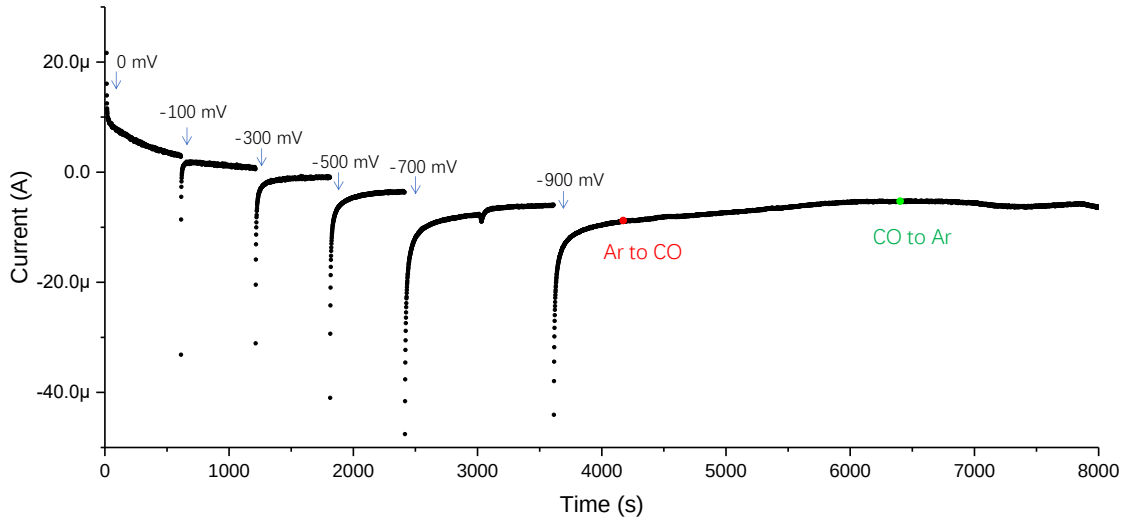


Figure 4-6: Current-time trace for an electrochemical experiment on Apo protein (lacking the active site) showing no effect of CO on the electrocatalytic proton reduction current. At the point shown in red (🔴), Ar to CO, the flow solution (Tris-HCl, pH 8.0 containing Eu-L) was bubbled by 100% CO gas, while the Ar-saturated buffer was flushed through the cell at the point shown in green (🟢), CO to Ar.

Figure 4-6 shows a control experiment using Apo protein which is lacking the active site, FeMo cofactor, of wild type MoFe protein. Different from the current trace of MoFe protein, there is no significant increase of current magnitude after applying -0.9 V in an analogous experiment. After 10 min to let the current stabilise, the mediator solution was flushed with 100% CO gas at 4200 s. The current remained close to -10 μA for the whole trace indicating no interaction between CO and Apo protein in this potential range. This supports the conclusion that the proton reduction happens in the active site of the native MoFe protein. Gas change back to Ar after 40 min (CO to Ar, Figure 4-6), also led to no significant change in reduction current.

4.2.2 Electrochemistry of MoFe protein in the presence of CO

In another set of experiments, a CO saturated solution was introduced to the SEC cell containing the wild type MoFe protein from the outset, before applying a potential.

Figure 4-7 shows only a small reduction current (-15 µA), most from Eu-L mediators, when the potential was decreased stepwise down to –0.9 V, compared with the catalytic current of proton reduction (- 50 µA) observed in the case of wild type protein in the absence of CO.

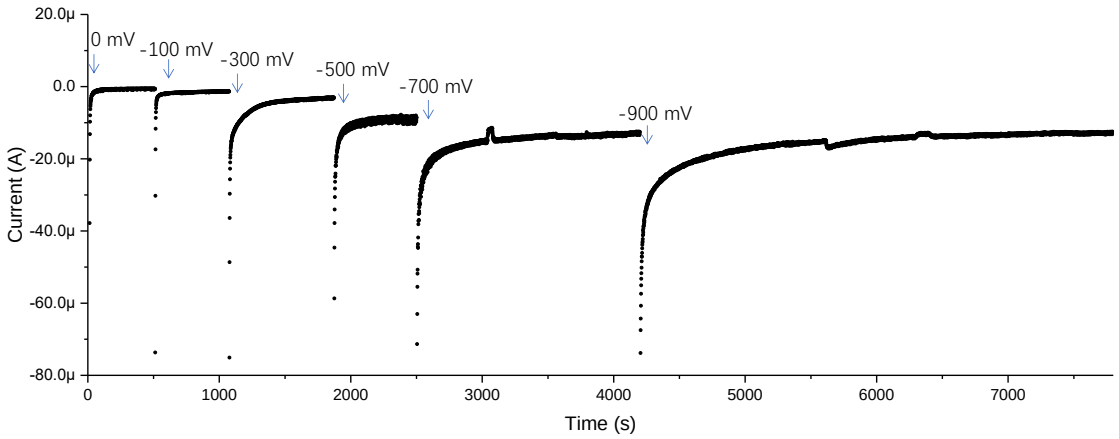


Figure 4-7: Current-time trace for an electrochemical experiment on wild type MoFe protein in the presence of CO (Tris-HCl, pH 8.0 containing Eu-L). A series of potential steps were applied, and flow of CO saturated mediator solution was started before applying potential.

4.3 CO binding to MoFe protein

In order to investigate the interaction between CO and the metal clusters that is responsible for the inhibition effect on the MoFe protein, an ATR-IR spectroscopy approach was employed using the same SEC cell as described in Chapter 3. Wild type and different variants of MoFe protein were investigated under carbon monoxide to study the mechanism of CO binding to nitrogenase.

4.3.1 Wild Type MoFe protein

Using the approach described in Section 3.1.2 for the wild type MoFe protein, 20 mg/mL carbon particle suspension was sonicated with Tris-HCl buffer for 1 hour, to allow particles evenly to

distribute in solution. Then 2 nmol protein was allowed to adsorb on 5 µL particle suspension in an ice box for another 2 hours. The mixture was deposited onto the prism of the base plate of the SEC cell. Tris-HCl buffer (pH 8.0) with Eu-L mediator mix (Eu-BAPTA, Eu-EGTA and Eu-DTPA) was used as a flow solution bubbled with different gases. Infrared spectra were collected, while electrochemistry was running to control the enzyme catalysis.

Figure 4-8 shows infrared spectra collected while the enzyme was under potential control as shown in Section 4.2.2. IR spectra recorded between potentials of –0.1 V and –0.7 V showed no significant spectral change in the ν(CO) region between 1750 cm^{-1} to 2200 cm^{-1}. Upon applying a potential of –0.9 V, the formation of a strong and broad absorption peak between 1850 cm^{-1} and 1950 cm^{-1}, was observed, together with a small peak above 2000 cm^{-1}. After applying a more negative potential, -1.1 V, these peaks grew and resolved into several peaks at 2021 cm^{-1}, 2009 cm^{-1}, 1980 cm^{-1}, 1964 cm^{-1}, 1933 cm^{-1}, 1916 cm^{-1} and 1900 cm^{-1}. This suggests a number of different CO-metal structures or CO bound species at multiple redox states. The onset potential for CO binding correlates with the onset potential for electrocatalytic protein by the enzyme.

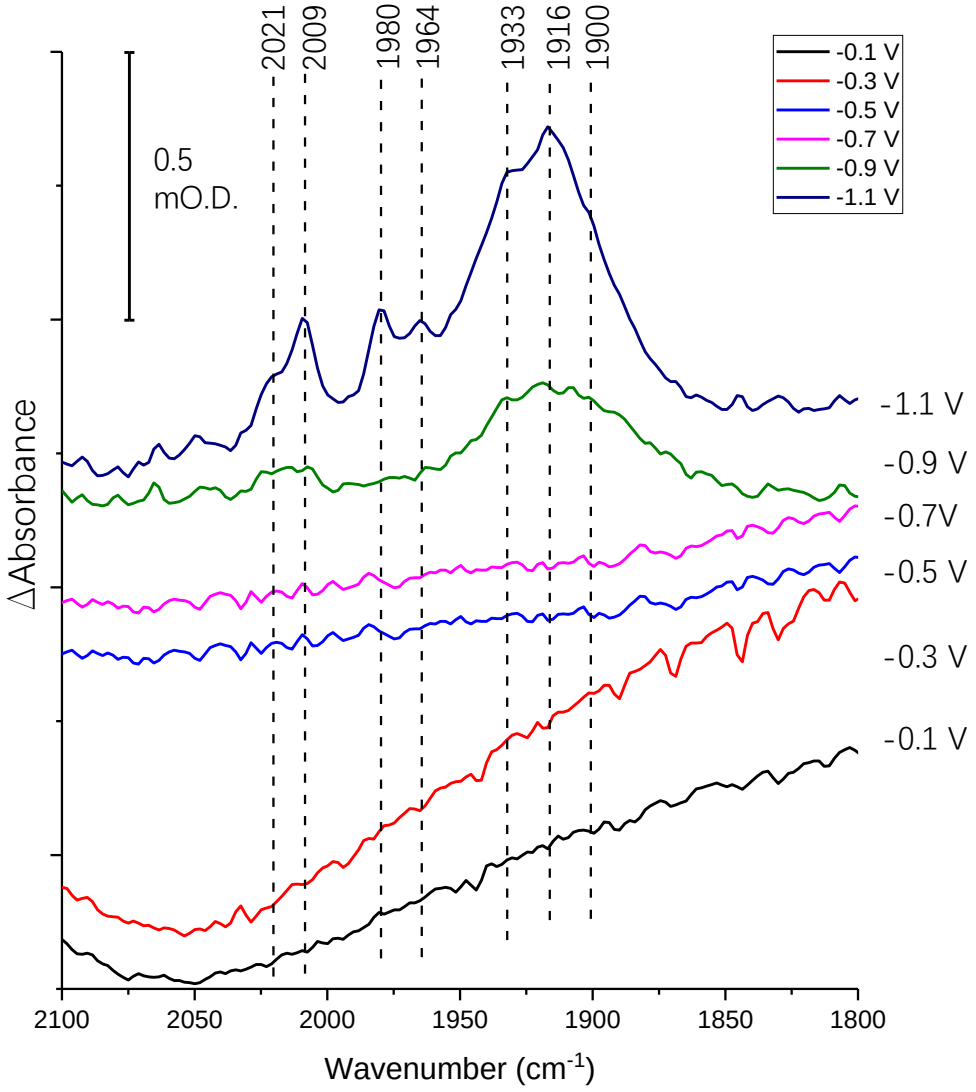


Figure 4-8: IR absorbance spectra of 2 nmol of wild type MoFe protein after the introduction of CO saturated solution (Tris-HCl, pH 8.0 containing Eu-L) followed by application of a sequence of potential steps. Each spectrum was recorded at least 30 min after the potential step, or when no further spectral changes occurred (-0.9 V and -1.1 V) and processed against a background spectrum at −0.1 V prior to addition of CO (512 scans, 4 cm^{-1} resolution).

In the control experiment without MoFe protein (just Eu-L), shown in Figure 4-9, IR spectra show no significant spectral changes in the region of v(CO) between 1800 cm^{-1} and 2200 cm^{-1}, when the same series of potential steps was applied in the presence of CO-saturated solution. Baseline

changes are probably due to re-arrangement of water in the film in response to the potential steps, especially in experiments with bare carbon particles.

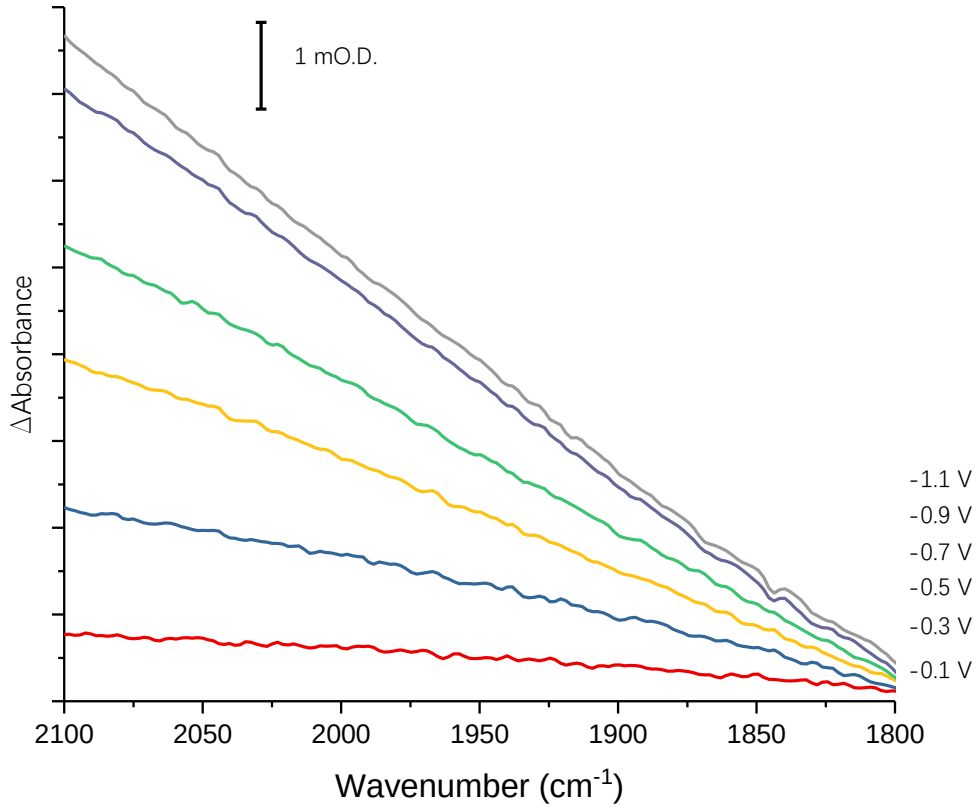


Figure 4-9: IR absorbance spectra of carbon particles without MoFe protein after addition of CO saturated solution (Tris-HCl, pH 8.0 containing Eu-L) followed by application of a sequence of potential steps. Each spectrum shown here was recorded after 30 min at each holding potential and processed against a background spectrum at –100 mV prior to addition of CO (512 scans, 4 cm^{-1} resolution).

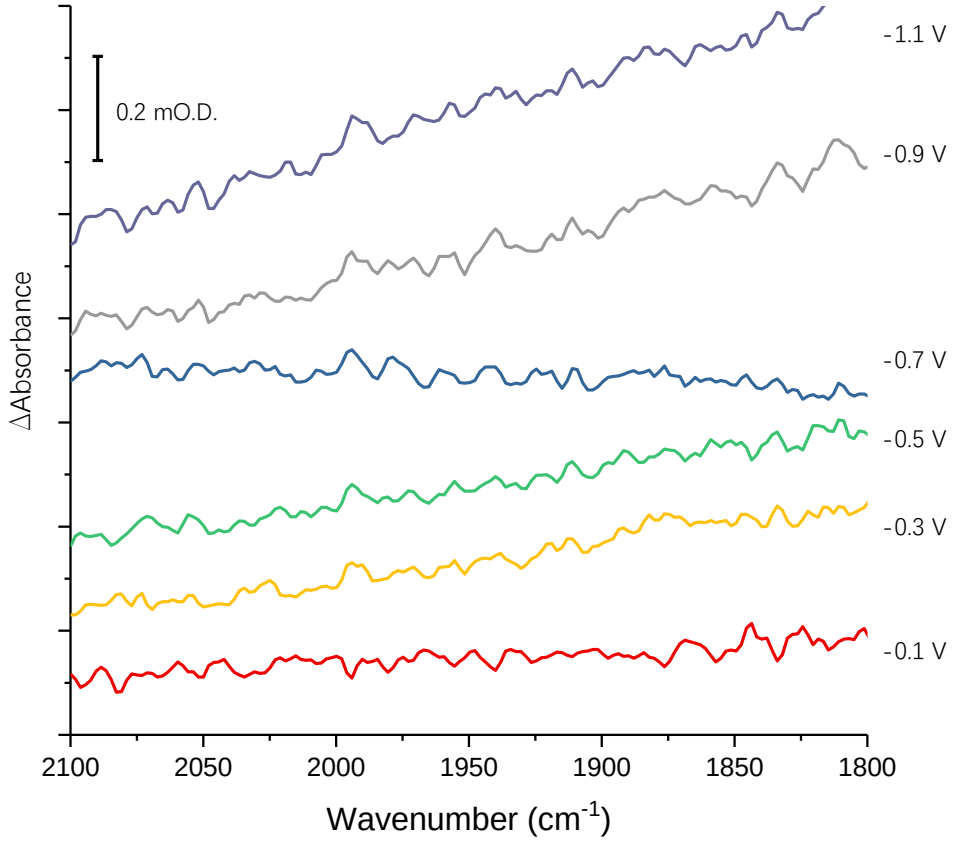


Figure 4-10: IR absorbance spectra of 2.0 nmol Apo protein after addition of CO saturated solution (Tris-HCl, pH 8.0 containing Eu-L) followed by application of a sequence of potential steps. Each spectrum shown here was recorded after 30 min at each holding potential and processed against a background spectrum at –100 mV prior to addition of CO (512 scans, 4 cm^{-1} resolution).

A similar control experiment was set up with Apo protein as shown in Figure 4-10. No *ν*(CO) peaks arose in the region from 1800 cm^{-1} to 2200 cm^{-1} when the protein was under CO saturated solution after applying potential steps from -0.1 V to -1.1 V.

Figure 4-11 displays another experiment designed to check the function of Eu-L mediators. Wild type MoFe protein on carbon particles was put onto the prism in the experiment above, while CO saturated solution without mediators (Tris-HCl buffer only) was introduced into the cell before applying a potential. There was no obvious increase in absorbance in the CO region from -0.1 V to -0.9 V. After 1 hour at -1.1 V, there was a weak, broad spectral change between 1900 cm^{-1} and

2050 cm^{-1}. However, the peaks were too weak to confirm as *v*(CO) peaks arising from CO binding under direct electron transfer to the active site. The absence of Eu-L mediators thus seems to slow electron transfer between carbon working electrode and the FeMo cofactor in the wild type MoFe protein leading to almost no CO binding as observed in IR spectra at proton reduction potential.

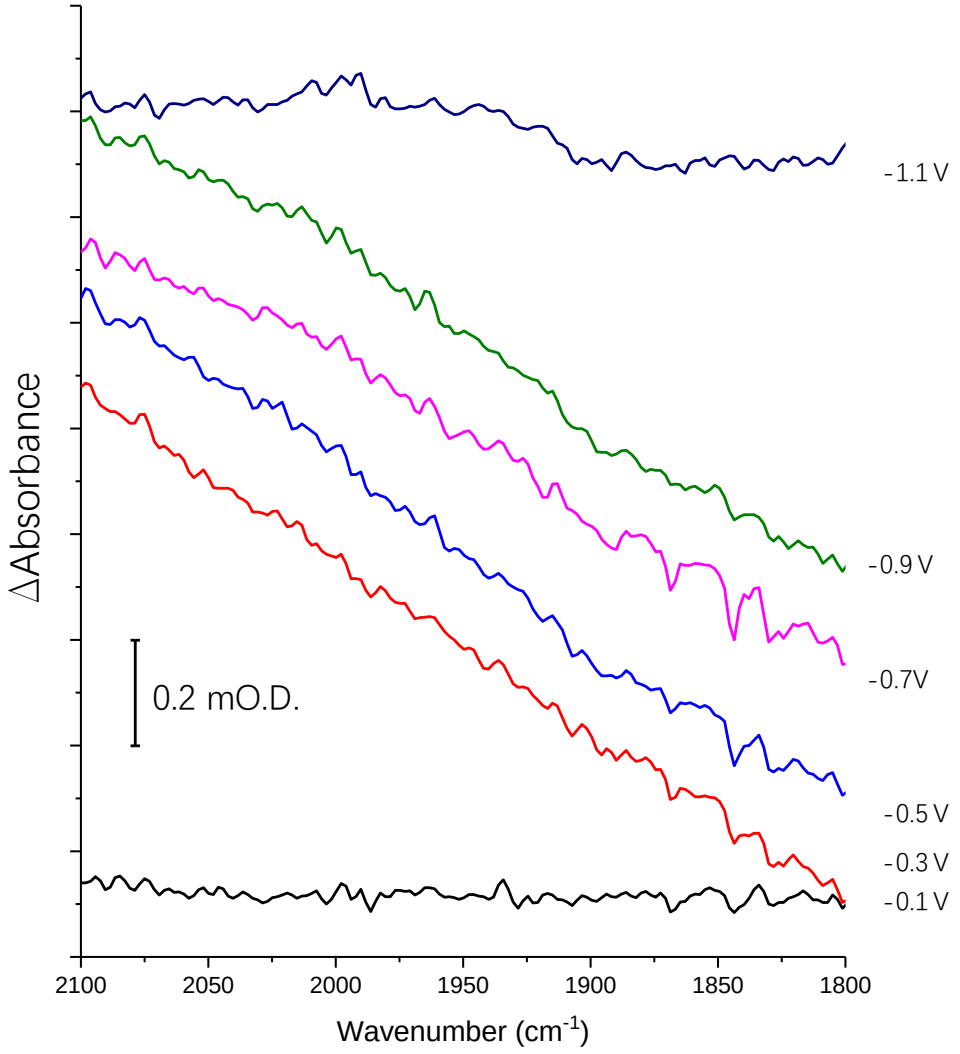


Figure 4-11: IR absorbance spectra of 2 nmol of wild type MoFe protein after the introduction of CO saturated solution (Tris-HCl, pH 8.0 without Eu-L mediator) followed by application of a sequence of potential steps. The spectra shown here from 0 V to -0.7 V were recorded 30 min after applying each holding potential, while the spectra at -0.9 V and -1.1 V were recorded after 1 hour. Each spectrum was processed against a background spectrum at –0.1 V prior to the addition of CO (512 scans, 4 cm^{-1} resolution).

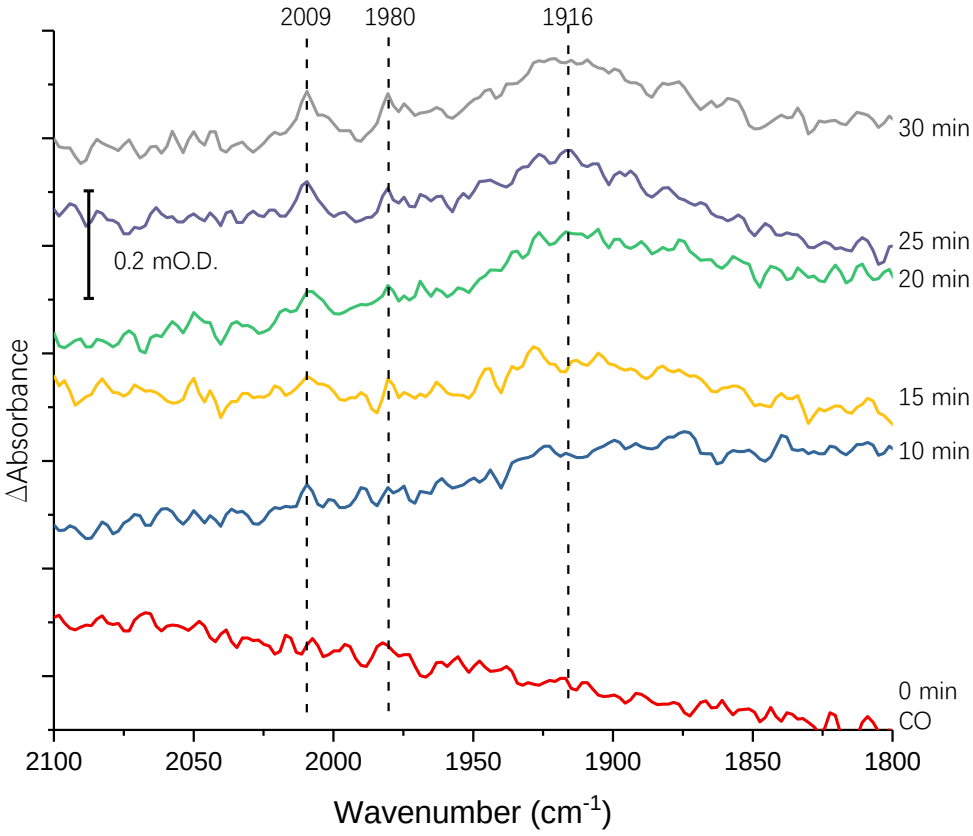


Figure 4-12: Time course IR absorbance spectra of 2 nmol of wild type MoFe protein after introduction of CO saturated solution (Tris-HCl, pH 8.0 with Eu-L mediator) at -0.9 V. Each spectrum by time was processed against a background spectrum before addition of CO (512 scans, 4 cm^{-1} resolution) at -0.9 V.

The experiment shown in Figure 4-12 was to study the effect of the introduction of CO saturated solution (Tris-HCl, pH 8.0 containing Eu-L) at a proton reduction potential. The electrochemical control was the same as shown in Figure 4-5. Spectra in Figure 4-12 were recorded when the current was stable and CO gas was introduced into the system. After about 15 min following the change to CO-saturated solution, a broad peak appeared between 1950 cm^{-1} and 1850 cm^{-1}. The peak grew slowly compared to the spectra in which MoFe protein was under CO before applying the array of potentials. The high wavenumber peaks at 2009 cm^{-1} and 1980 cm^{-1} appeared a bit later, from about 25 min all the peaks were consistent with the result in Figure 4-8, but were less intense due to the loss of MoFe protein over the long timeframe of this experiment.

4.3.2 Variant α-70$^{Val \rightarrow Ala}$ MoFe protein

The residue α-70^{Val} located around the FeMo cofactor displayed in Figure 4-13, appears to work as the substrate 'gatekeeper'.[8] Replacing the valine with an alanine amino acid residue allows bulky substrate (propargyl alcohol) to enter the active centre and be reduced.[27,28] Changing it to bulky leucine decreases the ability to reduce substrates like N_2 and Acetylene. A double exchange in the MoFe protein, α-70^{Ala}/α-195^{Gln}, allows the Mo-nitrogenase to reduce CO to methane and other hydrocarbons, like V-nitrogenase.[29]

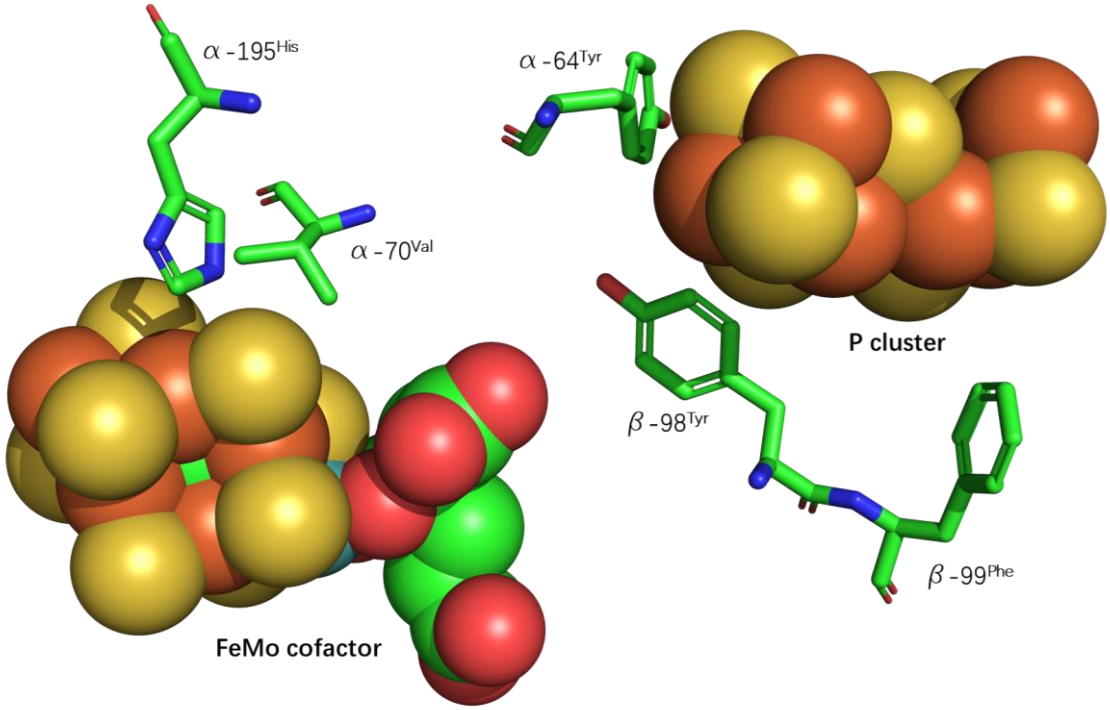


Figure 4-13: Relative positions of the two metal clusters and important amino acid residues (prepared using Pymol) in the MoFe protein which are mentioned in this chapter. (Generated from 3U7Q from RCSB PDB.)

To study the effect of the α-70 residue, variant α-70$^{Val\text{-}Ala}$ (70A) was introduced into our spectroelectrochemical system. In a similar experiment to those on the wild type enzyme, *ν*(CO) peaks appeared when the potential of -0.9 V was applied compared to the spectra at -0.7 V in Figure 4-14. The broad 1930-1900 cm^{-1} peak was only able to build up, as for wild type and other

variant MoFe proteins, at the beginning of application of the proton reduction potential (-0.9 V) but is absent in later spectra. High wavenumber peaks at 2009 cm^{-1}, 1980 cm^{-1} and 1964 cm^{-1} became the main CO-active site peaks later and correspond well to the higher wavenumber peaks for wild type MoFe protein.

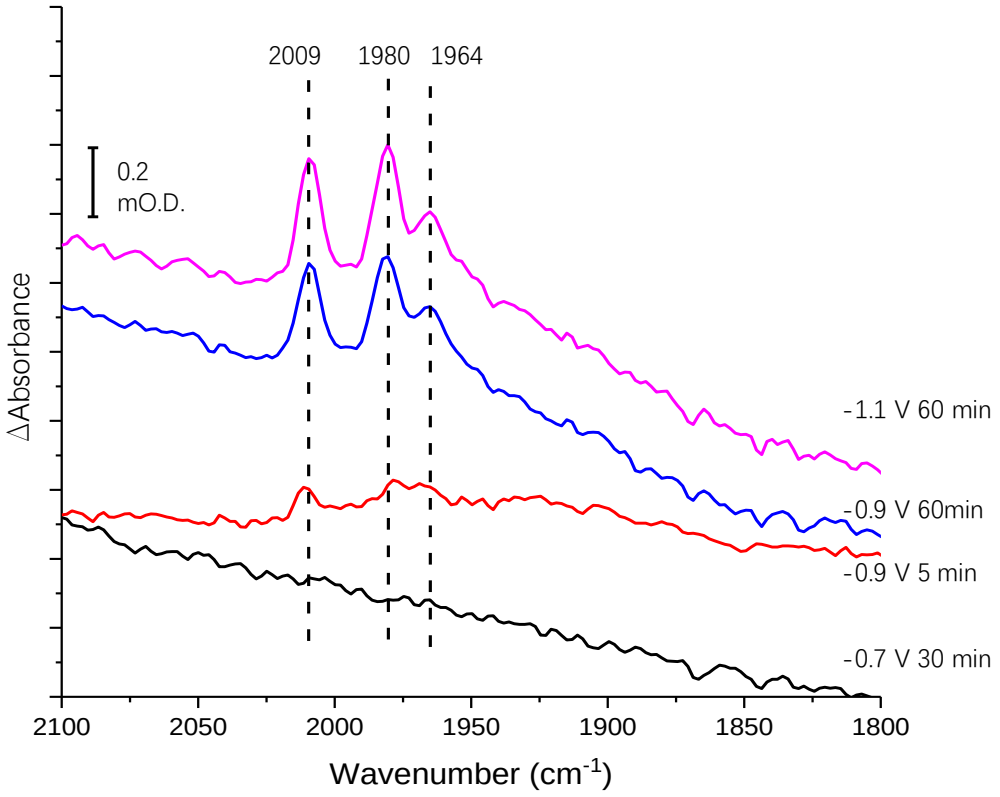


Figure 4-14: IR absorbance spectra of 2 nmol of variant 70A MoFe protein after the introduction of CO saturated solution (Tris-HCl, pH 8.0 containing Eu-L) followed by application of a sequence of potential steps. Each spectrum was processed against a background spectrum at 0 min after stepping to –0.7 V (512 scans, 4 cm^{-1} resolution).

4.3.3 Variant α-$64^{Tyr\rightarrow His}$ MoFe protein

Variant α-$64^{Tyr\rightarrow His}$(64H) is MoFe protein which replaces tyrosine by histidine and has a better proton reduction activity than wild type. The amino acid residue is located between the P cluster and FeMo cofactor, and results in the mutation MoFe protein to His with the capability to reduce substrates like hydrazine, azide, and protons at significant rates using Eu-L mediator as a reductant.

Figure 4-15 shows the spectroelectrochemical experiments with variant 64H with and without Eu-L mediators. Both experiments the *v*(CO) band appearing at -0.9 V. When 64H was posed at -0.9 V with mediators (A), there was no further growth in intensity of *v*(CO) peaks when the potential was stepped to -1.1 V. This contrasts with the result from wild type where the *v*(CO)bands grow more intense at -1.1 V. The 64H can also bind CO without the help of mediator (B), unlike the Wild type MoFe protein in the same period time, the *v*(CO) peaks shows no much difference to the peaks with the help of mediators. This is the first time we observed clearly direct electron transfer to the active site of MoFe protein and saw CO binding to MoFe protein without the help of mediators.

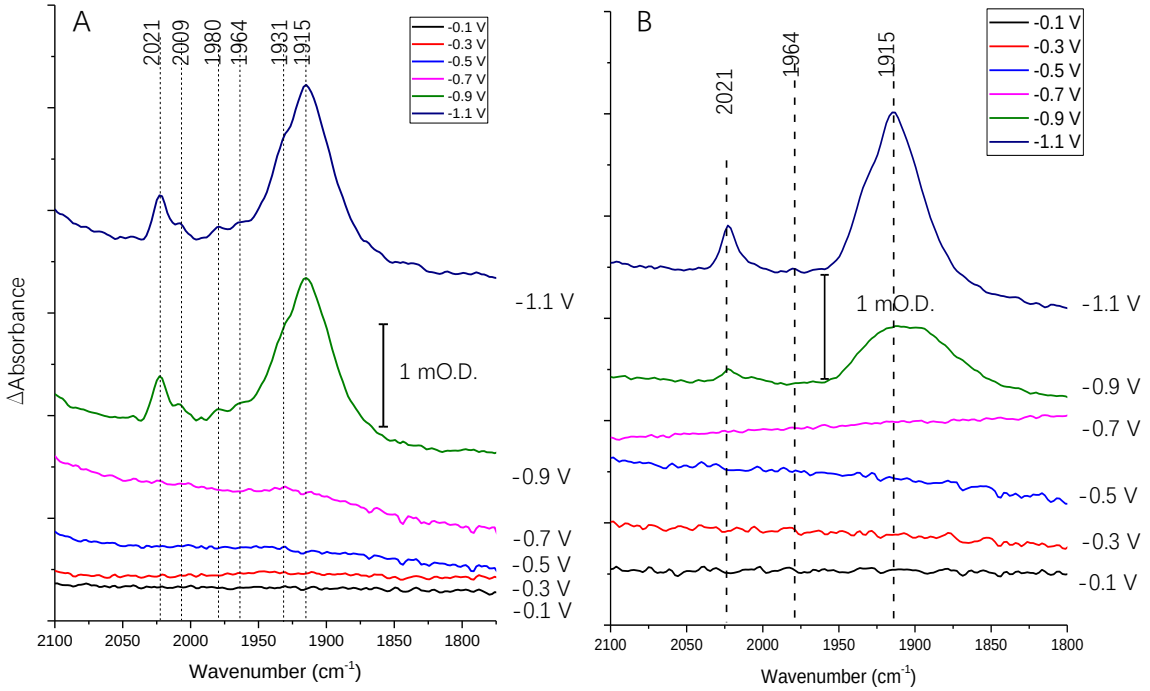


Figure 4-15: IR absorbance spectra of 2 nmol of variant 64H MoFe protein after the introduction of CO-saturated solution followed by application of a sequence of potential steps. Each spectrum was recorded after at least 30 min at each holding potential (60 min for -0.9 V and -1.1 V) and processed against a background spectrum at –100 mV prior to addition of CO (512 scans, 4 cm^{-1} resolution). CO binding peaks were obvious with the help of mediators (A) but gave a similar pattern in the buffer only system (B).

Brown et al. used cadmium sulphide (CdS) nanocrystals to photoreduce MoFe protein to reduce N_2 to ammonia.[30] Hickey et al. also demonstrated direct electroenzymatic reduction from N_2 to ammonia by using a novel pyrene-modified linear poly(ethyleneimine) to mediate electron transfer to MoFe protein.[31]

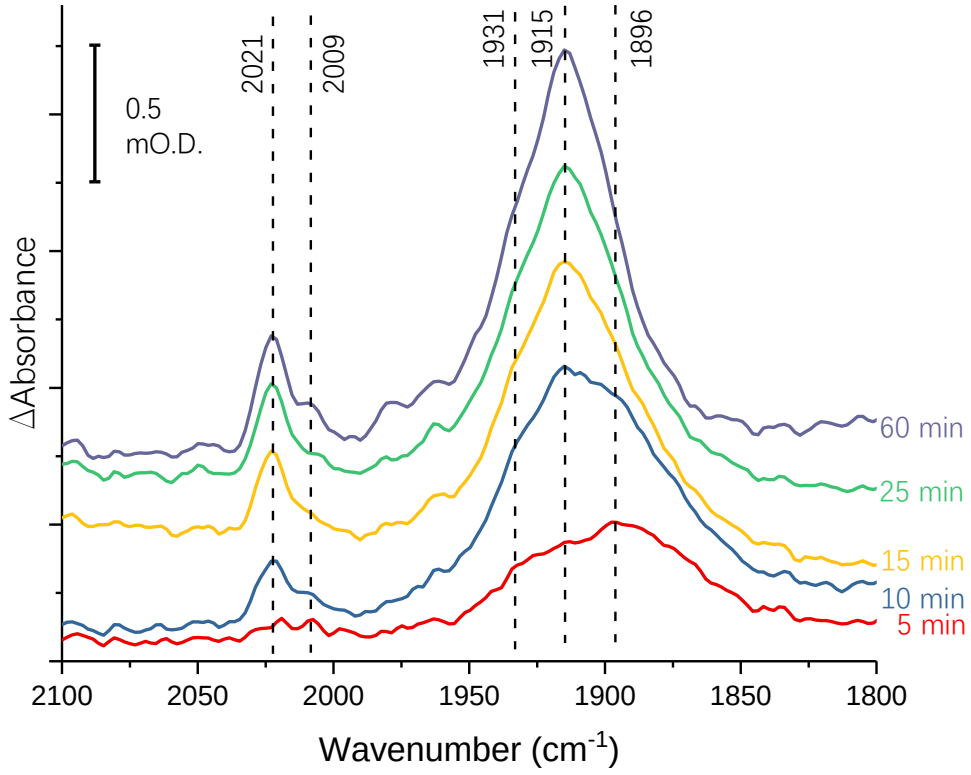


Figure 4-16: Time course IR absorbance spectra of variant 64H MoFe protein (Figure 4-15 A) in the presence of CO saturated solution (Tris-HCl, pH 8.0 containing Eu-L) at proton reduction potential (-0.9 V). Each spectrum was processed against a background spectrum at –0.7 V in the presence of CO (512 scans, 4 cm^{-1} resolution).

Figure 4-16 shows the time course of IR spectrum in Figure 4-15 (A) at -0.9 V, the centre of the main peak (1950-1850 cm^{-1}) was shifted from 1896 cm^{-1} (5 min) to 1915 cm^{-1} (10 min and later). And the peak 2021 cm^{-1} appeared clearly at this time and continuously grew as well as the peak 1915 cm^{-1}.

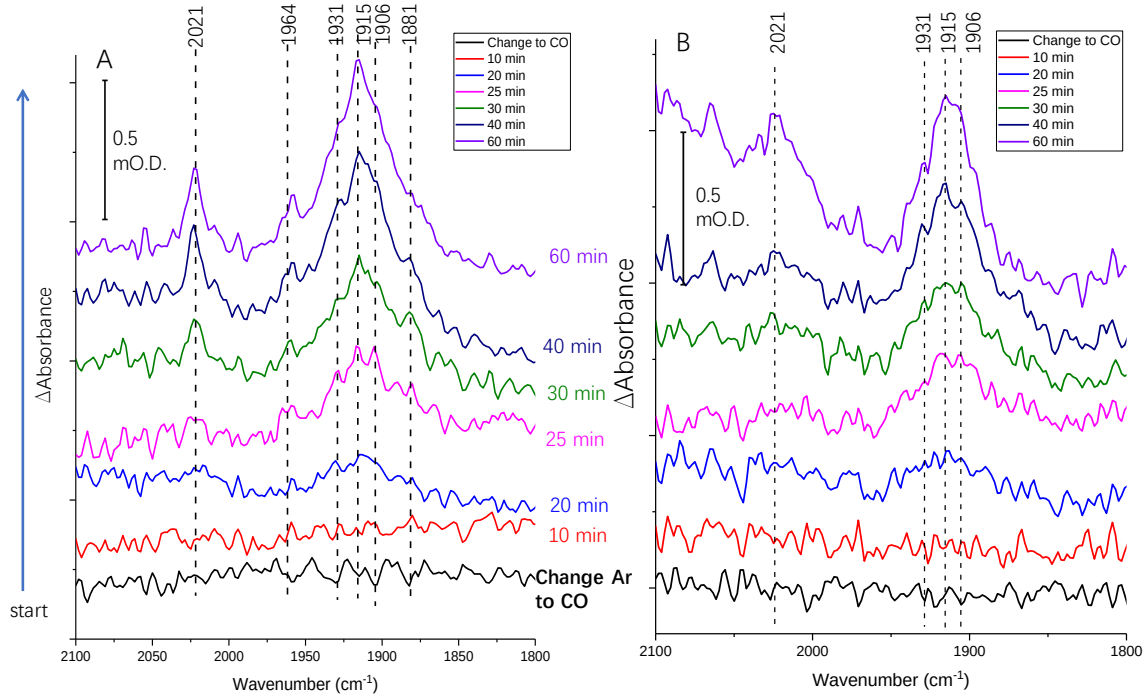


Figure 4-17: Time course IR absorbance spectra of 2 nmol of variant 64H MoFe protein after introduction of CO-saturated solution (Tris-HCl, pH 8.0 with the help of mediator (A) and buffer only system (B)) at -0.9 V. Each spectrum recorded by time was processed against a background spectrum before addition of CO at -0.9 V (512 scans, 4 cm^{-1} resolution).

The two experiments shown in Figure 4-17 were to study the effect when CO saturated solution was introduced under a proton reduction potential. The current was allowed to stabilise and then spectra were collected as CO-saturated buffer solution was introduced into the cell. About 25 min after the change to CO saturated solution, both spectra showed changes in the CO region.

The current trace was recorded at the same time at -0.9 V (shown in Figure 4-18) when collecting the IR spectra. The variant 64H MoFe protein showed a similar proton reduction inhibition tendency to the wild type MoFe protein, both with (black) and without (red) the help of Eu-L mediators. It took about 20 min CO bubbling for the inhibiton of proton reduction to stabilise, which is similar to the time in the spectral result. The catalytic current was about 15 µA greater in the presence of Eu-L suggesting that mediators help the electron transfer to some extent. In contrast the current showed no significant change with Apo protein with or without Eu-L. The

current for the variant at 100% CO was similar with and without Eu-L but was still 10 µA greater than for Apo protein, indicating that the proton reduction of the active site was not fully inhibited by CO with or without mediators.

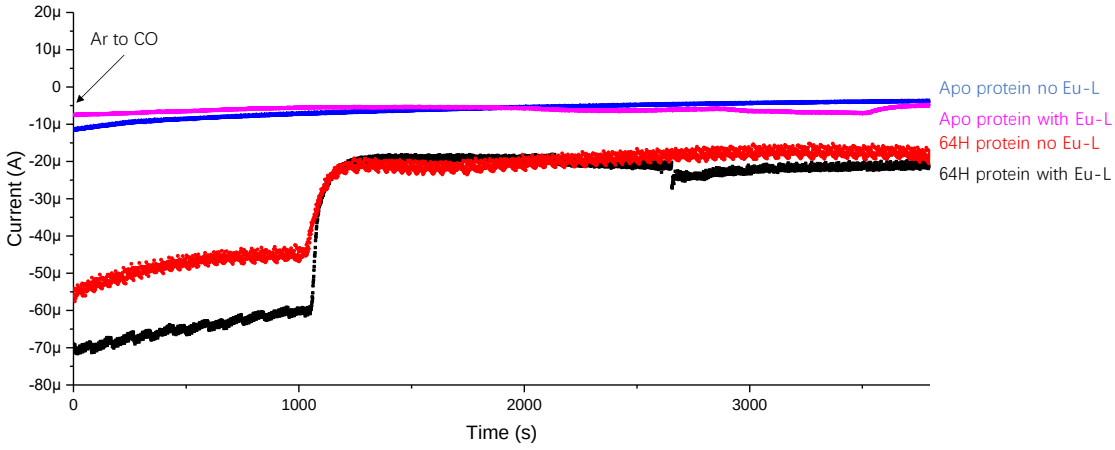


Figure 4-18: Current-time trace for electrochemical experiments on variant 64H MoFe protein and Apo protein showing the effect of CO on the electrocatalytic proton reduction current at -0.9 V. At the point 0 s, Ar to CO, the flow solution (Tris-HCl, pH 8.0 with and without the help of Eu-L) was flushed with 100% CO gas.

4.3.4 The reversibility of CO binding

In 2014 Spatzal et al. reported that the position of the ligand (CO) binding to the MoFe protein replaced a belt sulfur atom and the cluster was reactivated upon removal of CO, with the sulfur atom returning to the original place in the FeMo cofactor. These findings indicate that CO binding is reversible under certain experimental conditions.[22]

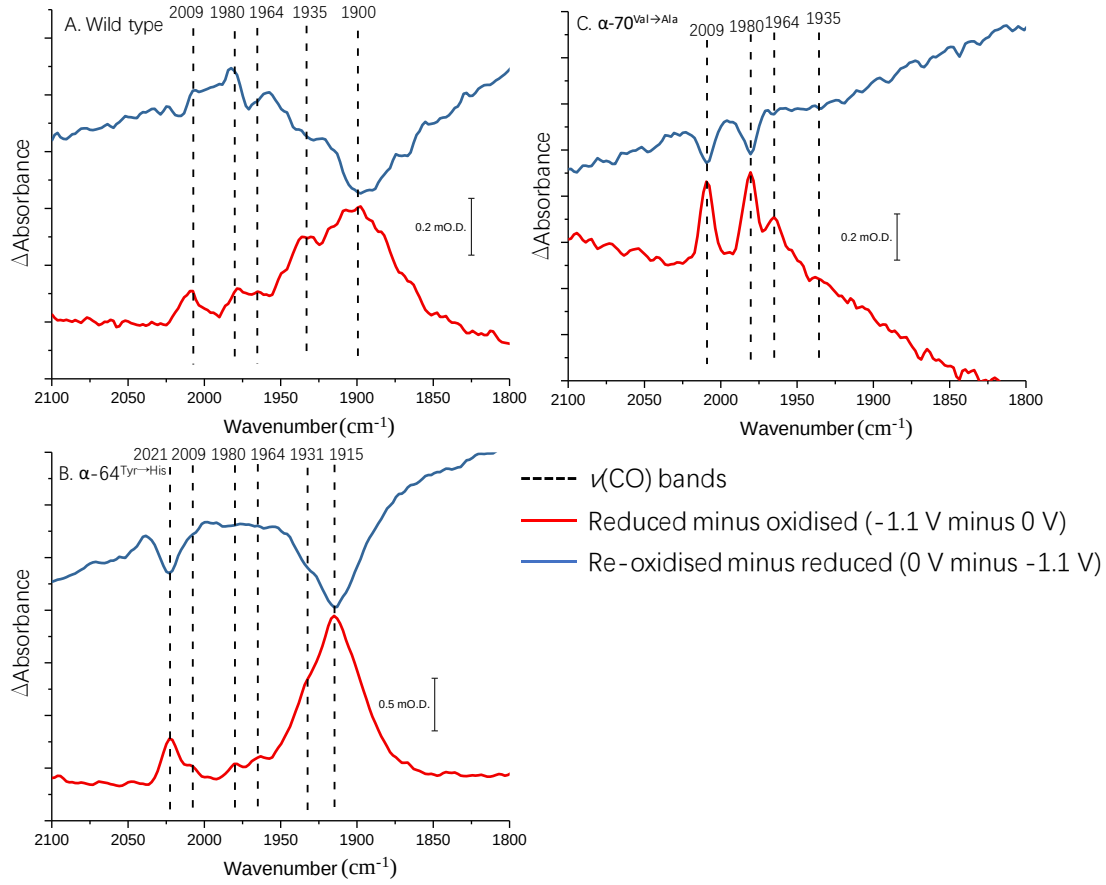


Figure 4-19: IR absorbance spectra of 2 nmol of Wild type (A), variant 64H (B) and variant 70A (C) MoFe protein under saturated CO solution (Tris-HCl, pH 8.0 with Eu-L mediators). In each diagram, the spectrum in red was the enzyme in the reduced state (-1.1 V) and use the oxidised state (0 V) as a background spectrum. The blue one was recorded after a step back to the oxidised state and used the spectrum at -1.1 V as a background spectrum. Each spectrum was collected after holding the potential for 30 min.

To study the reversibility of CO binding to the MoFe protein in the spectroelectrochemical cell, experiments were conducted as shown in Figure 4-19 by wild type, variant 64H and variant 70A MoFe protein. The experimental set up was the same as described above. The applied potentials were from the oxidised state of the protein (0 V vs SHE) to the reduced state (-1.1 V) and then back to the oxidised state again. Although all of the three enzymes showed significant reversibility after re-oxidation, there were some differences of *ν*(CO) peaks among these three proteins.

In Wild type (Figure 4-19 A), the broad and unresolved peak between 1850 cm^{-1} and 1950 cm^{-1} was similar to the main peak in Figure 4-8. Due to the low wavenumber CO species dominating, the highest point shifted to low wavelength (1900 cm^{-1}). This peak nearly disappeared after applying the oxidising potential, while the high wavenumber features like 2009 cm^{-1}, 1980 cm^{-1} and 1964 cm^{-1} changed little during the same period of time at 0 V.

There was not much difference between the two spectra of 64H and wild type. The CO binding peaks were almost completely lost at the oxidised potential in this case, even for the highest wavenumber peak at 2021 cm^{-1}.

Due to the main spectral features of CO-bound 70A being at high wavenumber, it is quite hard to compare the broad peak at low wavenumber with that of the other enzymes. The peaks at 2009 cm^{-1} and 1980 cm^{-1} decreased much faster than the peak 1964 cm^{-1} following re-oxidation.

From Figure 4-19, we can say most of the CO binding peaks are reversible under potential control. These CO-metal peaks may separate into several groups as they exhibited similar reversability in the different MoFe protein. The broad peak between 1850 cm^{-1} and 1950 cm^{-1} is the main peak for CO-metal bound species. The peaks at 2009 cm^{-1} and 1980 cm^{-1} may from one species as they seem to disappear together, and the peaks at 2021 cm^{-1} and 1964 cm^{-1} seem to be from two diverse bindings.

4.4 Using the attachment approach

4.4.1 Wild type MoFe protein

The attachment approach mentioned in Section 3.1.3 was then tested because the immobilised enzyme was much more stable on the electrode than directly absorbed on carbon particles. The CO binding experiments were conducted to determine whether the covalently coupled enzyme gave a result that was consistent with results without covalent bound enzyme (directly absorbed approach).

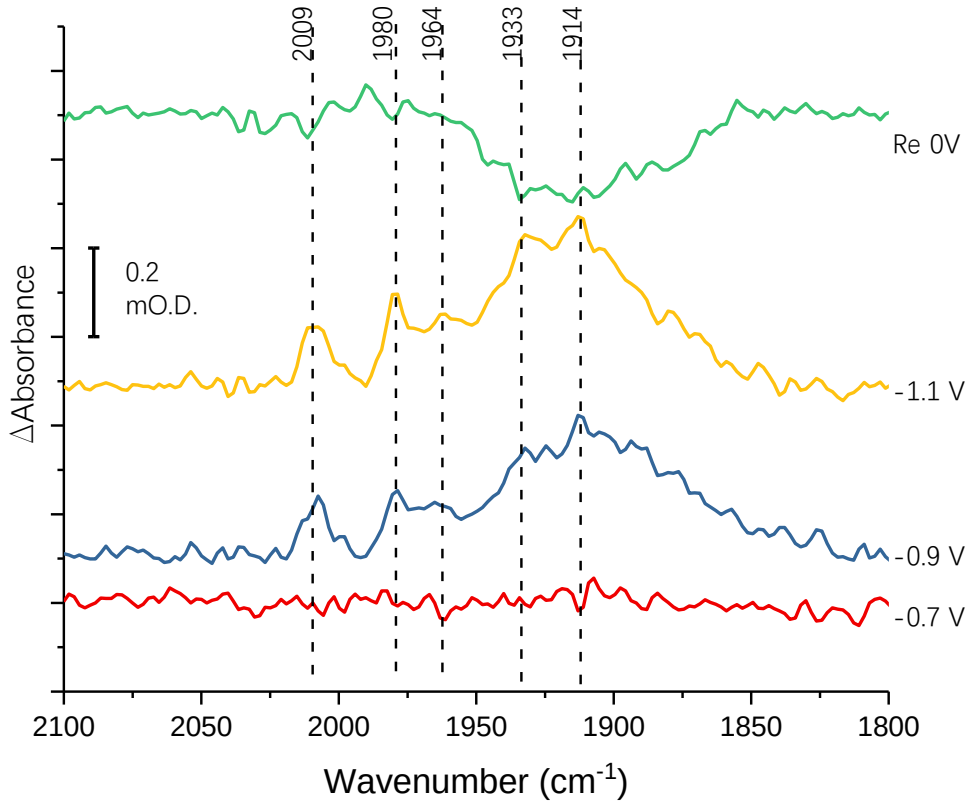


Figure 4-20: IR absorbance spectra of 2 nmol of wild type MoFe protein using the attachment approach to immobilise the protein spectra were recorded after introduction of CO saturated solution (Tris-HCl, pH 8.0 containing Eu-L) followed by application of a sequence of potential steps. The spectra at -0.7 V (—), -0.9 V (—) and -1.1 V (—) were processed against a background spectrum at –0.7 V. The spectra of protein in the re-oxidised state (Re 0 V —) used the spectrum at -1.1 V as the background (512 scans, 4 cm^{-1} resolution).

Following the method of modified carbon particles developed in Section 3.1.3, a small amount of modified carbon particle suspension was taken into the glovebox and rinsed with MilliQ water (deoxygenated) to remove DMF and minimize the O_2 content. The carboxylic group on the carbon particles was activated with EDC and NHSS and mixed with 2 nmol MoFe protein for another 6 hours. Then the protein-py-carbon mixture was rinsed with water 5 times before being deposited onto the prism and covered with carbon paper. The spectroelectrochemical cell was filled with Saturated CO solution (Tris-HCl, pH 8.0 with Eu-L mediators) through flow.

Figure 4-20 shows the results of an experiment designed to test the spectra of wild type MoFe protein under potential control. This shows similar peaks as using the direct absorbed method in Figure 4-8. However, the centre of the broad peak between 1850 cm^{-1} and 1950 cm^{-1} shifted to from 1896 cm^{-1} to higher wavenumber (1914 cm^{-1}) at the proton reduction potential, as also seen in Figure 4-21. The mid-position of the red spectrum (5 min) was at about 1896 cm^{-1} but then this species seemed to convert to another species which had higher wavenumber (1933 cm^{-1}). The centre of the main peak moved to about 1914 cm^{-1} after 25 min at -0.9 V and the peaks at 2009 cm^{-1} and 1980 cm^{-1} continuously increased in this duration, while the peak at 1896 cm^{-1} decreased with time.

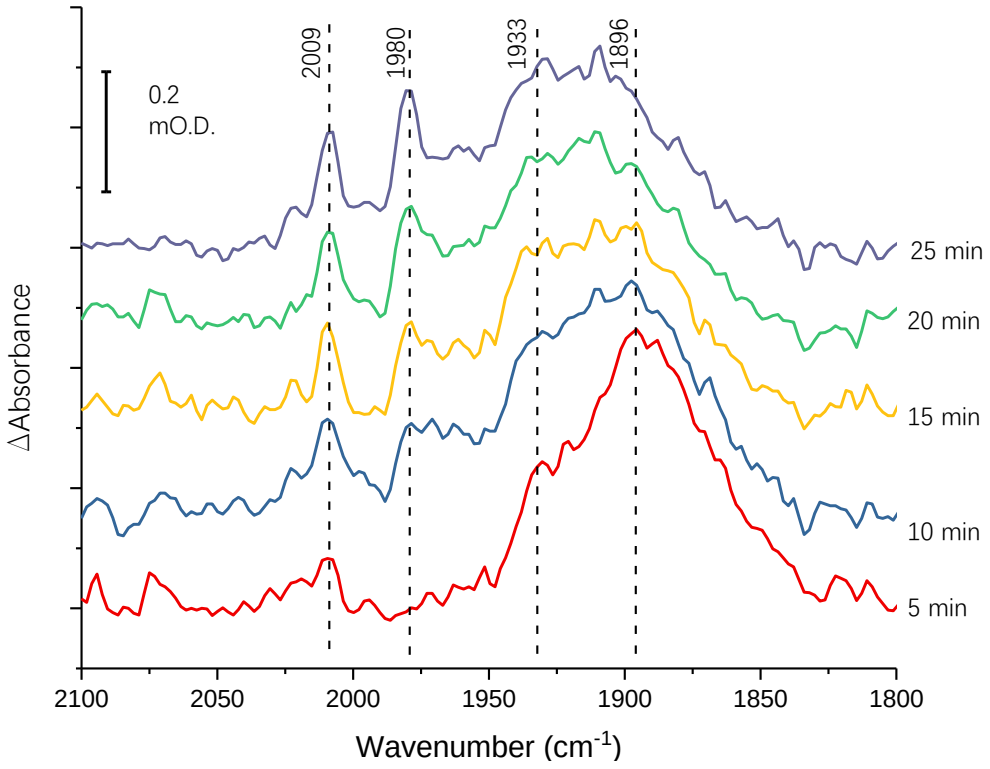


Figure 4-21: Time course IR absorbance spectra of 2 nmol of wild type MoFe protein using the attachment approach to immobilisation. Spectra were recorded after introduction of CO saturated solution (Tris-HCl, pH 8.0 containing Eu-L) at a proton reduction potential (-0.9 V). Each spectrum was processed against a background spectrum at –0.7 V (512 scans, 4 cm^{-1} resolution).

After applying a potential of 0 V to re-oxidise the protein, the result of 'Re 0 V' in Figure 4-20 was consistent with the spectrum shown in Figure 4-19. The broad spectral features lost the most intensity at 0 V, but the peaks at 2009 cm^{-1} and 1980 cm^{-1} seemed still to increase under these conditions. This indicates that these three peaks are from different CO-metal species.

4.4.2 Variant β-$98^{Tyr\rightarrow His}$ MoFe protein

According to the paper by Danyal et al., the genetically modified variant β-$98^{Tyr\rightarrow His}$ (98H) MoFe protein, is able to reduce hydrazine (N_2H_4) to ammonia using an Eu-polyaminocarboxylate complex, Eu^{II}-DTPA, as low potential reductant.[32] Study of this variant could also provide more insight into the substrate-catalytic pathway and the role of specific amino acid residues in controlling electron transfer. Coordination between CO and 'electron transfer' variant 98H MoFe protein was investigated in situ using IR spectroelectrochemistry. As the position of β-98 amino acid substitution is in a different location from the proposed CO binding sites on the FeMoco, this modification should not interfere with the CO binding to the FeMoco.

The experiment in Figure 4-22 was almost the same as the set-up of the experiment in Section 4.4.2. However, it only takes 4 hours to allow most of the enzyme to bind to the carbon particles, shown by a solution change to colourless as the enzyme-py-carbon formed together like a network in an Eppendorf tube.

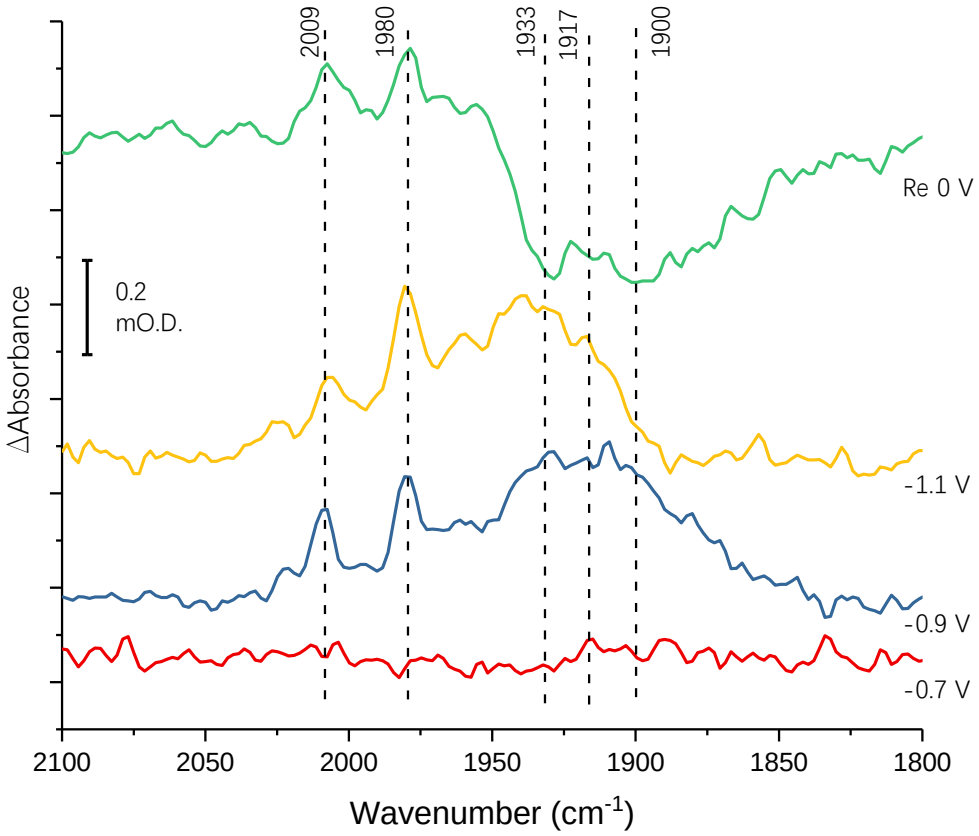


Figure 4-22: IR absorbance spectra of 2 nmol of variant 98H MoFe protein using the covalent attachment approach to immobilise protein. Spectra were recorded after introduction of CO saturated solution (Tris-HCl, pH 8.0 containing Eu-L) followed by application of a sequence of potential steps. The spectra at -0.7 V (—), -0.9 V (—) and -1.1 V (—) were processed against a background spectrum at -0.7 V. The spectra of protein in the re-oxidised state (re 0 V —) used the spectrum at -1.1 V as the background (512 scans, 4 cm^{-1} resolution).

Figure 4-19 gives the result of CO binding to the active site of variant 98H MoFe protein at different potentials. After applying -0.9 V, a broad but poorly resolved peak grew between 1950 cm^{-1} and 1850 cm^{-1}, and peaks at 2009 cm^{-1}, 1980 cm^{-1} and 1964 cm^{-1} could be observed in the spectra. It was found that the main CO binding peak to the variant 98H MoFe protein was reversible upon re-oxidation. However, the peaks at high wavenumber did not change significantly under the same conditions.

4.5 Discussion

4.5.1 CO inhibition of wildtype and variant MoFe protein

The electrochemical results from Section 4.2 showed clear catalytic current attributed to proton reduction after applying a potential of -0.9 V (vs SHE) to wild type MoFe protein and some variants of MoFe protein including variant 64H, as displayed in Figure 4-18. There was no significant evidence of proton reduction current at potentials more positive than -0.7 V compared to the control experiment in the absence of MoFe protein in the cell.

After introduction of CO saturated buffer into the spectroelectrochemical system, both wild type and variants of MoFe protein show similar inhibition of protein reduction by CO. Interestingly, proton reduction by the Fe protein/ATP-dependent nitrogenase system has been previously reported to be unaffected by CO under optimal assay conditions at pH 7.4.[33] However a study which looked into the pH dependence showed that CO inhibited the proton reduction only at basic pH values.[1] This study showed that H_2 evolution under CO is about 80% of H_2 under Ar at pH 8.0, still less than that obsevered in the present work. The earlier reported assays and SF experiment were under turnover conditions with Fe protein and ATP hydrolysis, and are likely to favour a different set of redox states of MoFe protein compared to the electrochemical experiment in this project.

For the negative current by Apo protein at -0.9 V seen in Figure 4-6 and Figure 4-18, we could see there is no change in the current after introducing CO-saturated solution into the cell, suggesting that the proton reduction happens in the FeMo cofactor of MoFe protein in this electrochemical study. The 10 μA of catalytic current by MoFe protein after inhibiting by CO was observed in contrast to Apo protein, which might indicate that CO does not fully inhibit the proton reduction by MoFe protein, or some other reduction reaction happened beyond just proton reduction.

4.5.2 *ν*(CO) peaks from CO coordination

For the wild type and variants of MoFe protein, *ν*(CO)peaks at 2009 cm^{-1}, 1980 cm^{-1} and 1964 cm^{-1} were observed from all proteins after applying -0.9 V. The broad and poorly resolved feature between 1950 cm^{-1} and 1850 cm^{-1} was centred at a slightly different position in the different variants of MoFe protein. The peak at 2021 cm^{-1} appeared only in the variant 64H and wild type MoFe protein.

From Figure 4-16 and Figure 4-21, we can see the centre of the broad peak between 1950 cm^{-1} and 1850 cm^{-1} is about 1896 cm^{-1}, soon after applying the potential of -0.9 V. The redox state of the MoFe protein or the active state of the MoFe protein was likely not fully in the reduced state. Then with time at -0.9 V, this CO species decreased, and new CO species formed at higher wavenumber compared to this broad peak, as the centre of it shifted to about 1915 cm^{-1}. This shift of the main peak was not observed from Figure 4-12 and Figure 4-17 in which CO was introduced to the solution some time after applying -0.9 V. The centre of the main peak at about 1915 cm^{-1} was gradually growing after 15-20 min bubbling with CO gas, and the CO species at 1896 cm^{-1} was not observed in theinfrared spectrum, indicating that this shift was not due to the concentration of CO in the solution.

For the high wavenumber peaks at 2021 cm^{-1}, 2009 cm^{-1}, 1980 cm^{-1} and 1964 cm^{-1}, it is difficult to make a comparison to the stop-flow literature as the spectra in that paper are shown only over the 2000 cm^{-1} to 1800 cm^{-1} region.[16] The advantage of the spectroelectrochemical experiment include better signal and further characterisation of the CO-bound complex which may be overlooked before forming the high wavenumber peak 2021 cm^{-1}, 2009 cm^{-1} and 1980 cm^{-1}. These peaks are a bit higher in wavenumber than normal mono Fe-CO species in Fe-S clusters previously reported. This suggests that these peaks may consist of $Fe(CO)_n$ structures where multiple CO ligands average the electron density on the cluster and increase the wavenumber. The result of

variant 70A in which the area near the active site is opened up shows easier formation of the higher wavenumber species under the same conditions than other MoFe proteins, consistent with the residue acting as a substrate gate. It is possible that some of the higher wavenumber peaks could be associated with CO binding to the Mo atom, (see for example, Molybdenum hexacarbonyl with ν(CO) at 2004 cm^{-1}).

4.5.3 Different sample handling approaches

In this chapter, two different methods were used to immobilise MoFe protein onto carbon particles (the working electrode), the direct adsorption and the covalent attachment. Both approaches were able to immobilise enzyme on carbon particles and did not change the property of the enzyme its own. The infrared spectra at electrodes formed in these two ways showed the same potential-dependent property for the proton reduction reaction and CO inhibition. The positions of the CO binding peaks from wild type and variants of MoFe proteins were consistent with each other.

The covalent attachment was able to keep the enzyme on carbon particles much longer (enzyme was still active in the second day) and there was almost no loss of amide II band observed from the infrared spectrum compared to the directly adsorbed approach. However, the accurate amount of enzyme immobilised onto carbon particles need to be further checked.

4.5.4 The potential scale

In the literature, a mediated electrochemical approach is often used to study the redox potential of metal clusters in nitrogenase. It was reported that the mid-point potential of the F cluster ($F^{+/2+}$) of the FeS cluster in the free Fe protein is about -300 mV (vs. SHE)[34] and shifts to -420 mV upon MgATP binding and -460 mV upon MgADP binding.[34,35] The P-cluster of the MoFe protein was found to have the same midpoint potential for the first two redox couples, $P^{N/+}$ and $P^{+/2+}$, at -307 mV, while the third couple $P^{2+/3+}$ had a higher midpoint potential at +90 mV.[36] The FeMo cofactor

of MoFe protein has a midpoint potential of first oxidised couple ($M^{N/OX}$) at -42 mV,[36] but it was found that a more reduced state of the FeMo cofactor required much lower potential redox mediators or specific reduction by the Fe protein.[37] The isolated FeMo cofactor in NMF was found to have at least two processes at different potentials (E_0= -0.3 V and E_1= -0.94 V).[38,39]

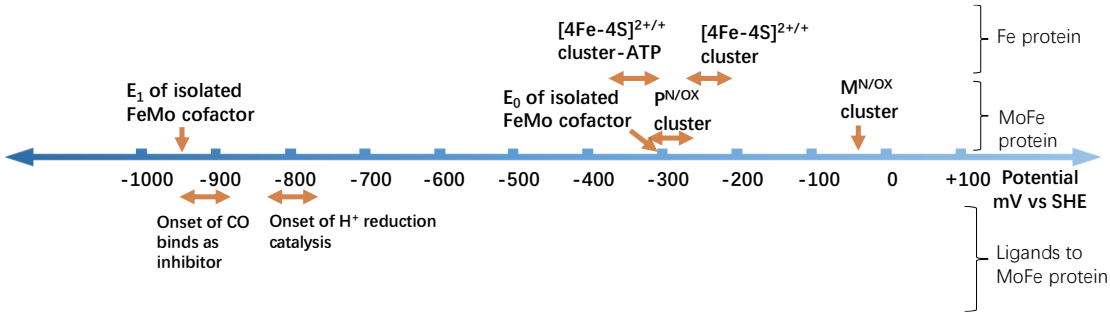


Figure 4-23: A potential scale shows the measured mid potentials of metal clusters in nitrogenase and potential of ligand binding events to MoFe protein in the electrochemical study.

Figure 4-23 displays these measured midpoint potentials on the scale and shows the potential for proton reduction and CO binding with MoFe protein in the electrochemical study. Combining the results from Paengnakorn[40] and from the present study, the onset of proton reduction by MoFe protein is about -800 mV,nd the potential for CO binding to the active site of MoFe protein is slightly more negative than the proton reduction potential.

Bibliography

1 D. N. Pham and B. K. Burgess, *Biochemistry*, 1993, **32**, 13725–13731.

2 R. N. F. Thorneley and D. J. Lowe, *J. Biol. Inorg. Chem.*, 1996, **1**, 576–580.

3 R. R. Eady and R. R. Eady, 1996, **96**, 3013–3030.

4 B. K. Burgess and D. J. Lowe, *Chem. Rev.*, 1996, **96**, 2983–3012.

5 I. Dance, *J. Am. Chem. Soc.*, 2005, **127**, 10925–10942.

6 B. M. Hoffman, D. R. Dean and L. C. Seefeldt, *Acc. Chem. Res.*, 2009, **42**, 609–619.

7 M. C. Durrant, *Biochemistry*, 2002, **41**, 13946–13955.

8 B. M. Hoffman, D. Lukoyanov, Z. Y. Yang, D. R. Dean and L. C. Seefeldt, *Chem. Rev.*, 2014, **114**, 4041–4062.

9 Z.-Y. Yang, N. Khadka, D. Lukoyanov, B. M. Hoffman, D. R. Dean and L. C. Seefeldt, *Proc. Natl. Acad. Sci.*, 2013, **110**, 16327–16332.

10 P. C. H. Mitchell, *J. Inorg. Biochem.*, 1986, **28**, 107–123.

11 B. Seger, A. B. Laursen, P. C. K. Vesborg, T. Pedersen, O. Hansen, S. Dahl and I. Chorkendorff, *Angew. Chemie - Int. Ed.*, 2012, **51**, 9128–9131.

12 M. Asadi, B. Kumar, A. Behranginia, B. A. Rosen, A. Baskin, N. Repnin, D. Pisasale, P. Phillips, W. Zhu, R. Haasch, R. F. Klie, P. Král, J. Abiade and A. Salehi-Khojin, *Nat. Commun.*, 2014, **5**, 1–8.

13 E. Skúlason, T. Bligaard, S. Gudmundsdóttir, F. Studt, J. Rossmeisl, F. Abild-Pedersen, T. Vegge, H. Jónsson and J. K. Nørskov, *Phys. Chem. Chem. Phys.*, 2012, **14**, 1235–1245.

14 D. Yang, T. Chen and Z. Wang, *J. Mater. Chem. A*, 2017, **5**, 18967–18971.

15 J. D. Tolland and R. N. F. Thorneley, *Biochemistry*, 2005, **44**, 9520–9527.

16 S. J. George, G. A. Ashby, C. W. Wharton and R. N. F. Thorneley, *J. Am. Chem. Soc.*, 1997, **119**, 6450–6451.

17 Z. Y. Yang, L. C. Seefeldt, D. R. Dean, S. P. Cramer and S. J. George, *Angew. Chemie - Int. Ed.*, 2011, **50**, 272–275.

18 Z. Yang, D. R. Dean and L. C. Seefeldt, *J. Biol. Chem.*, 2011, **286**, 19417–19421.

19 Z. Maskos and B. J. Hales, *J. Inorg. Biochem.*, 2003, **93**, 11–17.

20 L. Yan, C. H. Dapper, S. J. George, H. Wang, D. Mitra, W. Dong, W. E. Newton and S. P. Cramer, *Eur. J. Inorg. Chem.*, 2011, 2064–2074.

21 L. Yan, V. Pelmenschikov, C. H. Dapper, A. D. Scott, W. E. Newton and S. P. Cramer, *Chem. - A Eur. J.*, 2012, **18**, 16349–16357.

22 T. Spatzal, K. A. Perez, O. Einsle, J. B. Howard and D. C. Rees, *Science*, 2014, **345**, 1620–1623.

23 C. C. Lee, Y. Hu and M. W. Ribbe, *Science*, 2010, **329**, 642.

24 Y. Hu, C. C. Lee and M. W. Ribbe, *Science*, 2011, **333**, 753–755.

25 C. C. Lee, Y. Hu and M. W. Ribbe, *Angew. Chemie - Int. Ed.*, 2012, **51**, 1947–1949.

26 C. C. Lee, Y. Hu and M. W. Ribbe, *Proc. Natl. Acad. Sci.*, 2012, **109**, 6922–6926.

27 S. M. Mayer, W. G. Niehaus and D. R. Dean, *Dalt. Trans.*, 2002, 802–807.

28 R. Y. Igarashi, P. C. Dos Santos, W. G. Niehaus, I. G. Dance, D. E. Dean and L. C. Seefeldt, *J. Biol. Chem.*, 2004, **279**, 34770–34775.

29 Z. Y. Yang, D. R. Dean and L. C. Seefeldt, *J. Biol. Chem.*, 2011, **286**, 19417–19421.

30 K. A. Brown, D. F. Harris, M. B. Wilker, A. Rasmussen, N. Khadka, H. Hamby, S. Keable, G. Dukovic, J. W. Peters, L. C. Seefeldt and P. W. King, *Science*, 2016, **352**, 448–450.

31 D. P. Hickey, K. Lim, R. Cai, A. R. Patterson, M. Yuan, S. Sahin, S. Abdellaoui and S. D. Minteer, *Chem. Sci.*, 2018, **9**, 5172–5177.

32 K. Danyal, A. J. Rasmussen, S. M. Keable, B. S. Inglet, S. Shaw, O. A. Zadvornyy, S. Duval, D. R. Dean, S. Raugei, J. W. Peters and L. C. Seefeldt, *Biochemistry*, 2015, **54**, 2456–2462.

33 J. C. Hwang, C. H. Chen and R. H. Burris, *BBA - Bioenerg.*, 1973, **292**, 256–270.

34 G. D. Watt, R. R. Knotts and Z. C. Wang, *Biochemistry*, 1986, **25**, 8156–8162.

35 M. J. Ryle, W. N. Lanzilotta, L. E. Mortenson, G. D. Watt and L. C. Seefeldt, *J. Biol. Chem.*, 1995, 270, 13112–13117.

36 A. J. Pierik, H. Wassink, H. Haaker and W. R. Hagen, *Eur. J. Biochem.*, 1993, **212**, 51–61.

37 W. N. Lanzilotta and L. C. Seefeldt, *Biochemistry*, 1997, **36**, 12976–12983.

38 C. J. Pickett, K. A. Vincent, S. K. Ibrahim, C. A. Gormal, B. E. Smith and S. P. Best, *Chem. - A Eur. J.*, 2003, **9**, 76–87.

39 B. R. Lydon, C. C. Lee, K. Tanifuji, N. S. Sickerman, M. P. Newcomb, Y. Hu, M. Ribbe and J. Yang, *ChemBioChem*, 2019, **20**, 1–7.

40 P. Paengnakorn, P. A. Ash, S. Shaw, K. Danyal, T. Chen, D. R. Dean, L. C. Seefeldt and K. A. Vincent, *Chem. Sci.*, 2017, **8**, 1500–1505.

Chapter 5

Study of acetylene reduction by nitrogenase MoFe protein

Acetylene is one of the earliest studied nitrogenase substrates and is reduced to ethylene by Mo-nitrogenases. This chapter focuses on acetylene inhibition of proton reduction, and characterisation of products of acetylene reduction by the MoFe protein under electrochemical control. Several genetic variants were used to study the differences in acetylene reduction reaction under electrochemical control.

5.1 Introduction

In an early study, Dilworth observed that Mo-nitrogenase could reduce acetylene (HC≡CH) to ethylene ($(H_2C=CH_2)$ by two electrons and two protons.[1] This result opened the study of alternative substrates for nitrogenase in addition to dinitrogen and protons which are the native substrates for the protein.[2] It was shown that there is a wide range of different acetylene reduction mechanisms among the three nitrogenase proteins (Mo-, V- and Fe-), by the study of kinetics and spectroscopy. As the simplest alkyne, the molecular orbital diagram of acetylene is shown in Figure 5-1. The two sp-hybridized orbitals from each C atoms form a bond to H and the neighbouring C atom. And the pure p orbitals form two π bonds perpendicular to each other.

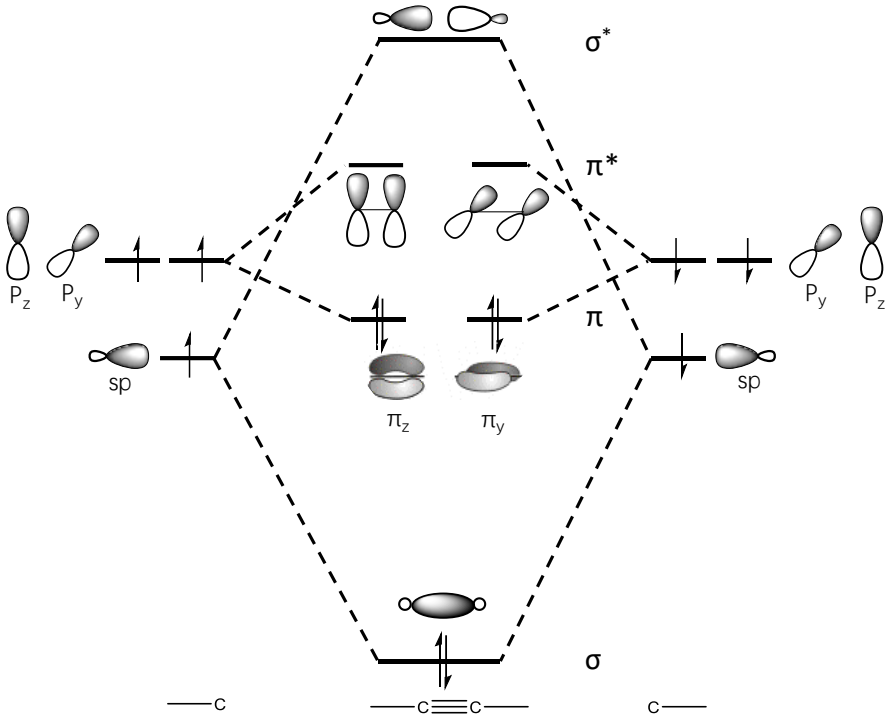


Figure 5-1: The diagram of the molecular orbital energy level of alkynes. The two sp hybrid orbitals combine and form a bonding σ orbital and an antibonding σ* orbital. The four p orbitals form two π and two π* orbitals.

The binding between acetylene and metal complexes is quite intricate. The *ν*(C≡C), and even the *ν*(C=C) are generally strong in the Raman spectra. However, their infrared intensities depend on

the metal involved and the binding between them. In the case of σ bonded acetylenic complex (M-C≡CH), the bond slightly shifts to lower wavenumber (2062 - 2000 cm^{-1}).[3] The peak of the triple bond shifts to a much lower frequency (1850 cm^{-1} for $Ti(Cp)_2(C \equiv CPh)_2Ni(CO)_4$ in Figure 5-2) due to the formation of both σ- and π-bonding. The weak π-bonding lowers the *ν*(C≡C) to about 2000 cm^{-1} in Na[Pt(RC≡CR')Cl_3] and[Pt(RC≡CR')Cl_2]$_2$ and the strong π-bonding to about 1700 cm^{-1} in Pt(RC≡CR')$(PPh_3)_2$.[4] The donation from filled d orbitals to empty π^* antibonding orbitals of acetylene weakens the triple bond and makes the frequency close to that of a double bond. The C≡C stretching exhibits at 1402 cm^{-1} when acetylene binds to two metals, as in $(HC{\equiv}CH)Co_2(CO)_6$.

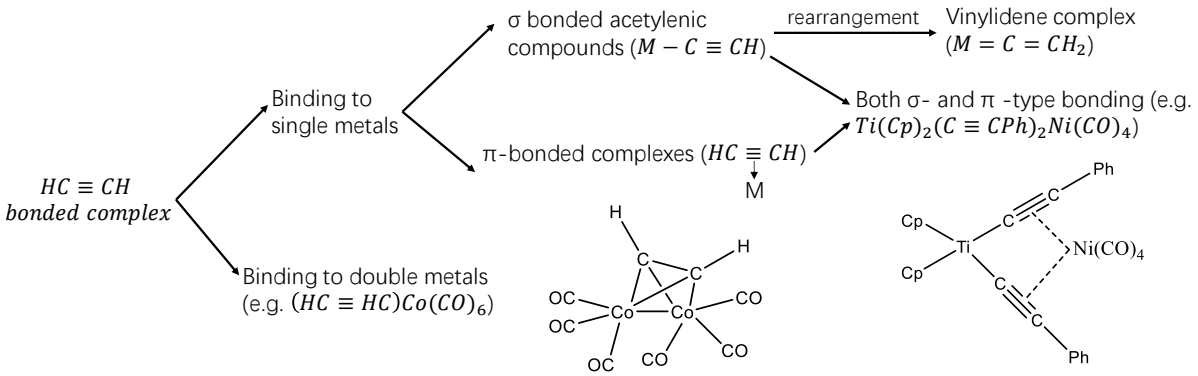


Figure 5-2: Proposed binding between acetylene (alkynes) and metal complexes.

The product of acetylene reduction by Mo-nitrogenase is mainly ethylene, with a very small amount of ethane ($H_3C–CH_3$) which is produced by a four-electron reduction process.[5,6] In contrast, both the V- and Fe-nitrogenase could produce ethylene and ethane.[7,8] Production of a mix of ethylene and ethane can also be achieved by mutation of an amino acid near the active site (FeMo cofactor) in the Mo-nitrogenase.[6,9]

An early stereochemical study of acetylene reduction showed the addition of hydrogen atoms by nitrogenase in the cis-position. This was proved by the formation of the cis-product released from either reducing acetylene gas by nitrogenase in the presence of D_2O or reducing

dideuteroacetylene (DC≡CD) in normal water.[7,10] This discovery indicated that the addition of both protons to the same side of acetylene in the nitrogenase which can be explained by a η^2-vinyl intermediate bound to the FeMo cofactor in the nitrogenase. Comparing wild type and variant nitrogenase, the more trans-product formed, the more ethane was detected.[11] Later, the characterisation of acetylene trapped in the MoFe protein by EPR and ENDOR spectroscopy showed that the reduced acetylene bound to one or more Fe atoms in the active site of the MoFe protein.[12]

Further studies on nitrogenase with bulky alkyne substrates like propyne ($CH_3C{\equiv}CH$) and 1-butyne ($CH_3CH_2C{\equiv}CH$) showed that these can also enter the active site and be subjected to two-electron and two-proton reduction reactions.[13] Propargyl alcohol ($HC{\equiv}CCH_2OH$) and propargyl amine ($HC{\equiv}CCH_2NH_2$) were also able to be reduced by nitrogenase at a very slow rate to form double bond compounds.[14,15]

5.2 Electrochemistry of acetylene reduction

The immobilisation of the MoFe protein in this chapter was carried out using the covalent approach as described in Section 3.1.3. The solution vial was filled with 6 mL Tris-HCl buffer, pH 8.0 and with 0.25 mM Eu-L mediators (Eu-BAPTA, Eu-EGTA and Eu-DTPA), and was flushed with Ar or acetylene individually using two inlet gas lines. Otherwise, the setup for the experiments with acetylene was the same as that for CO and isocyanides.

A small amount of acetylene gas used in experiments of my project was generated by reacting calcium carbide (CaC_2) with O_2-free MilliQ water in a custom-made Burris Bottle (Figure 5-3) inside the glove box. The CaC_2 stock was stored in the anaerobic glovebox to avoid possible release of O_2 during the C_2H_2 formation. An acetylene production reaction is shown below:

$$CaC_{2(s)} + 2H_2O_{(l)} \rightarrow C_2H_{2(g)} + Ca(OH)_{2(aq)} \qquad 5\text{-}1$$

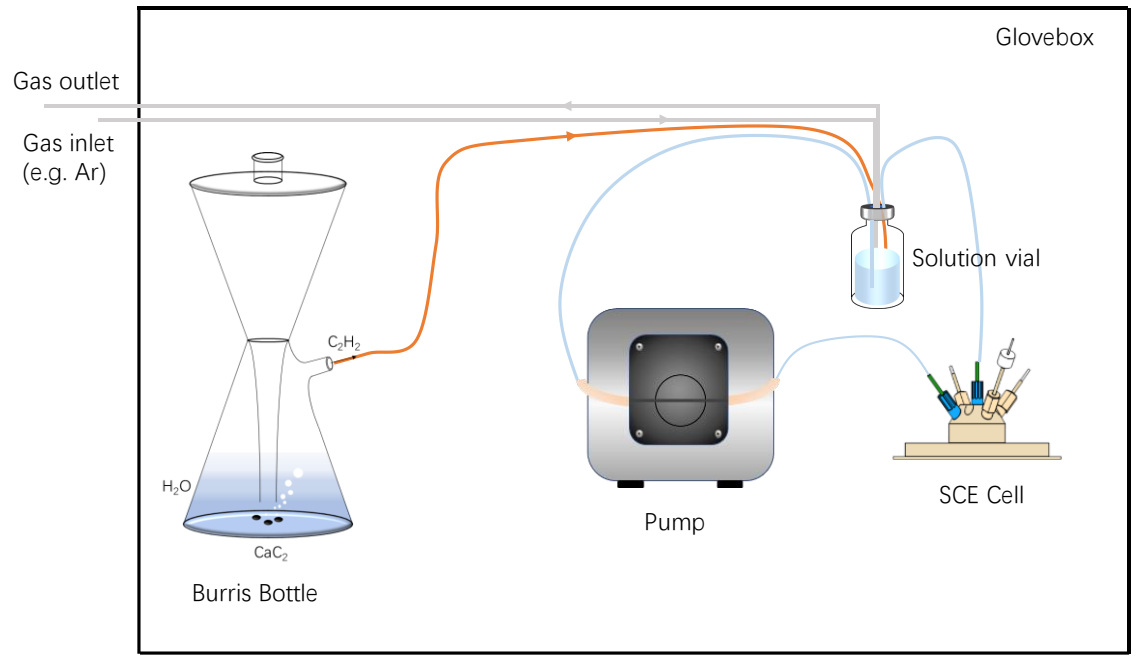


Figure 5-3: A schematic diagram of acetylene introduction to the SEC cell in a glovebox. A custom-made acetylene-generating bottle (Burris Bottle) was connected to a sealed solution vial so that acetylene gas could be bubbled into the solution (Tris-HCl buffer pH 8.0 and Eu-L mediators) which was flowed through the SEC cell by a pump.

The CaC_2 tablets were stored in a balloon which was fixed on the top of the Burris bottle by cable ties. The rate of acetylene gas production was controlled by the release of pieces of CaC_2, which react with O_2-free water as shown in Figure 5-3. The outlet of the Burris bottle was connected to a sealed solution vial as for the other gases, as described in Chapter 4. Acetylene-saturated solution (Tris-HCl buffer pH 8.0 and Eu-L mediators) was flowed into the SEC cell by the pump during the experiment. Other gases could mix with or replace acetylene in the flow system by bubbling the contents of the solution vial via another inlet (shown in Figure 5-3) at the same time. Gaseous products of nitrogenase catalysis like ethylene were able to accumulate in the headspace of the vial after disconnecting the inlet and outlet for gas flow and allowing the only solution flow into and out of the vial, and these gases in the headspace of the solution vial could be tested by other analytical methods.

5.2.1 Variant β-98$^{Tyr→His}$ MoFe protein

An experiment of Variant β-98$^{Tyr→His}$ (98H) MoFe protein in which tyrosine in β-98 position is replaced by histidine is shown in Figure 5-4. The applied potentials from 0 V to -1.1 V were the same as those used in most experiments described in my thesis. There was no significant change of the current trace in each potential step until application of -0.9 V potential. The proton reduction current reached about -40 μA at -0.9 V, while the same amount of Apo protein gave only -13 μA under analogous conditions.

After pouring the CaC_2 into the anaerobic Milli-Q water in the Burris bottle, the solution vial was bubbled with C_2H_2 gas. The Ar gas inlet was disconnected while the outlet remained open. The negative current at -0.9 V initially increased in magnitude to about -47 μA. Then the catalytic current rapidly dropped in magnitude and reached a similar current to that for the Apo protein in the control experiment. When Ar gas was used to flush C_2H_2 away from the cell, no change was observed in the current. The negative current was maintained at -10 μA during the poise at -0.9 V, during which the gas was switched between C_2H_2 and Ar.

The time of each gas bubbling after the switch was at least 10 min or until the current was stable to make the flow solution saturated with the new gas. In CO experiments from Chapter 4, it normally took about 10 min after introduction of CO to observe inhibition of proton reduction and bound CO peaks in the infrared spectra. Therefore, the rate of current change after the gas exchange between C_2H_2 and Ar suggests slow kinetics for these processes as the current change takes much longer than 10 min. Figure 5-4 shows much faster inhibition of proton reduction current by C_2H_2 which is likely due to the much higher solubility of C_2H_2 than CO.

The potential was then stepped down to -1.1 V while the solution was bubbled with Ar. The negative current initially fluctuated at around -200 μA, eventually increasing in magnitude to -280 μA at about 12300 s as shown in Figure 5-4. When a fairly stable proton reduction current was

maintained at approximately -280 µA, C_2H_2 was introduced into the flow solution. Again, the negative current briefly increased in magnitude before decaying in response to the C_2H_2 introduction, as shown in the grey region of Figure 5-4. The acetylene was flushed away from the cell with Ar when the decline of proton reduction current had stabilised. The catalytic current was able to recover this time, increasing in magnitude to about -70 µA over 1000 s. The recovery of proton reduction was confirmed by flowing acetylene gas into the cell again, which led to a drop in current again.

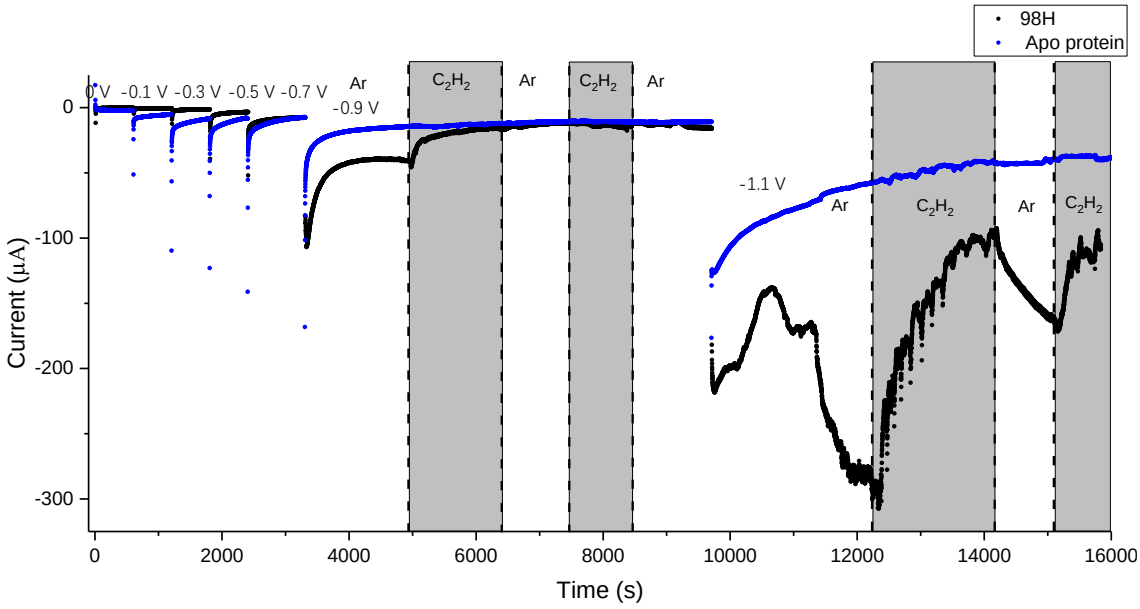


Figure 5-4: Current-time trace for an electrochemical experiment on variant 98H MoFe protein and apo protein showing the effect of C_2H_2 on the electrocatalytic proton reduction current at negative potentials. In the area shown in white, the enzyme was in Ar saturated solution (Tris-HCl buffer, pH 8.0 and Eu-L mediators). In the grey regions, the Ar gas flow was replaced by the C_2H_2 gas flow produced by calcium carbide and water in a Burris bottle.

In the control experiment on Apo protein, the negative currentshowed no change when the MoFe protein was under different gases (Ar or C_2H_2) at the low potentials (-0.9 V and -1.1 V). The proton reduction of variant 98H MoFe protein was fully inhibited by acetylene at -0.9 V (as the current

nearly overlapped that for apo protein). In contrast, at -1.1 V the current for the variant remained greater in magnitude than the current of apo protein at -1.1 V.

Acetylene is able to fully inhibit variant 98H MoFe protein at -0.9 V and the current does not recover under Ar which indicates an irreversible inhibition like CO. However, the proton reduction current recovers at least partially under Ar at a more negative potential (-1.1 V). Comparing to the Apo protein at -1.1 V, the inhibition of the variant is not complete at this potential, suggesting some residual proton reduction or some C_2H_2 reduction.

Figure 5-5 shows the current trace from an experiment designed to study the potential-dependent effect on the recovery of proton reduction by the MoFe protein when C_2H_2 is introduced and then flushed out. At the potential of -0.9 V, the proton reduction current was inhibited after bubbling with acetylene gas, as expected. The current decreased in magnitude to -13 μA and did not increase again after returning to the Ar saturated solution.

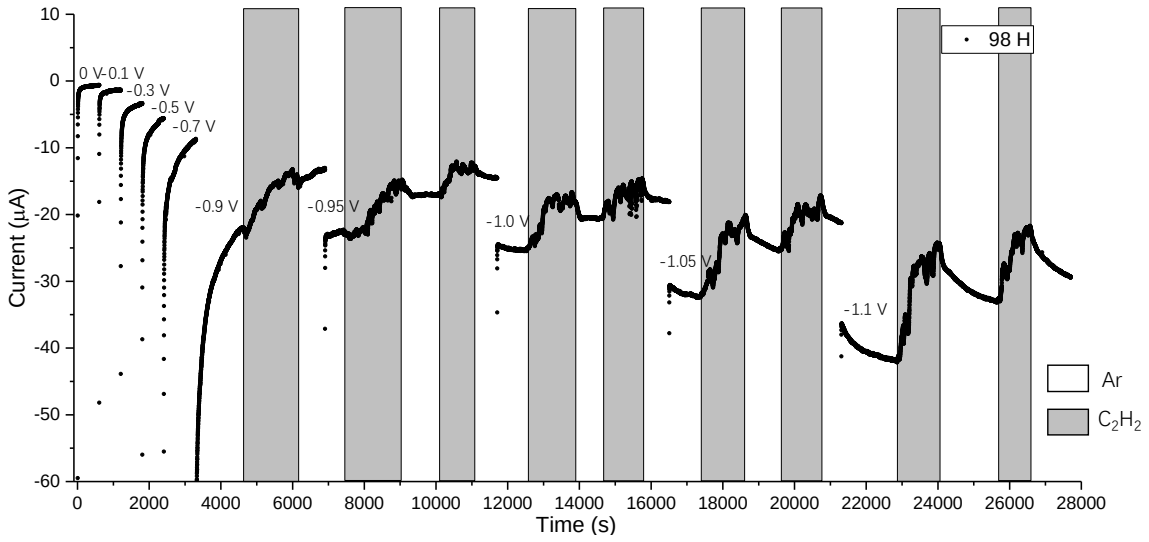


Figure 5-5: Current-time trace for an electrochemical experiment on variant 98H MoFe protein to determine the effect of potential on C_2H_2 inhibition of the electrocatalytic proton reduction current. In the area shown in white, the enzyme was under Ar-saturated solution (Tris-HCl buffer, pH 8.0 and Eu-

L mediators). In the grey region, the Ar gas flow was replaced by the C_2H_2 gas flow produced by calcium carbide and water in a Burris bottle.

After stepping to -0.95 V in Figure 5-5, the catalytic current was again inhibited by C_2H_2. However, there was some recovery in current after flushing C_2H_2 away with Ar and current was maintained at -17 μA. Repeating the gas exchange at this potential still saw a steady decrease in current magnitude under C_2H_2 (in the grey area), recovering under Ar (in the white area). Comparing three cycles of equilibration under Ar, the currents became successively lower and lower at -0.95 V. The current was first stable at about -23 μA, then arrived at -17 μA after bubbling with Ar, while the proton reduction current only reached at -15 μA during the third time under Ar.

The more negative potential of -1.0 V showed a similar result to that at -0.95 V. Here the current was stable at -25 μA, -20 μA and -18 μA respectively during each step under Ar, as displayed in Figure 5-5.

At -1.05 V and -1.1 V, there was a much more negative current as expected on increasing the driving force for catalysis and it took a longer time for the proton reduction current to level out. However, the change under different gases (Ar and C_2H_2) was the same as that at -0.95 V and -1.0 V. The negative current was partially recovered under Ar and lost again after bubbling with C_2H_2. Again, the ability to recover proton reduction dropped progressively with each cycle of gas change at one potential. The current stabilised at -33 μA, -25 μA and -22 μA at -1.05 V and at -42 μA, -33 μA and -30 μA at -1.1 V as shown in Figure 5-5. The fact that the overall current is much lower in this experiment compared to the one shown in Figure 5-4 might due to variation in protein immobilisation from one film to another or partial recovery of proton reduction at each potential as shown in Table 5-1.

Table 5-1: Negative current of variant 98H MoFe protein in saturated Ar solution after cycles of exposure to C_2H_2

Variant 98 H	-0.9 V	-0.95 V	-1.0 V	-1.05 V	-1.1 V
First under Ar	-22 μA	-23 μA	-25 μA	-33 μA	-42 μA
Second under Ar	-	-17 μA	-20 μA	-25 μA	-33 μA
Third under Ar	-	-15 μA	-18 μA	-22 μA	-30 μA

Figure 5-6 was the study of the interaction between acetylene and MoFe proteins under electrochemical control. The proton reduction current of variant 98H MoFe protein was not significant without Eu-L mediators in the flow solution before 8000 s, and there was no change in current at -1.0 V after a gas exchange between Ar and C_2H_2. After injecting Eu-L mediator into the solution vial to give a concentration of 0.25 mM, the current (black line, Figure 5-6) increased in magnitude rapidly as a result of direct reduction of the oxidised Eu-L. Then the catalytic current continued to increase in magnitude over time, which indicated the proton reduction by the variant 98H needed the help of Eu-L mediators at -1.0 V. The proton reduction current was stable at -60 μA and at 10800 s was inhibited after C_2H_2 gas was introduced into the cell. The proton reduction current showed an initial rapid increase in magnitude, and then slowly decreased to about -30 μA in saturated C_2H_2 solution. As observed previously, this inhibition could be removed after flushing C_2H_2 out of the solution, causing the current to reach -46 μA eventually.

When Apo protein was used in the control experiment in Figure 5-6, the blue current trace took a bit longer to stabilise at -1.0 V without Eu-L mediators, slowly decaying to less than -10 μA. Exchanging gas between Ar and C_2H_2 in this stage also did not give any change in current. Adding the Eu-L into the flow system caused the current to increase in magnitude to about -20 μA immediately. Introducing C_2H_2 gas into the solution did not affect the catalytic current. The

fluctuation of current in the grey area (shown in Figure 5-6) can be explained by variation in pressure when CaC_2 reacts in the Burris bottle and produces C_2H_2. The current of apo protein was maintained at about -20 µA in either Ar or C_2H_2 saturated solution at -1.0 V.

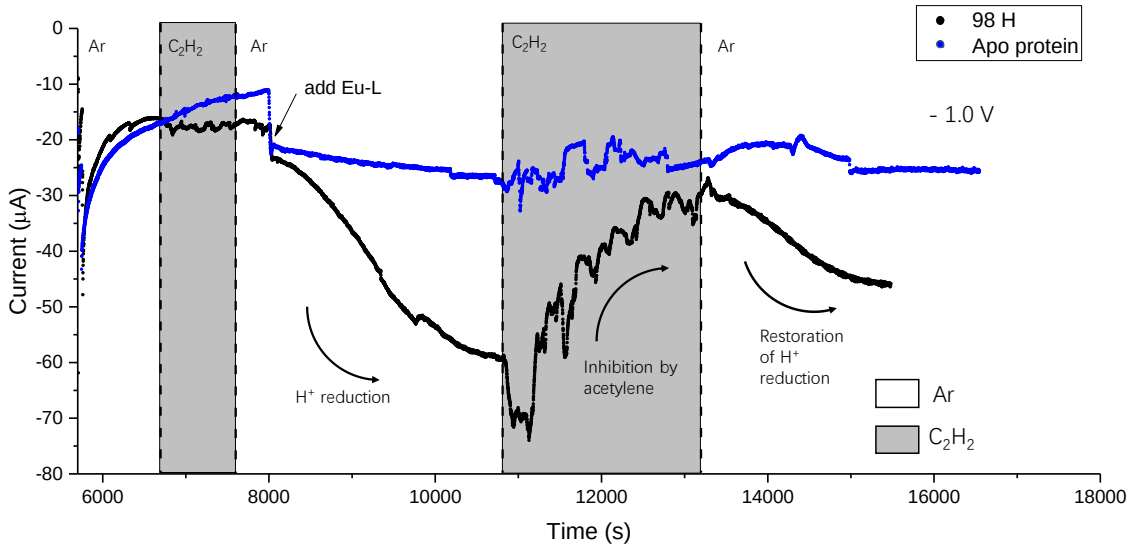


Figure 5-6: Current-time trace for an electrochemical experiment on variant 98H MoFe protein (black) and Apo protein (blue) of the MoFe protein showing the effect of C_2H_2 on the electrocatalytic proton reduction current with and without Eu-L. The 0.25 mM of Eu-L mediators was injected into the solution vial (containing Tris-HCl pH 8.0) at 8000s. In the area shown in white, the enzyme was under Ar-saturated solution. In the grey region, the Ar gas flow was replaced by the C_2H_2 gas flow produced by calcium carbide and water in a Burris bottle.

The proton reduction by variant 98H MoFe protein could be inhibited by acetylene at -0.9 V, and this inhibition was able to be relieved after flushing C_2H_2 out with Ar at -0.95 V. The recovered current did not reach its original level after each cycle of inhibition. Similar effects were seen at -1.0 V and -1.05 V, showing that the inhibition is partially reversible at potentials more negative than -0.9 V. At -1.1 V, the magnitude of current drop was greater in C_2H_2, but this inhibition was partially reversible again. Eu-L as mediator was confirmed as playing an important role in proton reduction by variant 98H MoFe protein at the low potential, and there was no inhibition of proton reduction current by C_2H_2 in the absence of Eu-L at -1.0 V.

5.3.2 Variant α-70$^{Val\rightarrow Ala}$ MoFe protein

For the experiments of variant α-70$^{Val\rightarrow Ala}$ (70A) MoFe protein, the cell and gases were set up as described above. The potential steps were applied from 0 V to -1.1 V as for 98H.From 0 V to -0.7 V, the current at each potential under Ar showed no significant change, as shown in Figure 5-7, indicating no significant proton reduction in this region. After a potential of -0.9 V, the proton reduction current increased to about -50 µA. The catalytic current was rapidly inhibited upon introduction of C_2H_2 and decreased to -12 µA at 8000 s. Unlike 98H, the proton reduction current was able to recover to about -26 µA over 20 min of poising at -0.9 V under Ar. Acetylene was then re-introduced, and the current was again inhibited, dropping to -12 µA. It took much longer (about 1 hour) for the current to recover to a stable level (-26 µA) after flushing C_2H_2 away.

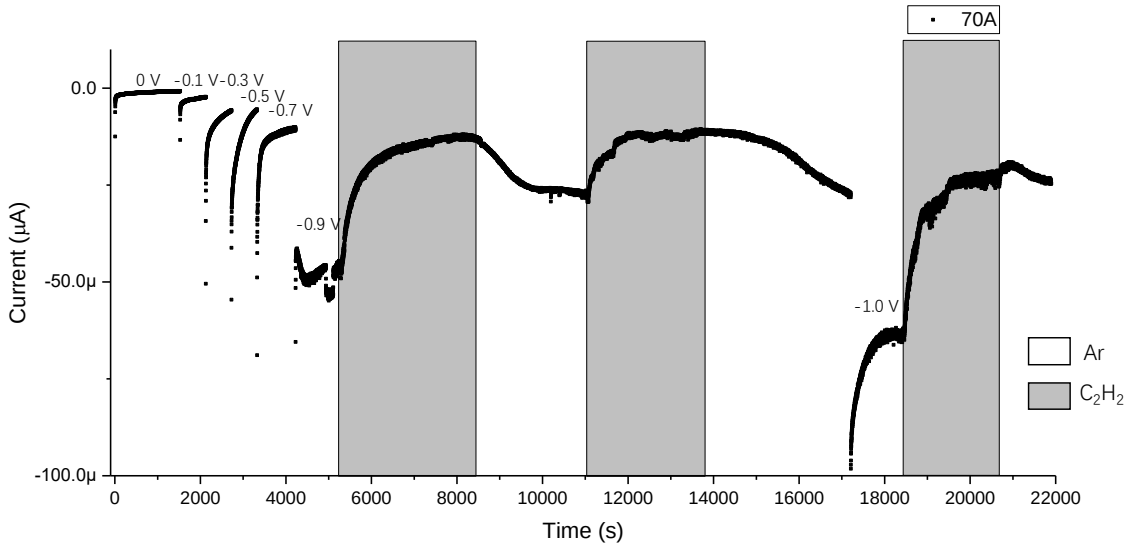


Figure 5-7: Current-time trace for an electrochemical experiment on variant 70A MoFe protein showing the effect of C_2H_2 on the electrocatalytic proton reduction current at low potential. In the area shown in white, the enzyme was in Ar saturated solution (Tris-HCl buffer, pH 8.0 and Eu-L mediators). In the grey region, the Ar gas flow was replaced by the C_2H_2 gas flow produced by calcium carbide and water in a Burris bottle.

Similar inhibition of catalytic current was observed at -1.0 V as shown in the later part of Figure 5-7. There was still some recovery under Ar at -1.0 V.

In contrast to 98H, the catalytic current for variant 70A MoFe protein could be restored under Ar at -0.9 V, a potential at which inhibition is irreversible for 98H.

5.3.3 Wild Type MoFe protein

The C_2H_2 introduction to the wild type MoFe protein showed a similar electrochemical profile to that of 98H with the help of Eu-L mediators at -0.9 V. The proton reduction current was inhibited by C_2H_2 at the potential of -0.9 V and this inhibition could not be removed by flushing the C_2H_2 gas away.

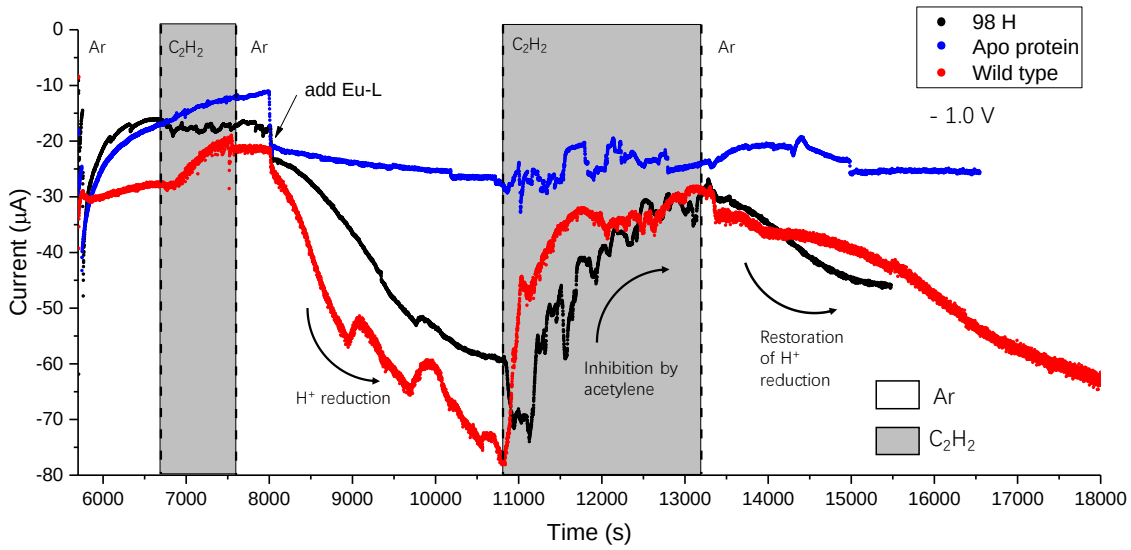


Figure 5-8: Current-time trace for an additional electrochemical experiment on wild type MoFe protein (red) showing the effect of C_2H_2 on the electrocatalytic proton reduction current. The 0.25 mM of Eu-L mediators was injected into the solution vial (containing Tris-HCl pH 8.0) at 8000s. In the area shown in white, the enzyme was under saturated Ar solution. In the grey region, the Ar gas flow was replaced by the C_2H_2 gas flow produced by calcium carbide and water in a Burris bottle.

Figure 5-8 shows an additional result of wild type MoFe protein at -1.0 V, superimposed on the plots shown previously in Figure 5-6. All setup of the experiment was the same as that for 98H and

apo protein, in which the enzyme was slowly stepped to -1.0 V under Ar in the absence of Eu-L mediator.

The current of wild type MoFe protein (red line) was much more negative under Ar at -1.0 V compared to variant 98H in the absence of Eu-L. The current was stable at -28 μA before the introduction of C_2H_2 gas into the SEC cell. The negative current shown in the first grey area decreased slowly in magnitude under C_2H_2 which indicated that the direct electron transfer to wild type MoFe protein happened at -1.0 V and could be inhibited by C_2H_2 without the help of Eu-L mediators. The inhibited current was close to the current of 98H. The negative current held at -21 μA when the cell was changed back to Ar saturated solution, showing that inhibition is irreversible for wild type MoFe protein under these conditions. The catalytic current of wild type MoFe protein showed similar changes as those observed for variant 98H MoFe protein after injecting 0.25 mM Eu-L mediators at 8000 s. However, it decreased in magnitude much faster and reached a more substantial current of -75 μA over the same period of time. The C_2H_2 gas caused the current of wild type MoFe protein to drop to about -30 μA which was a similar quantity of inhibition as observed for 98H. The restoration of proton reduction under Ar took a much longer period but the current could reach a similar level to the initial proton reduction current under Ar with Eu-L, showing that C_2H_2 inhibition is fully reversible at -1.0 V for wild type MoFe protein.

5.3 Infrared spectroscopy of alkyne reduction

There has been little literature study of acetylene reduction by nitrogenase using vibrational spectroscopy. In 1979, McMillian showed that a synthetic cluster $[Fe_4S_4(SPh)_4]^{3-}$ reduced acetylene to ethylene, and identified cis-1,2$C_2H_2D_2$ as the main product from acetylene in the presence of a deuterium source by gas-phase FT infrared spectroscopy.[16] Later stereospecific study by wild type and variant nitrogenase showed that the binding of acetylene to the active site of nitrogenase was not consistent with the σ bonded acetylenic terminated bound structure.[11] However, due to the

weak absorbance bands from the CC triple bond and the CC double bond of coordinated alkynes/alkenes in infrared spectroscopy, it is quite difficult to study intermediates directly from the infrared spectrum. Additionally, the overlap with the stretching bands *v*(OH) and *v*(NH) also make it hard to determine species unambiguously. All previous studies on nitrogenase focused on the gaseous products collected from the acetylene reduction.

5.3.1 Using acetylene as a ligand

Symmetric stretching of the carbon-carbon triple bond from acetylene is IR-inactive due to there being no change of dipole moment. Only if a terminal bond occurs, the peak of a carbon-carbon triple bond or double bond could be easily observed from IR spectra.

Figure 5-9 shows the infrared spectra of the variant 70A MoFe protein in the presence of C_2H_2, with the help of Eu-L mediators. The spectrum labelled "-0.9 V Ar" shows the protein under Ar at -0.9 V, against a background recorded 30 min earlier under the same conditions. This spectrum showed no significant peaks except a small loss of amide I&II bands. After the introduction of C_2H_2 into the flow system, three peaks (1626 cm^{-1}, 1558 cm^{-1} and 1518 cm^{-1}) increased in a similar region to the amide bands. This change could be observed at a low potential (-1.1 V C_2H_2, Figure 5-9). There was no peak appeared above 2000 cm^{-1} which indicated no terminal acetylenic species bound to the active site (M-C≡CH) observed from ATR-IR spectra at this potential.

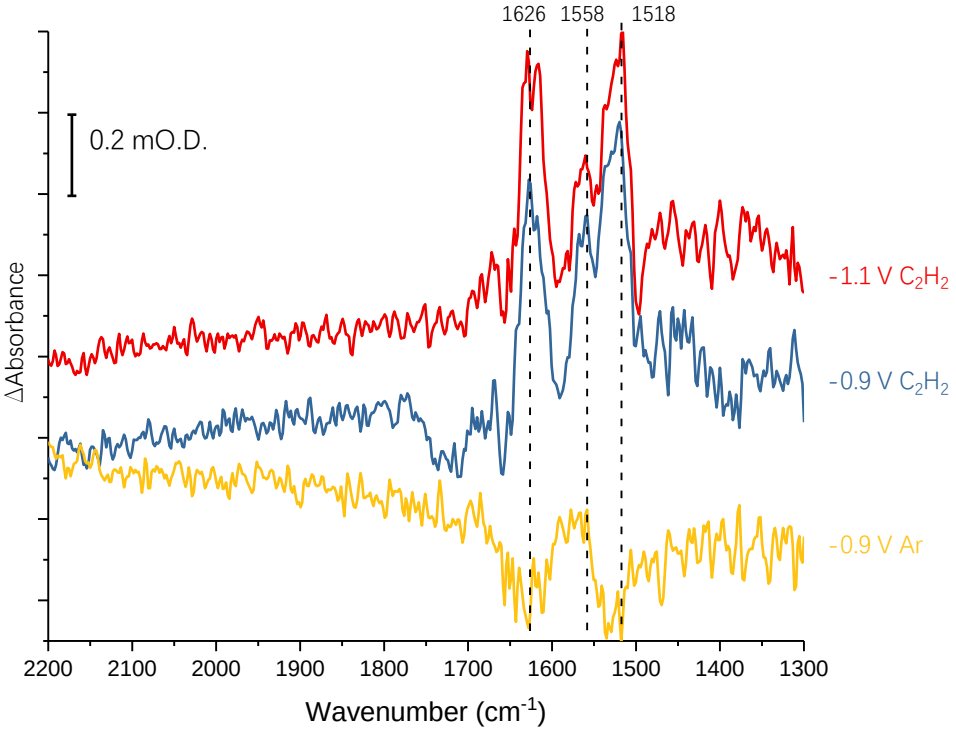


Figure 5-9: IR absorbance spectra of 4 nmol variant 70A MoFe protein in Tris-HCl buffer pH 8.0 containing Eu-L mediators at low potentials. Each spectrum was recorded when the system was in equilibrium at each holding potential and processed against a background spectrum recorded under Ar at the same potential (512 scans, 4 cm^{-1} resolution).

5.3.2 Using propargyl alcohol as a ligand

Variant 70A nitrogenase has been reported to reduce propargyl alcohol to allyl alcohol (CH_2=$CHCH_2OH$) by two protons and two electrons.[17] Due to unsymmetrical *v*(C≡C) stretching, the peak of the triple bond should be observable in infrared spectra. Figure 5-10 shows the infrared spectrum of 0.1 M propargyl alcohol (Sigma). The peak of *v*(C≡C) was observed at ca. 2119 cm^{-1}, and the peak at 1026 cm^{-1} was from *v*(C-O) which had much strong intensity. The vibrations of -OH and -CH from propargyl alcohol were covered by the solvent vibrational features.

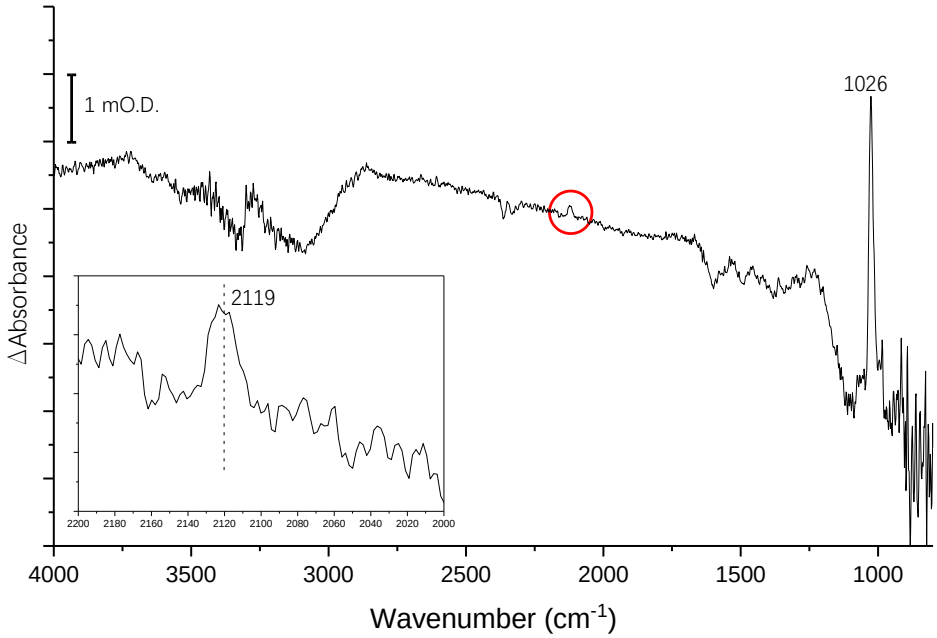


Figure 5-10: IR absorbance spectra of 0.1 M propargyl alcohol in Tris-HCl buffer pH 8.0 containing Eu-L mediators by ATR-IR (512 scans, 4 cm^{-1} resolution).

Figure 5-11 (A) shows that the *ν*(C≡C) appeared at 2119 cm^{-1} when 0.1 M propargyl alcohol was introduced into the spectroelectrochemical cell without applied any potential. There was not any change of this *ν*(C≡C) peak under electrochemical control to low potentials in the region from 2200 cm^{-1} to 2000 cm^{-1}. However, some new peaks (1497cm^{-1}, 1460 cm^{-1} and 1400 cm^{-1}) in the low wavenumber appeared at -1.1 V as clearly shown in Figure 5-11 (B). Changes in the amide bands and water absorption would cover any bands above 1500 cm^{-1}, like *ν*(C=C).

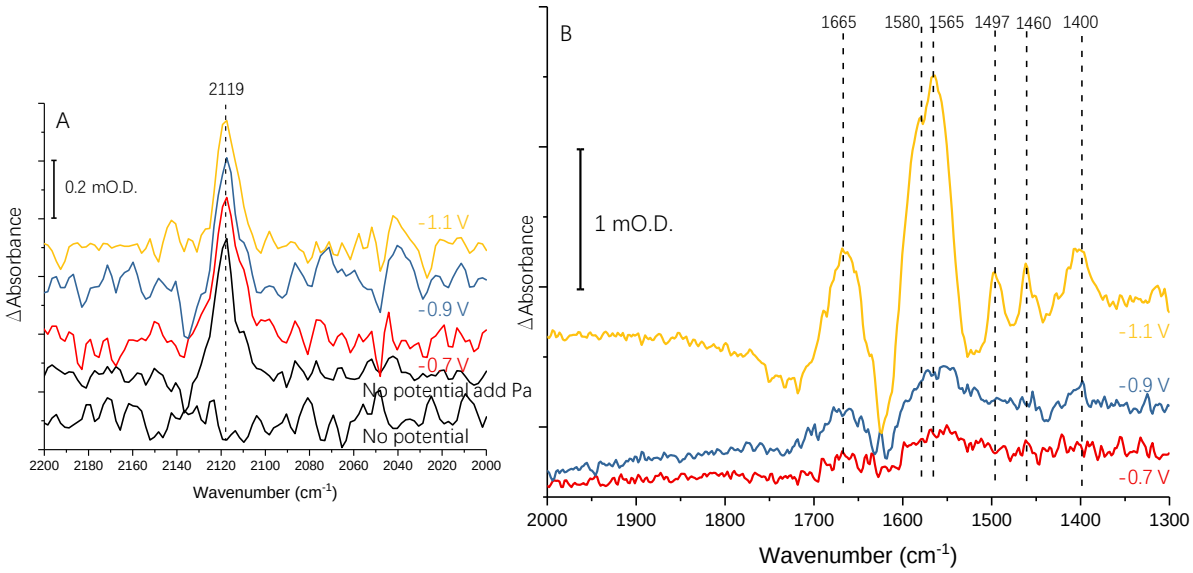


Figure 5-11: IR absorbance spectra of 4 nmol variant 70A MoFe protein in Tris-HCl buffer pH 8.0 containing Eu-L mediators with 0.1 M propargyl alcohol. (A) showed the region of ν(C≡C) before and after adding propargyl alcohol and the change with different potentials. Each spectrum was processed against a background in the absence of propargyl alcohol with no applied potential. (B) shows the spectra in the low wavenumber region and each spectrum was processed against a background at -0.7 V in the presence of propargyl alcohol (512 scans, 4 cm^{-1} resolution).

5.4 Ethylene determination by GC

To confirm the product of acetylene reduction, gas chromatography with a flame ionization detector was used to determine gases in the headspace of the solution vial. All experiments in this section were completed in Lance Seefeldt's group in the Department of Chemistry and Biochemistry, Utah State University, USA.

The experiment setup was the same as for the study by electrochemistry described above, because the electrochemical cell was taken to the Utah lab. The wild type MoFe protein was attached to modified carbon particles (10 µL, 10mg/mL) and deposited on the centre of the baseplate of the electrochemical cell. During experiments, 6 mL of 100 mM Tris-HCl buffer (pH 8.0) solution with 0.25 mM Eu-L mediators was flowed through the cell by a pump. The

electrochemistry was controlled by a PalmSens 4 potentiostat. All experiments were carried out in an anaerobic glove box filled with 98% Ar and 2% H_2. Instead of producing gas from a Burris Bottle, an acetylene gas cylinder was connected to the inlet gas line to the solution vial. Both inlet and outlet gas lines were closed during the acetylene reduction reaction in the flow system which allowed gaseous products to accumulate in the headspace of the solution vial. A 50 µL sample was taken for analysis each time from the headspace of the solution vial by an airtight syringe and analysed by GC as shown in Figure 5-12 (B). All data shown below were corrected by the standard curve which was found using pure ethylene gas.

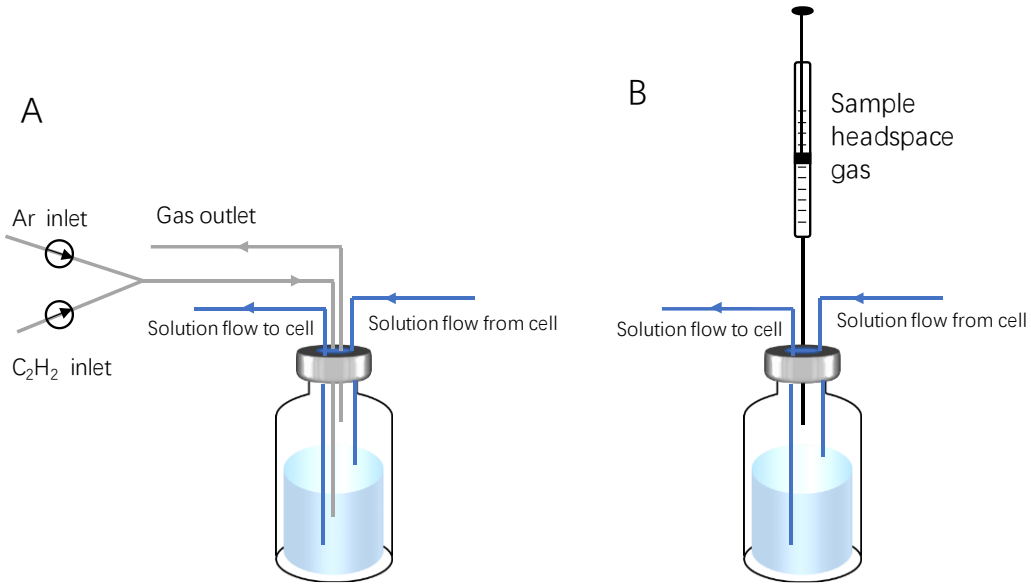


Figure 5-12: A schematic diagram of gas bubbling (A) and headspace gas sampling (B) in Lance Seefeldt's lab of Utah State University.

5.4.1 Acetylene reduction by wild type MoFe protein

Figure 5-13 shows a plot of ethylene production determined by GC with different applied potentials, from -0.7 V to -1.1 V. The flow solution was bubbled by acetylene from a pure gas cylinder at -0.7 V for 10 min. The initial sample was taken after closing the inlet and outlet to gas flow as shown in Figure 5-12.

There was a very small amount of ethylene produced at -0.7 V. Only about 1.2 nmol of ethylene was formed in 3 hours under electrochemical control. This production rate increased about 30 times after the applied the potential was stepped to -0.9 V, and about 40 nmol product was determined by GC after 3 hours at -0.9 V.

After stepping down to -1.1 V, the ethylene formation rate grew to about 10 nmol/min/mg protein which was about 14.5 times higher than that at -0.9 V. And this rate was quite stable over 5 hours, as the production of ethylene was nearly linear, as shown in Figure 5-13.

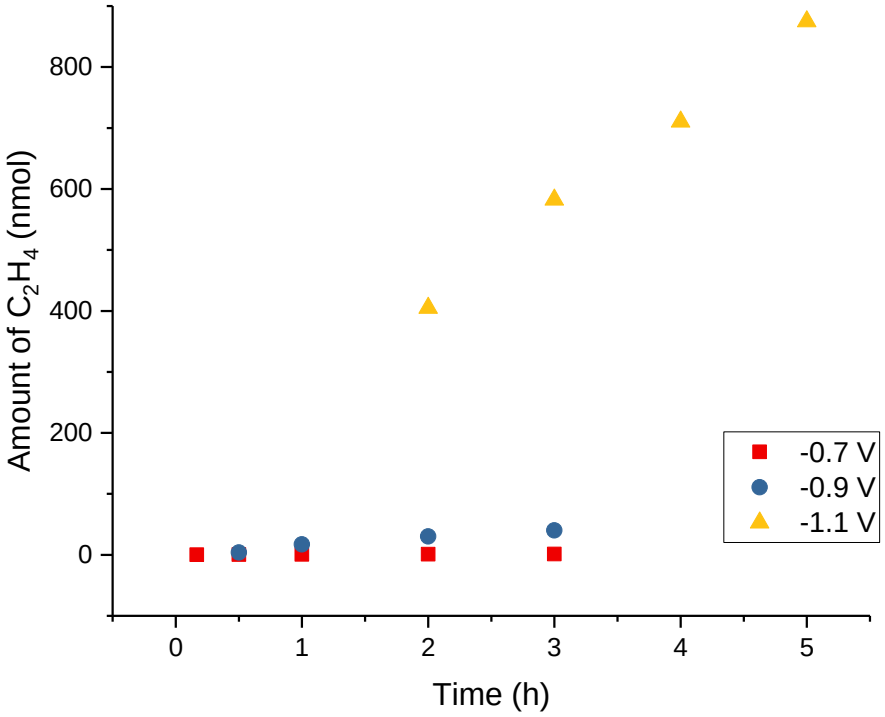


Figure 5-13: Time course of C_2H_4 production by 1.2 nmol wild type MoFe protein at different potential (■ -0.7 V, ● -0.9 V and ▲ -1.1 V). The quantity of C_2H_4 was determined from the headspace of the solution vial (which included 6 mL Tris-HCl, pH 8.0, with 0.25 mM Eu-L).

The faradaic efficiency of ethylene production by wild type MoFe protein at -1.1 V was calculated below over the period time of 5 hours. The quantity of electrical charge passed (Q) was 0.607 C and two electrons (n_1 = 2) are required for reducing the acetylene to ethylene. The total amount

of ethylene produced in 5 hours was 875 nmol, so the faradaic efficiency of ethylene production was about 27.8% in the experiment.

$$\mathrm{FE} = \frac{Mole\ of\ C_2H_4}{n_{e^-}}$$

$$n_{e^-} = \frac{Q}{n_1 * F}$$

Control experiments of acetylene reduction are shown in Figure 5-14. The setup of the experiment was similar to the experiments with the wild type MoFe protein. Rates of C_2H_4 production were quite low at both -0.7 V and -0.9 V in control experiments (not shown here). The 1.2 nmol Apo protein (● in Figure 5-14) produced approximately 120 nmol of C_2H_4 over 3 hours at -1.1 V which was about 20% of the rate of C_2H_4 formation by the wild type MoFe protein.

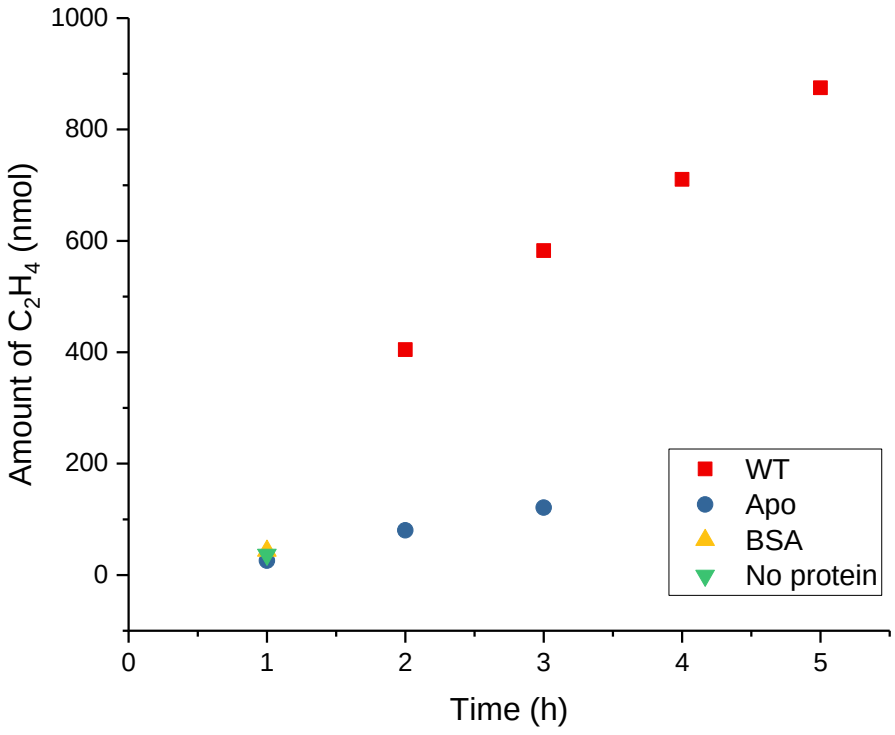


Figure 5-14: Time course of ethylene production by 1.2 nmol wild type MoFe protein (■) and substitutes in control experiments (● Apo protein, ▲ BSA and ▼ no protein) in -1.1 V. The quantity

of ethylene was determined from the headspace of the solution vial (which included 6 mL Tris-HCl, pH 8.0, with 0.25 mM Eu-L).

When a similar amount of the BSA (▲ in Figure 5-14, Bovine serum albumin) was used for immobilisation onto carbon particles and held at -1.1 V in saturated acetylene solution, about 43 nmol of C_2H_4 was created which was quite close to the quantity of the product by Apo protein.

In the last control experiment, bare modified carbon particles (▼ no protein in Figure 5-14) which were stacked with py and activated by EDC and NHSS before rinsing with water, were deposited onto the base plate of the cell. The amount of ethylene was about 37 nmol in one hour which was close to all other data from the control experiments. This indicated that there was about 40 nmol/h background ethylene produced from carbon particles at -1.1 V.

The rate of ethylene formation by the wild type MoFe protein at different potentials is shown in Figure 5-15. The enzyme was under a flow of solution which was bubbled with Ar during application of the potential of -0.7 V. Then, acetylene gas was bubbled for 10 min to make the flow solution saturated with acetylene before the inlet and outlet gas lines were closed for the remainder of the experiment. The potential continued to be held at -0.7 V for 1 hour, after which the first C_2H_4 reading was taken.

The rate of C_2H_4 formation at -0.7 V was 4.6 nmol/h which was 11% of the rate at -0.9 V displayed in Figure 5-15 (there is some variation between protein films, so these rates are higher than those shown in Figure 5-13. Data in Figure 5-15 were recorded on a single film). After stepping down to -1.0 V, the rate increased, and increased further at -1.1 V.

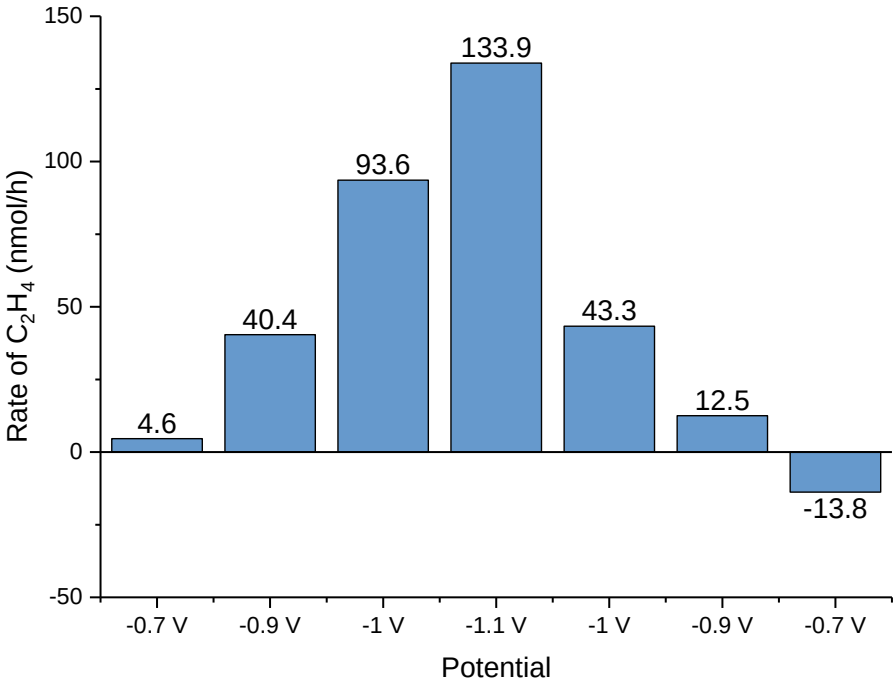


Figure 5-15: Potential-dependent column chart showing ethylene formation rate by 1.2 nmol wild type MoFe protein in the flow solution (Tris-HCl buffer, pH 8.0, with Eu-L mediators) saturated with acetylene. The quantity of ethylene was determined from the headspace of the solution vial.

The trend of rate with potential was mirrored when the potential was stepped more positive again, although the rates were lower during these steps, perhaps due to protein inactivation over the long experiment. The decrease of rate was also caused by loss of headspace gas during sampling each time, such that the apparent rate of C_2H_4 formation was negative when the potential was stepped back to -0.7 V in Figure 5-15. Overall, the results show that the reduction of acetylene was able to be well-controlled by electrochemistry and could be switched off after re-applying a positive potential.

5.4.2 Effect of partial pressure on the acetylene reduction reaction

The previous study of acetylene reduction during ATP and Fe protein-dependent nitrogenase catalysis has an interesting result that the highest rate was not at the highest acetylene level (from Lance Seefeldt's comments). The rate of ethylene formation by Mo-nitrogenase (Fe protein: MoFe

protein = 20: 1) reached a maximum point when the partial pressure of C_2H_2 was about 0.2 bar and then decreased gradually as the concentration of acetylene was raised.

To study the effect of the partial pressure of acetylene on the wild type MoFe protein at -1.1 V in the mediated electrochemical system, pure acetylene gas was injected by an airtight needle into the headspace of a solution vial which was first bubbled with Ar for 10 min. The closed system was connected to the atmosphere by opening the outlet gas flow after 10 min mixing with additional acetylene gas to equilibrate to atmospheric pressure.

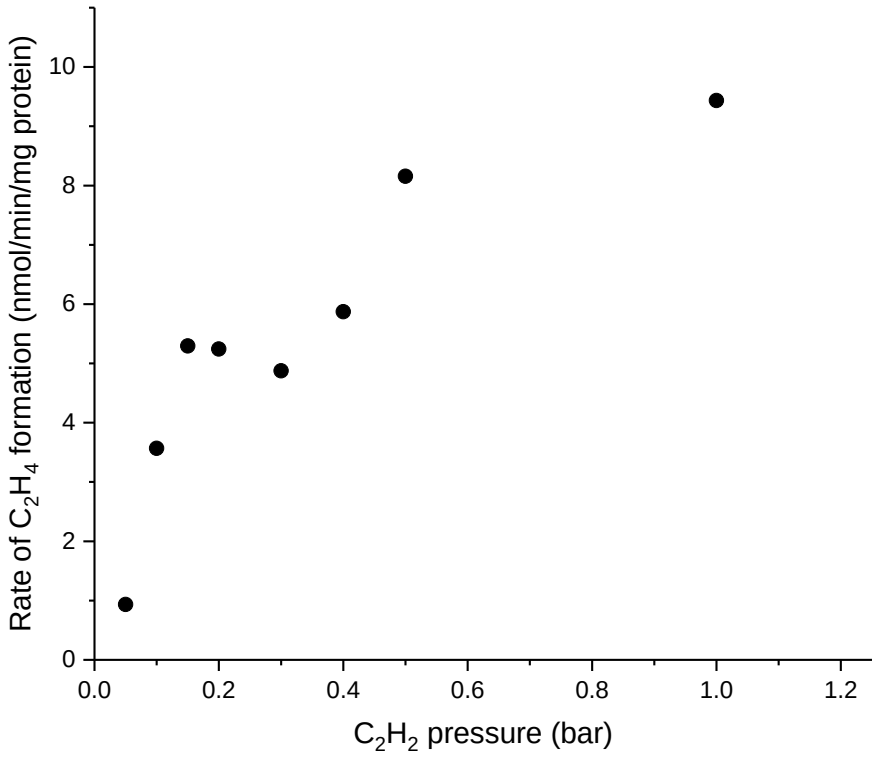


Figure 5-16: Plot of C_2H_4 formation rate at different partial pressures of C_2H_2 by wild type MoFe protein. The rate was average of ethylene produced over 1 hour at -1.1 V. The acetylene pressure was adjusted by injecting pure acetylene gas into an Ar filled vial containing 6 mL Tris-HCl buffer with pH 8.0 in the presence of 0.25 mM Eu-L mediators.

Figure 5-16 shows that the C_2H_4 formation rate at -1.1 V increases to 5.3 nmol/min/mg MoFe protein dramatically in the C_2H_2 partial pressure range of 0 bar to 0.15 bar, and that the rate

started decreasing after 0.2 bar of acetylene pressure which was quite similar to the result from acetylene reduction by native Mo-nitrogenase (Fe protein and MoFe protein). However, the ethylene formation rate increased again when acetylene gas was injected to 0.4 bar, and the increase in rate (9.5 nmol/min/mg MoFe protein, the rate of bare carbon under pure C_2H_2 is 0.6 nmol/min) was continuous until the system was under pure acetylene. This change contrasted with acetylene reduction in the ATP-dependent system. The result is nevertheless consistent with different modes of acetylene interaction, as an inhibitor and as a substrate.

5.4.3 Other proteins

Experiments on other nitrogenase proteins, variant 98H MoFe protein (●), native VFe protein from V-nitrogenase (▼) and native FeFe protein from Fe-nitrogenase (▲) were also studied as shown in Figure 5-17. The data on all these proteins were collected after bubbling acetylene gas for 10 min at -1.1 V. From the plot, the rate of ethylene formation was quite constant in the first three hours by each protein. The wild type MoFe protein (■) had a rate of 10.3 nmol/min/mg protein over 3 hours. The variant 98H only reached 3.6 nmol/min/mg protein, and VFe protein and FeFe protein had rates of 3.8 nmol/min/mg protein and 7.1 nmol/min/mg protein respectively. The apo protein as a control had a rate of 0.67 nmol/min/mg protein.

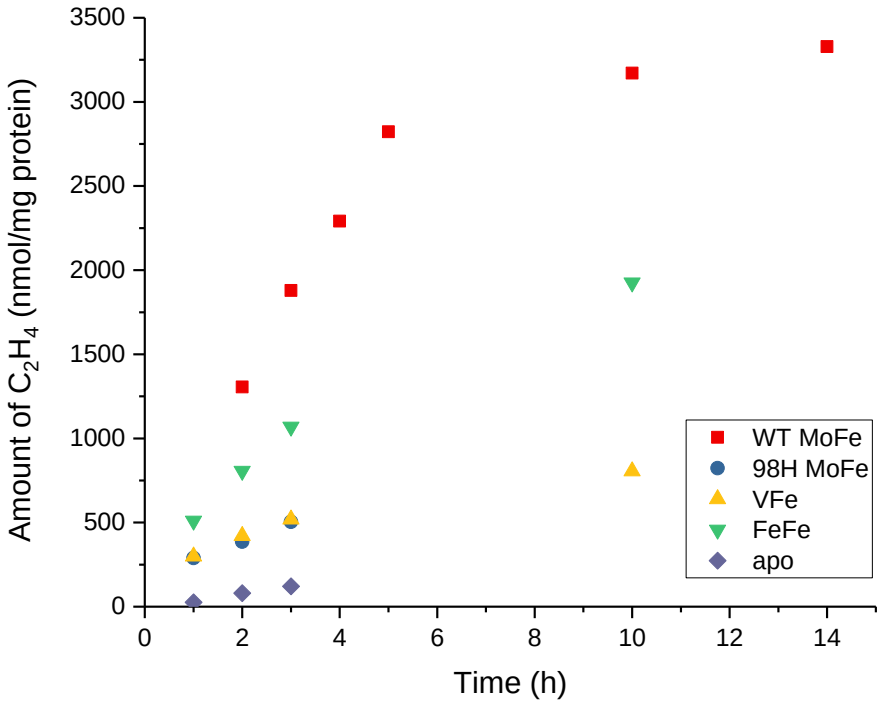


Figure 5-17: Time course of ethylene production by ■ wild type MoFe protein, ◆ apo protein, ● variant 98H MoFe protein from Mo-nitrogenase, ▲ native VFe protein from V-nitrogenase and ▼ native FeFe protein from Fe-nitrogenase at -1.1 V. The quantity of ethylene was determined from the headspace of the solution vial (filled with 6 mL Tris-HCl, pH 8.0, with 0.25 mM Eu-L).

Figure 5-18 shows the result of acetylene reduction by MoFe protein with and without the help of Eu-L mediators. The amount of ethylene formation by 1.2 nmol MoFe protein at -1.1 V was about 160 nmol in 1 hour and 300 nmol at 2 hours in buffer only solution. This formation rate reached about 80% of that with the help of Eu-L mediators, if not considering the background effect from carbon particles.

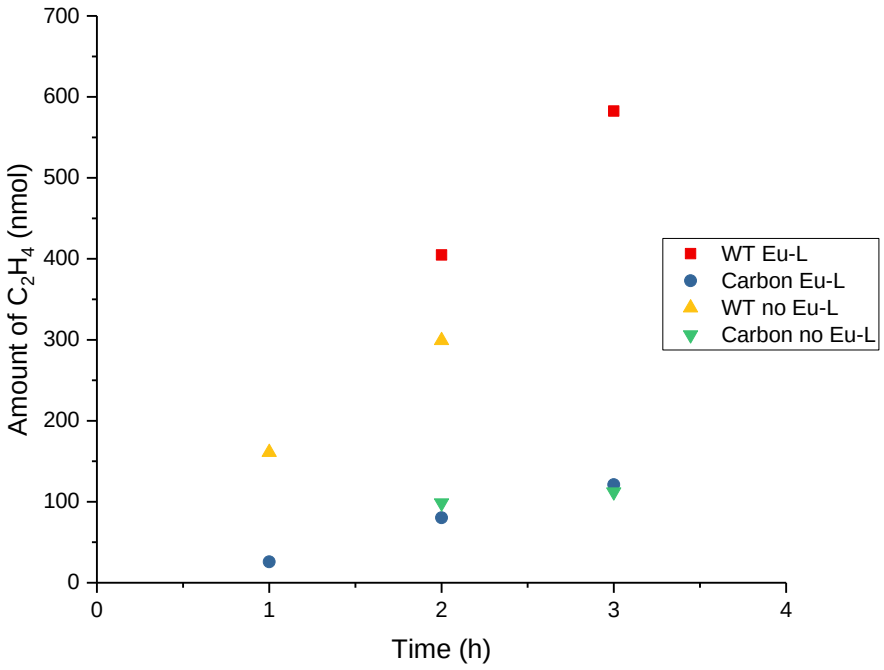


Figure 5-18: Time course of ethylene production by 1.2 nmol wild type MoFe protein with (■)and without Eu-L mediators (▲) and modified carbon particles in control experiments (● with Eu-L, ▼ without Eu-L) at -1.1 V. The quantity of ethylene was determined from the headspace of the solution vial (which included 6 ml Tris-HCl, pH 8.0, with 0.25 mM Eu-L).

The rate of ethylene formation (ca. 40 nmol/h) from carbon particles under Tris-HCl buffer was similar to that with Eu-L mediators in Figure 5-18, indicating that the mediators may not contribute to the background reaction. This shows that wild type MoFe protein is able to take up electrons reasonably efficiently from the carbon particles without Eu-L, confirming direct electron transfer is possible.

5.5 Discussion

Electrochemical experiments on wild type and the variant 98H MoFe protein described in Section 5.2 clearly show that proton reduction by MoFe protein is inhibited by acetylene near the onset of proton reduction at -0.9 V, and that this process is irreversible (even when C_2H_2 is flushed out with Ar) at this potential. At slightly more negative potentials, the inhibitor becomes partially reversible, with the substantial recovery of current under Ar. This suggests that a different redox

level of the FeMo cofactor centre is accessed at about -0.95 V. Control experiments on apo protein show that the C_2H_2 effect must occur at the FeMo cofactor centre of intact nitrogenase. The behaviour of the variant 70A MoFe protein, in which the cavity at the active site is opened up, was slightly different with inhibition being reversible even at -0.9 V when C_2H_2 was flushed out with Ar. This could be due to a particular binding mode for acetylene being favoured in this variant.

GC analysis of the gas phase products confirmed MoFe protein electrocatalytic reduction of C_2H_2 to C_2H_4 for wild type and 98H, with a higher rate for wild type MoFe protein. The rate of ethylene formation was about 10 nmol/min/mg MoFe protein within 5 hours at -1.1 V. This rate was quite low (~1%) compared to acetylene reduction by the ATP-dependent nitrogenase. The potential-dependence observed for wild type was consistent with the extent to which the protein reduction current could recover under Ar at different potentials.

The fact that current decreases, rather than increases, when C_2H_2 reduction occurs, indicates that C_2H_2 reduction must suppress proton reduction so that the net current drops. The ability to electrochemically drive the reduction of a triple bond substrate in preference to proton reduction is exciting as it suggests it may be possible to find conditions for electrochemically driving N_2 reduction.

From Figure 5-8, Eu-L mediators helped to increase the rate of proton reduction by wild type and variant MoFe protein. Although acetylene could inhibit the catalytic current of wild type MoFe protein at -1.0 V, there was no restoration of current after bubbling Ar gas again without mediators, so they are clearly important in allowing the MoFe protein to access the required redox level.

The relatively low Faradaic efficiency of ~28% for wild type MoFe protein at -1.1 V is not surprising as many e^- will be consumed for proton reduction.

From control experiments, we found that a certain amount of ethylene was produced by carbon particles at negative potential. All the control experiments of Apo protein, BSA and no protein gave a similar rate of ethylene formation from GC analysis.

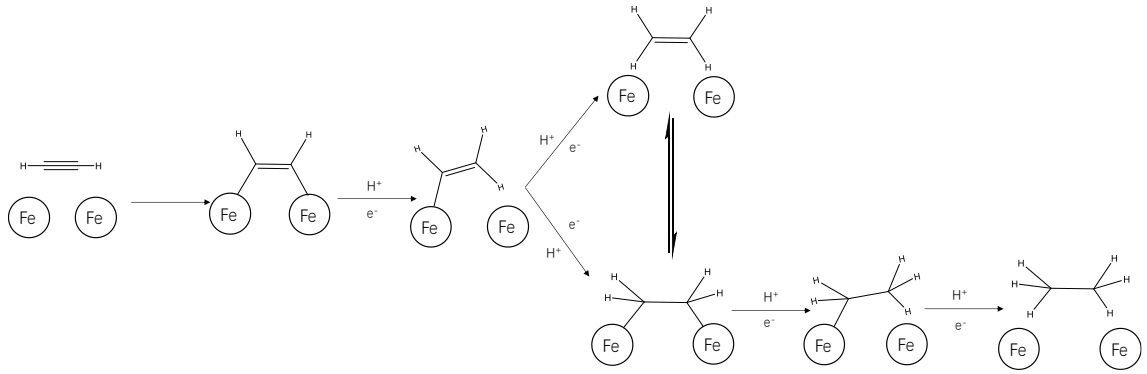


Figure 5-19: Proposed mechanism for acetylene reduction to ethylene and ethane by nitrogenase. The scheme describes a model for acetylene bound to the active site of nitrogenase and reduced to both ethylene and ethane

The spectroscopic experiments were conducted to try to detect coordinated acetylene or intermediates in its reduction. It showed no significant *ν*(C≡C) peak of solution acetylene with potentials in the infrared spectra, so there was no evidence for end on terminal C_2H_2 binding. The carbon-carbon triple bond might be π-bonded to two Fe atoms as the proposed mechanism shown in Figure 5-19.[11] Some changes were observed below 1700 cm^{-1} but were hard to define due to overlap with changes in amide bands and water. Even with propargyl alcohol, it was difficult to determine whether any new peaks appeared. Further experiments with ^{2}H and ^{13}C acetylene may help in studying the mechanism using infrared spectroscopy.

Figure 5-15 shows that acetylene reduction by MoFe protein was controlled by potential. More negative potentials could accelerate the rate of ethylene formation. And this change could be reversed after stepping the potential back to more positive values. This is expected for an electrocatalytic reaction where increasing the driving force should increase the rate.

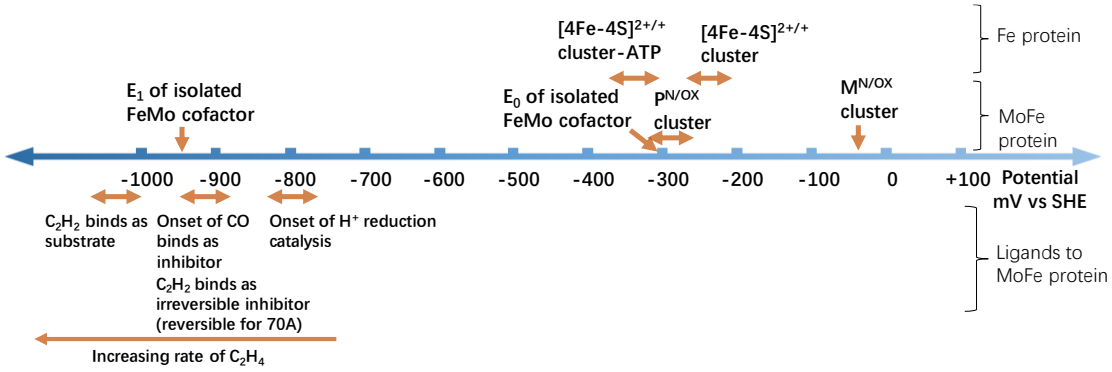


Figure 5-20: A potential scale shows the measured mid potentials of metal clusters in nitrogenase and the potentials of ligands binding to the MoFe protein in the electrochemical study.

Figure 5-20 presents the potentials for acetylene binding to the MoFe protein. It shows that the acetylene inhibited the proton reduction current by the MoFe protein at the potential ca. -900 mV. At -900 mV, the rate of forming ethylene is quite low compared to that at -1100 mV, where reversible reduction reaction of acetylene by the MoFe protein occurs. The inhibition of proton reduction current could be recovered quickly by flushing acetylene out at this potential. The rate of C_2H_4 formation increased from -0.7 V to -1.1 V and this change could be well-controlled by the potential.

Bibliography

1 M. J. Dilworth, *Biochim. Biophys. Acta - Rev. Biomembr.*, 1966, **127**, 285–294.

2 B. K. Burgess and D. J. Lowe, *Chem. Rev.*, 1996, **96**, 2983–3012.

3 M. A. Coles and F. A. Hart, *J. Organomet. Chem.*, 1971, **32**, 279–284.

4 K. Nakamoto, *Infrared and Raman Spectra of Inorganic and Coordination Compounds*, John Wiley & Sons, New Jersey, 6th edn., 2009.

5 M. J. Dilworth, M. E. Eldridge and R. R. Eady, *Biochem. J.*, 1993, **289**, 395–400.

6 D. J. Scott, D. R. Dean and W. E. Newton, *J. Biol. Chem.*, 1992, **267**, 20002–20010.

7 M. J. Dilworth, R. R. Eady, R. L. Robson and R. W. Miller, *Nature*, 1987, **327**, 167–168.

8 K. Schneider, U. Gollan, S. Selsemeier-Voigt, W. Plass and M. Mtiller, *Naturwissenschaften*, 1994, **81**, 405–408.

9 C. H. Kim, W. E. Newton and D. R. Dean, *Biochemistry*, 1995, **34**, 2798–2808.

10 R. W. F. Hardy, R. D. Holsten, E. K. Jackson and R. C. Burns, *Plant Physiol.*, 2008, **43**, 1185–1207.

11 P. M. C. Benton, J. Christiansen, D. R. Dean and L. C. Seefeldt, *J. Am. Chem. Soc.*, 2001, **123**, 1822–1827.

12 H. I. Lee, M. Sørlie, J. Christiansen, T. C. Yang, J. Shao, D. R. Dean, B. J. Hales and B. M. Hoffman, *J. Am. Chem. Soc.*, 2005, **127**, 15880–15890.

13 C. E. McKenna, M. C. McKenna and C. W. Huang, *Proc. Natl. Acad. Sci.*, 1979, **76**, 4773–4777.

14 H. I. Lee, R. Y. Igarashi, M. Laryukhin, P. E. Doan, P. C. Dos Santos, D. R. Dean, L. C. Seefeld and B. M. Hoffman, *J. Am. Chem. Soc.*, 2004, **126**, 9563–9569.

15 R. Y. Igarashi, P. C. Dos Santos, W. G. Niehaus, I. G. Dance, D. E. Dean and L. C. Seefeldt, *J. Biol. Chem.*, 2004, **279**, 34770–34775.

16 R. S. McMillan, J. Renaud, J. G. Reynolds and R. H. Holm, *J. Inorg. Biochem.*, 1979, **11**, 213–227.

17 S. M. Mayer, W. G. Niehaus and D. R. Dean, *Dalt. Trans.*, 2002, 802–807.

Chapter 6

Study of isocyanide binding to the metal centres of nitrogenase

This chapter focuses on isocyanide binding and reduction by the MoFe protein in different oxidation levels and characterisation of the interaction between isocyanide and the metal clusters of the MoFe protein and several genetic variants.

6.1 Introduction

A study of isocyanide binding to metal clusters is another way to explore redox-dependent ligands binding to nitrogenase as isocyanide is isoelectronic with both CO, N_2 and cyanide. However, isocyanide has different electronic properties; the stronger σ-donor characteristics of isocyanide enable it to coordinate with higher oxidation number metal centres, although it is also a π acceptor.

6.1.1 Isocyanide binding to isolated FeMo cofactor

As coordinated isocyanide exhibits a strong Infrared absorption peak in the range 2165–2110 cm^{-1},[1] it is a reasonable probe to determine the mechanism of isocyanide binding to the mental centres of the MoFe protein. Terminal isocyanide ligands usually have approximately linear CNC angles, but bent geometries are known, and in these cases, the *ν*(NC) stretching frequency is significantly lowered, consistent with a diminished NC bond order. Bridging between two metal centres is another possible mode for isocyanide binding, which would also lower the *ν*(NC) frequency.

One previous isocyanide binding study was carried out on the isolated FeMo cofactor, the active site of nitrogenase, by Pickett and coworkers. An electrochemical study of the isolated FeMoco, extracted into an organic solvent, showed that isocyanide is able to bind to the isolated FeMoco. IR spectra recorded during titration of cyclohexyl isocyanide with the oxidised form of the isolated FeMo cofactor showed a peak at 2170 cm^{-1} appearing first, followed by a peak at 2137 cm^{-1} which was the same as the free cyclohexyl isocyanide in solution. The t-butyl isocyanide gave bands at 2166 cm^{-1} and 2135 cm^{-1} at the oxidised level of the FeMo cofactor. These two peaks were lost upon application of a reducing potential (-0.8 V), while two new peaks at 2147 cm^{-1} and 2098 cm^{-1} arose indicating isocyanide bound the cofactor at the semi-reduced level (the S = 3/2, one-electron reduced state) of the isolated FeMo cofactor.[2]

6.1.2 Reducing isocyanides by nitrogenase

Kelly et al. were the first to demonstrate the reduction of methyl isocyanide by a N_2-fixing extract from *Azotobacter chroococcum* (Ac) in 1967.[3] They determined methylamine and methane as the main products from the 6-electron reduction reaction which also needed MgATP and was inhibited by carbon monoxide. A small amount of ethane and ethylene were also formed from methyl isocyanide. When the reaction was run in D_2O, all methane was found as CD_4 which indicated the carbon of methane was from the isocyanide group (-NC). The products from ethyl isocyanide reduction were the same as those from methyl isocyanide and favoured formation of methane rather than C_2 products. This was interpreted as an indication that CH_3NC bound end-on to the active site of nitrogenase through the terminal carbon atom rather than the nitrogen atom in the isocyanide group.[3] Later, Kelly demonstrated that both carbon atoms in the C_2 products arose from different isocyanide carbons in a D_2O experiment,[4] showing that C-C coupling can occur on the nitrogenase active site. The rate of methane production started to decrease when the concentration of CH_3NC was above 5 mM. On the basis of this information, Hardy (1979) suggested a reduction followed by an insertion mechanism whereby C_2 products were formed by the interaction of a single bound C_1 radical with a free molecule of CH_3NC.[5]

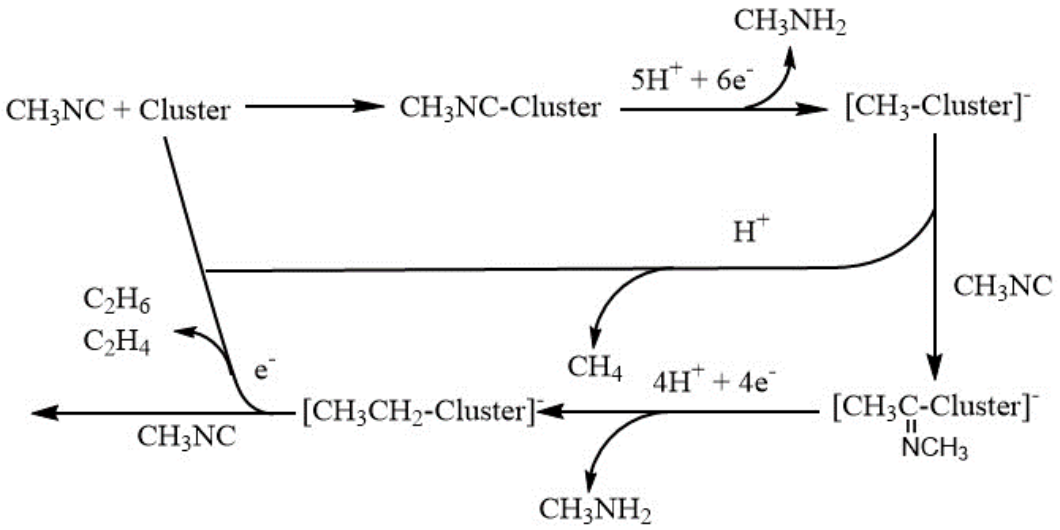


Figure 6-1: The scheme of nitrogenase reduction of methyl isocyanide to methylamine and hydrocarbon.

Later in 1982, it was shown that $[Fe_4S_4(SPh)_4]^{2-}$ and $[Mo_2Fe_6S_8(SPh)_9]^{3-}$ are able to reduce C_2H_2 to C_2H_4 in MeOH/THF electrochemically, and give similar stereoselectivity of products as nitrogenase in D_2O experiments. Tanaka et al. used these species as models for studying the methyl isocyanide reduction reaction by nitrogenase.[6] Figure 6-1 shows the Scheme of this reaction. The first step in the figure is adduct formation between CH_3NC and the cluster, which is followed by the five-proton and six-electron reduction reaction to form CH_3NH_2 and $[CH_3\text{-cluster}]^-$. Then another protonation forms the main product, methane. Alternatively the insertion of additional CH_3NC affords $[CH_3C(=NCH_3)\text{-cluster}]^-$, which could give ethane or ethylene in the subsequent reactions. Longer chain hydrocarbons might be formed as further byproducts in this mechanism. Therefore, the ratio of the amount of CH_4 and other hydrocarbon products from CH_3NC may primarily depend on the relative ease of the insertion reactions of H^+ and CH_3NC.[6]

In 1983, Burgess et al. studied the interaction between methyl isocyanide and the purified component proteins of *Azotobacter vinelandii* nitrogenase (Av). They found that CH_3NC was an effective reversible inhibitor of total electron flow and could fully remove proton reduction by nitrogenase at a certain concentration. The rate of MgATP hydrolysis remained constant as the

concentration of methyl isocyanide was increased up to 0.5 mM, but the amount of all CH_3NC products increased with a continuous decrease in the rate of H_2 production. However, the rate of these products started decreasing after 5 mM CH_3NC concentration due to a dramatic decrease in total electron flow. Methyl isocyanide seems to be reduced at a state of nitrogenase that is more oxidized than the state responsible for proton reduction or dinitrogen fixation, as it required a much lower ratio of Fe protein to MoFe protein. Ethane and ethylene as products of CH_3NC appear to be formed through an insertion reaction as mentioned in discussion of Figure 6-1. Apart from H_2, all reagents like acetylene, N_2, azide and N_2O, could relieve the inhibition and reduction of methyl isocyanide by nitrogenase.[7]

Using ^{19}F NMR and p-$CF_3C_6H_4S^-$ as the reporter ligand to study methyl isocyanide and cyanide binding to isolated FeMo cofactor in the S=3/2 state, with parallel EXAFS work on the MoFe protein, showed no interaction with the Molybdenum centre.[8]

6.2 Electrochemical investigation of isocyanide inhibition of MoFe protein

The new attachment approach for immobilization of enzyme onto the working electrode which was tested in Section 4.4 was used in all experiments shown in this Chapter, as this approach is able to provide a very stable enzyme situation in the spectroelectrochemical cell.

Therefore, an 8 µL mixture of activated py-carbon suspension (carbon particles modified by 1-pyrenebutyric acid, described in chapter 3) was mixed with 4 nmol MoFe protein and stored on ice under anaerobic conditions to form the covalent bond between the protein and carbon particles. Then the protein-py-carbon mixture was rinsed with water and deposited onto the ATR-IR prism and covered with a carbon paper.

As isocyanide is an extremely smelly and poisonous compound with a low boiling temperature, experiments were carried out in a fume hood and a glovebox. A headspace vial of a buffer solution with Eu-L mediators was sealed inside the glovebox. Then isocyanide was injected into the sealed

vial in the fume hood and taken back to the glovebox immediately. The bottle was cooled down on ice to minimise the evaporation of the isocyanide. The O_2 level in the vial was minimized by bubbling Ar gas into the headspace of the vial for 2 min, which might slightly lower the concentration of the isocyanide stock. The isocyanide solution was introduced into the spectroelectrochemical cell by changing the solution vial as shown in Figure 4-2.

Figure 6-2 shows the current trace for wild type MoFe protein with 25 mM methyl isocyanide under a series of potentials in the spectroelectrochemical cell. There was no significant change of current from 0 V to -1.1 V (vs SHE). This contrasts with the current in the absence of methyl isocyanide shown in Figure 6-3, in which there was a much larger negative current at potentials (-0.9 V and -1.1 V) where proton reduction occurs until the addition of methyl isocyanide.

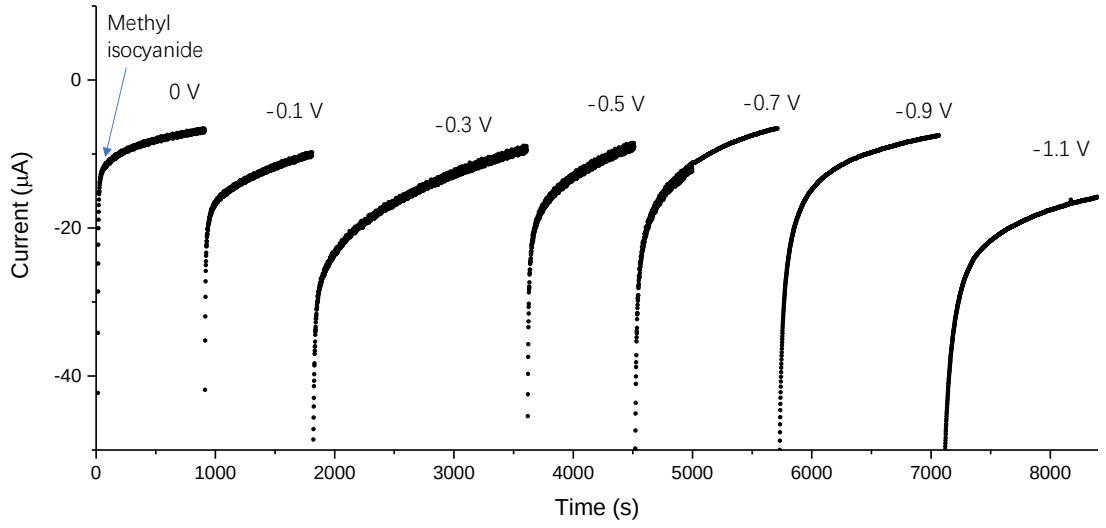


Figure 6-2: Current-time trace for an electrochemical experiment on wild type MoFe protein showing that there is no electrocatalytic proton reduction current in the presence of 25 mM methyl isocyanide under potential control.

The difference is highlighted in the experiment shown in Figure 6-3, the catalytic current was about -200 μA at -1.1 V before adding methyl isocyanide. Changing to a solution vial containing 25mM methyl isocyanide caused the current to drop about -40 μA. The current at -0.9 V was at least -30 μA more negative than the current at the same potential in Figure 6-2. There was no

meaningful difference from 0 V to -0.7 V in the absence and presence of methyl isocyanide, which was prior to the onset of proton reduction presented in Section 4.2.

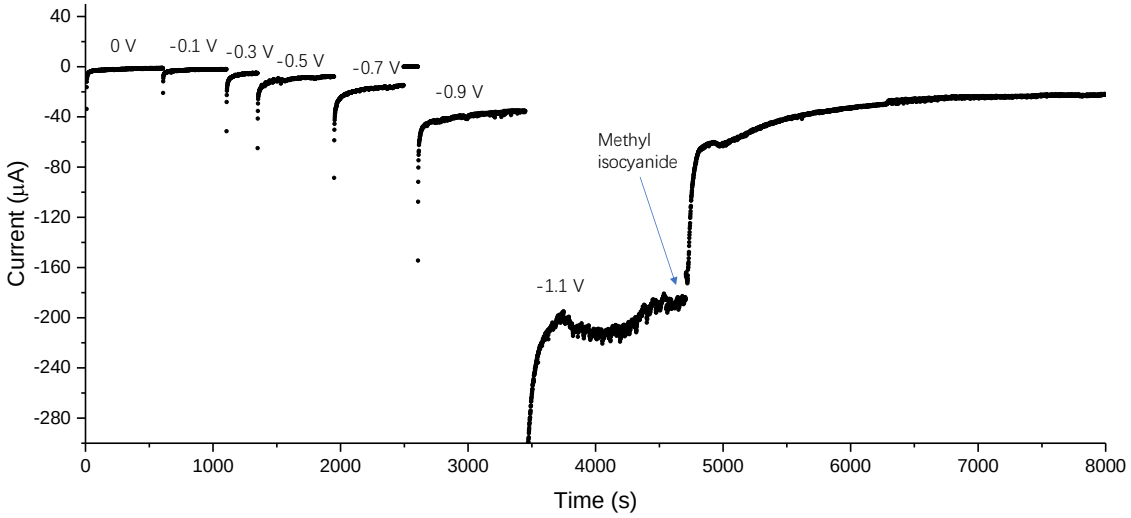


Figure 6-3: Current-time trace for an electrochemical experiment on wild type MoFe protein showing the inhibition of electrocatalytic proton reduction current in the presence of 25 mM methyl isocyanide under -1.1 V.

Figure 6-3 shows that after the introduction of methyl isocyanide solution into the cell, proton reduction was immediately inhibited at -1.1 V. The negative current decreased to about -60 µA and remained at ca. -20 µA after 1 hour, indicating the methyl isocyanide was able to inhibit the electrocatalytic H^+ reduction by nitrogenase MoFe protein.

In control experiments for the apo protein and bare carbon, about -5 µA electrochemical current was observed from both experiments at -1.1 V with the same concentration of methyl isocyanide.

6.3 IR SEC study of Isocyanide binding to MoFe protein

In this Infrared spectroelectrochemical study, the effect of isocyanide on wild type and different variants of the MoFe protein was investigated. An interaction between isocyanide ligands and the metal clusters at different redox potentials was examined spectroscopically with the help of

mediators. The SEC results will be presented and discussed in this section. This should give some useful insights into the complex substrate-binding mechanism of nitrogenase.

6.3.1 Isocyanide in the solution

In a control experiment, a 25 mM methyl isocyanide solution was prepared in Tris-HCl pH 8.0 buffer containing Eu-L mediators as well. Infrared spectra were collected before and after the introduction of the methyl isocyanide solution into the spectroelectrochemical cell before applying a potential. No peaks appeared in the range of 2300 cm^{-1} to 2100 cm^{-1} before changing to CH_3NC solution as shown by Figure 6-4 (red line). After changing to 25 mM methyl isocyanide solution, a strong peak appeared at 2187 cm^{-1} immediately (blue line, the background spectrum was recorded in the absence of CH_3NC). This peak is observed at 21 cm^{-1} higher than the peak of neat methyl isocyanide due to the hydrogen bonding interaction between water molecules and the carbon of isocyanides.[9] The peak 2166 cm^{-1} (blue line) shown in Figure 6-4 is consistent with the *v*(NC) stretch of neat methyl isocyanide in the infrared spectrum. The difference of two infrared peaks for the *v*(NC) stretch is due to the hydrogen bonding interaction between water molecules and the carbon of isocyanides, which has been suggested to be the site of proton acceptor in hydrogen bonding.[9]

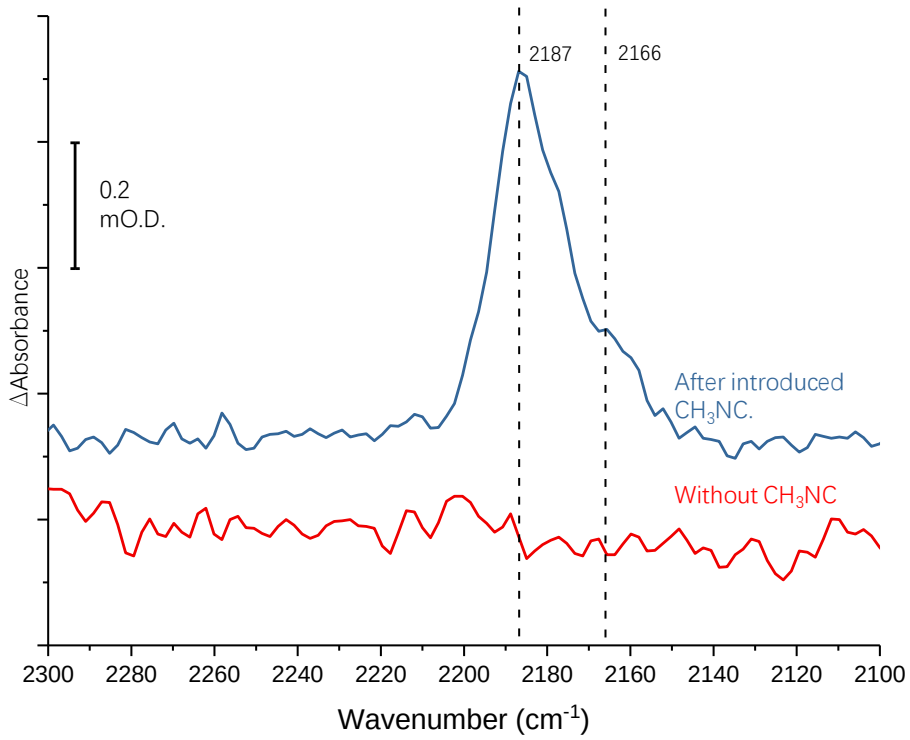


Figure 6-4: IR absorbance spectra for a layer of carbon particles in solution (Tris-HCl buffer pH 8.0 containing Eu-L mediators) without nitrogenase and without applied potential. The spectrum in red was recorded before applying CH_3NC (25 mM) and the spectrum in blue was recorded when no more change was observed after the introduction of CH_3NC. Both spectra processed against a background spectrum before the addition of methyl isocyanide (512 scans, 4 cm^{-1} resolution).

In the second control experiment shown in Figure 6-5 (A), 4 nmol of apo protein of MoFe protein was attached onto the modified carbon particles before they were deposited onto the ATR-IR prism. 25 mM methyl isocyanide was introduced into the cell after a background spectrum recorded in Tris-HCl buffer (containing Eu-L) with no applied potential. An intense *v*(-NC) peak appeared at 2187 cm^{-1} which is consistent with the *v*(-NC) peak of methyl isocyanide in free solution at bare carbon particles without applied any potential (as shown in Figure 6-4). After applying a range of potentials from 0 V to -1.1 V in several steps, no obvious change was observed in the spectra, indicating that no binding happened here between the methyl isocyanide and apo protein.

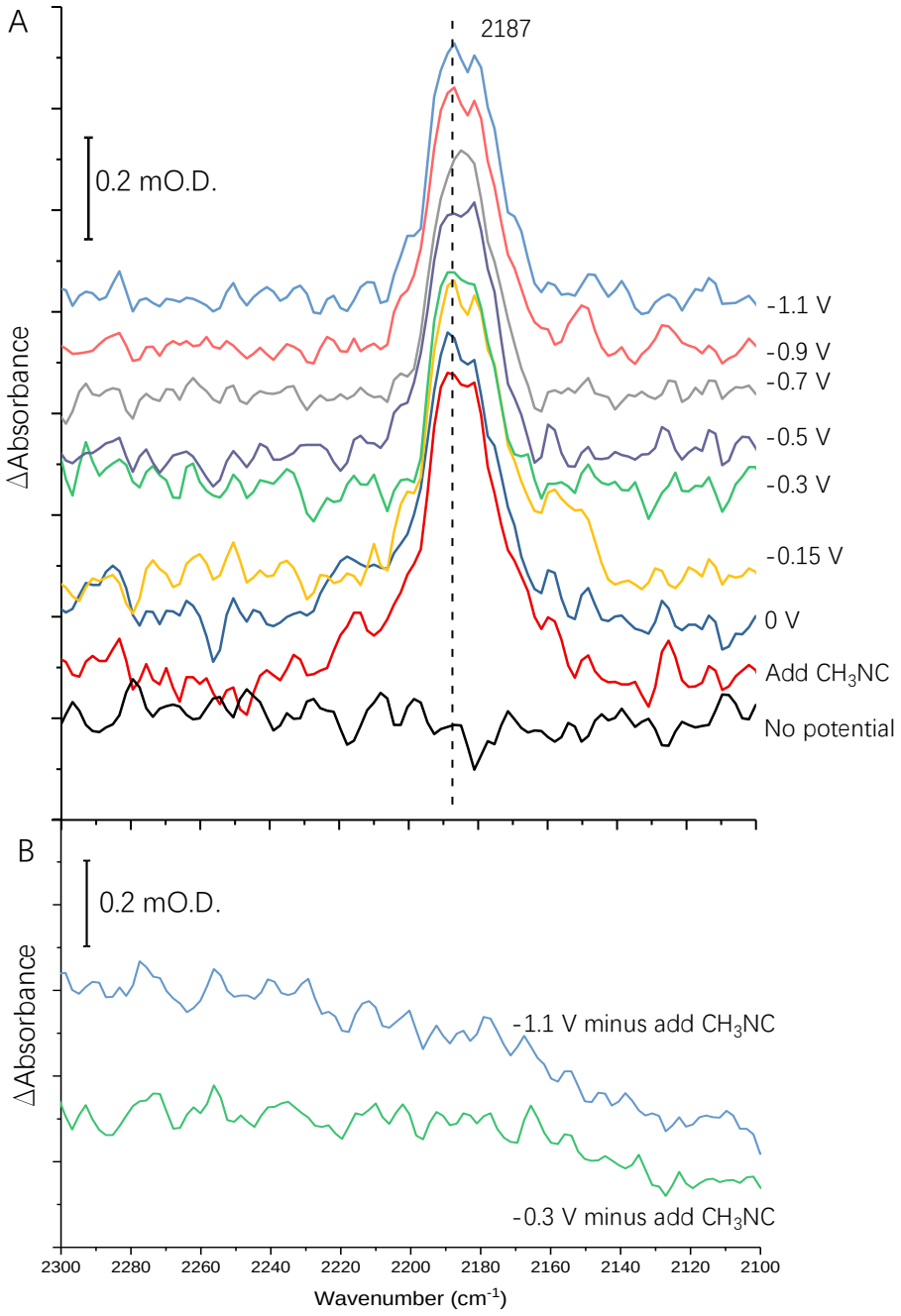


Figure 6-5: IR absorbance spectra of 4 nmol apo protein on carbon particles in 25 mM methyl isocyanide solution (Tris-HCl buffer pH 8.0 containing Eu-L mediators) with a series of applied potentials. Each spectrum in (A) was recorded after a 30 min poise at the specified potential and processed against a background spectrum before the addition of methyl isocyanide with no applied potential. The spectra in (B) show the difference between isocyanide peaks at negative potentials (-0.3 V and -1.1 V) and that after applying CH_3NC with no applied potential.

Figure 6-5 (B) presents the change after applying negative potentials in the same control experiment. No difference was observed in the range from 2300 cm^{-1} to 2100 cm^{-1} after equilibration of methyl isocyanide in the flow solution with the series of potentials from 0 V to -1.1 V.

6.3.2 Variant β-98$^{Tyr\rightarrow His}$ MoFe protein

Variant β-98$^{Tyr\rightarrow His}$ (98H) MoFe protein was the first MoFe protein studied here with isocyanides, as it took a short immobilisation time to form stable covalent bonds to the modified carbon particles. A 4 nmol aliquot of 98H MoFe protein was used here to study the interactions between variant MoFe protein and isocyanides.

Figure 6-6 shows a series of spectra recorded as 98H MoFe protein is exposed to methyl isocyanide (25 mM) at different potentials. There was no significant feature in the infrared range from 2300 cm^{-1} to 2100 cm^{-1} before the introduction of methyl isocyanide into the spectroelectrochemical cell without any applied potential. After the reagent solution contacted the enzyme, a narrow peak appeared at 2187 cm^{-1} (displayed in Figure 6-6, blue line) which was at the same position as the methyl isocyanide peak in the absence of protein. Potentials were applied to the protein until no further change was observed in the infrared spectrum. The infrared spectra at 0 V (vs SHE) showed a new peak at about 2203 cm^{-1}, 16 cm^{-1} higher than the *ν*(NC) solution peak from methyl isocyanide. This redshift was consistent with the results reported for isocyanide binding to the isolated FeMo cofactor described in section 6.1.1. Therefore, this new peak was considered to indicate methyl isocyanide binding to the active site of the MoFe protein. The mild potential at 0 V was in agreement with the conclusion of Burgess et al. that methyl isocyanide might be reduced at a state of nitrogenase that is more oxidized than the state responsible for proton reduction or N_2 reduction.[7,10] After applying potentials, the main peak from 2200 cm^{-1} to 2170 cm^{-1} still grew and the centre of this peak moved from 2187 cm^{-1} to 2190 cm^{-1} in Figure 6-6. As the result from

Figure 6-5 B shows that the *ν*(NC) solution peak does not increase or shift after applying potentials, this suggests that another peak corresponding to bound isocyanide might be hidden between the 2203 cm^{-1} and 2187 cm^{-1} peaks.

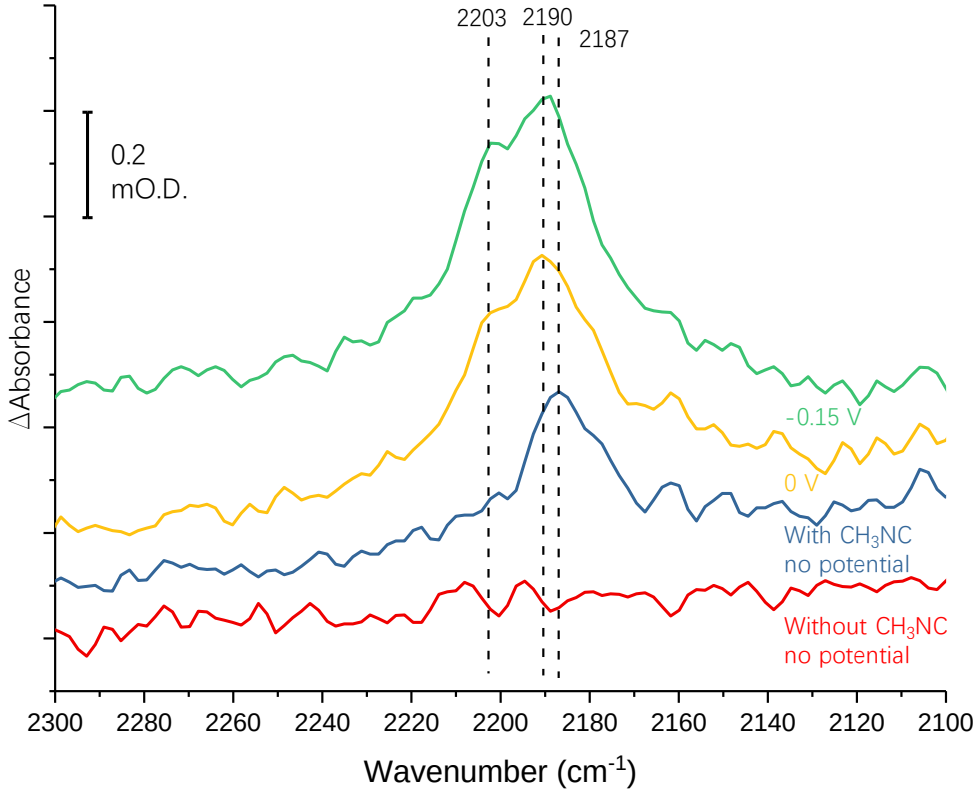


Figure 6-6: IR absorbance spectra of 4 nmol variant 98H MoFe protein in 25 mM methyl isocyanide solution (Tris-HCl buffer pH 8.0 containing Eu-L mediators) at a series of potentials. Each spectrum was recorded 30 min after switching to the given potential and processed against a background spectrum recorded before the addition of methyl isocyanide with no applied potential.

Figure 6-7 displays time course spectra of methyl isocyanide binding to the MoFe protein at 0 V in the same experiment as shown in Figure 6-6. Subtracting a spectrum recorded with no applied potential but in the presence of 25 mM methyl isocyanide (Figure 6-6, blue line) reveals a new broad feature (from 5 min) raised between 2215 cm^{-1} and 2185 cm^{-1}, which had a higher wavenumber than the peak of solution methyl isocyanide. This peak rapidly increased over the

next 30 min and seemed to separate into two peaks at 2203 cm^{-1} and 2195 cm^{-1}, which may overlap with a slight change in the free isocyanide peak (2187 cm^{-1}) as mentioned above.

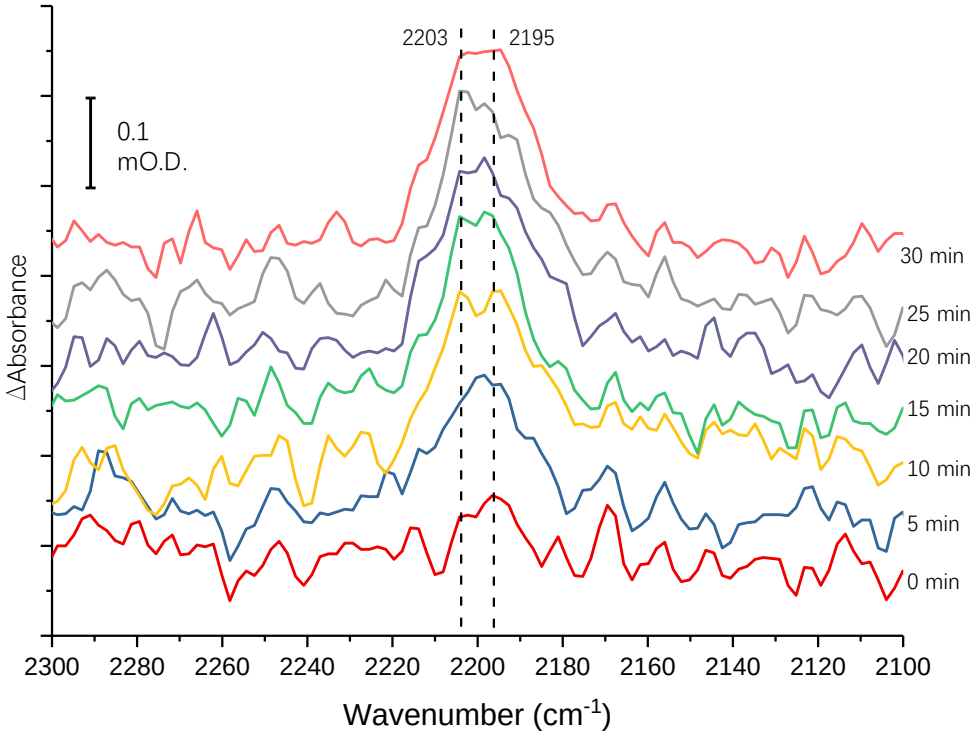


Figure 6-7: Time course IR absorbance spectra of variant 98H MoFe protein in 25 mM methyl isocyanide solution (Tris-HCl buffer pH 8.0 containing Eu-L mediators) at 0 V. Spectra were recorded at 5 min intervals and processed against a background spectrum in the presence of methyl isocyanide with no applied potential.

Further steps to more negative potential (-0.2 V and -0.3 V vs SHE) did not make any change to the IR spectra, as shown in Figure 6-8. Moreover, stepping the potential successively more positive also had no effect on the spectra.

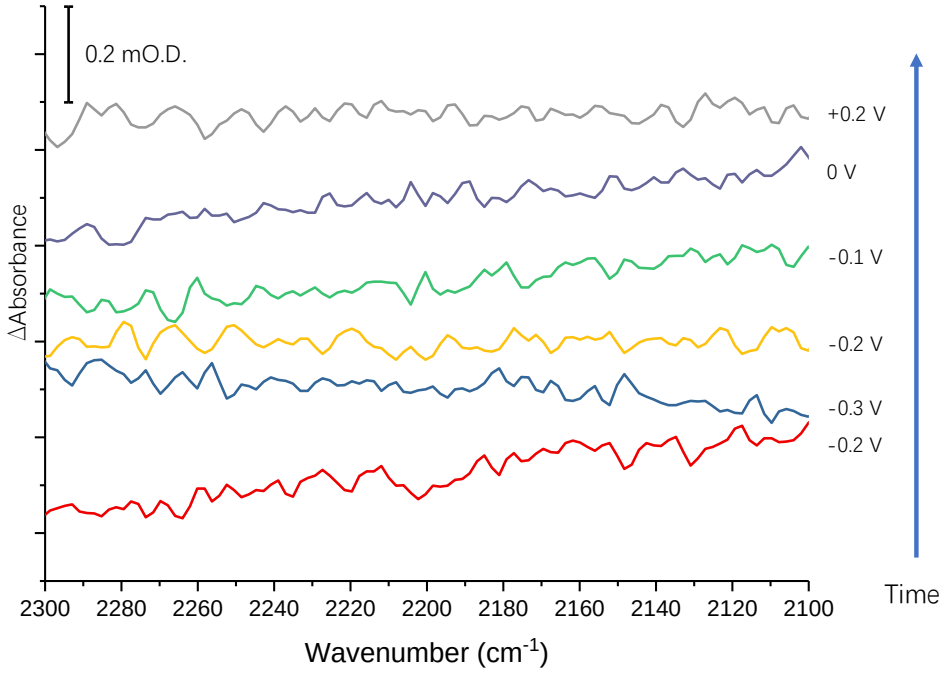


Figure 6-8: IR absorbance spectra of variant 98H MoFe protein in 25 mM methyl isocyanide solution at a series of potentials. Each spectrum was recorded after equilibration at the specified potential and processed against a background of the spectrum one step before.

6.3.3 Variant α-70$^{Val\rightarrow Ala}$ MoFe protein

The interaction between the variant α-70$^{Val\rightarrow Ala}$ (70A) MoFe protein (in which α-70^{Val} near the FeMo cofactor is replaced by Alanine) and methyl isocyanide was then studied in the spectroelectrochemical cell. A similar experiment was set up as in Figure 6-6 without methylene blue as an extra mediator.

After addition of 25 mM methyl isocyanide solution, the free CH_3NC solution peak appeared at 2187 cm^{-1} before any potential was applied. After applying a series of potentials, the bound CH_3NC peak at 2203 cm^{-1} appeared at +0.05 V (Figure 6-9 (A), yellow line), and intensity between 2240 cm^{-1} and 2140 cm^{-1} continuously increased at this potential. At the potentials, -0.15 V and -0.3 V, the broad feature between 2240 cm^{-1} and 2140 cm^{-1} continued to increase, which is likely due to underlying contributions from the bound methyl isocyanide peaks. This is confirmed by the

spectrum in Figure 6-9 (B), in which peaks at 2195 cm^{-1}, 2203 cm^{-1} and 2222 cm^{-1} appear when using the spectrum with no applied potential after applying 25 mM CH_3NC as background.

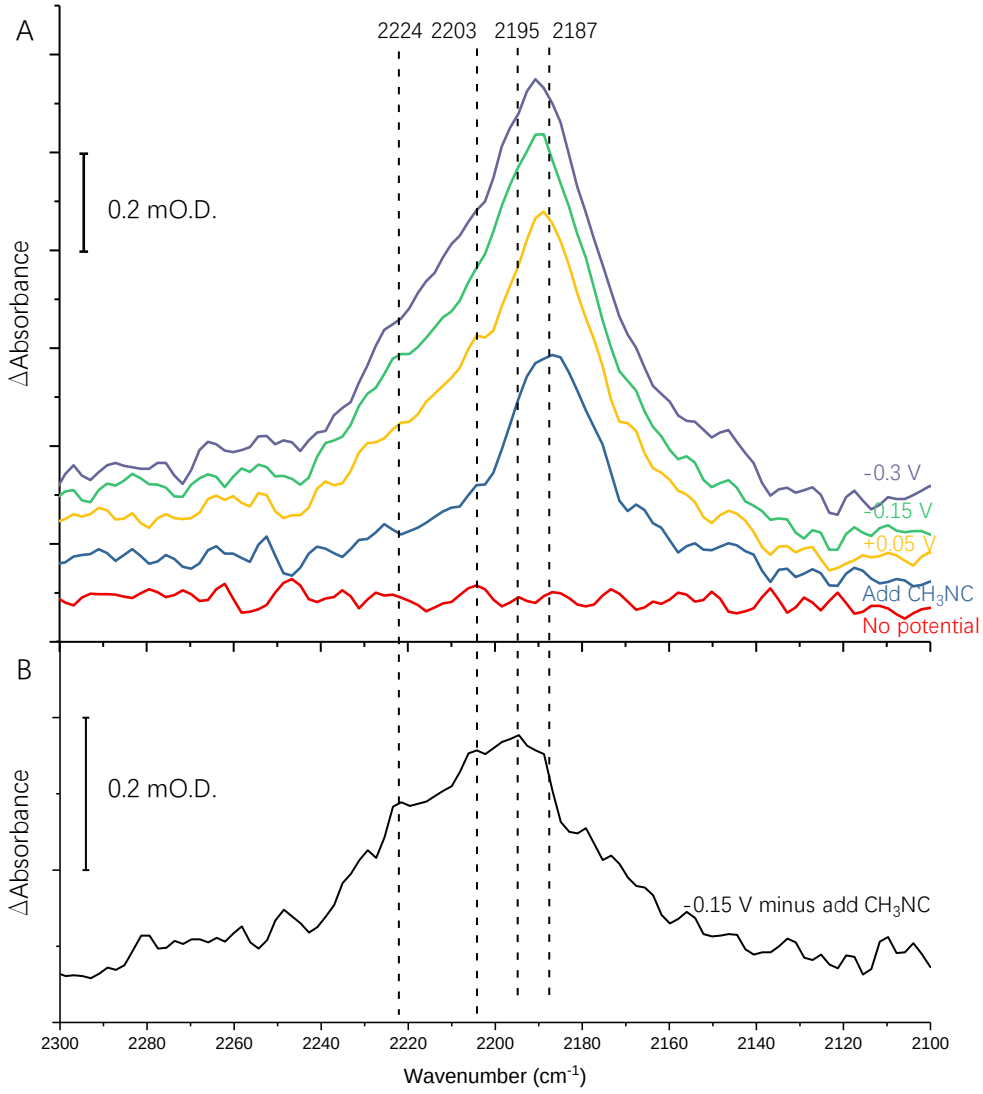


Figure 6-9: IR absorbance spectra of 4 nmol variant 70A MoFe protein in 25 mM methyl isocyanide solution (Tris-HCl buffer pH 8.0 containing Eu-L mediators) with a series of potentials. Each spectrum in (A) was recorded 30 min after applying the specified potential and processed against a background spectrum recorded before the addition of methyl isocyanide with no applied potential (512 scans, 4 cm^{-1} resolution). The spectrum in (B) shows the difference between the spectra at -0.15 and one with no applied potential after adding CH_3NC.

The peak at 2195 cm^{-1} is covered by the peak for bound isocyanide at 2203 cm^{-1} and the free CH_3NC solution peak, similar to the corresponding peak for the variant 98 H MoFe protein. An additional peak appeared at high wavenumber (2222 cm^{-1}) for the variant 70A MoFe protein, quite close to the bound CH_3NC peak at 2218 cm^{-1} for the variant 98H MoFe protein which was discussed in Section 6.3.2.

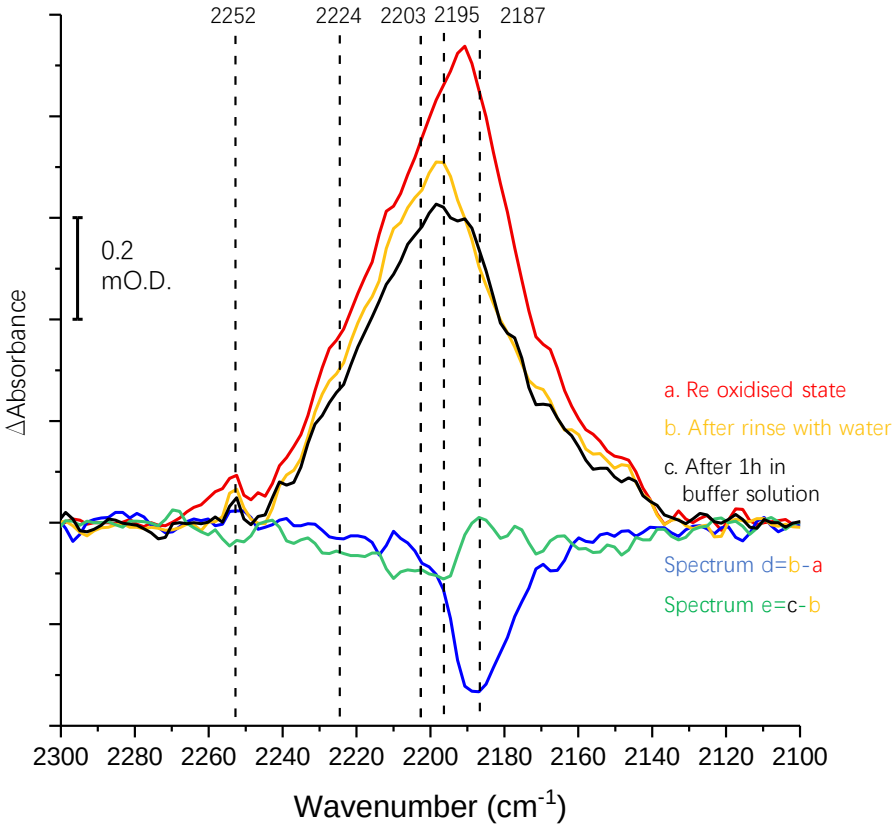


Figure 6-10: IR absorbance spectra of 4 nmol variant 70A MoFe protein after exposure to 25 mM methyl isocyanide with no applied potential, after applying 0 V from Figure 6-9. The a, b and c spectra were processed against a background spectrum before the addition of methyl isocyanide with no applied potential. The spectra d and e show the difference between these three spectra as indicated.

After returning to the oxidising potential of 0 V and switching off the potentiostat, the methyl isocyanide was rinsed out of the cell with plenty of Tris-HCl buffer for 10 min until there was no negative peak observed in the infrared spectra from free CH_3NC loss. In Figure 6-10, the red spectrum shows the variant 70A MoFe protein at open circuit potential following the step to 0 V.

Compared to the spectra at -0.3 V shown in Figure 6-9, there was not much difference in the main peak from 2240 cm^{-1} to 2140 cm^{-1}. However, a small peak at 2252 cm^{-1} was observed in the spectra recorded at open circuit potential after the step to 0 V.

After 10 min of rinsing with buffer, the main peak dramatically dropped in intensity, especially in the region around 2187 cm^{-1}. This is clearly observed from the difference (spectrum d, Figure 6-10) between the spectra before and after rinsing with buffer where the only loss was from the free CH_3NC solution peak at 2187 cm^{-1}. The result shown in Figure 6-10 spectrum e shows that the binding of isocyanide and MoFe protein is almost completely irreversible at the potentials applied here. There were only very small negative peaks observed at the position of bound CH_3NC peaks after one hour under Tris-HCl buffer solution with no applied potential.

Following the experimentshown in Figure 6-10, the methyl isocyanide solution was introduced again back to the cell without any electrochemical control which restored the free CH_3NC solution peak in Figure 6-11 (A) (no potential). A series of low potentials (down to -1.1 V) applied to the cell and enhanced the broad peak from 2240 cm^{-1} to 2140 cm^{-1} by increasing the intensity of bound methyl isocyanide peaks as shown in Figure 6-11 (B).

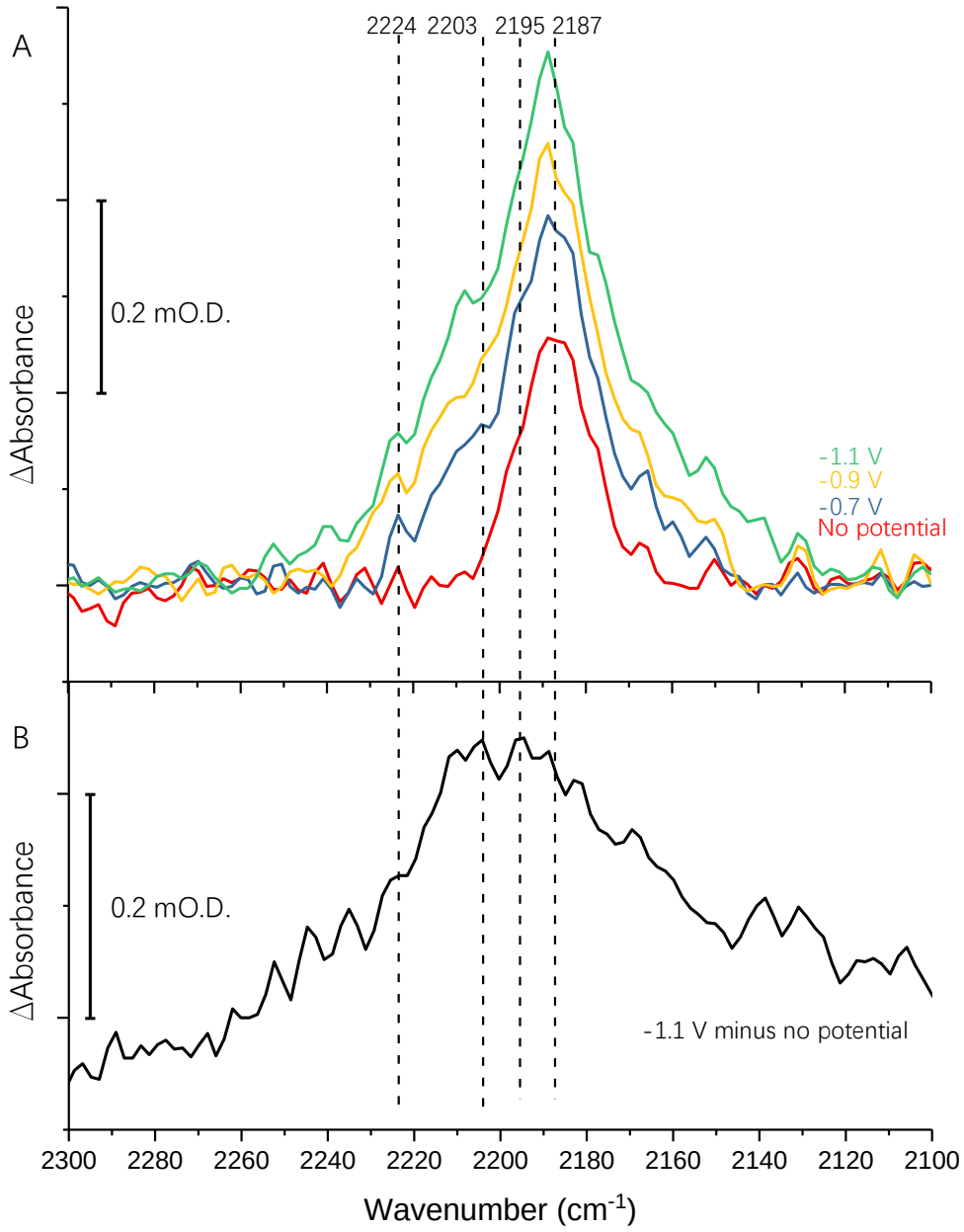


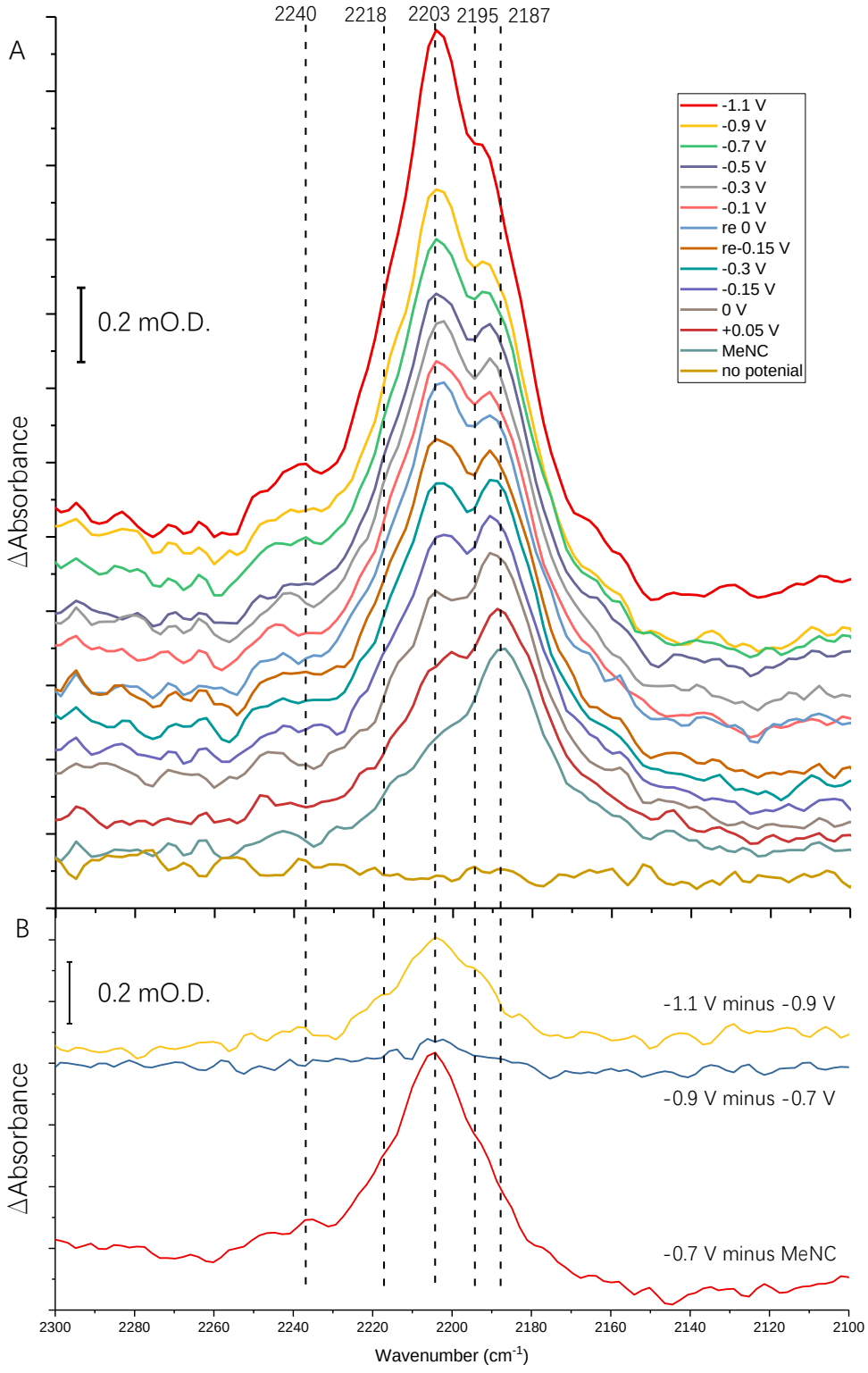
Figure 6-11: IR absorbance spectra of variant 70A MoFe protein at 25 mM methyl isocyanide solution with a series of potentials. Each spectrum in (A) was recorded 30 min at each holding potential and processed against a background spectrum recorded before the addition of methyl isocyanide re-introduced with no applied potential. The spectrum in (B) shows the difference between the spectra at -1.1 V and with no applied potential at CH_3NC.

6.3.4 Wild Type MoFe protein

For the experiments on wild type MoFe protein, a similar spectroelectrochemical cell was setup in the glovebox. Compared to the variant 98H and 70A MoFe proteins, it took an extra 2 hours to allow the wild type MoFe protein fully attach to carbon particles through covalent bonds on ice.

As for the MoFe protein variants, there were no peaks in the *v*(NC) region of the infrared spectra in the absence of 25 mM methyl isocyanide solution. Figure 6-12 (A) shows an experiment in which CH_3NC was introduced into the buffer which contained 0.25 mM Eu-L mediator with no applied potential. The free CH_3NC solution peak at 2187 cm^{-1} quickly reached a height of 0.5 mO.D. after introducing the methyl isocyanide. After no further spectral changes were observed, a series of potentials were applied with the help of mediators. Even with no applied potential, additional bands consistent with coordinated methyl isocyanide were observed: a shoulder at 2203 cm^{-1} and a weak band at ca. 2240 cm^{-1}.

As the applied potential was stepped more negative, the 2203 cm^{-1} increased in intensity and dominated the spectra at -1.1 V. There was also a slight increase in intensity for the 2240 cm^{-1} peak at low potentials. The centre of low wavenumber peak below 2203 cm^{-1} moved from 2187 cm^{-1} (free CH_3NC solution peak) at no applied potential to 2195 cm^{-1} at the potential of -1.1 V, indicating an additional peak between 2203 cm^{-1} and 2187 cm^{-1} increasing in intensity at low potential. The red line in Figure 6-12 (B) shows the bound CH_3NC peak growing at -0.7 V after applying methyl isocyanide. The bound peak at 2203 cm^{-1} dominated at this set of potentials and might cover the other bound peaks at 2195 cm^{-1} and 2218 cm^{-1} which were observed in the experiments of variants of MoFe protein. After applying the -1.1 V potential, the peaks at 2218 cm^{-1}, 2203 cm^{-1} and 2195 cm^{-1} were clearly evident in the yellow spectra of Figure 6-12 (B).


A
2240
2218
2203
2195
2187
-1.1 V
-0.9 V
-0.7 V
-0.5 V
-0.3 V
-0.1 V
re 0 V
re-0.15 V
-0.3 V
-0.15 V
0 V
+0.05 V
MeNC
no potenial
0.2 mO.D.
ΔAbsorbance
B
0.2 mO.D.
-1.1 V minus -0.9 V
-0.9 V minus -0.7 V
-0.7 V minus MeNC
ΔAbsorbance
2300
2280
2260
2240
2220
2200
2180
2160
2140
2120
2100
Wavenumber (cm-1)

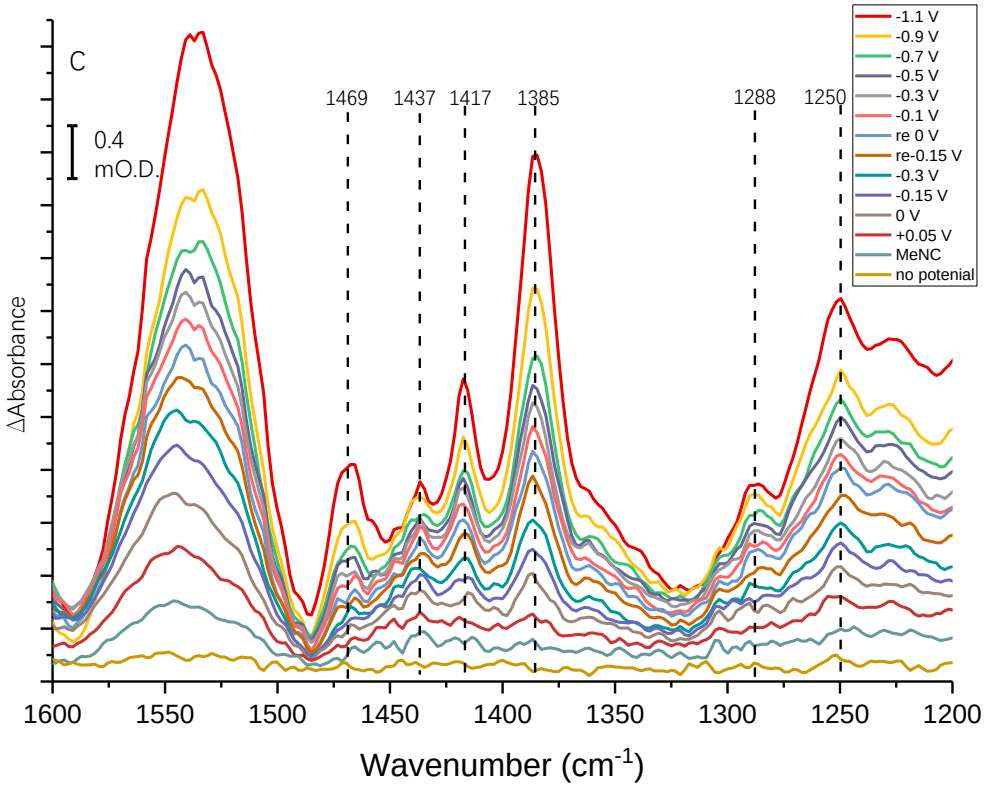


Figure 6-12: IR absorbance spectra of 4 nmol wild type MoFe protein at 25 mM methyl isocyanide solution (Tris-HCl buffer pH 8.0 containing Eu-L mediators) with a series of potentials. Each spectrum in (A) (2300 cm^{-1}-2100 cm^{-1}) and (C) (1600 cm^{-1}-100 cm^{-1}) was recorded 30 min after stepping to the specified potential and processed against a background spectrum recorded before the addition of methyl isocyanide with no applied potential (512 scans, 4 cm^{-1} resolution). The spectra in (B) show the difference at low potentials as indicated.

Figure 6-12 (C) shows IR spectra in the range from 1600 cm^{-1} to 1200 cm^{-1} collected from the same experiment shown in Figure 6-12 (A). There were several peaks arising within the potential series in the presence of methyl isocyanide, which were quite close to the area of *v*(NH) deformation vibration and *v*(CH) deformation vibration.

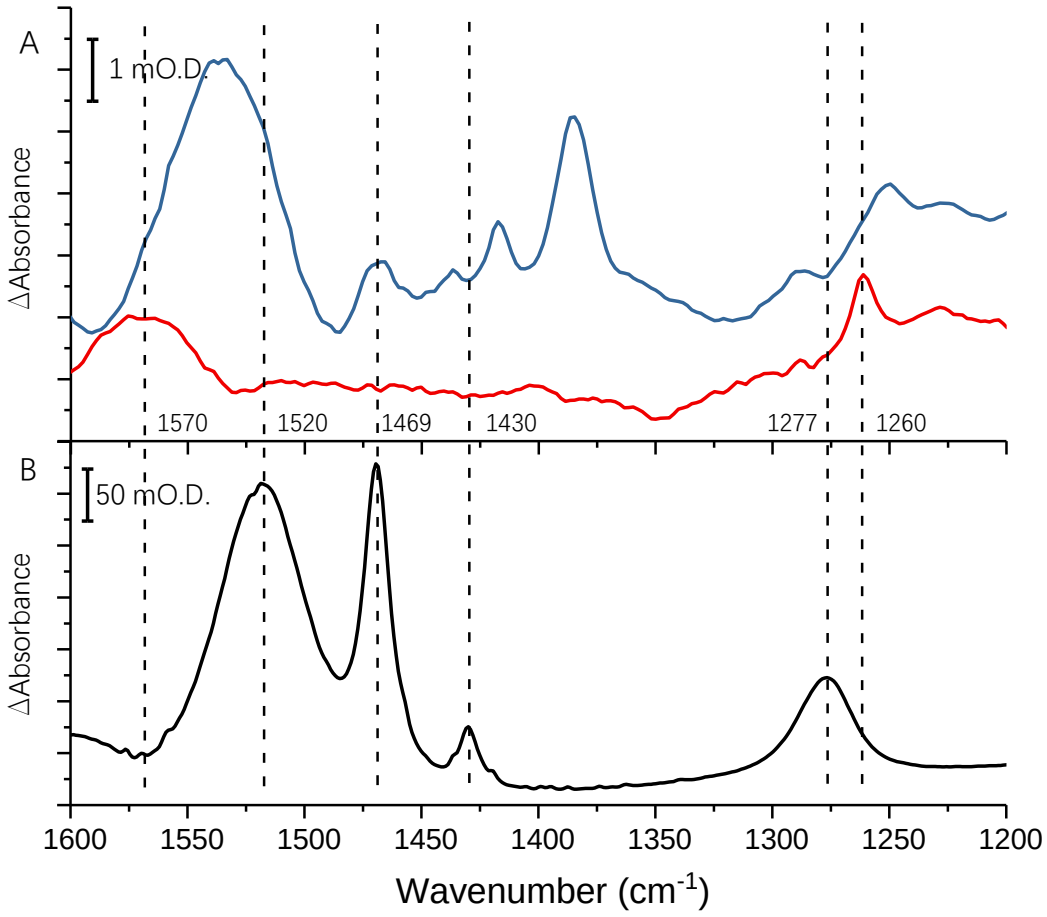


Figure 6-13: IR absorbance spectra of 4 nmol apo protein (red) and wild type (blue) at 25 mM methyl isocyanide at -1.1 V processed against a background spectrum recorded at 0 V in panel (A) (512 scans, 4 cm^{-1} resolution). IR absorbance spectra of 1.5 M methylamine (Tris-HCl buffer pH 8.0) processed against a background spectrum of Tris-HCl Buffer by FT-IR in panel (B) (1024 scans, 2 cm^{-1} resolution).

Figure 6-13 (A) shows the difference of spectra between -1.1 V and 0 V in the range 1600 cm^{-1} to 1200 cm^{-1} for apo protein (red line) and wild type MoFe protein (blue line). In contrast to wild type MoFe protein, no peak was observed in the range 1500 cm^{-1} to 1300 cm^{-1} in the spectra of apo protein. The broad peak at around 1570 cm^{-1} may be caused by slight changes in the amide II band from apo protein. The solution flow might push the carbon-enzyme film much closer to the prism and increase the amide peaks from protein. The peak 1260 cm^{-1} should come from the Si-CH_3 groups on the ATR-IR prism. It indicates that no similar peaks appeared in this infrared spectral range when apo protein was at 25 mM methyl isocyanide with applied potentials.

An IR spectrum of 1.5 M methylamine (Sigma) recorded by FT-IR is shown in Figure 6-13 (B). There were several functional groups displaying vibrational bands in the range from 1600 cm^{-1} to 1200 cm^{-1}. The broad peak around 1500 cm^{-1} is probably from the vibration of $-NH_2$. The peaks at 1469 cm^{-1} and 1430 cm^{-1} of CH_3NH_2 are very similar to the peak shown in Figure 6-12 C which might result from asymmetric bending of $-CH_3$ or $-CH_2$. The peak at 1277 cm^{-1} should be contributed by the vibrational modes of C-N stretching or C-H wagging.

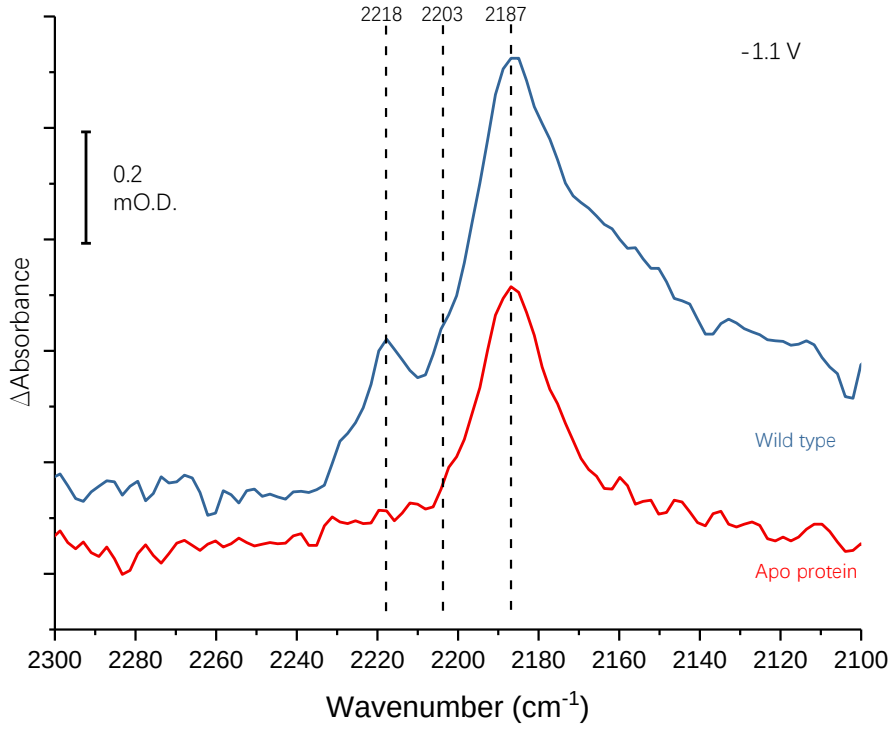


Figure 6-14: IR absorbance spectra of 4 nmol wild type MoFe protein and apo protein with 25 mM methyl isocyanide solution (Tris-HCl buffer pH 8.0 containing Eu-L mediators) at -1.1 V. Each spectrum was recorded when the system had equilibrated after introduction of CH_3NC and is processed against a background spectrum before addition of methyl isocyanide at -1.1 V (512 scans, 4 cm^{-1} resolution).

To study the substrate binding to MoFe protein at a low potential, 25 mM methyl isocyanide was introduced to the cell after the proton reduction current was stable at -1.1 V (the current trace in Figure 6-3). The free isocyanide solution peak appeared and was stable within 5 min in the control experiment with Apo protein in Figure 6-14. There was no additional peak observed, in contrast,

a clear binding peak was displayed in the spectrum of wild type MoFe protein after the same amount of time. However, there was little further change or growth of the bound CH_3NC peak later in the experiment. The spectra were a bit different from the earlier experiments in which CH_3NC was introduced at more positive potentials or without an applied potential. In particular, the 2203 cm^{-1} peak was much less prominent in Figure 6-14.

After the *ν*(NC) peaks were stable in the range from 2300 cm^{-1} and 2100 cm^{-1}, infrared spectra were collected over time without any substrate solution flow. Ignoring osmotic pressure, the amount of reaction solution was about 150 μL. Figure 6-15 (A) shows a significant loss band at 2187 cm^{-1} (0.76 mO.D. of peak height in 15 hours), suggesting methyl isocyanide consumption overnight by the wild type MoFe protein in the spectroelectrochemical cell. The bound isocyanide peaks were also lost during the experiment, consistent with a decrease pf methyl isocyanide concentration in the cell. In the control experiment on apo protein in Figure 6-15 (B), the free CH_3NC solution peak had a slight loss (0.14 mO.D. of peak height in 15 hours) which might be due to the evaporation of methyl isocyanide or background reduction reaction (from the apo protein or carbon particles).

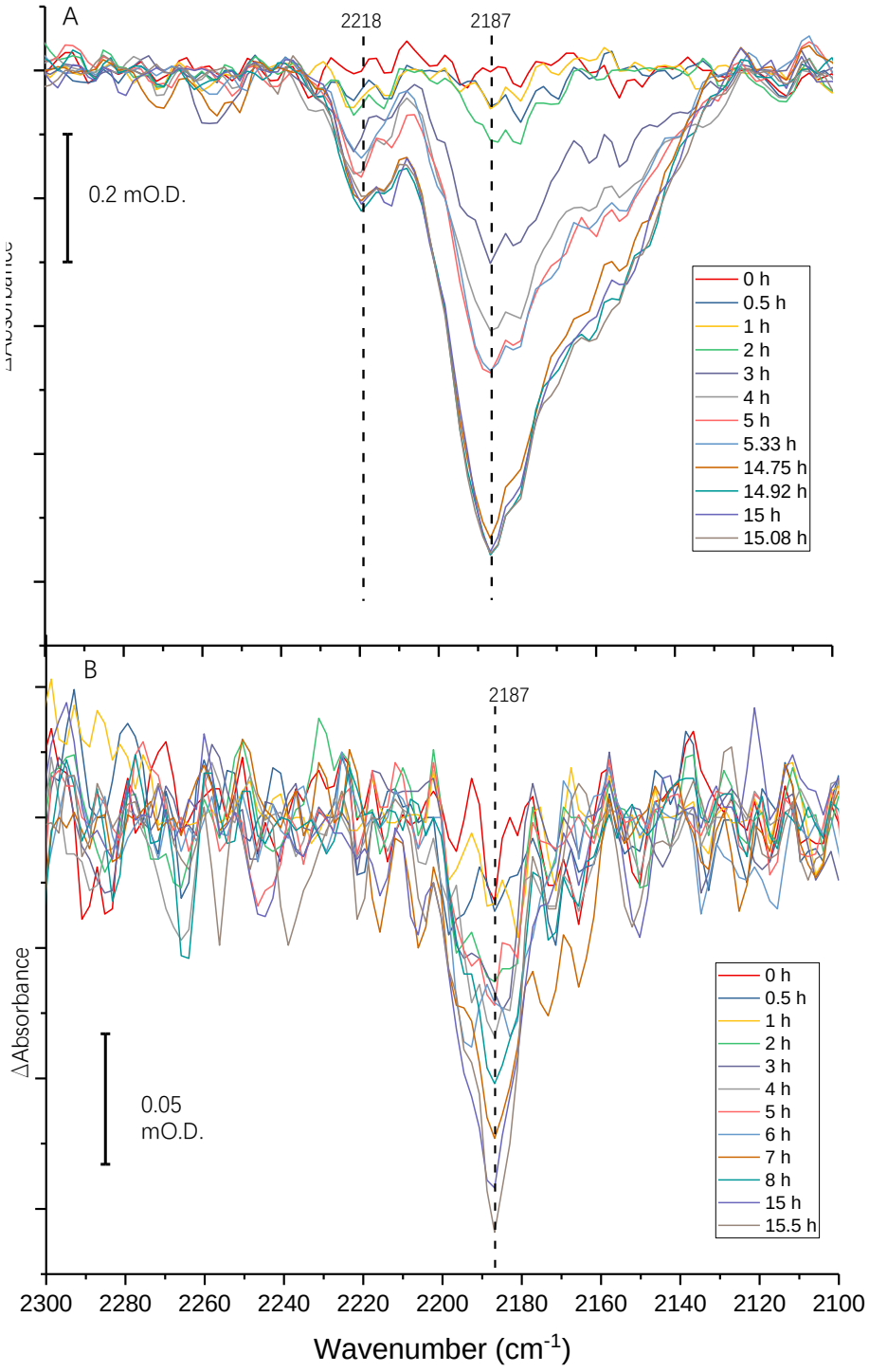


Figure 6-15: Time course IR absorbance spectra of 4 nmol wild type MoFe protein (A) and apo protein (B) showing consumption of methyl isocyanide at -1.1 V with no pumping flow. Each spectrum was recorded at the time shown on the right and processed against a background spectrum recorded in the presence of methyl isocyanide when the *ν*(NC) peak was stable at the potential of -1.1 V (512 scans, 4 cm^{-1} resolution).

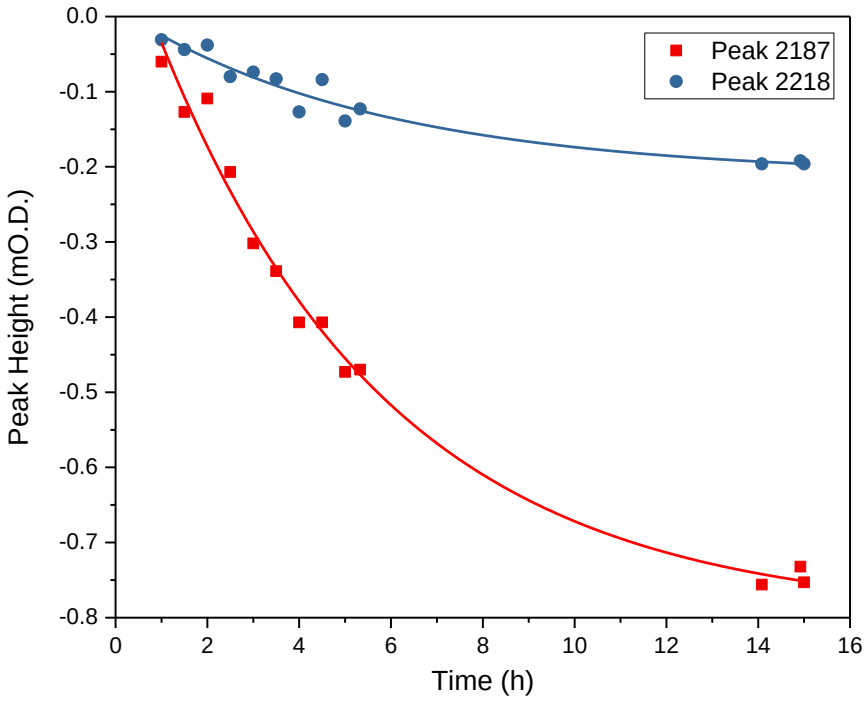


Figure 6-16: A plot showing the change in peak height of ν(NC) peaks at 2187 cm^{-1} (red) and 2218 cm^{-1} (black) as a function of time at a potential of -1.1 V. The peak heights were obtained from a set of time-series difference spectra of the wild type MoFe protein in the presence of 25 mM methyl isocyanide solution recorded at -1.1 V and processed against a spectrum recorded after the isocyanide peaks were stable. (Raw data are shown as points with fitted traces calculated by exponential growth function, Origin Programme 2017.)

Methyl isocyanide consumption continued over more than 10 hours as shown in Figure 6-16. The height of the free CH_3NC solution peak was 1.19 m O.D. at the beginning and lost 63.9% of the height over 15 hours. The peak for bound CH_3NC at 2218 cm^{-1} had a height of 0.34 mO.D. and lost 55.8% in the same amount of time.

6.3.5 Ethyl isocyanide

Figure 6-17 depicts FTIR spectra of ethyl isocyanide determined by Min-Wen Chung, one of the previous group members. The spectrum of neat ethyl isocyanide is depicted as a black line. With the longer ethyl chain of the ethyl substituent, which has a stronger electron-donating ability relative to the methyl group (2166 cm^{-1}), the *ν*(NC) shifts to lower wavenumber at 2149 cm^{-1}. The

aqueous ethyl isocyanide (300 mM, red line) shows three characteristic bands at 2168 cm^{-1}, 2185 cm^{-1}, and 2149 cm^{-1}. The Fermi resonances of *v*(NC) change the donor or acceptor frequency, giving rise to two strong absorption peaks at the high wavenumber for the aqueous isocyanide.[11]

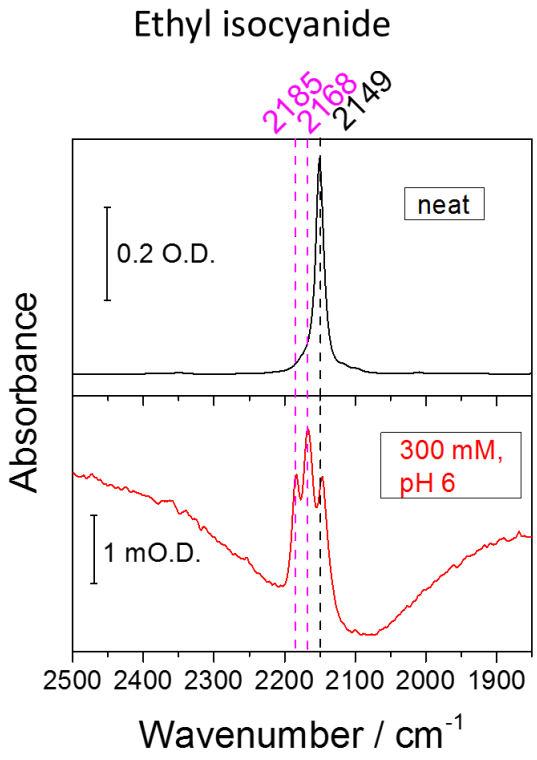


Figure 6-17: FTIR spectra of ethyl isocyanide by Min-Wen Chung (a previous group member). The neat form is shown in black, and the spectra collected in the presence of a buffer solution (pH 6, mixed buffer) is represented in red.

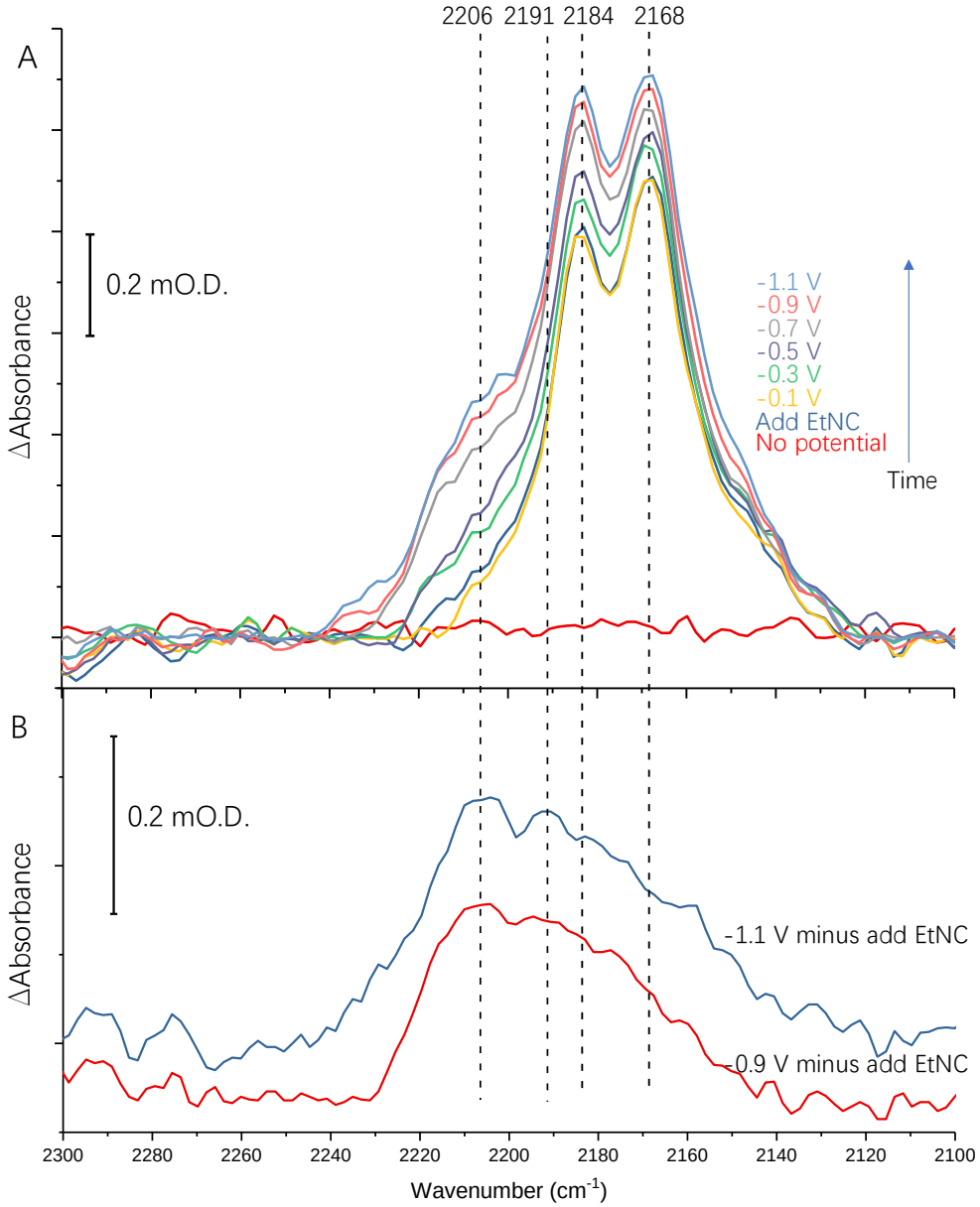


Figure 6-18: IR absorbance spectra of 4 nmol wild type MoFe protein in 50 mM ethyl isocyanide solution (Tris-HCl buffer pH 8.0 containing Eu-L mediators) at a series of potentials. Each spectrum in (A) was recorded 30 min after stepping to the specified potential and processed against a background spectrum recorded before the addition of ethyl isocyanide without any applied potential (512 scans, 4 cm^{-1} resolution). Spectra in (B) show the low potential spectra processed against a background with no applied potential after the introduction of ethyl isocyanide as indicated.

A series of negative potentials was applied to the wild type MoFe protein after two free ethyl isocyanide solution peaks were stable at no applied potential. The shoulder peakabove 2200 cm^{-1}

was observed at low potential. Especially in the spectra at -1.1 and –0.9 V (Figure 6-18 (A)), this additional part of the isocyanide peak was clearly displayed at ca. 2206 cm^{-1}. In the subtracted spectra, peaks at about 2206 cm^{-1} at and 2191 cm^{-1} were clearly observed, which could be peaks from ethyl isocyanide bound to the MoFe protein due to similar shift of the binding peak shown in Figure 6-18 (B).

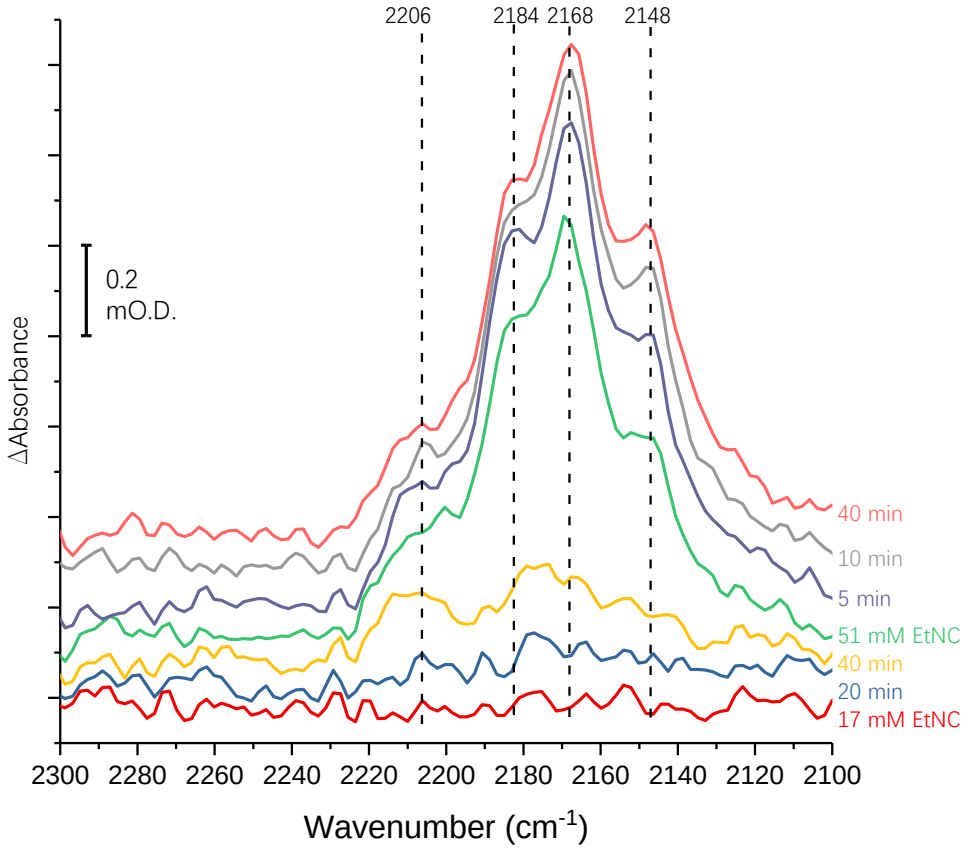


Figure 6-19: IR absorbance spectra of 4 nmol wild type MoFe protein with different concentration of ethyl isocyanide solution (Tris-HCl buffer pH 8.0 containing Eu-L mediators) at -1.1 V. Each spectrum was recorded by time in ethyl isocyanide solution and processed against a background spectrum in the absence of ethyl isocyanide at -1.1 V (512 scans, 4 cm^{-1} resolution).

A low concentration of ethyl isocyanide (~17 mM) was first introduced into the flow system at -1.1 V. There was no significant change until 20 min in the range from 2300 cm^{-1} to 2100 cm^{1} in

Figure 6-19. The peak in the position of about 2206 cm^{-1} and the mixture of solution peaks were observed clearly after 40 min at this ethyl isocyanide concentration.

A further increase in the concentration of ethyl isocyanide to 51 mM made the peaks grow dramatically. The *v*(NC) stretch from free ethyl isocyanide was clearly split into three peaks at this time, 2184 cm^{1}, 2168 cm^{-1} and 2148 cm^{-1}. The additional band at 2148 cm^{-1} was in agreement with the isocyanide group being in an organic microenvironment of the ethyl isocyanide micelle-like droplets, due to the poor solubility of ethyl isocyanide. The binding peaks at 2206 cm^{-1} also increased as the ethyl isocyanide solution concentration increased. The peak at 2191 cm^{-1} was covered by the free C_2H_5NC solution peaks.

6.3.6 Methylene blue as an extra mediator

As the methyl isocyanide was found to bind to 98H MoFe protein at such a mild potential, a new mediator, methylene blue, was added to help control the potential experienced by the protein and find out the requirement of mediator for the MoFe protein at mild potentials. Figure 6-20 shows the cyclic voltammogram of 2 mM methylene blue in Tris-HCl buffer, revealing the reduction peak at -15 mV (vs SHE) and oxidation peak at 12 mV. This mid potential is also close to the first oxidised couple of the active site of nitrogenase ($M^{N/OX}$) which is reported to have a measured midpoint potential around -42 mV.[12]

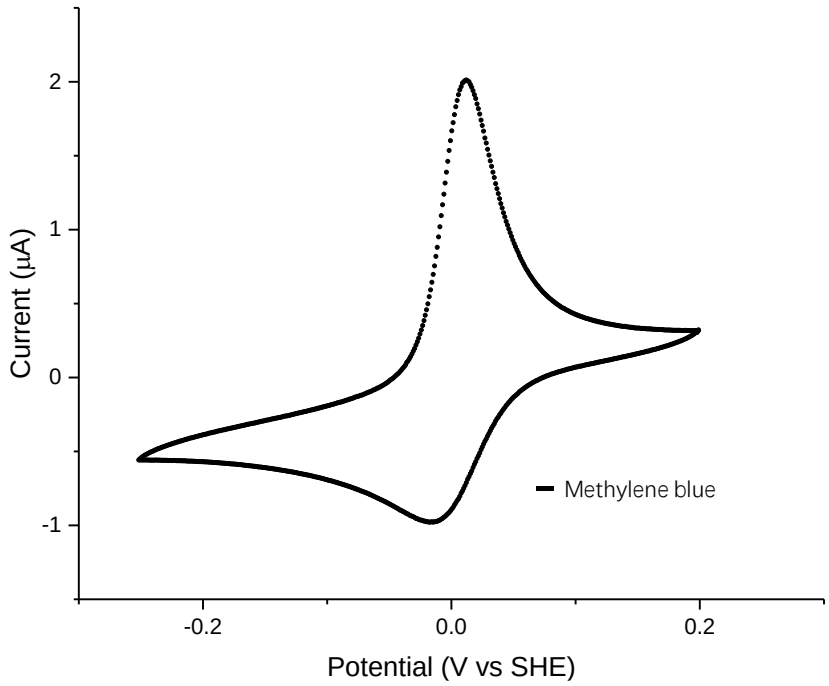


Figure 6-20: Cyclic voltammogram of methylene blue (concentration 2 mM), in 100 mM pH 8 Tris-HCl buffer, scan rate 10 mV s^{-1}.

Using an extra 0.25 mM methylene blue as a mediator, to support MoFe protein at the mild potentials, an infrared spectral study was carried out as shown in Figure 6-21. This time, methyl isocyanide was introduced into the cell at +0.1 V, as methyl isocyanide was shown to bind to the active site of 98H MoFe protein at ca. 0 V in Figure 6-7. Applying a more positive potential risks destroying the clusters of nitrogenase. There were clearly no peaks at +0.1 V before adding CH_3NC, but after introducing isocyanide, a broad peak appeared between 2240 cm^{-1} and 2140 cm^{-1} at the same potential. It took 30 min for spectra to stabilise after introducing methyl isocyanide before stepping to the next potential. It was quite apparent that this broad peak could be separated into two peaks (2203 cm^{-1} bound CH_3NC peak, and 2187 cm^{-1} free CH_3NC solution peak). Other peaks might be covered by the powerful free isocyanide peak in this study. The peak became much broader and less resolved in the spectra at -0.15 V and -0.45 V in Figure 6-21. However, not much detail can be found from this general spectrum.

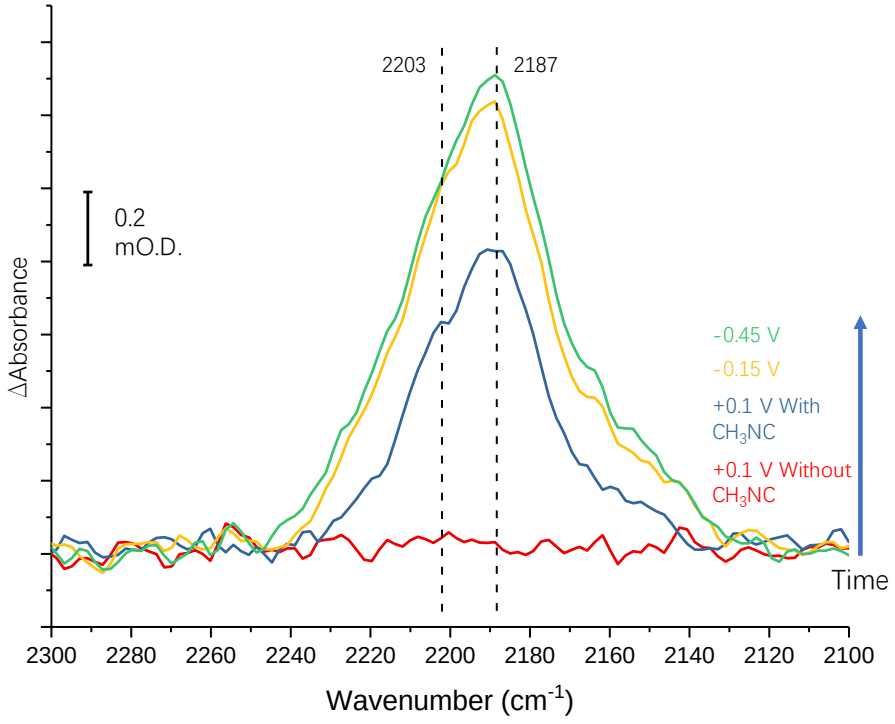


Figure 6-21: IR absorbance spectra of variant 98H MoFe protein at 25 mM methyl isocyanide (Tris-HCl buffer pH 8.0 containing Eu-L and Methylene Blue mediators) with a series of potentials. Each spectrum was recorded after holding for 30 min at each potential and processed against a background spectrum recorded before the addition of methyl isocyanide at +0.1 V.

Figure 6-22 shows the time course spectra of methyl isocyanide and the MoFe protein at -0.15 V with the help of methylene blue as an extra mediator. All spectra are processed using data with the same concentration of methyl isocyanide at +0.1 V as the reference (as shown in Figure 6-21, blue line). After applying -0.15 V, the broad peak between 2230 cm^{-1} and 2160 cm^{-1} rapidly increased in the first 5 min, with the species at 2203 cm^{-1} being more intense than the other bound CH_3NC peaks in Figure 6-22 (A). The low wavenumber components (2203cm^{-1} and 2195 cm^{-1}) in this broad peak started to decrease later at this potential. It is clearly shown in Figure 6-22 (B) that these two peaks are lost in the infrared spectra at later times.

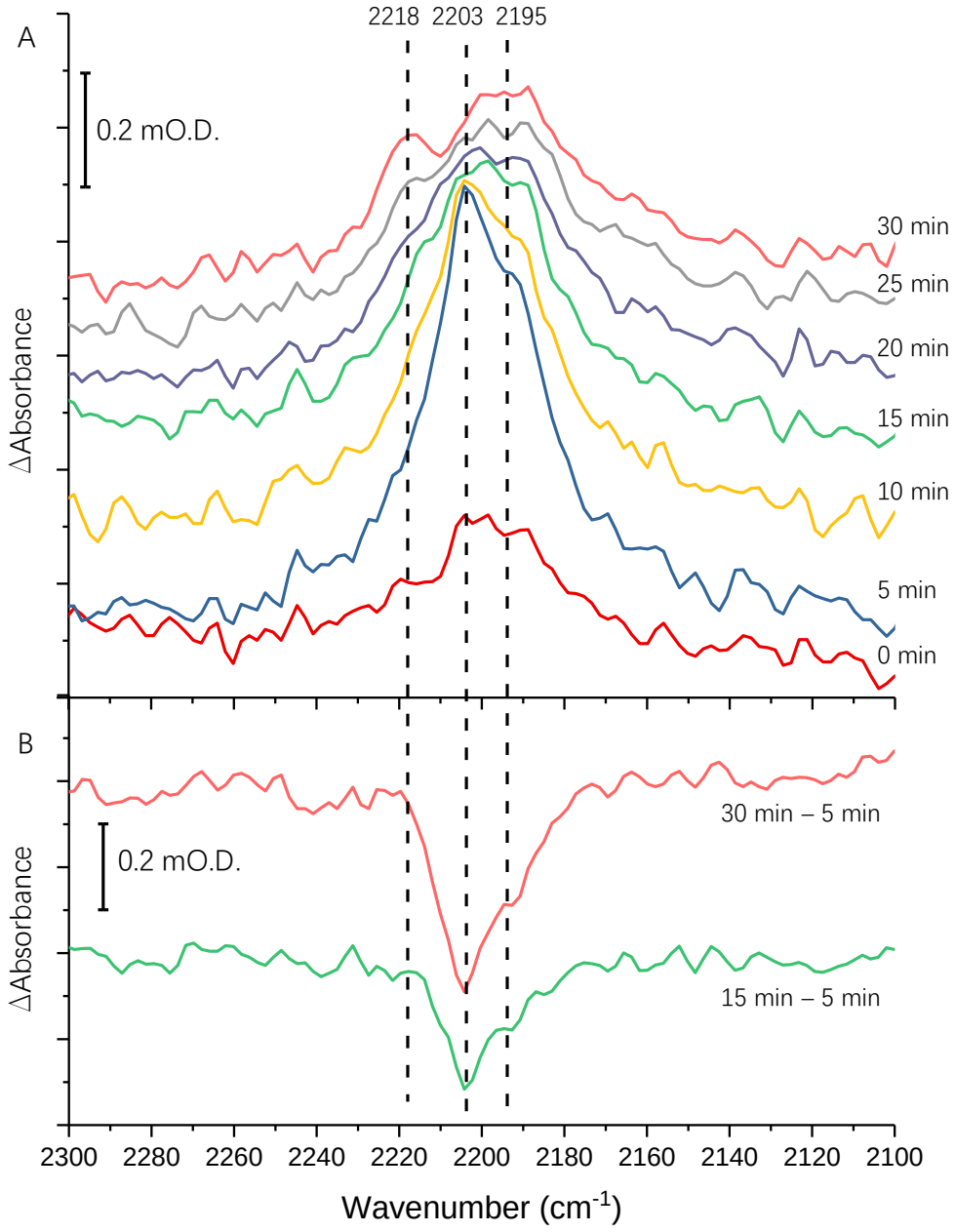


Figure 6-22: Time course IR absorbance spectra of variant 98H MoFe protein in 25 mM methyl isocyanide solution (Tris-HCl buffer pH 8.0 containing Eu-L and Methylene Blue mediators) at -0.15 V. Each spectrum in (A) was recorded at 5 min intervals and processed against a background spectrum recorded in the presence of methyl isocyanide at +0.1 V. The spectra in (B) show the changes at 15 min and 30 min against the spectra recorded after 5 min at -0.15 V.

Meanwhile, a new peak became visible in the high wavenumber feature at 2218 cm^{-1} after the loss of low wavenumber features, which indicated a new bound methyl isocyanide species was

formed at -0.15 V with the help of the extra mediator, methylene blue. This peak arose in the first 5 min and did not decrease by time as displayed in Figure 6-22 (B).

There was no reverse change in the range from 2300 cm^{-1} to 2100 cm^{-1} observed when the applied potential was stepped back to +0.1 V. And the further negative potential of -1.1 V also did not give any significant change in the *v*(NC) region of the infrared spectrum with the extra mediator.

6.4 Product determination by chromatography

To determine the identity of the main product formed from electrochemical catalysis, a derivatization method was used to identify any methylamine in the flow solution.

An OPT reagent (including phthaldialdehyde and 2-mercaptoethanol) was trialled for determining different amino acids and ammonia by HPLC (High-Performance Liquid Chromatography, C18 column).[13] However, the approach did not work well when used with a UV-vis detector instead of a fluorescence detector. The derivatization product was too sensitive to the temperature which made the result not reproducible.

The BOC group (Di-tert-butyl dicarbonate) is an agent which can add to amines in aqueous conditions to help with analysis of the group by GC (Gas Chromatography, a chiral stationary phase column).[14] BOC_2O (1 mmol, 0.235 mL) was diluted with 1 mL THF (Tetrahydrofuran) in a large centrifuge tube. The 150 µL BOC solution which was left for one hour was added to 50 µL sample. After 2 hours waiting, 200 µL ethyl acetate was added to extract the product. The top phase was removed after 20 minutes and dried by adding anhydrous sodium sulphate. The solution was then injected into a vial for GC determination.

This approach produced a more reliable result from a test experiment to generate a methylamine standard curve. It was also able to determine a small amount of ammonia from an ammonium chloride standard solution as well.

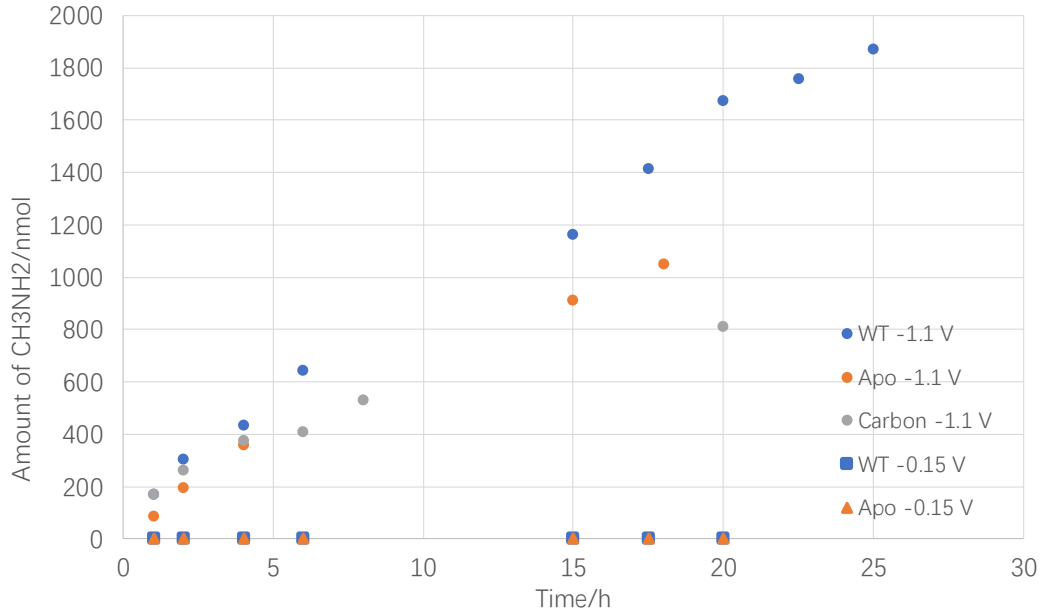


Figure 6-23: Plot of methylamine from the reduction of 25 mM methyl isocyanide by wild type MoFe protein (●/■), Apo protein (●/▲) and carbon particles only (●) as indicated. Each sample (50 µl) was taken from the flow solution as a time-point and derivatized by BOC reagent before determination by GC.

Figure 6-23 shows the amount of methylamine determined by GC. The total reduction rate still had about 1.4 nmol/min/mg protein over 20 hours at -1.1 V. However, the amount of methylamine detected from electrodes containing only Apo protein on carbon, or only carbon particles, was more than 50% of that from wild type MoFe protein, indicating that there was quite a considerable background isocyanide reduction at -1.1 V by the carbon material itself.

For the sample taken at mild potential (-0.15 V), the GC determination from experiments on wild type MoFe protein and Apo protein did not detect any amount of methylamine within 20 hours. Using methylene blue as the extra mediator also did not get any signal in the position of product peak from GC.

6.5 Discussion

6.5.1 Isocyanide bound peaks

To study the interaction between isocyanide and nitrogenase MoFe protein, we introduced quite a high concentration (about 25 mM) of methyl isocyanide into the spectroelectrochemical cell. Such concentration could allow *ν*(NC) peaks to be observed in infrared spectra, but the high concentration of isocyanide decreased the activity of nitrogenase,[7] which lowered the proton reduction reaction by the enzyme as well.

The free methyl isocyanide solution peak 2187 cm^{-1} was able to be observed from infrared spectroscopy after the introduction of methyl isocyanide immediately. After the intensity of this peak was stable, there was not much change observed at different potentials in a short period of time. In a long-period experiment, the free CH_3NC peak was gradually lost due to the reduction reaction by the MoFe protein as shown in Figure 6-15 (A). However, the slight weakening of 2187 cm^{-1} peak was observed in the control experiment of the apo protein, which lost 18.4% height of the free CH_3NC peak in the same amount time (15 hours). This background decline might come from methyl isocyanide evaporation or reduction reaction by the apo protein or carbon particles at low potentials.

With methyl isocyanide as the ligand binding to MoFe protein under potential control, the peak at 2203 cm^{-1} was the feature observed first at mild potentials. This binding peak was observed in all variants and wild type of MoFe protein and was not clearly potential-dependent like the bound peaks between CO and the active site of the MoFe protein. Application of negative potentials could only increase the intensity of this binding peak. The binding peak possessed higher wavenumber than the free solution peak which contrasted with the CO binding peak. As the isocyanide is a strong σ donor as well as a π-acceptor, π back-donation is less important and orbital overlap is dominated by σ-bonding when isocyanide is coordinated to high oxidation state metal.[15]

The isocyanide might therefore transfer electron density to metal atoms in the active site of the MoFe protein giving a higher frequency than in free solution.

There was an additional bound methyl isocyanide peak covered by the intensities of the bound peak at 2203 cm^1 and the free solution peak at 2187 cm^{-1}, revealed by a slight shift in the centre of the free CH_3NC solution peak to higher frequency after applying a negative potential. The subtraction spectra from all enzymes above indicated that a bound CH_3NC peak appeared at about 2195 cm^{-1} after applying potentials.

There was some evidence of an additional binding peak arising later at higher wavenumber, in other words, slowly increasing at low potential. This peak may come from methyl isocyanide bound to higher oxidation state metal (like Mo or Fe^{III}). For the variant 98H MoFe protein, there was no such peak observed at low potentials until methylene blue was introduced as an extra mediator. An additional peak at 2218 cm^{-1} then appeared at -0.15 V in Figure 6-22 and not much change was observed in low potentials in the *ν*(NC) region (from 2300 cm^{-1} to 2100 cm^{-1}).

The similar binding peak (2218 cm^{-1}) was observed in the experiment on wild type MoFe protein upon the introduction of methyl isocyanide at -1.1 V, while the bound CH_3NC peak at 2203 cm^{-1} was in low intensity. If methyl isocyanide was introduced before applying any potentials, the peak at 2203 cm^{-1} dominated, and the peak for bound isocyanide at 2218 cm^{-1} only built up at negative potentials below -0.9 V. There was a new peak at much higher wavenumber, 2240 cm^{-1}.

In the spectra of variant 70A MoFe protein, these additional binding peaks both shifted to much higher frequencies of 2224 cm^{-1} and 2252 cm^{-1}. And these high-frequency peaks appeared at mild potentials and did not change at low potential.

Table 6-1: All peaks observed from wild type and variants of MoFe protein with methyl isocyanide in the infrared spectral range between 2300 cm^{-1} and 2100 cm^{-1}

MoFe protein	Free solution peak (cm^{-1})	1st peak (cm^{-1})	2nd peak (cm^{-1})	3rd peak (cm^{-1})	4th peak (cm^{-1})
Wild type	2187	2195 (m)	2203 (m)	2218 (L)	2240 (m)
98H variant	2187	2195 (m)	2203 (m)	2218 (m, with MB)	
70A variant	2187	2195 (m)	2203 (m)	2224 (m)	2252 (m)

*The order of bound methyl isocyanide is from low to high in wavenumber.
First to appear: m (mild potentials); L (low potentials)

All these peaks shown in Table 6-1 did not show any reversible property under potential control although they were gradually lost in isocyanide-free solution. It still a problem to define the bound peaks shown in Table 6-1 as well as the peaks in the range from 1600 cm^{-1} to 1200 cm^{-1} shown in Figure 6-12 (C).

In the study of ethyl isocyanide, two binding peaks were appeared at higher wavenumber (ca. 2206 cm^{-1} and 2191 cm^{-1}), compared to free ethyl isocyanide solution peaks 2184 cm^{-1} and 2168 cm^{-1}, which had a similar shift to the result from methyl isocyanide experiments.

6.5.2 Methylamine determination

The results of product determination from GC showed that wild type MoFe protein did not do much work on the isocyanide reduction. The carbon particles and Apo protein both produced at least 50% of methylamine in the same time compared to the wild type MoFe protein.

The concentration of methyl isocyanide (at least 25 mM) for oberserving from ATR-IR spectroscopy was too high to affect the activity of the enzyme. Further experiments at a low concentration of isocyanide (1 mM) and further control experiments might help to provide an answer.

The faradaic efficiency of methylamine production by MoFe protein was calculated below in the time period of 20 hours. The current (I) was considered as -20 μA which was the equilibrium current shown in Figure 6-3. Assuming two electrons are used to produceCH_3NH_2, the efficiency is about 22.4% for the production of methylamine. If six electrons are given to access CH_3NH_4, it would be 67.2%.

$$\mathrm{FE} = \frac{n_{CH3NH2}}{n_{e^-}}$$

$$n_{e^-} = \frac{I * t}{n_1 * F}$$

6.5.3 The potential scale

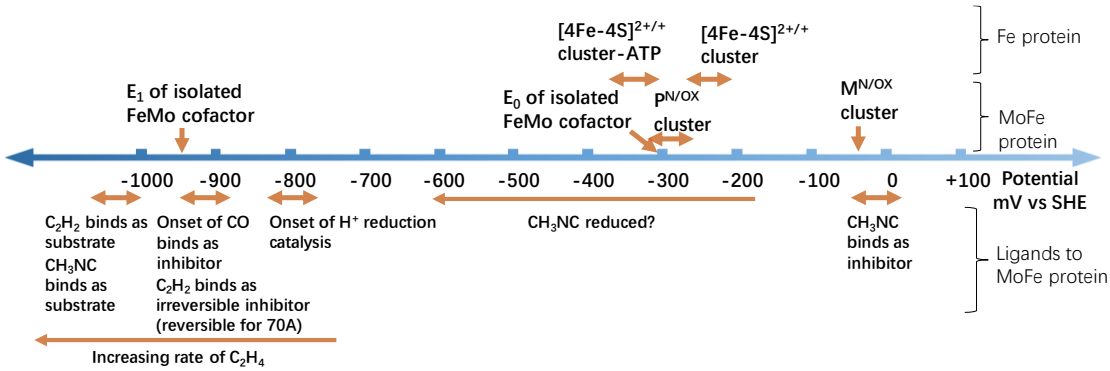


Figure 6-24: A potential scale shows the measured mid potentials of metal clusters in nitrogenase and potential of ligands to MoFe protein in the electrochemical study.

Figure 6-24 displays the additional midpoint potential of isocyanide (methyl isocyanide) to nitrogenase MoFe protein on the potential scale. Methyl isocyanide binds to MoFe protein at a quite mild potential, about 0 mV, while reduction of isocyanide required a much more negative potential at about -1100 mV. There was a mystery for isocyanide binding between these two potentials where bound peaks only slightly increased in intensity in the infrared spectra.

Bibliography

1 R. W. Stephany, M. J. A. de Bie and W. Drenth, *Org. Magn. Reson.*, 1974, **6**, 45–47.

2 C. J. Pickett, K. A. Vincent, S. K. Ibrahim, C. A. Gormal, B. E. Smith and S. P. Best, *Chem. - A Eur. J.*, 2003, **9**, 76–87.

3 M. Kelly and J. R. Postgate, *Biochem. J.*, 1967, **102**, 100–102.

4 M. Kelly, *Biochem. J.*, 1968, **107**, 1–6.

5 R. W. F. Hardy, *A Treatise on Dinitrogen fixation*, Wiley, New York, 1979.

6 K. Tanaka, Y. Imasaka, M. Tanaka, M. Honjo and T. Tanaka, *J. Am. Chem. Soc.*, 1982, **104**, 4258–4260.

7 J. F. Rubinson, J. L. Corbin and B. K. Burgess, *Biochemistry*, 1983, **22**, 6260–6268.

8 Eager, *J. Biol. Chem.*, 1989, **264**, 15967.

9 R. Von Schleyer and A. Allerhand, *J. Am. Chem. Soc.*, 1962, **84**, 1322–1323.

10 B. K. Burgess and D. J. Lowe, *Chem. Rev.*, 1996, **96**, 2983–3012.

11 G. C. Blouin and J. S. Olson, *Biochemistry*, 2010, **49**, 4968–4976.

12 W. N. Lanzilotta and L. C. Seefeldt, *Biochemistry*, 1997, **36**, 12976–12983.

13 J. L. Corbin, *Appl. Environ. Microbiol.*, 1984, **47**, 1027–1030.

14 M. Bertrand, A. Chabin, A. Brack and F. Westall, *J. Chromatogr. A*, 2008, **1180**, 131–137.

15 Y. Yamamoto, *Coord. Chem. Rev.*, 1980, **32**, 193–233.

Chapter 7

Conclusion

This thesis presents the work of an IR spectroelectrochemical study of nitrogenase MoFe protein. The immobilisation approaches were developed from Nafion-entrapment to direct adsorption and the attachment approach for MoFe protein was used in the SEC study. The improvement offered by the immobilisation approach is faster electron transfer from the electrode to the enzyme and it also allows ligands to diffuse through the electrode/protein film efficiently. The stability of the covalent bond between the MoFe protein and pyrene butyric acid means there is a stable protein-carbon film, allowing the long-time experiment to be possible.

In Chapter 4, the inhibition by CO on the MoFe protein was discussed. Compared to the previous study by Paengnakorn in the Vincent group, the new immobilisation approach gives a much stronger intensity of peaks for CO bound to the active site of MoFe proteins. CO binding could be well-controlled by potential, and presents quite observable changes between the oxidised state and reduced state. Wild type MoFe protein and other variants (98H, 70A and 64H) all give consistent positions of CO bound peaks (2009 cm^{-1}, 1980 cm^{-1}, 1964 cm^{1} and a broad peak from 1950 cm^{-1} to 1850 cm^{-1}). Bound CO peaks at high wavenumber are dominant in the IR spectra of variant 70A MoFe protein, in which the cavity at the active site is opened up, showing that the alteration in the cavity affects the CO binding sites.

One of the main important findings is that direct electron transfer from the electrode to one variant of the MoFe protein (64H) was observed for the first time, which might avoid the need for mediators in experiments in the Fe protein-independent system, thus avoiding possible background contributions of the Eu-L complexes to electrochemical current in future experiments on this variant.

In Chapter 5, acetylene reduction by nitrogenase MoFe protein was studied. From electrochemical experiments, the proton reduction by MoFe protein is inhibited by C_2H_2 at -0.9 V, which is irreversible at this potential under Ar. A slightly more negative potential allowed the protein to

recover from this inhibition when Ar was introduced to flush out C_2H_2, showing that this process is at least partly reversible at negative potentials. This change suggests a different redox level of FeMo cofactor is accessed below -0.9 V. The result from variant 70A MoFe protein shows this inhibition is reversible even at -0.9 V when C_2H_2 was flushed out with Ar, confirming that the change of cavity at the active site affects ligand binding at different redox levels.

Although IR studies of acetylene with MoFe protein were not conclusive, analysis by GC (in Lance Seefeldt's labs) confirmed ethylene as the main product. The rate of ethylene formation is reasonably high compared to the results from a series of control experiments. However, it is far lower than that from the ATP and Fe protein-dependent system (~1%). The reduction rate of acetylene could be controlled by potential, and more negative potentials give a faster reduction rate. This effect is reversed after stepping the potential back to more positive values, showing the effect of driving force in the electrocatalytic reaction.

The study of the interaction between isocyanide and MoFe protein is displayed in Chapter 6. Isocyanide, especially methyl isocyanide, was found to give new peaks in the IR spectra, consistent with isocyanide bound to the MoFe protein. The peaks were shifted slightly to higher wavenumber compared to the free isocyanide solution peak, indicating that the sigma-donor interaction dominates. Several different species were observed from spectra recorded both at mild potentials and low potentials, which was consistent with the previous study that there are two different redox potentials for isocyanide reduction by nitrogenase.[1]

Although GC confirms that methyl isocyanide was reduced to methylamine at -1.1 V in the SEC cell, no methylamine was detected by GC at mild potentials. The reduction rate of CH_3NC by the wild type MoFe protein is quite close to the rate observed in control experiments with apo protein, showing the difficulty in confirming electrochemical substrate reduction by nitrogenase and the importance of control experiments with the apo-protein. The very negative potentials required

for substrate reduction mean that competing background reactions at the electrode / mediators or P-cluster in the MoFe protein are likely, and need to be corrected-for in control experiments.

Overall, the work in this thesis is summarised on a potential scale in Figure 7-1. Isocyanide (methyl isocyanide) bound as an inhibitor to the active site of MoFe protein at quite a mild potential (about 0 mV), even above the midpoint potential of the first redox couple of the FeMo cofactor at -42 mV. The onset of CO binding, and the binding of C_2H_2 to MoFe protein as an irreversible inhibitor is about -900 mV, the same potential where proton reduction starts to be detected from the current. The reduction of C_2H_2 and methyl isocyanide as substrates by the MoFe protein required slightly more negative potentials which is consistent with a potential that would access the second redox process of isolated FeMo cofactor at ca. -940 mV.

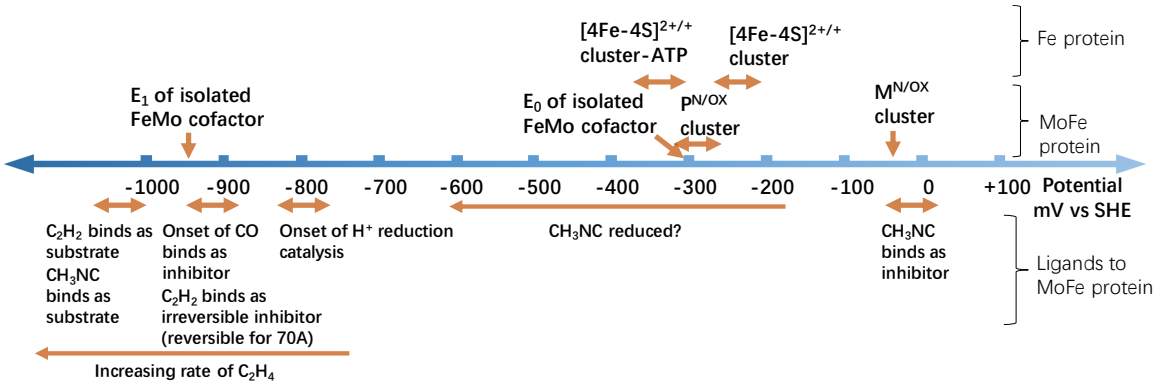


Figure 7-1: A potential scale shows the measured mid potentials of metal clusters in nitrogenase and potential of ligands binding to MoFe protein in the electrochemical study.

Future work should focus on the potential between -100 mV and -800 mV, and for this a wider range mediator cocktail, offering control from 0 mV to -1100 mV might be helpful in the studies. A better approach to quantify amines or ammonia should be developed to analyse the dilute products of isocyanide reduction more accurately. Analysing different products at different potentials could help to understand the effect of electrochemical driving force on the reduction

reaction by MoFe protein, which could provide new insight toward understanding the mechanism of nitrogenase.

It is very promising that it was possible to drive reduction of acetylene by nitrogenase, as this shows that the reduction of a triple-bond substrate is possible for nitrogenase under electrochemical control. Preliminary results for methyl isocyanide reduction support this. It is intriguing that acetylene reduction was observed for wild type nitrogenase even without Eu-L, suggesting follow-up studies without mediators. Different carbon materials could be trialled to see whether direct electron transfer can be improved.

Minteer and coworkers have recently presented data they interpret as direct N_2 reduction by MoFe protein attached via a similar pyrene linker approach,[2] but they do not present control data for apo-protein, and so it is difficult to confidently attribute the current in their work to N_2 reduction by MoFe protein. To study the interactions between N_2 and MoFe protein, it may be necessary to find conditions that lower the competing proton reduction reaction, as the evolution of H_2 (involving loss of a bound hydride) would re-oxidise the FeMo cofactor and prevent accessing levels suitable for N_2 binding. It may be useful to raise the pH. Another possibility could be to try working under a partial H_2 atmosphere to see if this would suppress proton reduction and enable N_2 reduction.

Overall, the work presented in this thesis presents the first information on potentials required for different ligands interacting with the MoFe protein, and should form the basis for future mechanistic studies of nitrogenase. It will be interesting to look at the V- and Fe- nitrogenases to see how their behaviour differs.

Bibliography

1 B. K. Burgess and D. J. Lowe, *Chem. Rev.*, 1996, **96**, 2983–3012.

2 D. P. Hickey, K. Lim, R. Cai, A. R. Patterson, M. Yuan, S. Sahin, S. Abdellaoui and S. D. Minteer, *Chem. Sci.*, 2018, **9**, 5172–5177.